Supramolecular Chemistry of Some New Schiff Base Ligands:

From Single and Triple-Strand Helices to Polymers

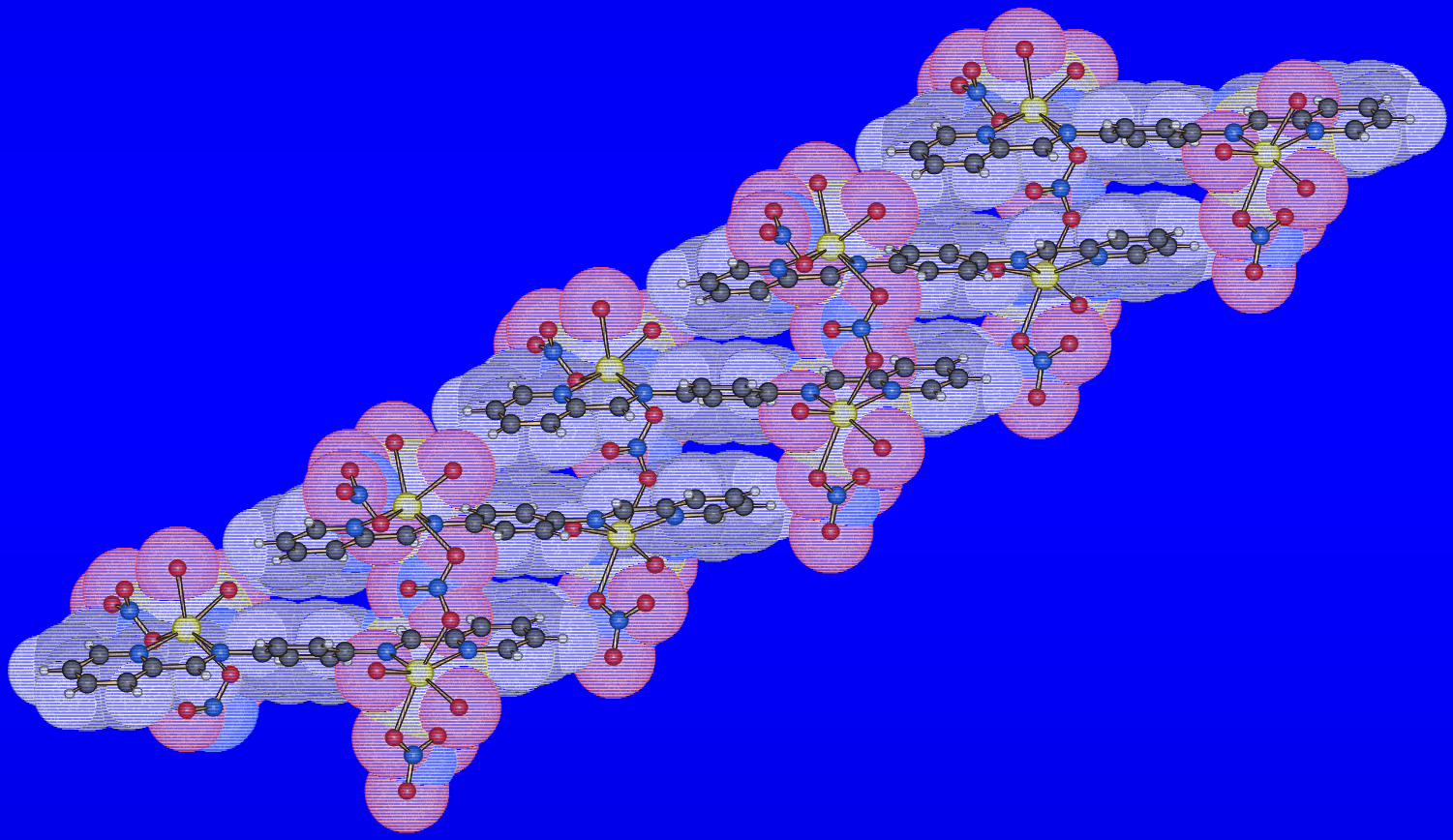

Ana Tesouro Vallina

Neuchâtel 2001

UNIVERSITÉ DE NEUCHÂTEL

FACULTÉ DES SCIENCES

INSTITUT DE CHIMIE

Supramolecular Chemistry of Some New Schiff Base Ligands: From Single and Triple-Strand Helices to Polymers

Thèse Présentée à la Faculté des Sciences de l'Université de Neuchâtel par

Ana Tesouro Vallina

Chimiste diplômée de

l'Université de Oviedo (Espagne)

pour l'obtention du titre

de Docteur ès Sciences

Institut de Chimie

Université de Neuchâtel Juillet 2001

IMPRIMATUR POUR LA THESE

Supramolecular chemistry of some new Schiff base ligands: From single and triple-strand helices to polymers

de Mme Ana Tesouro Vallina

UNIVERSITE DE NEUCHATEL

FACULTE DES SCIENCES

La Faculté des sciences de l'Université de Neuchâtel sur le rapport des membres du jury,

Mme H. Stoeckli-Evans (directrice de thèse),
K. Bernauer et P. Belser (Fribourg)

autorise l'impression de la présente thèse.

Neuchâtel, le 31 août 2001

Le doyen:

J.-P. Derendinger

Remerciements

Le présent travail a été effectué d'octobre 1997 à juillet 2001 dans les laboratoires de Chimie Physique II de l'Université de Neuchâtel, sous la direction de Madame le professeur Helen Stoeckli-Evans.

En premier lieu, j'aimerais exprimer ma gratitude à ma directrice de thèse, Madame le professeur Helen Stoeckli-Evans, pour m'avoir donné l'opportunité de travailler dans son groupe ainsi que pour sa constante bonne humeur et gentillesse. Elle a la capacité de favoriser la bonne entente dans son groupe, ce qui est, en principe, plus difficile dans un groupe formé par des personnes venant des quatre coins de la planète comme le nôtre ! Je la remercie sincèrement de m'avoir initié à la cristallographie et de m'avoir laissé une grande liberté dans la réalisation de ce travail. Cette liberté liée à sa grande disponibilité nous permet d'apprendre à réfléchir et de se développer et je la remercie pour cela.

Je remercie les membres de mon jury de thèse, Monsieur le Professeur Klaus Bernauer et Monsieur le Professeur Peter Belser (Université de Fribourg) pour avoir accepté d'examiner ce travail et pour m'avoir donné leur avis surtout sur la partie concernant les mesures en solution.

Je remercie Monsieur le Professeur Bernhard Erni (Université de Bern) pour m'avoir laissé utiliser le spectrophotomètre Spectramax-250 pour faire des titrations spectrophotomètriques. J'adresse aussi mes remerciements aux personnels des services d'analyses spectroscopiques RMN et MS de notre institut et ceux des services d'analyses élémentaires de l'Ecole d'Ingénieurs de Fribourg.

Je ne peux pas oublier dire merci à notre grand CHEF, Monsieur Philippe Stauffer, « la crème de la crème » pour être si serviable et si sympathique ainsi que pour ses jeux de mots pas toujours faciles pour les non-francophones !

Je ne peux pas non plus oublier ni Piotr ni Radek pour être disponibles à plus que 100% pour résoudre de petits et grands problèmes informatiques, électriques et autres !

Comme assistante, j'aimerais remercier mes étudiants de première et deuxième année et également à Pascal Grossenbacher, mon apprenti dans ma deuxième année de thèse, qui a travaillé beaucoup et très bien, même si, quelque fois, il ne comprenait pas tout à fait ma manière de parler en français !

Je n'oublie pas non plus à Gilles Gasser qui a réalisé son travail de diplôme avec moi et qui maintenant est en train d'effectuer sa thèse dans notre groupe. Je crois que cela veut dire que la première expérience était bonne ! Remarque : Gilles est le premier « produit du terroir suisse authentique » dans le groupe !

Mes remerciements s'adressent aussi (bien sur qu'oui!) à TOUS les membres du groupe sans exception, les anciens et les nouveaux. Je ne vais jamais oublier ces quatre ans qu'on a passé ensemble. J'espère pouvoir trouver dans l'avenir une ambiance de travail si agréable et gai et surtout, la même absence de rivalité.

Parmi ces personnes, j'aimerais en citer, en particulier, quatre (et dans l'ordre « d'apparition » dans le groupe !) : Montse, Piotr, Dilovan et Jessica. Je les remercie pour leur amitié très enrichissante que j'espère garder très longtemps (surtout si EasyJet continue à exister !). Un « gracias » aussi pour l'équipe d'espagnols de l'Institut qui m'ont permis de me sentir comme à la maison !

Enfin, j'aimerais très particulièrement remercier mes parents, ma sœur, ma tante, mon oncle et Luis pour m'avoir écouté et « supporté » tout le temps. Muchísimas gracias!

Je remercie bien sûr l'Etat de Neuchâtel et le Fonds National Suisse de la Recherche Scientifique de m'avoir confié un poste d'assistant ainsi que pour leur soutien financier.

CONTENTS

ABBREVIATIONS

1D, 2D, 3D	one-, two- and three-dimensional
DCI, EI, ES	desorption chemical ionisation, electronic impact, electrospray
MS	mass spectrometry
IR	infrared
NMR	nuclear magnetic resonance
UV	ultraviolet
Vis	visible
L	ligand
M	metal
Py	pyridine
Pz	pyrazine
Ph, ϕ	phenyl
s, d, t, m	singlet, doublet triplet and multiplet (NMR spectroscopy)
vs, s, m, w, b	very strong, strong, medium, weak, broad (IR spectroscopy)
RT	room temperature
TBr	2,3,5,6-tetrakis(bromomethyl)pyrazine
tamp	2,3,5,6-tetrakis(aminomethyl)pyrazine
bamp	2,6-bis(aminomethyl)pyridine
tppz	2,3,5,6-tetra(2-pyridyl)pyrazine
TLC	thin layer chromatography
X	halogen
χ	magnetic susceptibility
δ	chemical shift
ε	extinction coefficient
λ	wavelength
τ	index of trigonality
υ	stretching vibration (IR spectroscopy)

I. INTRODUCTION

Supramolecular chemistry: overview of structural motifs in Coordination Chemistry

The origin of coordination chemistry is normally dated from 1798 with the discovery of the cobaltammines by Tassaert[1]. In 1913 Alfred Werner received the Nobel Prize for his theory of transition metal-amine complexes. After one century modern coordination chemistry has developed considerably. Traditional coordination chemistry focuses on the type and arrangement of bonds present in classical metal complexes, coordination compounds and organometallic chemistry[2]. The innovative approach of the recently established field of **Supramolecular Chemistry** considers[3] "*the chemistry of molecular assemblies and of the intermolecular bond*" that is "*the chemistry beyond the molecule*". This includes topics such as molecular recognition, host-guest processes, crystal engineering, templating, self-assembly, self-organization and molecular machines[4a].

The scope of this introduction is to focus on the self-assembly processes in coordination chemistry. Several very interesting books and reviews[4] cover the enormous literature existing in this field and some of them have been used to prepare this introduction. For example, Piguet *et al.*[5] have written a comprehensive review of single, double and triple helicates and Swiegers *et al.*[6] have recently published a wide compilation of the new structural motifs in Coordination chemistry that covers compounds published up to April 2000.

One of the main goals today in coordination chemistry is to synthesize molecules with predefined geometry using the concepts of supramolecular chemistry and, moreover, to mimic structural shapes present in nature (proteins, viruses, see-shells…). In fact, chemists have borrowed from biologists the concept of **self-assembly** in order to explain how several

subunits associate spontaneously to form complex molecular entities in a hierarchic and well-defined manner.

For instance, one of the best-known examples is the 3D-organization (tertiary and quaternary structure) of a protein from a specific amino acid sequence (primary structure), a process that takes place in a very precise and well-established manner. In coordination compounds, analogous levels of organization can be defined. The bond connections inside the **building blocks** form the primary structure. The motif (for instance, a double helix) obtained by the assembly of these blocks gives the secondary structure, the so-called **supermolecule**. When several of these motifs, come together to form, for example, a circular helix they give rise to the tertiary structure, a **supramolecular array**. If a number of them aggregate together, this will lead to a macroscopic **conglomerate** (highest level of organization).

The nature of coordinate bonds is placed in between biological intra and intermolecular interactions (*weak and labile*) and covalent bonds (*strong and kinetically inert*). The driving force for biology and for most metal assisted self-assembly processes is the thermodynamics. Normally, self-assembly processes are kinetically fast and only the thermodynamically most stable compound will be obtained, even if other species were present in solution. This is because, in the reversible equilibrium, the *self-correcting* principle is effective allowing each possible product to inter-convert on the rest, and vice versa, as many times as necessary to reach the lowest energy product in spite of some local energy minima products.

The general approach to influence the final structure (to program the result) is by playing with external parameters such as ligand structure, metal stereochemical preferences, counter-ion used, temperature, concentration of the species, solvent and reaction time. It is known that the metal's coordination number and its geometrical preferences are variable and depend on the

size, the charge and the electronic structure. For example, Ag^{+} and Cu^{+} prefer to coordinate in a tetrahedral manner while Co^{2+} and Ni^{2+} are normally in an octahedral geometry. Metals also present variable affinity for different donor atoms. Many organic molecules have already been synthesized and used as ligands in metal self-assembly processes. The goal is now to learn how to use all of this available information in a database or **library of building blocks**. This has been achieved in a number of cases and predefined molecular fragments have been assembled to produce a wide array of compounds with predefined geometry as will be detailed during this introduction.

All the 3D structural motifs obtained so far can be organized into different groups, from a strictly structural point of view. The following section describes this classification in five main groups subdivided in several categories.

1. Helicates

One of the most studied systems obtained *via* self-assembly processes are the helicates[4b,5]. A **helicate** is defined as a complex consisting of one or more threads (if 2 = double helix, 3 = triple helix and so on) coordinated in a wrapping manner to a series of metallic ions (two at least), which define the helicoidal C_2 (if double) or C_3 (if triple) axis. A molecular **thread** or **strand** is an extended ligand molecule that contains two or more separate domains that can coordinate to different metal ions.

- **What are the main characteristics of a helical structure?**

1. The **chirality** associated with the screw axis. A helical compound can exist in the right-handed (Δ=*P*) and in the left-handed (Λ=*M*) forms.

2. The **pitch**: distance between repeated units along the screw axis.

- **What do we need to generate a helicate?**

Some requirements need to be fulfilled (as much as possible) to obtain a helicate. Both the metal ion and the thread must be unambiguously coded if we want to obtain a unique helical motif. The geometric and donor atom preferences of the metal should be checked. The ligand should possess the correct type and number of donor atoms and should be carefully designed. It should have a certain degree of flexibility, sufficient to permit twisting but not too much to avoid the coordination of all binding sites to the same metal atom.

- **How can the helicates be classified?**

According to the number of ligands wrapped around the metals, we have **single**[7-19], **double**[20-31], **triple helicates**[32-49] and so on. Most helicates known at present are either double or triple helicates. The synthetic strategy is, in theory, quite simple. For instance, to obtain a binuclear double-helix we need two molecular threads containing two *n*-dentate metal coordination sites and two metal ions with a preferred coordination number of *2n*.

By analogy, a binuclear triple-helix needs three ligands containing two *m*-dentate metal coordinating sites and two metal ions with a preferred coordination number of *3m*. Helicates can be divided into **homostranded** (all the strands are the same) or **heterostranded** (presence of different strands). Strands in helicates can be classified in two major groups: **homotopic**, if they present the same binding units along the strand and **heterotopic** when they include different binding units and have, therefore, directionality.

The Scheme I[5] illustrates this classification with all possible sub-categories for the case of double helical complexes.

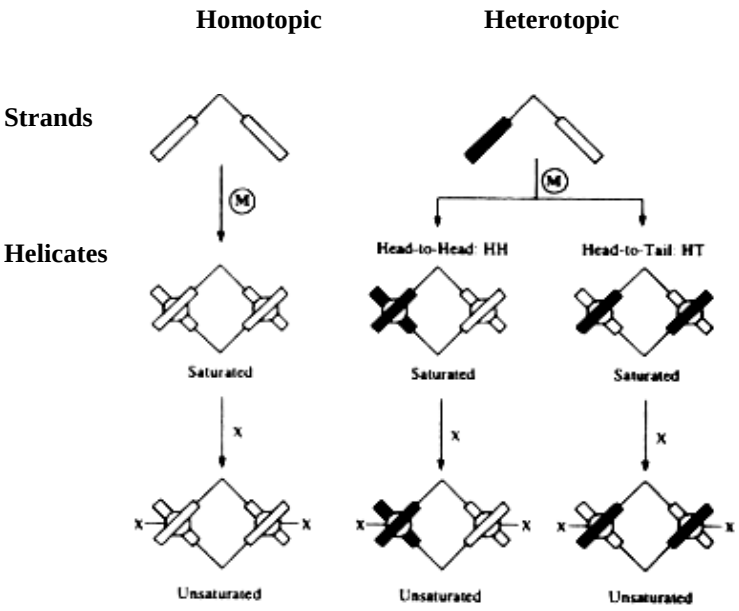

Scheme I

Saturated → if the donor atoms of the ligands fulfil the stereochemical requirements of the metal ions.

Unsaturated → when additional ligands are necessary to complete the coordination sphere of the metal ions.

The same classification used in Scheme I can be applied for triple helicates.

From the point of view of the metal, the helicates can be **homo**- or **heteronuclear**. If the ligands used are homotopic, one should expect to obtain a homonuclear helicate because two different metals will not bind to the same coordinating unit without any special reason. On the other hand, if the aim is to synthesize a heteronuclear helicate, the ligand should be designed to have two or more different metal-binding units according to the metal preferences.

The two most common metal coordination geometries associated with helicates are tetrahedral (for example Ag(I) and Cu(I)) and octahedral (for example Co(II) and (III), Ni(II), Zn(II) and Cd(II)) although examples of other coordination geometries are known (helicates containing lanthanides[37]) .

If the metal or the ligand are not perfectly coded, the reactions become complicated and several products are possible. For instance, **non-helical** compounds, named **side-by-side**, can be obtained and sometimes it is difficult to force the formation of the desired compound. The

following scheme[5] shows the chiral and helical properties of single-double- and triple-stranded helicates.

Scheme II

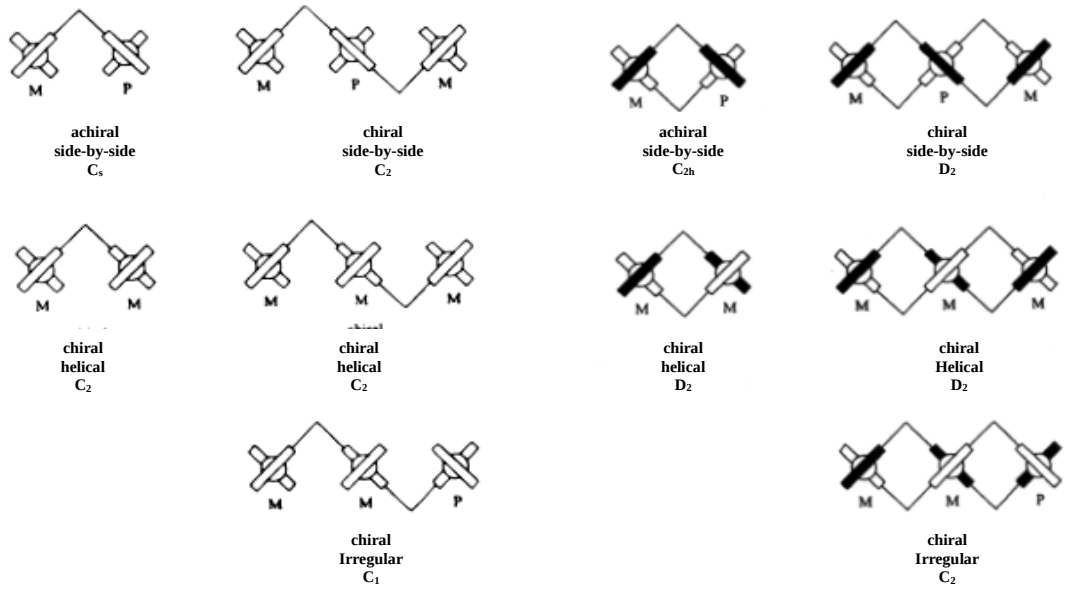

Single stranded helicates **Double stranded helicates**

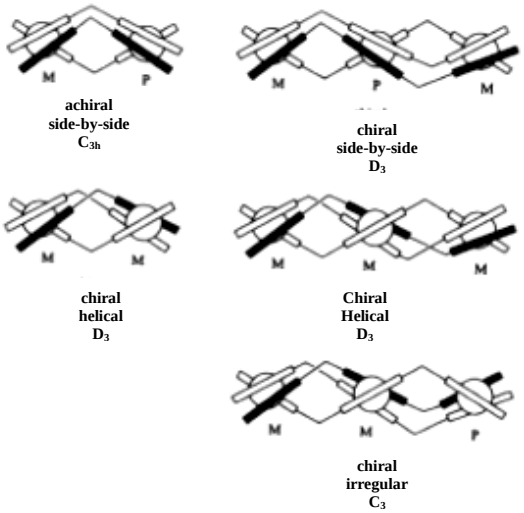

Triple stranded helicates

For example, in a binuclear saturated homotopic helicate, if both metals display opposite absolute configuration, the achiral *side-by-side* arrangement is observed and *vice versa*. In the case of an odd number of metal centres, chirality is always observed. The term irregular is used to describe heterotopic helicates.

- **What analytical methods can we use to characterize self-assembled helicates?**

The most complete structural information can be obtained from **X-ray diffraction**. Of course, for that, the first requisite is to obtain good quality crystals and this is not always possible. Helices are very often difficult to crystallize and when they do it, they sometimes diffract

poorly and problems of disorder, mainly due to counter ions and solvent molecules, make the process of refining the structure difficult. However, most known helicates have been studied by X-ray crystallography.

The behaviour of the species in solution is very interesting because occasionally during the crystallization process the modification of certain conditions can lead to a different structure(s) than the one(s) present in solution. The most used techniques are the NMR, ES-MS (*Electrospray mass spectrometry*) and UV-Vis spectroscopies for qualitative, quantitative and structural investigation.

NMR studies are sometimes complicated depending on the metal atom present and some groups[27,28,37] have developed a *savoir-faire* in this domain. The symmetry in the molecule can be determined by ^{1}H NMR studies. For example, if some selected signals of the free ligand spectrum are compared with the same appearing in the complex(es) it can be seen how many times this signal appears and this can be related with the number of ligands present in the structure or with the symmetry of the compound. Sometimes a model can be proposed.

Evolving Factor Analysis[50] can be used to estimate the number and relative proportion of the species present in the solution as well as values for their equilibrium formation constants using data from **spectrophotometric titrations**[37]. This works well in simple cases but when the number of species present in solution increases (3-5 maximum), it can fail or give only approximate results.

ES-MS is a powerful tool because as it is a soft technique, the molecules are not destroyed during the measurements and all the m/z values observed correspond to species present

originally in the solution. High resolution is necessary in order to calculate the charge of each peak in the spectra. As a general approach, the best analysis will be obtained from a combination of all these techniques. For instance, by analysing ES-MS spectra we could neglect some of the *a priori* possible products and then the UV-Vis treatment will be simplified.

- **Applications of helicates**

First of all, until recently, the research in this field has been mainly academic. However, some specific applications taking advantages of the inherent properties of helicates such as **chirality** are being developed. Helicates can be used as building blocks in helical macromolecular structures[51]. Another application uses the chiral cavity formed by the spacers when wrapping around the metal atoms for selective **host-guest** recognition processes[52]. Although helicates present only a small interest as biomimetic models some studies of helical compounds interacting with DNA[53] have shown that they have a good complementarity with the major-groove of B-form DNA.

Helicates containing lanthanide metal ions are also being intensely studied[37] because of their **luminescent properties**. In helicates, the metal ions are very well protected, enveloped by the ligands and they are not easily accessible. Therefore, they usually conserve their intrinsic properties (in any solvent) and these helicates can be used as light-converting devices.

2. Latticed motifs

This category includes grids, racks and ladders or any 2D coordination arrays build up entirely by orthogonal binding. Their coordination bonds are formed at alternating right angles to each other using, generally, tetrahedral (Ag(I), Cu(I)) or octahedral (Ni(II), Co(II), Zn(II)) metal ions and rigid linear ligands with several chelating units.

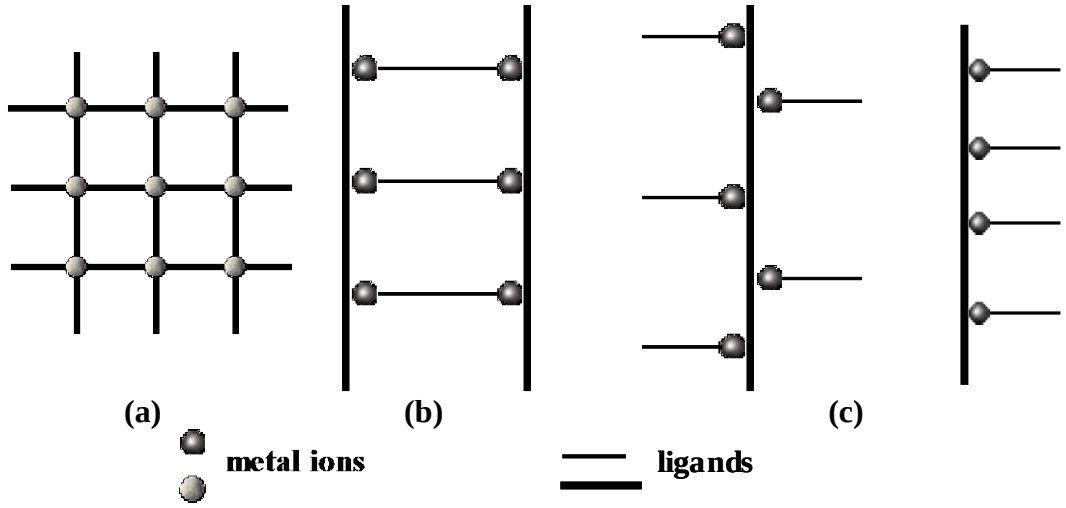

Figure I. Schematic drawing of (a) **grid**, (b) **ladder** and (c) ***syn***- and ***trans***- **rack** motifs.

To obtain **grids**[54-59], planar ligands, with a rigid spacer between their binding sites, for instance, bidentate heteroaromatic linkers, like oligopyridines, have been used. They are described with the nomenclature **[n x n']G** (ligands containing n and n' coordinating sites where n + n' = total number of ligands and n.n' = total number of metals).

In the case of **ladders** and **racks**[60-1], besides the previous requisite, a second mono- or bidentate ligand with coordinating sites at one or both ends, is also necessary. Ladders are structurally rigid and are described as **[2 x n]L** while racks are described as **[n]R** (with n = nuclearity of the compound). Other non-infinite coordination arrays are included in this group; for example, the combination of T and L and X shaped ligands to give an interesting porphyrin based complex was reported by Drain *et al*[62].

The magnetic[56] and photophysical properties[61] as well as the capacity for information storage[55] are possible applications of these compounds.

3. Cyclic motifs

This term includes a large variety of compounds displaying closed 2D and 3D structures incorporating metal ions, the so-called **metallocycles**. Their cyclic nature is the only common characteristic among them. As it can be seen in Figure II many different polygonal (a) and polyhedral (b) shapes can be obtained by using building blocks with a systematic and logical design.

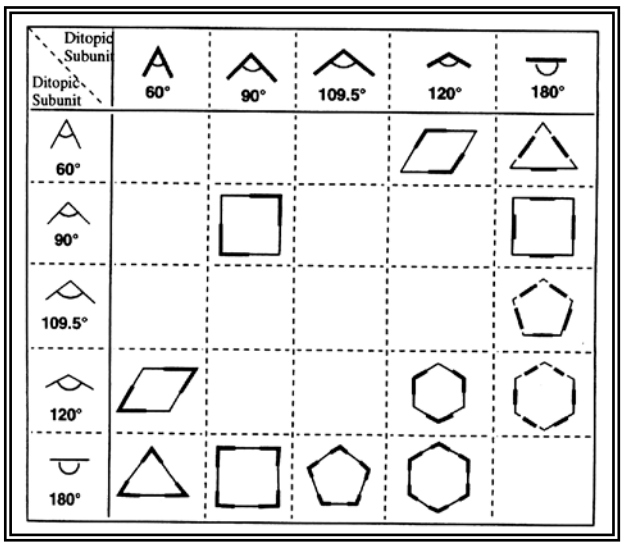

(a)

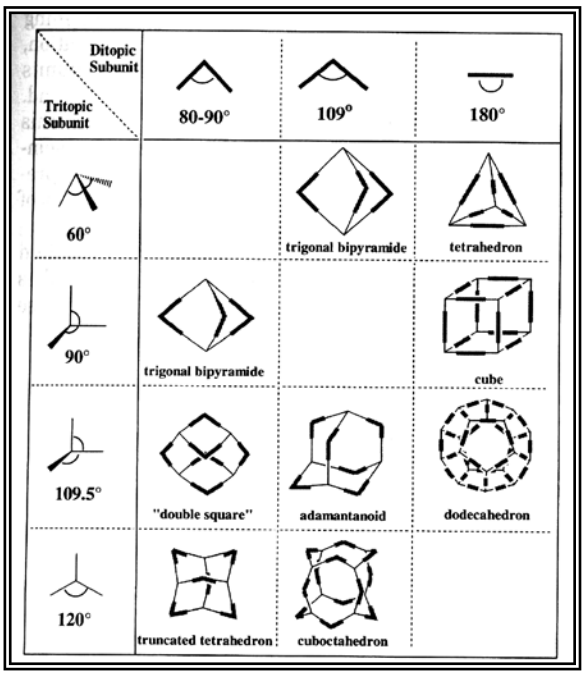

(b)

Figure II. Molecular library approach[63]

The appropriate complementarities between *donor* (ligands) and *acceptor* (metal) building blocks play a critical role in the formation of these polygonal (such as triangles, squares, pentagons, hexagons) and polyhedral (such as cubes, tetrahedrons, octahedrons) assemblies. Raymond *et al.* have reported[64] a *symmetry-interaction model* to explain their formation, using the hypothesis that symmetry-driven processes and lock-and-key interactions form these closed structures. As for most self-assembly processes, the formation of metallocycles is ruled by thermodynamics. In general, cyclic structures are preferred over open ones for enthalpic

reasons (larger number of bonds formed per unit) and, at low concentrations, small cycles are more favored than big ones for entropic reasons (Le Chatelier law).

A large number of publications concerning metallocyclic polygons and polyhedra have been reported: triangles[65], squares[65f, 66], rectangles[67], hexagonal, cubic and rectangular boxes[68], cylinders[27b, 69], cyclophane boxes[70] and adamantanoid boxes[71.]

Among the applications of these compounds one can mention their use in host-guest processes as receptors, transporters or containers. Luminescent properties as well as their use in catalysis due to the formation of channels have been described[63].

Another very interesting type of cyclic motif is the so-called **circular helicates**[72]**.** They consist of double-helicates whose ends have been closed to give a toroidal structure. They can be described using the nomenclature **[n]^{m}cH** (n = number of metal atoms, m = helicity, i.e. 2 for a double helix). For example, a schematic drawing of a [6]^{2}cH is shown in Scheme III[72a].

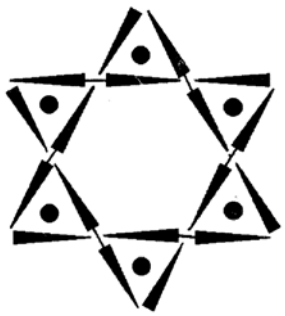

Scheme III

Circular helicates are a very beautiful example of the, before mentioned, *tertiary structure* level of organization. They are formed in a thermodynamic one-step self-assembly process although sometimes the kinetic product is observed.

In some cases[72] mixtures of circular helicates of different nuclearity have been observed during the same reaction.

The template effect is also observed in cases containing anion molecules in their cavity that define the final nuclearity of the compound. Normally, the racemic mixture of the *P* and *M* configurations is observed except for cases where the design of the ligand favours one of the configurations. These are the most interesting cases in view of their use in selective host-guest or catalytic processes.

4. Filamentous motifs

The 1D, 2D or 3D linear coordination oligomers formed with ligand strands having their donor binding sites at their ends (i.e. 4,4'-bipyridine) are included in this group. The metals are coordinated to the ligands in an alternate sequence forming a molecular strand. The binding angle is 180° except for branched oligomers. In order to avoid the formation of infinite polymers, a terminator ligand able to bind with the remaining positions at both ends is necessary.

Two main subclasses can be considered:

4.1. rods[73] → are inflexible linear coordination oligomers where the entire molecule lies on a straight axis. The synthetic approach is to start with a bidentate rigid ligand and progressively attach more ligands (*bricks*) using the coordination to the metal as the *cement*. Figure III depicts a rod-shaped oligomer. The principal applications for these materials can be found in the domain of photophysics when using luminescent metal ions and in electron-transfer processes[73g].

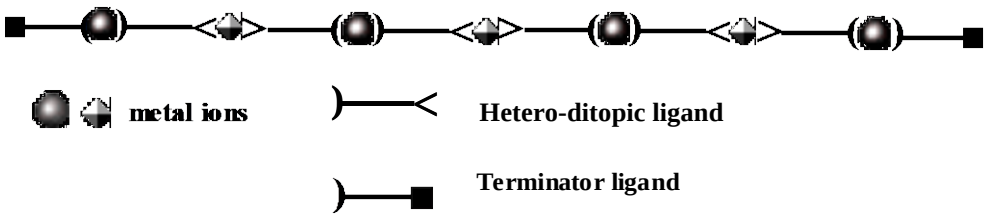

Figure III. Schematic illustration of a rod coordination oligomer.

4.2. metallodendrimers → are highly branched (Greek *δεντρο, dendro = tree*) coordination oligomers produced by using branched spacers and having in the centre, as the *creator*, a branched ligand as well. Two synthetic strategies can be used in dendrimer chemistry, the so-called ***divergent strategy*** (the dendrimer is build up starting from the centre, the *core*- this is

the most general approach) and the ***convergent strategy*** (the dendrimer is build up from the outside border to the core)[4c]. The **core** represents the, using dendrimer terminology, **generation zero**. Then, each reaction step will give rise to a new generation and it should have a very high yield, ideally, quantitative yield. Low yields together with steric problems, can inhibit the synthesis of high (and even low) generation dendrimers. Figure IV[74] shows the structure of a third-generation dendrimer (each circle with a different colour represents a new generation), presenting a functionalised surface.

Figure IV. Metallodendrimer structure

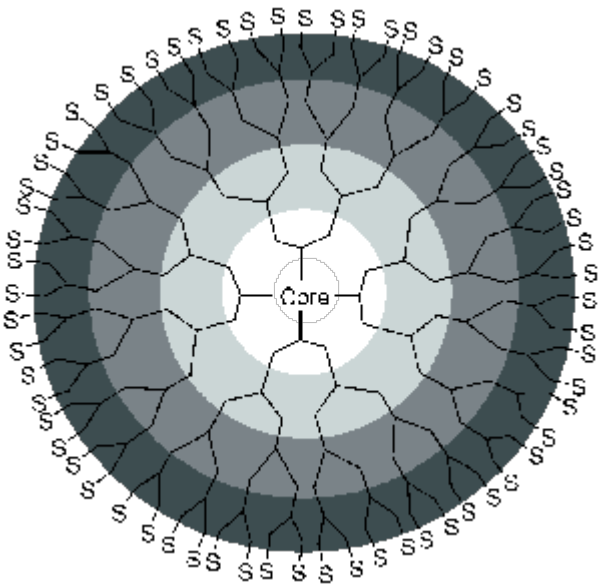

Using this approach, many applications emerge due to the properties of the surface of the dendrimers. For instance, if a certain functional group is known to exhibit a particular property, using it as the terminal group in a dendrimer will increase its concentration and the intensity of such property, in many cases, not only with an additive effect.

There are applications of interest in several areas of research: surface chemistry magnetism, catalysis, sensoring, electrochemistry or photochemistry[75].

5. Interlaced motifs

In this class are included the complexes presenting interpenetrating groups, for instance, one ligand rolled up through itself or through another ligand.

We can distinguishes several sub-types:

5.1. Catenanes: if both groups are cyclic and they are closed like the links of a chain. When more than two rings are present in the structure, the complexes are named **polycatenanes**.

A schematic representation of a polycatenane is given in Figure V[76].

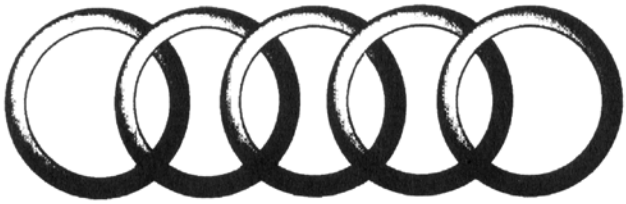

Figure V

A large number of studies on electron-transfer properties and behaviour in controlled molecular motion of catenanes have been reported[76f]. Sauvage *et al*. have carried out a considerably amount of research in this domain including work on catenane switches[76b,d,e,f].

5.2. Rotaxanes: If one of the groups is an open structure but with large terminal groups that do not allow it to escape from the ring (wheel + axis)[77] (see Figure VI).

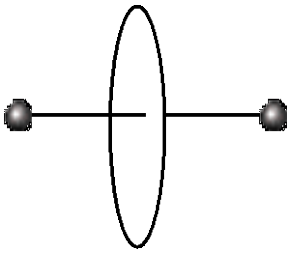

***Pseudo*-rotaxanes** are a particular case where the open structure does not posses the bulky stopper groups and therefore, it is theoretically able to escape from the *wheel* after the formation of the rotaxane.

Figure VI

The synthesis can be achieved using a tetrahedral metal ion and a mixture of a linear bidentate strand and a macrocyclic bidentate ligand. Rotaxanes exhibit extremely interesting properties. They could be useful to examine in electron-transfer processes. They can also be seen as nanomachines or motors inducing molecular motion. For example, by changing the oxidation state of the metal, the geometrical preferences change (i.e. Cu(I), tetrahedral to Cu(II), pentacoordinate) and if the macrocycle contains two different binding domains that can be

selectively accessible , the ring will rotate in function of the oxidation state of the metal[77a]. This processes is reversible.

5.3. Knots: when a single strand passes over and under itself several times to form a continuous loop. They are named or classified depending on the number of times that the ligand crosses with itself. The synthetic strategy for obtaining knots is to connect the opposite ends of the two ligands of a double helix by an irreversible organic step (not by a one-step self-assembly process). The synthetic chemistry needed is in general quite arduous[78,80]. Figure VII shows a schematic drawing of a knot (a) and its two possible chiral conformations (b).

(a) **Figure VII** **(b)**

Finally, one should mention compounds containing several secondary motifs at the same time, the *mixed-motif* complexes. These compounds exhibit *tertiary structure* that comes from the different possible ways of spatial disposition of the secondary motifs. Examples combining a rotaxane with a rack[79] or a helicate with a grid[80] have been reported (Figure VIII. (a) and (b), respectively).

(a) **(b)**

Figure VIII

II. RESULTS AND DISCUSSION

Objective of this work

As it has been showed in the *Introduction,* the design of new nitrogen-donor multidentate ligands and the study of their metallosupramolecular chemistry are of interest not only from the point of view of their potential applications but also from a strictly structural point of view.

The condensation reaction of an aromatic carbaldehyde with a primary amine has been shown to offer an easy and inexpensive way of forming a variety of bis-bidentate and bis-tridentate imine-based ligands and it has been reported that this type of ligand can lead to the formation of different metallic supramolecular assemblies[1-8] such as helicates, and single-stranded polymers. Depending on ligand structural features such as flexibility, the length and nature of the spacer group between the coordinating moieties, and the type of donor atoms, a large variety of different 3D motifs can be generated.

Taking into account all of these parameters, plus the electronic and geometrical preferences of the metal atom, the synthesis of a series of N_x and N_xO_y ligands presenting different spacer groups, together with the systematic study of their reactivity towards metal ions, was carried out. The nature of the spacers has been selected according to parameters such as length and flexibility. All of the ligands selected possess two chelating units that can bind to two different metal atoms or sometimes to a single metal atom, depending on the spacer unit.

1. THE LIGANDS

1.1. Imino based ligands

In general, imines can be formed in high yield by mixing aldehydes and amines. In our case, the ligands **L2-L9** were prepared by the general procedure for a condensation reaction between a carbaldehyde and a diamine in a 2:1 ratio (**L1** was prepared from terephthalaldehyde and 2-(2-aminoethyl)pyridine in a 1:2 ratio) and all of them possess two bidentate Schiff base chelating units linked by a different central spacer unit.

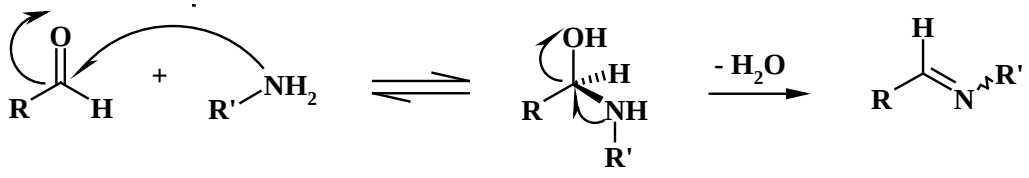

Scheme 1. General mechanism for the condensation between a carbaldehyde and an amine.

Both imine configurations, *Z* and *E* can, theoretically, be obtained. As it will be shown, this was not the case for our ligands. The solvent used for the reaction, as well as the reaction time and the temperature, vary from one synthesis to another. The use of dry solvents or molecular sieves to absorb the water formed during the reaction was tried but these conditions did not improve the yields of the synthesis.

The following scheme illustrates the schematic representation of the imine base ligands **L1-L9** prepared during this work.

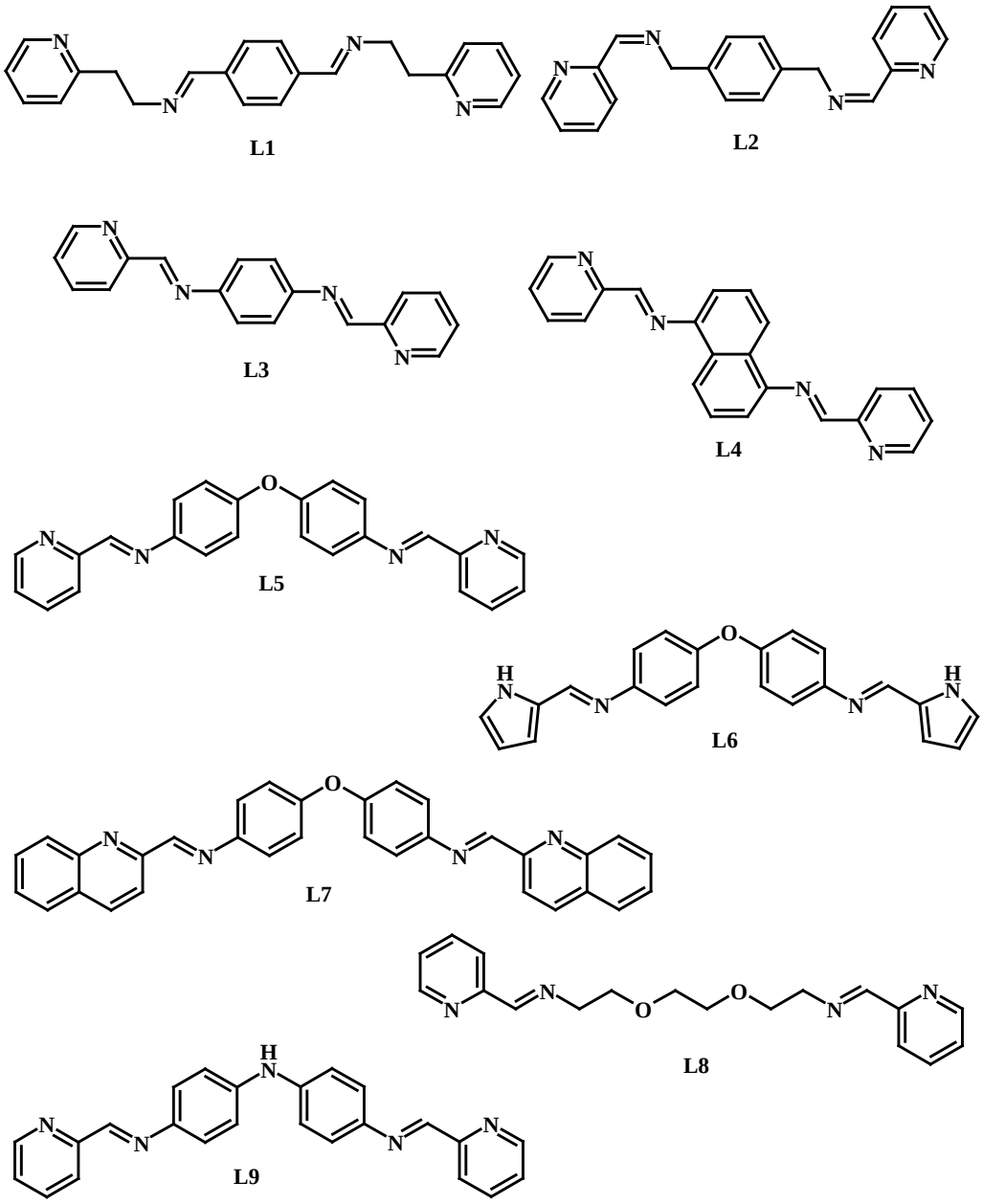

Scheme 2

1.1.1. L1 (*N,N'-Bis[2-(2-pyridinylethyl)-amino]-terephthalalimine)* (1)

L1 was obtained from the condensation reaction between terephtalaldehyde and 2-(2-aminoethyl)pyridine in a 1:2 ratio with quantitative yield. The IR spectrum of **L1** exhibits some weak peaks in the region between 3043 and 2918 cm^{-1}, corresponding to the arC-H

stretching vibrations. The characteristic imine-stretching band appears at 1642 cm^{-1} in addition to several strong bands at 1588, 1567 and 1476 cm^{-1} assigned to the arC-arC and arC-arN stretching vibrations. Some other intense bands at lower wavelengths correspond to the bending C-H vibrations at 830 and 769 cm^{-1}. The ^1H NMR spectrum of **L1** presents five sets of resonances in the aromatic region and two more in the CH_2 region. As the ligand is symmetric each set of resonances was assigned to one half of the molecule. It was possible to assign each independent proton except for Hb, Hd (Scheme 19, p 37) that appeared together as a multiplete at 7.19 ppm. The UV-Vis spectrum (250-600 nm region) of **L1** in ethanol at a concentration 125 μM shows a band around 275 nm related with a pyridine $\pi \rightarrow \pi^*$ transition.

Crystals suitable for X-ray analysis of **L1** were obtained by slow diffusion of cyclohexane into a solution of the ligand in ethylacetate. The X-ray characterisation shows that the structure is centrosymmetric (Figure 1). The bond distances and angles are normal within experimental error.

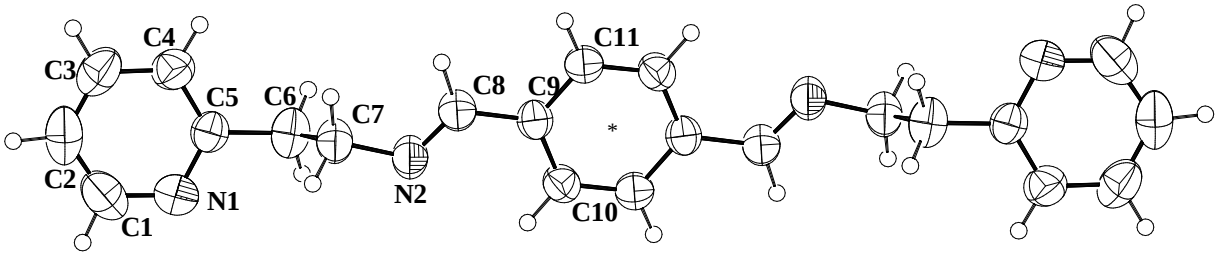

Figure 1. Molecular structure of **L1**.

The imine C=N groups have an *E* configuration with a distance of 1.255 (2) Å, typical for a double bond showing that electron delocalisation does not take place between the phenyl ring and the imine group. As expected, the CH_2 groups break up the π-system. The dihedral angle between the mean planes of the pyridine and phenyl rings is 12.4 (1)°.

The shape of **L1** can be described as a *step-like* (Figure 1a) with a *step* of 1.268 (4) Å (distance between N2 and the pyridine mean plane).

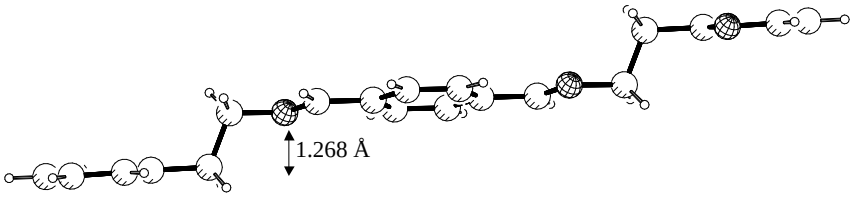

Figure 1a. Side view of **L1**.

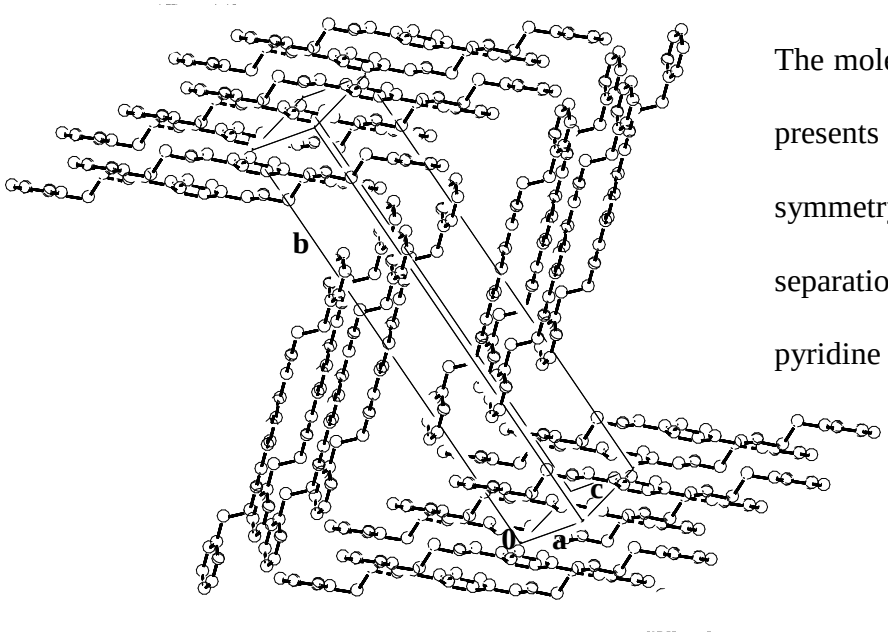

The molecular packing of **L1** (Figure 1b) presents a head-to-tail arrangement of symmetry related molecules with a separation of 5.239 (4) Å between the pyridine rings (i = x-1/2, -y+1/2, z+1/2).

Figure 1b. Molecular packing of **L1** with hydrogen atoms omitted for clarity.

1.1.2. L2 *(N,N'-Bis(2-pyridinylmethylene)-1,4-diamino-p-xylene)* (2)

Ligand **L2** was obtained by the condensation between α,α'-diamino-p-xylene and pyridine-2-carboxaldehyde in a 1:2 ratio with a quantitative yield. The IR spectrum of **L2** exhibits some weak peaks in the region between 3060 and 2850 cm^{-1}, related to the arC-H stretching vibrations. The imine-stretching band is observed at 1640 cm^{-1} and the arC-arC and arC-arN stretching vibrations bands at 1587, 1565 and 1469 cm^{-1}. The bending C-H vibrations are found at 849 and 777 cm^{-1}. The ^{1}H NMR spectrum of **L2** exhibits six sets of resonances in the

aromatic region corresponding to the pyridine and imine protons and one in the CH_2 region. The UV-Vis spectrum (250-600 nm region) of **L2** in EtOH at a concentration 125 μM shows a band around 270 nm corresponding to the pyridine $\pi \rightarrow \pi^*$ transition.

Slow diffusion of acetonitrile into a solution of the ligand in chloroform gives crystals suitable for X-ray analysis. The crystal structure of **L2** is also centrosymmetric as depicted in Figure 2.

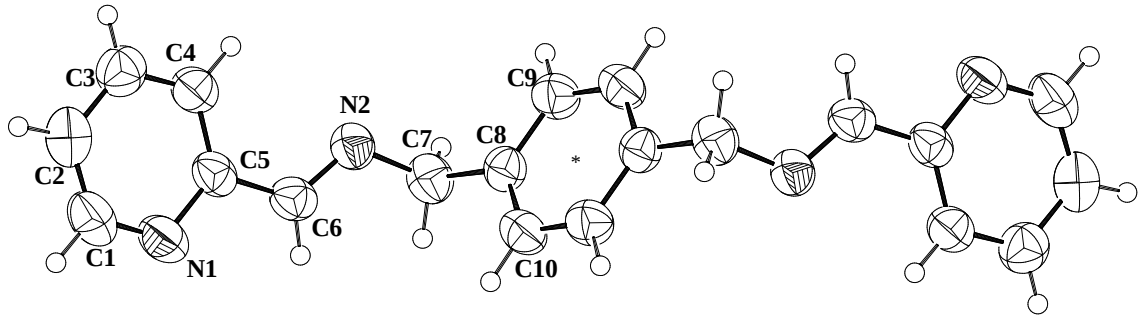

Figure 2. Molecular structure of **L2**.

As for **L1**, the imine group presents *E* conformation and a C=N double bond distance, 1.262(3) Å. The aromaticity of the system is interrupted by the CH_2 groups.

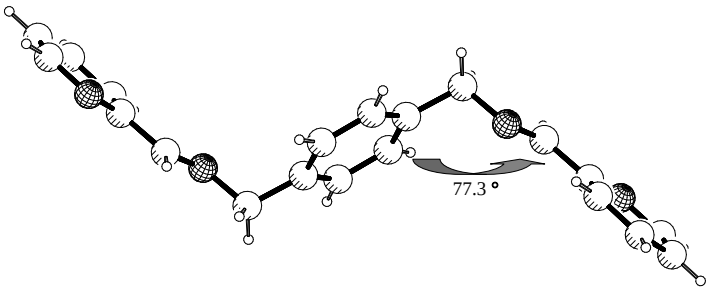

Figure 2a. Side view of **L2**.

Compared to **L1**, the form of **L2** looks more *zigzag* in shape with a dihedral angle of 77.3 (1)°, close to perpendicular, between the mean planes of the pyridine and phenyl rings (Figure 2a).

The molecular packing of **L2** is depicted in Figure 2b. Symmetry related molecules arrange in an intercalated head-to-tail manner.

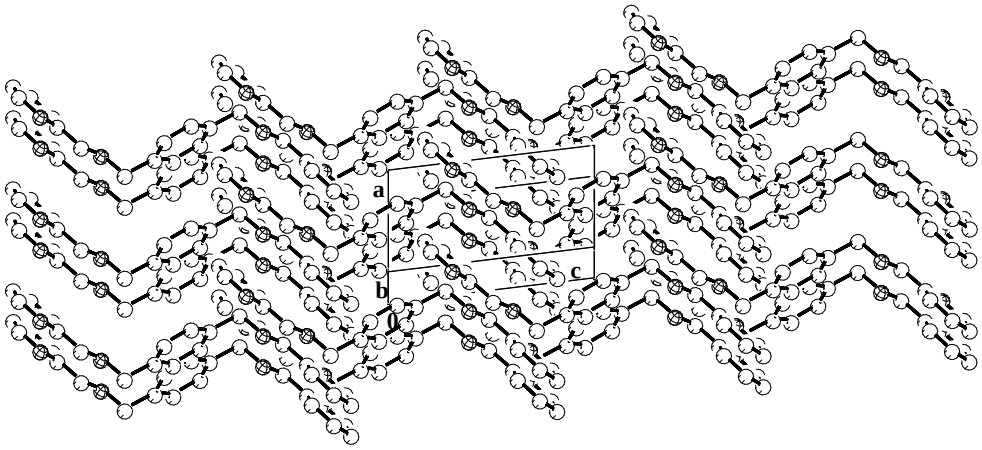

Figure 2b. Molecular packing of **L2** with H atoms omitted for clarity.

1.1.3. L2R *(N,N'-Bis(2-pyridinylmethyl)-1,4-diamino-p-xylene)* (3)

In order to avoid the hydrolysis problems[#] upon complexation of ligands **L1** and **L2**, the double imine bonds were reduced to simple amine groups. The two imino groups of the ligand **L2** were reduced by treating an ethanolic solution of the ligand with $NaBH_4$ in excess, and then extracting the residue obtained in CH_2Cl_2 to afford **L2R**, in a very good yield, as an orange oil.

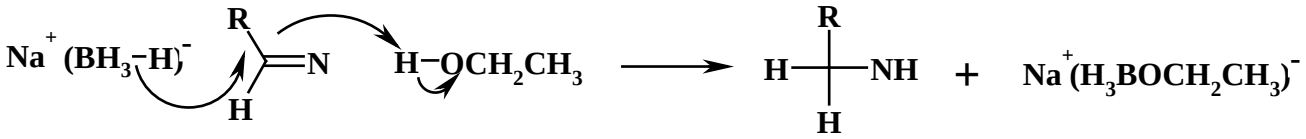

Scheme 3. General mechanism of the reduction with $NaBH_4$.

The IR spectrum of **L2R** shows clearly the absence of the imine vibrational band and the presence of a NH stretching vibration at 3054 cm^{-1}. The arC-arC and arC-arN stretching vibrations bands are found at 1593, 1570 1514 and 1475 cm^{-1} displaced upwards compared to the same bands in **L2** and the bending C-H vibrations at 841 and 762 cm^{-1} are displaced

[#] This will be discussed later on (*Results and discussion*: *The complexes*).

downwards. In the ^{1}H NMR spectrum of **L2R** the peak corresponding to the imine group is clearly absent. This spectrum exhibits four sets of resonances in the aromatic region, one in the CH_2 region and one more at 2.12 ppm that corresponds to the amine group. The aromatic signals are slightly displaced to higher or lower chemical shifts with respect to the NMR spectrum for **L2**. With the aim of obtaining an image of this molecule in the solid state, it was necessary to have the product in solid form. Therefore, its hydrochloride was prepared by bubbling through a methanolic solution of **L2R** a stream of HCl freshly formed by the reaction of H_2SO_4 with NaCl. A white solid that immediately precipitated was filtered and dried but it was not possible to obtain X-ray quality crystals. The protonated form of **L2R** was finally obtained by the reaction of **L2R** with 2 equivalents of $Fe(ClO_4)_2 \cdot 6H_2O$ in MeCN. The brown-red crystals obtained were analysed by X-ray diffraction and were found to be $\mathbf{L2RH_4^{4+}}$ with perchlorate as counter ions

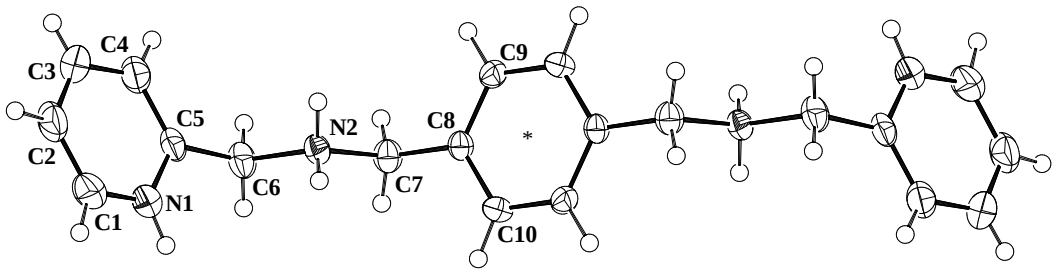

Figure 3. Molecular structure of $\mathbf{L2RH_4^{4+}}$ with labelling scheme and counter ions omitted.

The crystal structure of $\mathbf{L2RH_4^{4+}}$ is centrosymmetric as observed in Figure 3. The structure determination confirms that **L2** was reduced to **L2R** and that the amino groups and the pyridine rings are protonated. In the crystal structure, it can be seen that both N atoms, from the pyridine and from the amine group, are involved in some intra and intermolecular N-H…O interactions with the perchlorate oxygen atoms (see Figure 4).

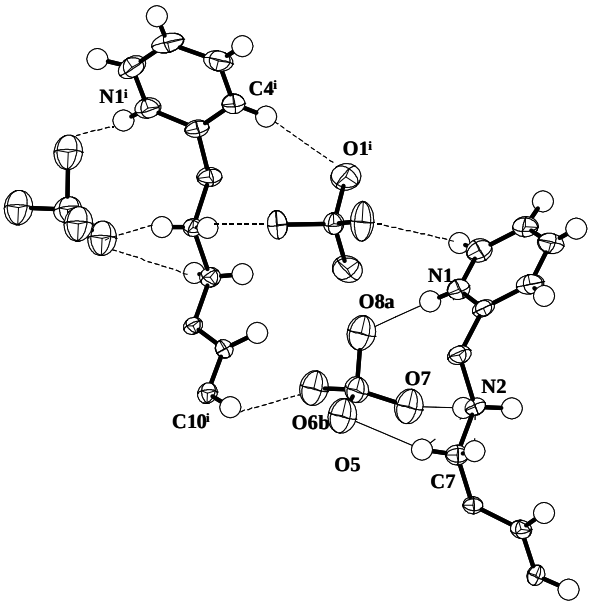

The 3D packing of **L2RH$_4$$^{4+}$** is also influenced by some weak intermolecular C-H…O and N-H…O interactions. The shortest interactions are found for C10…O6b^{i} (symmetry operation i = x, -y, z-1/2) and N1…O8a with distances of 3.12(1) and 2.83(1) Å, respectively.

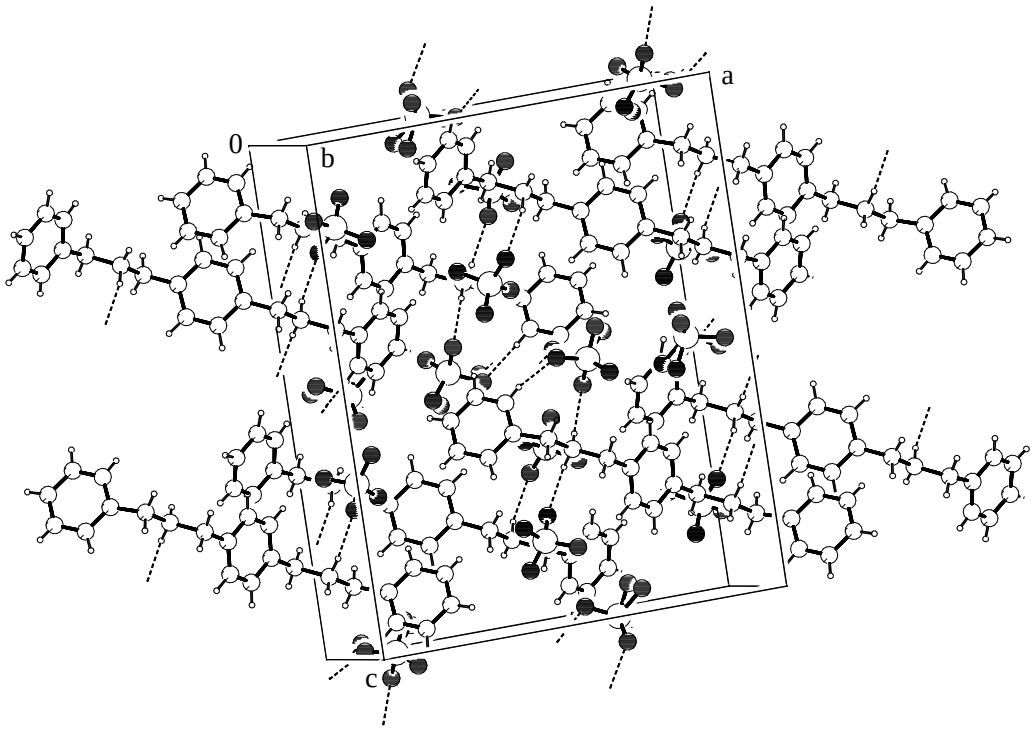

Figure 4. Crystal packing in compound **L2RH$_4$$^{4+}$** showing the hydrogen bonding. A closer view is showed as well for clarity.

One perchlorate anion was found to be disordered with three of the oxygen atoms refined in two different positions with occupancies of 50% each.

1.1.4. L3 *(N,N'-Bis(2-pyridylmethylene)-1,4-diaminobenzene)* (4)

Ligand **L3** was obtained by the condensation reaction between 1,4-phenylendiamine and pyridine-2-carboxaldehyde in a 1:2 ratio with a quantitative yield.

The IR spectrum of **L3** exhibits some weak peaks in the region between 3048 and 2918 cm^{-1}, corresponding to the arC-H stretching vibrations. The characteristic strong imine-stretching band is found at 1619 cm^{-1} and the arC-arC and arC-arN stretching vibrations bands at 1584, 1563, 1494, 1462 and 1434 cm^{-1}, all of them as strong intense peaks. The bending C-H vibrations are found at 844 and 773 cm^{-1}.

The ^{1}H NMR spectrum of **L3** exhibits six sets of resonances in the aromatic region corresponding to the aromatic and imine protons that have been individually assigned. The UV-Vis spectrum (250-600 nm region) of **L3** in EtOH at a concentration 125 μM shows two clear bands at 285 and 360 nm corresponding to the pyridine $\pi \rightarrow \pi^*$ transition and to the absorption of the imine chromophore group.

Slow diffusion of cyclohexane into a solution of the ligand in ethylacetate produced light yellow-brown crystals appropriate for X-ray analysis (Figure 5).

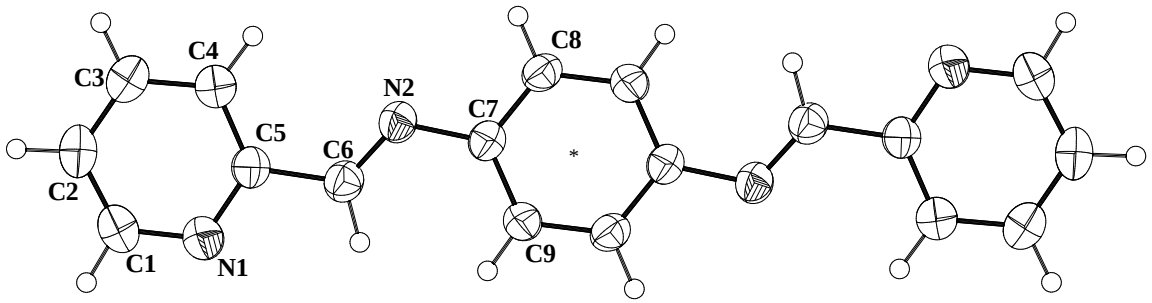

Figure 5. Molecular structure of **L3**.

The molecule presents C_i symmetry. All geometric parameters correspond to standard values. The imino group exhibits an *E* configuration and the entire molecule is almost planar with a dihedral angle of 11.1 (1)° between the mean planes of the pyridine and phenyl rings.

This planarity is coherent with the complete delocalisation present in the aromatic system although this electronic conjugation is not observed at a bond distance level. The C=N bond distance is 1.258(2) Å, indicative of a double bond and distances of 1.471(2) and 1.420(2) Å for C5-C6 and N2-C7, respectively, are standard values for single C-C and N-C bonds.

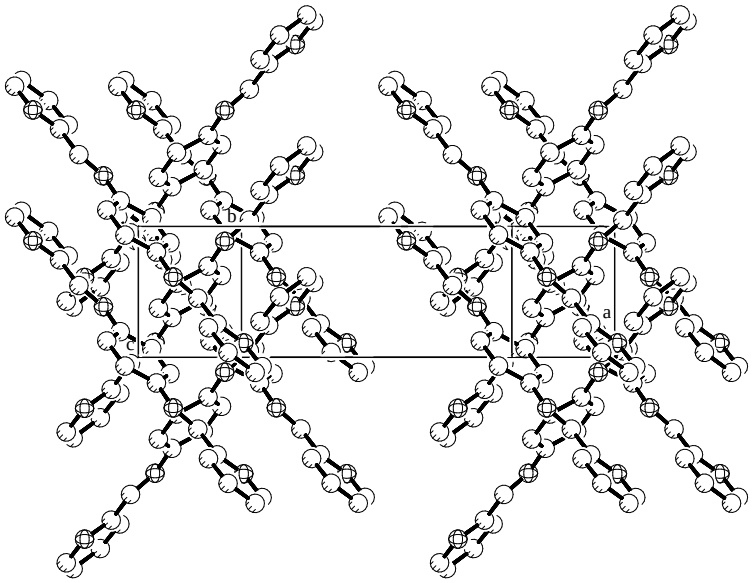

Figure 5a. Crystal packing in compound **L3**.

Some weak C-H…N intra and intermolecular contacts are present between N2…C8 (2.39 (2) Å), N2…C4 (2.90 (2) Å) and between N1…$C3^i$ (3.49 (2) Å) (i = x, -y – 1/2, -z + 1/2). The intramolecular contacts come from the electronic repulsion that forces the two N atoms of the pyridine and the imine to adopt a *trans* configuration. In the crystal packing (Figure 5a), the molecules of **L3** are disposed in a perpendicular manner one with respect to the other and stack in columns up the c axis. No π-π interactions between the aromatic rings are observed.

1.1.5. L4 *(N,N'-Bis(2-pyridylmethylene)-1,5-diamino-naphthalene)* (5)

This ligand was obtained by the condensation reaction between 1,5-diaminonaphthalene and pyridine-2-carboxaldehyde in a 1:2 ratio with a quantitative yield. The IR spectrum of **L4** displays some weak peaks at 3074, 3055 and 3041 cm^{-1}, due to the arC-H stretching vibrations. The imine-stretching band appears at 1622 cm^{-1} as an intense peak and the arC-arC and arC-arN characteristic stretching vibrations bands at 1581, 1566 and 1495 cm^{-1}.

The strong bending C-H vibrations are found at 799, 780 and 743 cm^{-1}. The ^{1}H NMR spectrum of **L4** exhibits eight sets of resonances in the aromatic region, corresponding to the aromatic and imine protons. The UV-Vis spectrum (250-600 nm region) of **L4** in EtOH at a concentration 125 μM shows one clear band at 370 nm and a small shoulder at 280 nm corresponding to the pyridine $\pi \rightarrow \pi^*$ transition and to the absorption of the imine chromophore group. The naphthalene group band appears as a broad band at *ca.* 250 nm.

Crystals suitable for X-ray analysis were obtained by slow diffusion of methanol into a solution of the ligand in dichloromethane. The molecular structure is depicted in Figure 6.

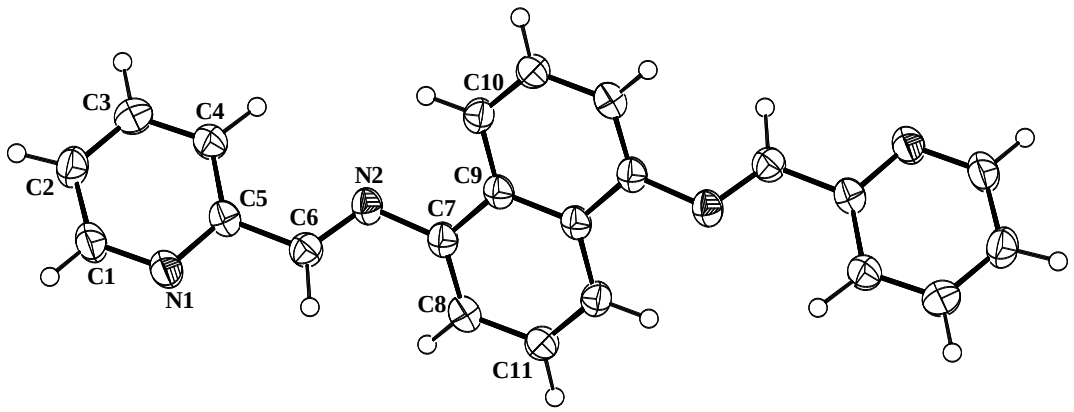

Figure 6. Molecular structure of **L4**.

The molecule possesses a symmetry centre with half of the molecule generated by the symmetry operation: -x+1, -y+1, -z+1. The imino group shows again the *E* configuration but the structure differs significantly from that of **L3**.

The pyridine rings are twisted out of the naphthalene plane by 47.21 (1)° and consequently the ligand has completely lost its planarity although, in principle, it is designed to be fully aromatic. This conformation gives rise to two weak C-H…N intramolecular interactions for the couples N2…C10 and N2…C4 of 2.90 (2) and 2.84 (2) Å, respectively.

The packing motif of **L4** differs considerably from that of **L3** having a zigzag form that is represented in Figure 6a. Symmetry related molecules stack head-to-tail with a separation of 5.053 (4) Å between the pyridine rings.

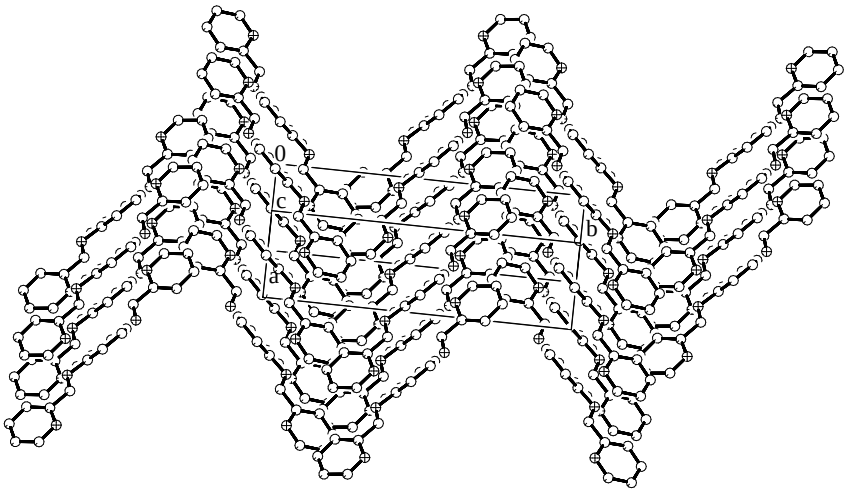

Figure 6a. Crystal packing in compound **L4**.

1.1.6. L5 *(N,N'-Bis(2-pyridylmethylene)-1,4-diamino-diphenyl ether)* (6)

L5[33] was obtained by the condensation reaction between 4,4'-diaminophenyl ether and pyridine-2-carboxaldehyde in a 1:2 ratio with a quantitative yield. The IR spectrum of **L5** displays some weak peaks at 3047 and 2905 cm^{-1}, associated to the arC-H stretching

vibrations. The imine-stretching band is found at 1624 cm^{-1} as a strong intense peak and the arC-arC and arC-arN stretching vibrations bands at 1584, 1566, 1467 and 1438 cm^{-1}. The asymmetric stretching vibrations associated with the ether function show up at 1240 and 1198 cm^{-1}. Bending C-H vibrations are found at 859, 832 and 776 cm^{-1}.

The ^{1}H NMR spectrum exhibits seven resonances in the aromatic region corresponding to the aromatic and imine protons, proving clearly the C_2 symmetry of the molecule in solution. The UV-Vis spectrum (250-600 nm region) of **L5** in EtOH at a concentration 125 μM shows two clear bands at 285 and 340 nm corresponding to the pyridine $\pi \rightarrow \pi^*$ transition and to the absorption of the imine chromophore group.

Slow diffusion of hexane into a solution of the ligand in dichloromethane gave crystals of sufficient quality to be analysed by X-ray diffraction.

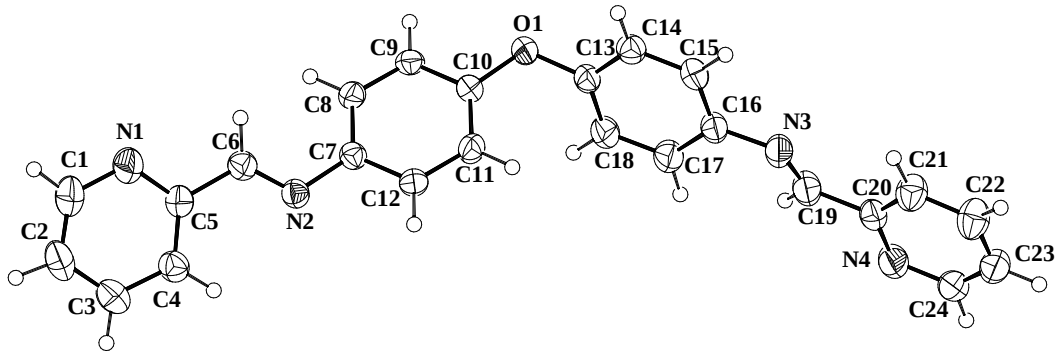

Figure 7. Molecular structure of **L5**.

As for the precedent ligands, **L5** has an imine *E* configuration. The molecule possesses *pseudo*-C_2 symmetry with the twofold axis running through the central O atom. The conformation of the two halves of the molecule is quite different. One moiety, to the right in Figure 7, is almost flat with a dihedral angle of 10.77 (8) ° between the phenyl and the

pyridine rings. In the second half of the molecule the rings are inclined to one another by 46.35 (5) °.

The pyridine-imine system is almost planar within the two moieties. Torsion angles N1-C5-C6-N2 and C7-N2-C6-C5 are 178.3 (1) and 173.3 (1) °, respectively, whereas torsion angles N3-C19-C20-N4 and C16-N3-C19-C20 are 170.0(1) and –177.7 (1) °, respectively. This is consistent with the presence of a π-system, only interrupted by the central O atom, although bond-length alternation is always observed (the average C=N bond distance of 1.263 (1) ° is indicative of double-bond character).

In the crystal packing, Figure 7a, it can be seen that the pyridine N atoms are involved in weak intermolecular C-H…N interactions with symmetry-related molecules. The shortest interactions (Table 1) are found for C18…N4^{i} and C21…N1^{ii} with distances of 3.527 (2) and 3.405 (2) Å, respectively.

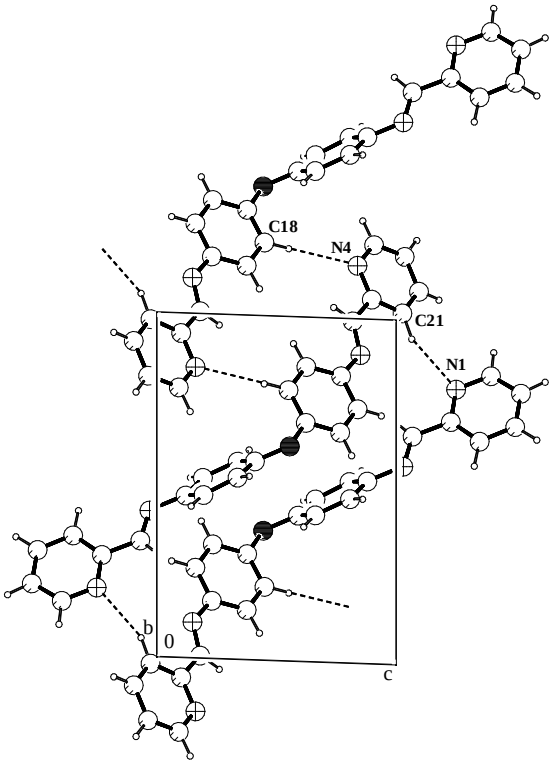

The more planar moieties of symmetry-related molecules are also considerably overlapped. A separation of *ca.* 3.75 Å was found between the best plane through the benzene ring (C13-18) and the pyridine ring (N4,C20-C24)^{iii}, (iii = 2-x, -y, 2-z), indicating weak π-stacking in the crystal.

Figure 7a. Crystal packing of compound **L5** showing C-H…N interactions as dotted lines.

Table 1. Short non-bonding interactions (Å,º) for **L5**.

D-H...A	d(D-H)	d(H...A)	d(D...A)	<(DHA)
C18-H18...N4^{i}	0.97(2)	2.57(2)	3.526(2)	168(1)
C21-H21...N1^{ii}	1.01(2)	2.55(2)	3.405(2)	142(1)

Symmetry transformations used to generate equivalent atoms:

i = -x+2,-y,-z+1 ii = -x+1,-y,-z+1

1.1.7. L6 *(N,N'-Bis(2-pyrrolidinmethylene)-1,4-diamino-diphenyl ether)* (7)

Ligand **L6** (Scheme 4) was obtained by the condensation reaction between 4,4'-diaminophenyl ether and pyrrol-2-carboxaldehyde in a 1:2 ratio with a high yield.

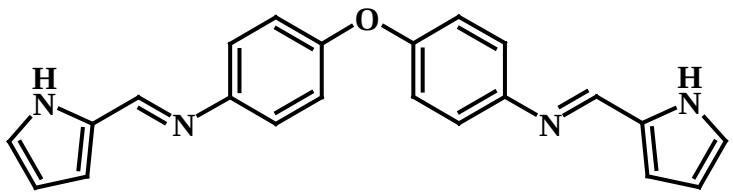

Scheme 4. Schematic diagram of **L6**.

The IR spectrum of **L6** exhibits a very strong peak at 3413 cm^{-1} that corresponds to the free pyrrol NH group vibration and several weak peaks at 3113, 3063, 3032, 2959 and 2889 cm^{-1}, associated with the arC-H stretching vibrations. The imine-stretching band appears at 1617 cm^{-1} as an intense signal and the arC-arC stretching vibrations bands at 1549, 1499, 1452 and 1421 cm^{-1}. The peaks associated with the ether function asymmetric stretching band are found at 1260, 1240 and 1196 cm^{-1}. Bending C-H vibrations appear at 836 and 728 cm^{-1}.

The ^{1}H NMR spectrum exhibits six sets of resonances, five of them in the aromatic region. The proton of the pyrrol NH group is observed at 11.74 ppm. The UV-Vis spectrum (250-600 nm region) of **L6** in EtOH at a concentration 125 μM shows one clear band at 340 nm with a small shoulder at about 295 nm corresponding to the absorption of the imine chromophore and the diphenyl ether groups. The pyrrol $\pi \rightarrow \pi^*$ transition absorption takes place below 250 nm and the maximum was not recorded. It was impossible to obtain X-ray quality crystals of **L6**. A crystalline solid was obtained using different solvents for crystallization but, unfortunately, no single crystals suitable for X-ray analysis.

1.1.8. L7 *(N,N'-Bis(2- quinolidinmethylene)-1,4-diamino-diphenyl ether)* (8)

L7 was obtained by the condensation reaction between 4,4'-diaminophenyl ether and quinoline-2-carboxaldehyde in a 1:2 ratio with a quantitative yield.

The IR spectrum of **L7** presents some weak peaks between 3050 and 3000 cm^{-1}, assigned to the arC-H stretching vibrations. The intense imine-stretching band is found at 1622 cm^{-1} and the arC-arC and arC-arN stretching vibrations bands at 1594, 1584, 1572, 1560, 1497 and 1428 cm^{-1}. The intense asymmetric stretching vibration signals associated with the ether function appear at 1282, 1246, 1237 and 1197 cm^{-1}. Bending C-H vibrations are found at 834 and 757 cm^{-1}. The ^{1}H RMN spectrum exhibits nine sets of resonances, eight corresponding to aromatic protons and one for the imine proton signal. This is coherent with the symmetry of the molecule in solution.

X-ray quality crystals were obtained by slow diffusion of methanol into a solution of the ligand in dichloromethane. Like all of this series of imino Schiff-base ligands, **L7** presents an imine *E* configuration (Figure 8).

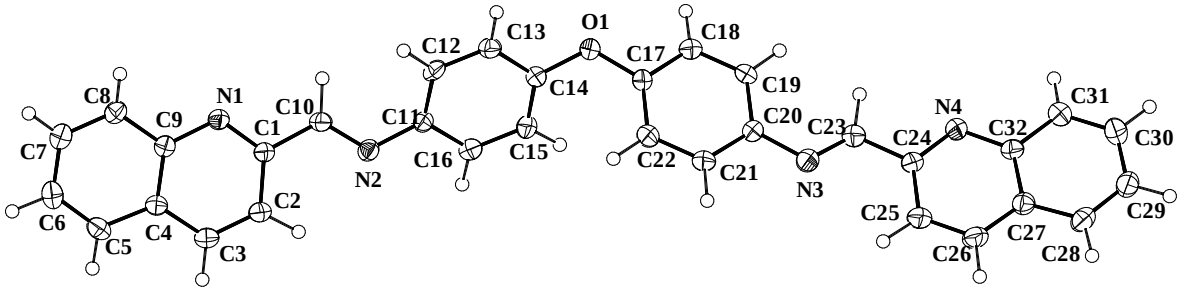

Figure 8. Molecular structure of **L7**.

As in **L5**, the solid-state structure for **L7** presents *pseudo*-C_2 symmetry with the twofold axis running through the central O atom. The ligand **L7** is more planar than **L5** and the conformation of the two halves of the molecules does not differ as much.

The moiety to the right in Figure 8 is the most planar with a dihedral angle of 9.73 (2) º between the quinoline and the benzene rings. The second half is almost twice as twisted with a dihedral angle of 17.85 (1) º. The pyridine-imine system is nearly planar in both halves with dihedral angles of 5.09 (2) and 6.51 (2) º between the quinoline rings from both moieties and the planes formed by atoms C2-C1-C10-N2 and atoms C25-C24-C23-N3 respectively.

The average C=N bond distance is 1.271 (3) Å, indicating typical double-bond character. Once again, bond-length alternation is observed in this π-system only broken by the central oxygen atom. In the crystal packing, Figure 8a, the quinoline N atoms are involved in weak intermolecular C-H…N interactions with symmetry related molecules. These values are reported in Table 2.

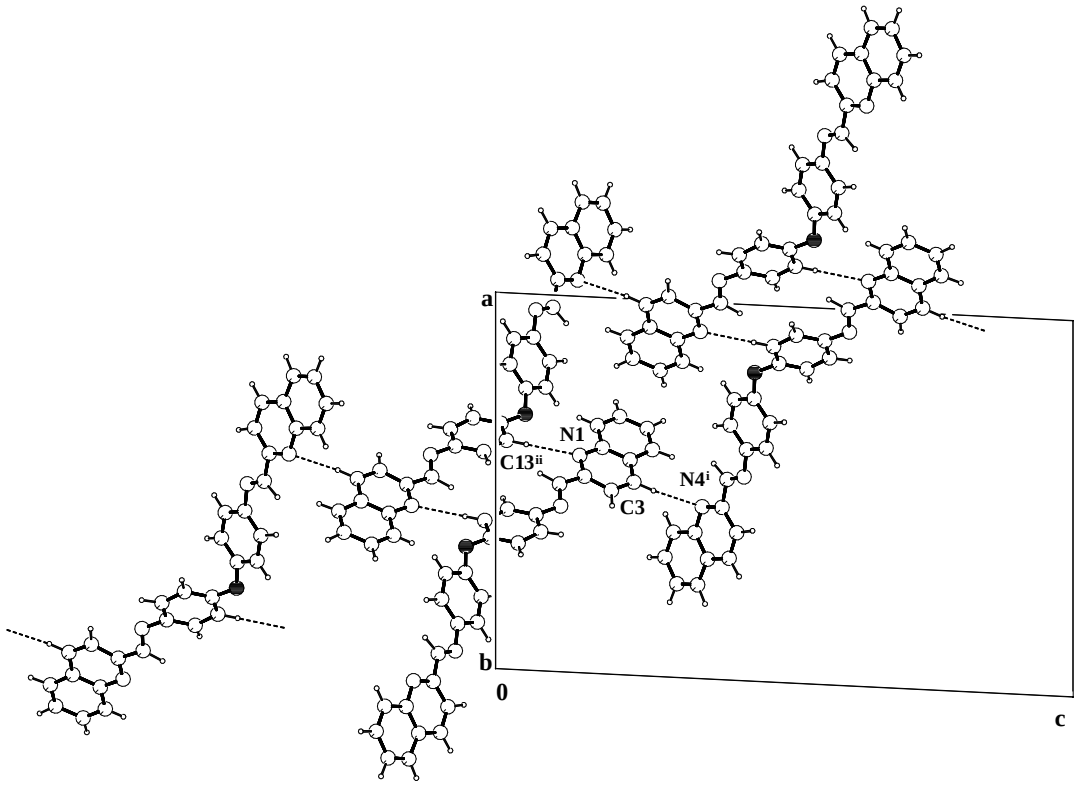

Figure 8a. Crystal packing of compound **L7** showing C-H…N interactions as dotted lines.

Table 2. Short non-bonded interactions (Å,º) for **L7**.

D-H...A	d(D-H)	d(H...A)	d(D...A)	<(DHA)
C3-H3...N4^{i}	1.01(2)	2.51(3)	3.435(4)	153(2)
C13-H13...N1^{ii}	0.98(2)	2.59(2)	3.568(3)	176(2)

Symmetry transformations used to generate equivalent atoms:

i = x+1/2,-y+3/2,z+1/2 ii = -x+1,-y,-z

The shortest interactions are found for C3…N4^{i} (3.435 (4) Å) and C13…N1^{ii} (3.568 (3) Å). In the crystal π-stacking is observed between the phenyl rings (C11-16 and C17-22) of symmetry-related molecules stacked up the b axis (symmetry operations x, y-1, z and x, y+1, z). A separation of *ca.* 3 Å was found which is much shorter than the similar distance found in the crystal for **L5**.

1.1.9. L8 *(N,N'-Bis(2-pyridylmethylene)-2,2'-(ethylenedioxy)bis(ethylamine))* (9)

This ligand was obtained by the condensation reaction between 2,2'-(ethylenedioxy)bis(ethylamine) and pyridine-2-carboxaldehyde in a 1:2 ratio with a quantitative yield as an orange oil.

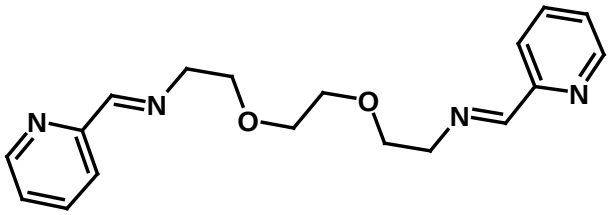

Scheme 5. Schematic diagram of **L8**.

The IR spectrum of **L8** presents some medium intensity peaks at 3054 and 3008 cm^{-1}, assigned to the arC-H stretching vibrations and a very strong peak at 2863 cm^{-1} that is associated to the O-CH_2 group stretching vibration. The intense imine-stretching band is found at 1651 cm^{-1} and the arC-arC and arC-arN stretching vibrations bands at 1588, 1568, 1469 and 1436 cm^{-1}. The strong asymmetric stretching vibration signals associated with the ether function appear at 1122 and 1048 cm^{-1}as a broad band. Bending C-H vibrations are found at 993 and 776 cm^{-1}.

The ^{1}H NMR, spectrum of the ligand **L8** displays five sets of resonances in the aromatic region. As the ligand is symmetric each set of resonances was assigned to a given pair of equivalent H's, one for the imine H's and four for the pyridine H's. Two supplementary signals were observed in the CH_2 region, in the form of a multiplet and a singlet, corresponding to the alkane chain protons. The UV-Vis spectrum (250-750 nm region) of **L8** in ethanol at a concentration 125 μM shows one clear band at 271 nm and another at *ca.* 250 nm corresponding to the pyridine $\pi \rightarrow \pi^*$ transition and to the absorption of the imine chromophore group.

1.1.10. L9 *(N,N'-Bis(2-pyridylmethylene)-1,4-diamino-diphenylamine)* (10)

Ligand **L9** (Scheme 6) was obtained by the condensation reaction between 4,4'-diaminodiphenylamine sulphate (previously deprotonated with KOH) and pyridine-2-carboxaldehyde in a 1:2 ratio with good yield.

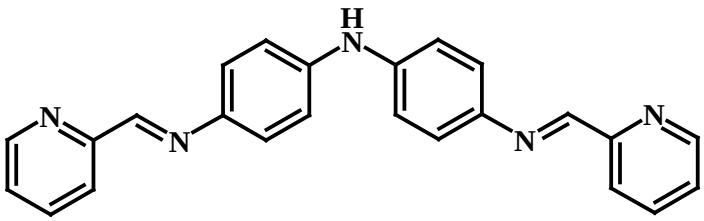

Scheme 6. Schematic diagram of **L9**

The IR spectrum of **L9** exhibits a medium intensity peak at 3242 cm^{-1} that corresponds to the NH group vibration and several weak peaks at 3168, 3073, 3051, 3028, 2987 and 2922 cm^{-1}, associated to the arC-H stretching vibrations. The imine-stretching band appears at 1621 cm^{-1} and the arC-arC and arC-arN stretching vibrations bands at 1593, 1572, 1520, 1499 and 1468 cm^{-1}. The very strong stretching band associated with the C-N vibration is found at 1325 cm^{-1}. Bending C-H vibrations appear at 998, 839 and 775 cm^{-1}.

The ^{1}H NMR spectrum exhibits eight sets of resonances. Seven of them belong to the aromatic region and have been independently assigned to each of the pyridine and benzene hydrogen atoms and one at 4.10 ppm was assigned to the NH group chemical shift. The UV-Vis spectrum (250-600 nm region) of **L9** in EtOH at a concentration 125 μM shows two clear bands at 270 and 420 nm corresponding to absorption of the imine chromophore and the biphenyl amino groups. It was impossible to obtain X-ray quality crystals for **L9**. A crystalline solid was obtained using different solvents for crystallization but, unfortunately, no single crystals suitable for X-ray analyses.

1.2. Spectroscopical and structural comparison between imino ligands

The ligands **L1**-**L9** belong to the same family of compounds and in Tables 3a and 3b some interesting structural X-ray and spectroscopic features, such as, ^{1}H NMR, IR and UV-Vis spectra, are compared. As the common unit in some of the ligands is the pyridylimine-chelating unit, the following parameters have been defined (Scheme 7).

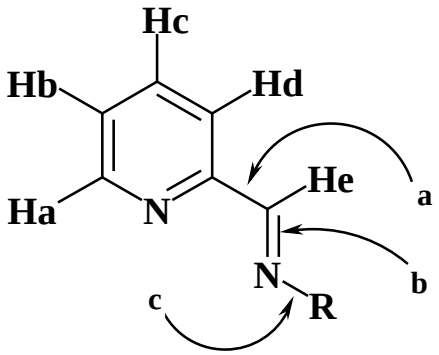

Scheme 7

Table 3a. For ^{1}H NMR comparison, the pyridine H atoms are labelled as Ha to Hd and the imine H atom as He. The stretching vibrations characteristic of the imine group in the IR is $\nu_{C=N}$. The absorption bands of the ligands in UV-Vis spectroscopy are noted with λ_{max}.

Table 3a. A comparison of ^{1}H NMR (ppm), IR (cm^{-1}) and UV-Vis (nm) for imine base ligands.

	Ha	**Hb**	**Hc**	**Hd**	**He**	**$\nu_{C=N}$**	**λ_{max}**
L1*	8.55	7.19	7.55	7.19	8.22	1642	275
L2*	8.64	7.31	7.74	8.06	8.48	1640	270
L3	8.74	7.55	7.98	8.19	8.67	1619	285, 360
L4	8.44	7.93	8.00	8.33	8.75	1622	280, 370
L5	8.70	7.54	8.00	8.24	8.66	1624	285, 340
L6*	6.69	6.21	7.04	-	8.33	1617	340
L7*	7.26	8.20	7.91_{qui}	7.80_{qui}	8.86	1622	-
L8	8.62	7.48	7.90	8.01	8.36	1651	271
L9	8.70	7.41	7.93	8.15	8.66	1621	270, 420

The ligands marked with * do not exactly match with the general scheme because they contain pyrrol (**L6**) or quinoline (**L7**) units instead of pyridine or they incorporate CH_2 groups between the pyridine and the imine group as in **L1** or between the imine group and the central phenyl ring as in **L2.** In **Table 3b** the bond distances for the imine group are labelled **a**, **b** and **c**. The symbol **#** means that the mean value has been taken for the non-centrosymmetric structures. Some ligands were either oils or it was not possible to obtain X-ray diffraction quality crystals. **ϕ** represents the torsion angle involving the atoms contained in bonds **a**, **b** and **c; φ** corresponds to the dihedral angle between the pyridine (or quinoline) and the phenyl central spacer rings. If the ligand is non-centrosymmetric two **φ** values are given for the two different moieties. A search in the CSD[9] for related compounds[10-13] has been carried out and the average values for parameters **a**, **b**, **c** and **ϕ** are given as standard values. The values obtained from the International Tables for Crystallography[24] are also presented.

Table 3b. A comparison of bond distances (Å) and angles (°) for imine base ligands.

	a	**b**	**c**	**ϕ**	**φ**
L1*	1.468(2)	1.255(2)	1.460(2)	179.6(1)	12.4
L2*	1.461(3)	1.262(3)	1.458(3)	177.5(2)	77.3
L3	1.471(2)	1.258(2)	1.420(2)	178.1(1)	11.1
L4	1.477(3)	1.272(3)	1.416(2)	178.2(2)	47.2
L5	1.473(2)#	1.263(2)#	1.417(2)#	175.5(1)#	10.77, 46.35
L7*	1.470(3)#	1.271(3)#	1.419(3)#	175.6(3)#	17.85, 9.73
Average	1.470(2)	1.263(2)	1.459(2), 1.418(2)	177.4(2)	-
Standard&	1.466, 1.476	1.260, 1.279	1.467, 1.431 1.465, 1.420	178.5	-

& Above, values obtained from the CCDC, Cambridge Crystallographic Data Centre, using the VISTA program and below, values from the International Tables for Crystallography.

It can be seen from Table 3b that in all seven structures, the **ϕ** torsion angle very close to 180°, the theoretical value for an *E* imine configuration [its average value of 177.4 ° is very similar to the standard value of 178.5 °]. It is interesting to point out that regardless of the structure of the ligand the imine C=N bond (**b**) exhibits a well-defined double bond character, which rules out its participation in the creation of a extended delocalised π system. The average C=N distance of 1.263 Å is very close to the standard values of 1.260 and 1.270 Å for a Schiff base system. The average values for the parameters (**a**) and (**c**) of 1.470 and 1.459 (L1 and L2) and 1.418 (rest of the ligands) Å, are also close to the standard values found for similar systems, 1.466 / 1.476 and 1.467 / 1.465 (L1 and L2) and 1.431/1.420 (rest of the ligands) Å, respectively. In the case of L1 and L2, (c) corresponds to a C_{aliph}-N_{im} bond distance whereas for the rest of the ligands it corresponds to a C_{ar}-N_{im} bond distance.

This situation might be expected for cases where electron delocalisation is more difficult to achieve, for example, when an oxygen atom links both aromatic moieties as in ligands **L5** and **L7**. However, the reasons for the non-"appartenance" of the imine group to a "supposedly" extended π system are not clear. Perhaps it could be due to the electronic repulsion of the pyridine, or quinoline, N atom lone pair electrons with the aromatic central rings that forces the molecule to avoid a perfectly planar conformation. In any case, the analysis of the bond distances and of the planarity of all of these systems, suggest that delocalisation is only achieved to a certain degree.

1.3. Other ligands

Two bis-tridentate ligands were also synthesized in the present work. They were obtained by a nucleophilic substitution reaction using, as electrophilic reactant in both cases, 2,3,5,6-tetrakis(bromomethyl)pyrazine.

1.3.1. tma (*2,3,5,6-Tetrakis(N-methylanilin-methyl)pyrazine)* (11)

This compound was obtained by the general reaction of substitution of the four bromine atoms of 2,3,5,6-tetrakis(bromomethyl)pyrazine (**TBr**) by nucleophilic attack from the nitrogen atom of N-methylaniline, as shown in Scheme 8.

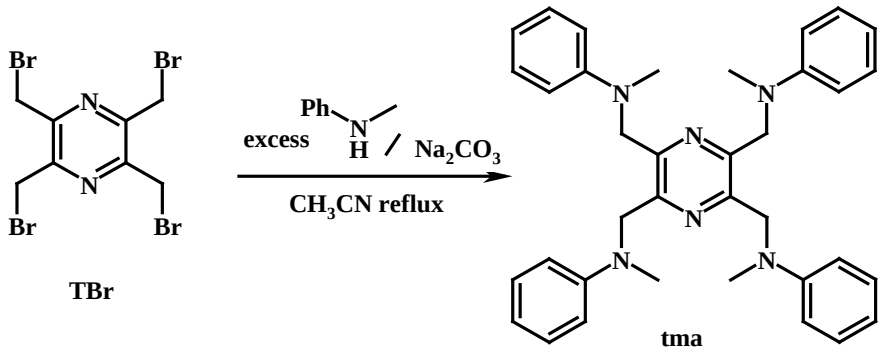

Scheme 8

Na_2CO_3 in large excess was used to deprotonate the amine. Other bases, such as NEt_3, were tried but the product formed was more difficult to purify. The reaction was followed by TLC using a mixture of hexane: ether (8:2) as eluent. After 30 minutes of reaction, the spot corresponding to **TBr** had already disappeared. After 2 hours, no change was observed and the reaction was stopped. The excess Na_2CO_3 and the NaBr formed were filtered off and the solvent evaporated. The ligand was purified by dissolving the excess amine in hexane

resulting in a medium yield. The use of a flash column (hexane:ether 8:2) is also possible but it did not improve the yield.

The IR spectrum of **tma** exhibits several weak signals in the region between 3037 and 2926 cm^{-1} corresponding to the Ph-H and Pz-H stretching vibrations. The arC-arC and arC-arN stretching vibrations are composed of two very strong peaks at 1601 and 1508 cm^{-1} and some of lower intensity at 1573, 1479, 1446 and 1430 cm^{-1}. A signal at 1117 cm^{-1} corresponds to the Pz-CH_2 bending vibrations. Other bending C-H vibrations appear at 745 and 689 cm^{-1}. The ^1H NMR spectrum exhibits four sets of resonances. Two of them belong to the phenyl H atoms, another one at 4.58 ppm was assigned to the CH_2 group and the last at 2.79 ppm corresponds to the CH_3 chemical shift.

X-ray quality crystals were obtained by slow evaporation of a $CDCl_3$ solution of **tma** in a NMR tube. The crystal structure is illustrated in Figure 9.

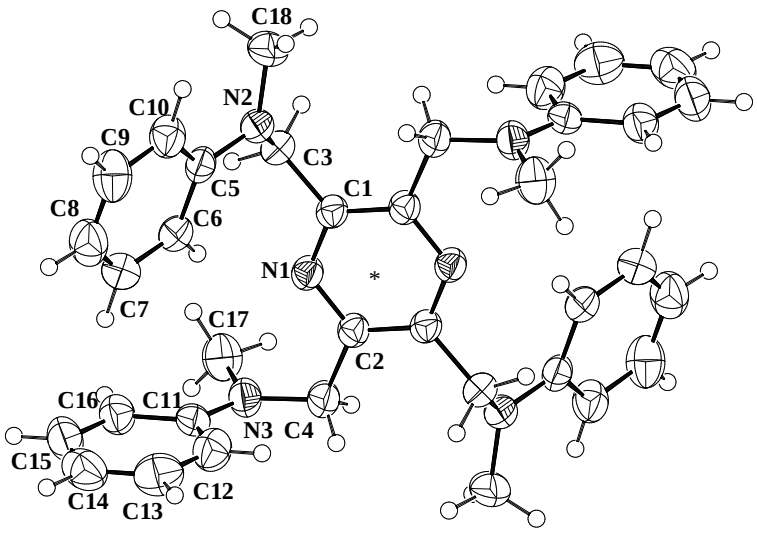

The molecule is centrosymmetric. The N amino atoms do not lie in the pyrazine mean plane and due to the symmetry of the molecule two adjacent substituents are located above this plane while the other two on the other side of the pyrazine are directed below.

Figure 9. Molecular structure of **tma**.

The dihedral angles between the phenyl rings C5-10 and C11-16 is 78.3 (1) º, close to perpendicular to each other. The dihedral angles between these two rings and the pyrazine mean plane are 63.6 (1) º and 86.8 (1) º, respectively.

All geometrical parameters (Table 4) are in reasonable agreement with expected values. The average C-N bond distance of 1.435 Å is close to the standard value[24] of 1.426 for a C-N distance corresponding to a nitrogen located in a pyramidal environment [although the C11-N3 bond distance of 1.382 Å is closer to the value given for a nitrogen atom in a planar environment]. Both N2 and N3 possess a rather planar geometry as it can be deduced from the values of the angles C-N-C (Table 4) that are very close to 120 º, value for a perfect planar geometry. By adding the three angles around the N and calculating the difference from 360 °, it is possible to observe that N2 (6.39 °) is more pyramidal than N3 (1.34 °).

Table 4. Selected geometric parameters [Å, º] for **tma.**

C1-N1	1.340(2)	C2-N1	1.336(2)
C1-C2^{i}	1.394(3)	C2-C4	1.524(3)
C1-C3	1.514(3)	C11-N3	1.382(3)
C3-N2	1.458(3)	C4-N3	1.443(3)
C5-N2	1.396(3)	C17-N3	1.446(3)
C18-N2	1.455(3)	N3-C4-C2	114.94(18)
N1-C1-C2^{i}	120.76(17)	N3-C11-C12	122.8(2)
N1-C1-C3	115.82(17)	N2-C3-C1	114.75(17)
N1-C2-C1^{i}	120.79(17)	N2-C5-C6	121.97(19)
N1-C2-C4	117.02(17)	C1^{i}-C2-C4	122.19(17)
C5-N2-C3	118.66(17)	C4-N3-C11	121.93(19)
C5-N2-C18	117.55(18)	C4-N3-C17	116.7(2)
C3-N2-C18	117.4(2)	C17-N3-C11	120.13(19)
C1-N1-C2-C4	-179.95(19)	C1-C3-N2-C5	83.9(2)
C2-N1-C1-C3	178.70(17)	C2-C4-N3-C17	-81.1(3)
C1-C3-N2-C18	-125.0(2)	C2-C4-N3-C11	86.3(3)

Symmetry transformation used to generate equivalent atoms: i -x+1,-y+1,-z+2

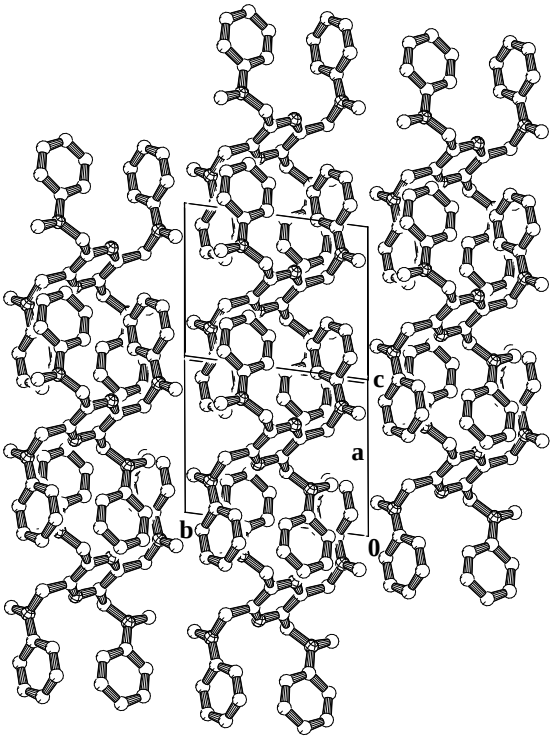

Figure 9a. Crystal packing of **tma**.

In the crystal, the molecules of **tma** stack in columns as showed in Figure 9a. No π-π interactions between the aromatic rings are observed being the shortest distance between parallel phenyl rings of symmetry related molecules about 5 Å.

A search in the CSD[9] for ligands similar to **tma** was carried out. The compound 2,3,5,6-tetra-(2-pyridyl)pyrazine (**tppz**) is a bis-tridentate N_3N_3 ligand and its coordination chemistry has been largely studied[14-15]. Its crystal structure differs considerably from that of **tma** due to the reduced flexibility of **tppz** in comparison to **tma**. In **tppz**, the pyridine rings are inclined towards the pyrazine ring by 48.9(1) and 51.7(1) ° and to one another by 62.4(1) °. The two crystallized forms (monoclinic and tetragonal) [16] are very similar.

1.3.2. tda (*2,3,5,6-Tetrakis(dimethylaminomethyl)pyrazine)* (12)

The same type of reaction as for **tma** using dimethyl-amine instead of N-methylaniline as nucleophilic reactant was used to synthesize **tda**:

$$\mathbf{(CH_3)_2NH.HCl}\ \text{in}\ \mathbf{H_2O} \xrightarrow[\mathbf{0\ ^oC}]{\mathbf{NaOH}} \mathbf{(CH_3)_2NH}_{\text{condensed}}^{\text{gas}} \quad \mathbf{-60\ ^oC}$$

In a first step, the amine, $(CH_3)_2NH{\cdot}HCl$, was deprotonated with NaOH in an ice bath. In this manner, dimethyl amine was formed and as it is a gas, it was condensed at a temperature maintained between –60 º C and –40 º C.

The second step of the reaction was the very slow addition of **TBr** in CH_2Cl_2 to the amine at low temperature. At this point, it is important to note that **TBr** should be added as slowly as

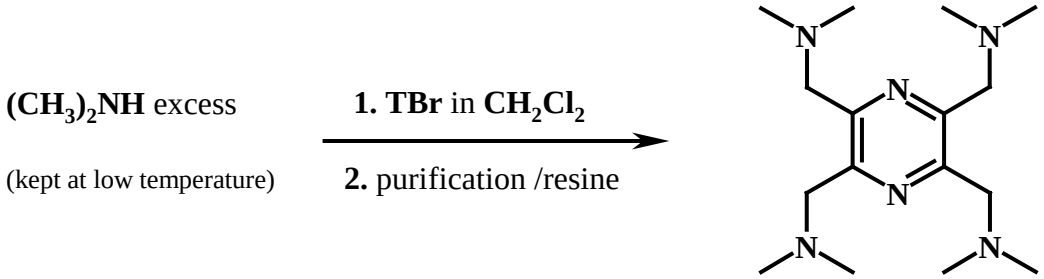

tda

possible and that the order of addition plays a central role in order to avoid the intramolecular reaction that could take place (product II).

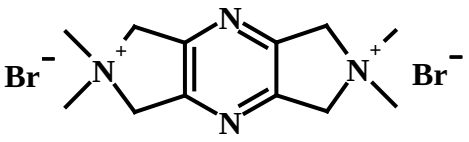

(II)

Finally, the last step is to purify the ligand. The $(CH_3)_2NH{\cdot}HBr$ formed during the reaction as well as the HBr molecules attached to a percentage of the **tda** molecules were eliminated using a resin column charged with OH^- ions. In this manner, the Br^- ions could be exchanged by OH^- ions to form water molecules. The $(CH_3)_2NH$ formed, gases out from the solution and the rest is easily evaporated to yield **tda** as a light yellow solid.

The IR spectrum of **tda** exhibits several sharp and intense signals at 3573, 3427, 2974, 2942, 2854 and 2820 cm^{-1} corresponding to the Pz-CH_2 and CH_3-H stretching vibrations. The arC-arC and arC-arN stretching vibrations bands consist of strong peaks at 1464, 1456 and 1414 cm^{-1}. The signal at 1259 cm^{-1} corresponds to the Pz-CH_2 bending vibrations. Other bending C-H vibrations appear at 1027, 987, 841 and 779 cm^{-1}. The ^1H NMR spectrum exhibits two

sets of resonances; a singlet at 3.65 ppm corresponding to the CH_2 group and a singlet at 2.15 ppm assigned to the CH_3 group.

X-ray quality crystals were obtained by slow diffusion of hexane into a solution of the ligand in dichloromethane. The molecular structure is given in Figure 10.

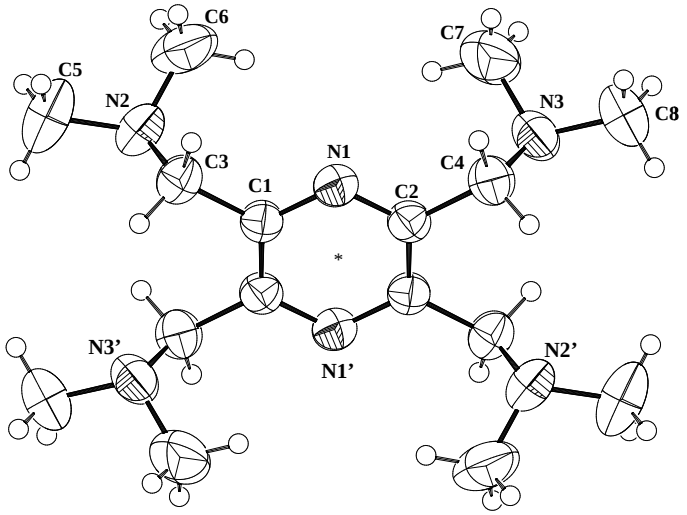

The molecule is centrosymmetric. The N amino atoms do not lie in the pyrazine mean plane and due to the symmetry of the molecule adjacent groups are placed above and below the plane of the pyrazine ring.

Figure 10. Molecular structure of **tda**.

The methyl groups thermal parameters are within the normal values for groups presenting some freedom of movement and have been refined in only one position. All geometrical parameters (Table 5) agree with standard bond distances and angles values.

The compound 2,3,5,6-tetra-(aminoethyl)-pyrazine (**tamp**) is also a bis-tridentate N_3N_3 ligand and its coordination chemistry has been largely studied in our group[13-14]. The pyridine analogue (**bamp**) is also comparable with **tda** [although only the crystal structures of their hydrochloride form are known].

Table 5. Selected geometric parameters [Å, º] for **tda**.

C1-N1	1.343(3)	C3-N2	1.458(3)
C1-C2^{i}	1.393(3)	C4-N3	1.454(3)
C1-C3	1.506(3)	C2-C4	1.507(3)
C2-N1	1.340(3)	C4-N3-C8	110.8(2)
N1-C1-C2^{i}	121.0(2)	C6-N2-C3	111.0(2)
N1-C1-C3	117.3(2)	C3-N2-C5	111.2(2)
C2^{i}-C1-C3	121.7(2)	N1-C2-C1^{i}	121.6(2)
N1-C1-C3-N2	103.3(3)	C1-C3-N2-C5	159.1(3)
N1-C2-C4-N3	-108.8(2)	C2-C4-N3-C8	-165.7(2)
C1-C3-N2-C6	-77.0(3)	C2-C4-N3-C7	71.6(3)

Symmetry operation: i -x,-y,-z+1

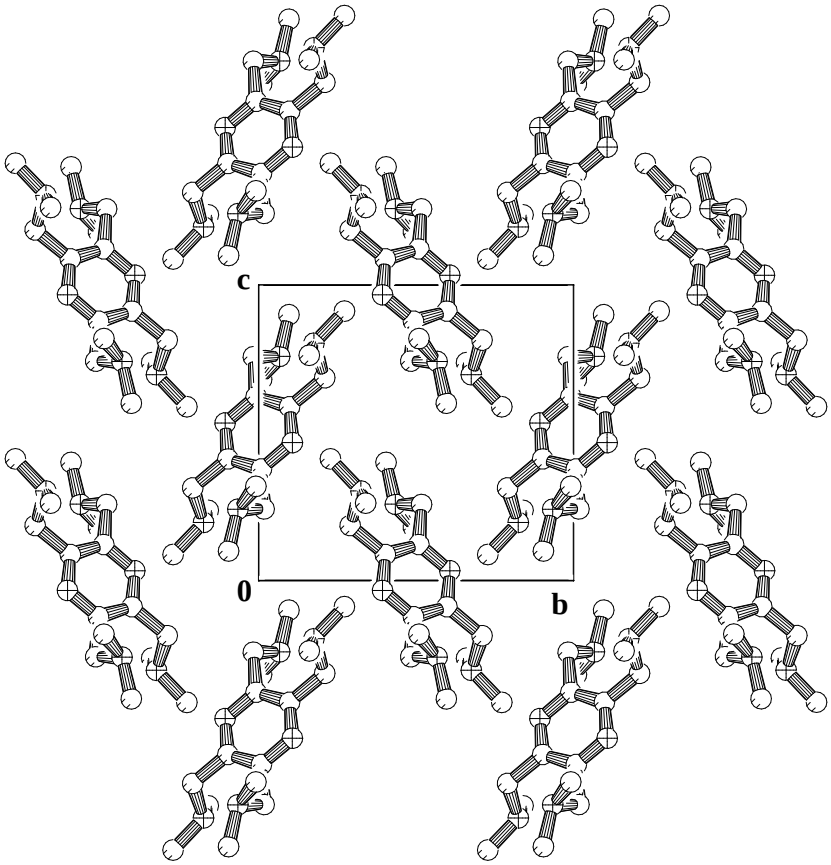

In the crystal, the molecules of **tda** are disposed as showed in Figure 10a. No π-π interactions are observed between pyrazine rings of symmetry related molecules.

Figure 10a. Crystal packing of **tda** down the *a* axis.

1.3.3. bptz *(3,6-Bis(2-pyridil)-1,2,4,5-tetrazine)* (13)

Finally, **bptz**, a commercial product, was briefly studied. The compound was used as supplied and hence no analyses were carried out. The IR spectrum was recorded in order to compare how the bands were displaced during the synthesis of metal complexes containing this ligand. This spectrum displays a series of sharp peaks. At 3096 and 3060 cm^{-1} two weak signals, assigned to arC-H stretching vibrations are observed. Several peaks corresponding to the arC-arC and arC-arN stretching bands appear at 1640, 1582, 1479, 1444 and 1427. A very strong signal is observed at 1391 $cm^{-1}$and it was assigned to the N-N stretching vibration. Bending C-H vibrations appear at 799, 745, 733 and 597 cm^{-1}.

X-ray quality crystals were obtained by slow diffusion of hexane into a solution of **bptz** in dichloromethane. The crystal structure is depicted in Figure 11.

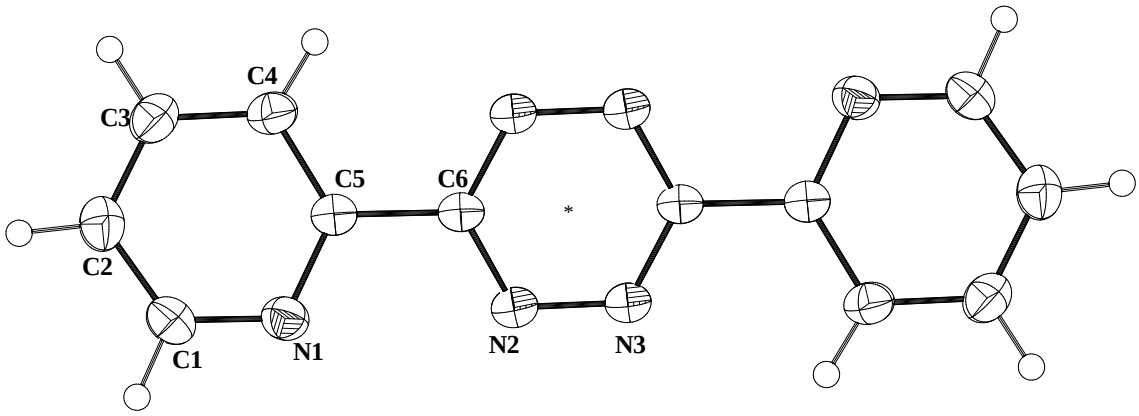

Figure 11. Molecular structure of **bptz**.

The molecule presents C_i symmetry and it is moderately planar with a dihedral angle of 19.5 (1) ° between the pyridine and the tetrazine rings. The bond-distances (Table 6) are consistent with an extended π-system, including the tetrazine ring (the distance N2-N3 is 1.327 (2) Å, characteristic of a delocalised bond distance).

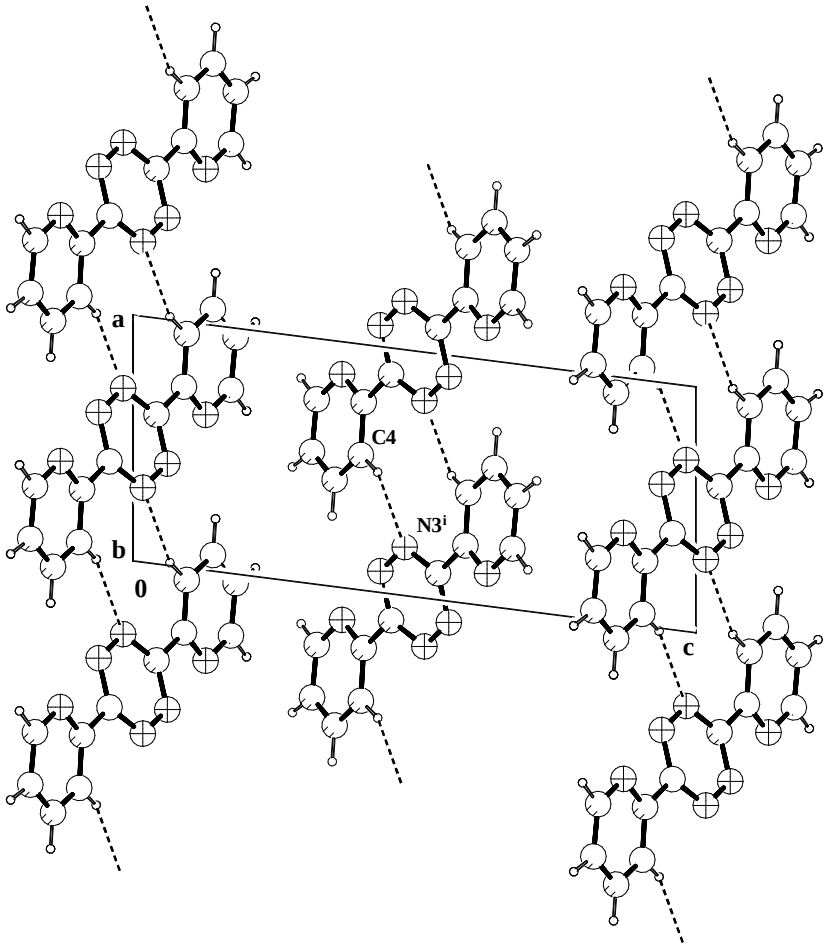

Figure 11a. Crystal packing of compound **bptz** showing C-H…N interactions as dotted lines.

In the crystal packing, Figure 11a, it can be seen that the tetrazine atom N3 is involved in intermolecular C-H…N interactions with symmetry-related molecules (C4…$N3^{i}$ = 2.82 (1) Å, with i = -x, -y, -z+1).

Table 6. Selected geometric parameters [Å, º] for **bptz**.

C1-N1	1.333(3)	C5-N1	1.344(2)
C5-C6	1.485(3)	N3-$C6^{i}$	1.337(2)
C6-N2	1.338(2)	N2-N3	1.327(2)
N1-C5-C4	123.5(2)	N2-C6-C5	118.0(2)
N1-C1-C2	124.3(2)	N3-N2-C6	117.1(2)
N1-C5-C6	116.6(2)	$N3^{i}$-C6-N2	124.9(2)
N2-N3-$C6^{i}$	118.1(2)		

Symmetry transformation used to generate equivalent atoms: i -x,-y,-z+1

A separation of *ca.* 3.60 Å was found between the best planes through the pyridine rings of symmetry related molecules (symmetry operation: 1-x, 1-y, 1-z), indicating weak π-stacking in the crystal down the a direction (Figure 11b).

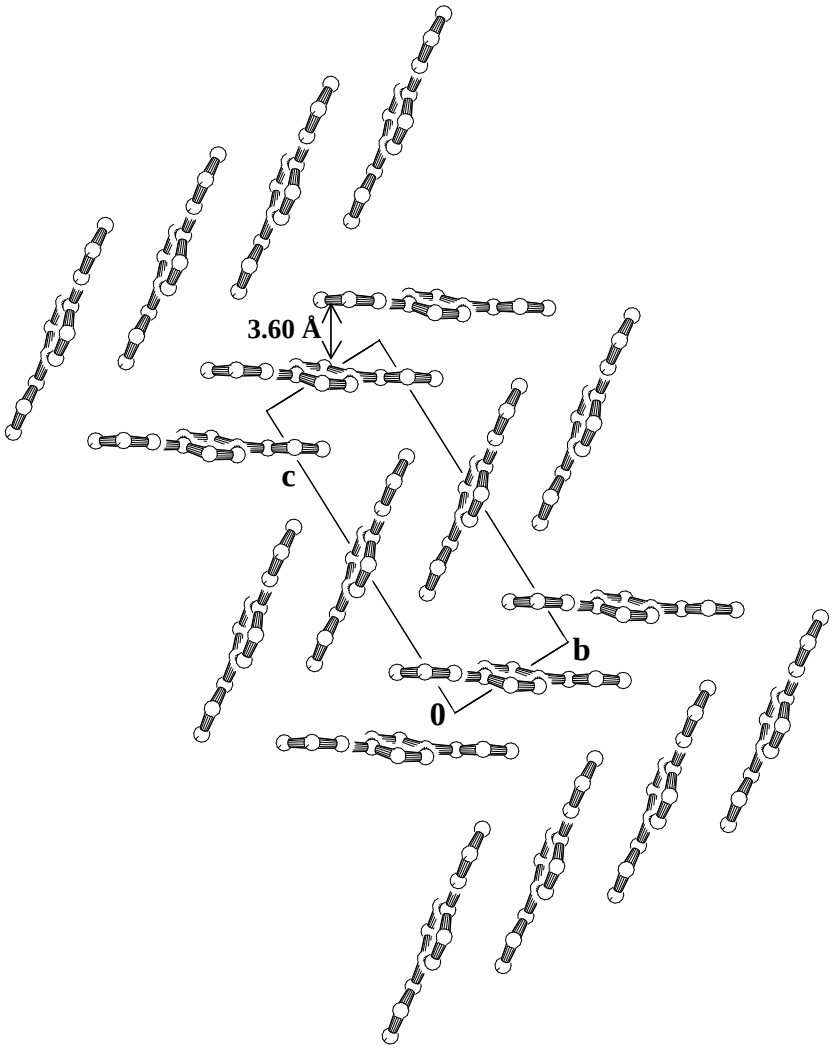

Figure 11b. Crystal packing of compound **bptz** down the *a* axis showing the stacking of the molecules. H atoms have been omitted for clarity.

2. THE COMPLEXES

The second part of this work concerns the study of the reactivity of the ligands (presented in the first part) towards the metal atoms. The reactions with a large number of different metal salts (transition metal and d^{10} metal salts) have been carried out in different reaction conditions (varying solvent, temperature and reaction time; using diffusion techniques or by mixing the reactants, etc…). The structure of the different complexes obtained has been mainly determined by X-ray crystallography. Although a number of compounds yielded good quality single crystals, in many other cases, X-ray diffraction could not be employed due to the poor quality or to the absence of crystals. However, UV-Vis titration experiments have been carried out in order to compare the reactivity of the ligands with a series of metal salts and to obtain some information about the behaviour of these complexes in solution. These experiments have provided a great deal of useful information. In this context, before starting any measurement, two different approaches have to be considered.

Although the best would be to study *a large* number of cases in *an intense* manner, this process is very time consuming. To resolve this problem, two possibilities are available:

1. To study a small number of cases in depth: a large number of measurements need to be done, for example, to study the reaction between one ligand and all the possible salts of one particular metal atom, or
2. To study a large number of cases in less detail and perform a general screening.

Here, we have chosen the second approach with the aim of getting a general impression of the coordination chemistry of the synthesised ligands, for instance, to see whether they react with a large number of metals or to have an idea about the complexity of the reactions: is only one or several new species formed?

2.1. Coordination behaviour of ligands L1 and L2

Unfortunately, it was impossible to obtain crystals of metal complexes containing these two ligands. Only several compounds resulting from the metal-catalysed hydrolysis of the **L1** imine groups were isolated as single crystals. These are the complexes: $[Cu(L1')_2](ClO_4)_2$[17], $[Cu(L1')Cl_2]$[18] and $[Ni(L1')Cl(H_2O)_3]Cl$ where L1' is 2-(2-aminoethyl)pyridine resulting from the hydrolysis of **L1**. For **L2**, crystals of α,α'-diamino-p-xylene were found after reaction with several metal salts, proving the hydrolysis of this ligand.

Despite this, UV-Vis titration experiments of the ligands **L1** and **L2** (125 μM in EtOH) with addition of increasing quantities of different metal salt solutions ([M] = 0, 4.7, 9.4, 18.7, 37.5, 75, 150 and 300 μM, in EtOH) have been carried out. For **L1**, when $HgCl_2$, $Cd(NO_3)_2 \cdot 4H_2O$, CuAcO and $Mn(ClO_4)_2.6H_2O$ were added to the ligand solution no reaction was observed under the conditions of the experiment (no changes in the UV-Vis spectrum of the ligand).

The case of the titration of **L1** with $AgNO_3$ is more interesting. The next figure shows the change in the UV-Vis spectrum (only the significant region from 250 to 350 nm is presented) that occurs when **L1** coordinates to Ag^+ ion in EtOH. Upon addition of Ag^+ ion to the ligand solution, the intensity of the ligand band at 275 nm progressively decreases and the absorbance increases at the region of about 305 nm. The presence of a very clear isosbestic point at 290 nm is the confirmation of a clean reaction (only one product is formed). The mole ratio plot made using the change in absorbance at 275 and 305 nm suggests that the stability constant of this new species might be rather small. Although is not clear, the formation of a Ag^+:L1 1:1 complex could be proposed. This formulation could be consistent with a polymeric structure as proposed in Scheme 9.

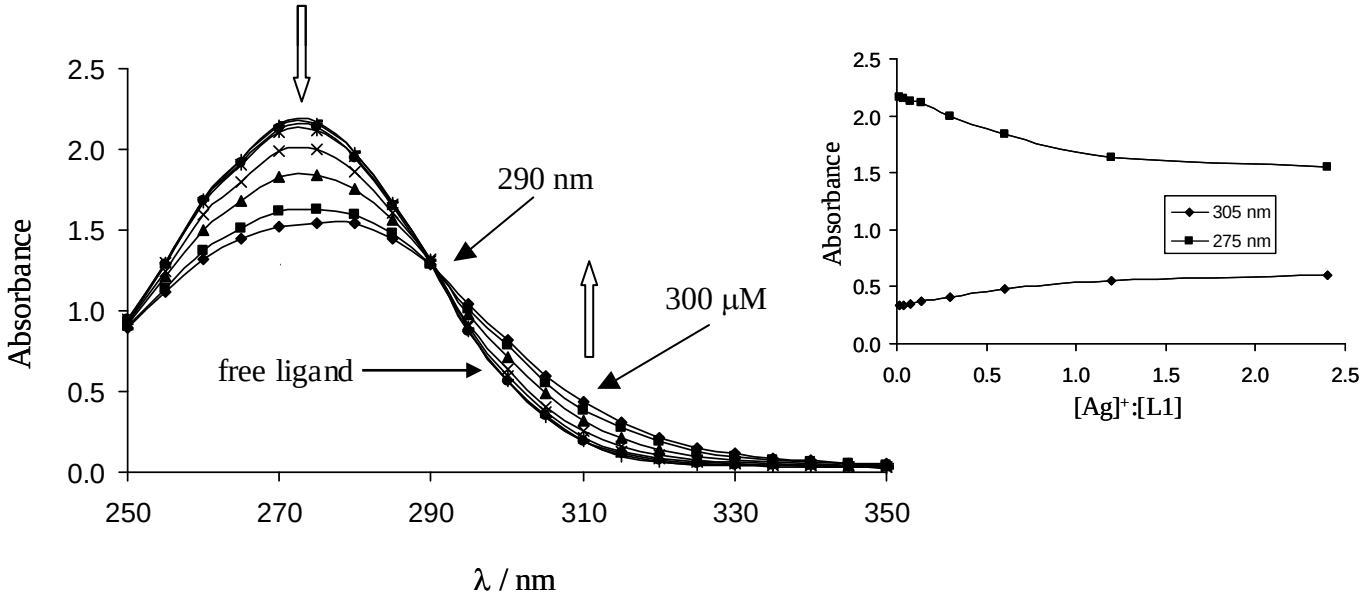

Figure 12. UV spectra of **L1** upon incremental addition of Ag^{+} in EtOH and ratio plot of the absorption at 275 and 305 nm.

Scheme 9. Proposed structure for the reaction of **L1** with $AgNO_3$.

Titration of **L1** with Ni^{2+}, Co^{2+} or Zn^{2+}ions gave very similar results. Very slight changes in the **L1** UV-Vis spectrum were detected apart from the decrease in intensity of the ligand band at 275 nm. In any case, the coordination must be very weak. The case of Cu^{2+} is slightly different. Isosbestic points at 265 and 310 nm are observed until a metal concentration of 75 μM (although the changes in absorbance are very small) and then, when higher metal concentrations are used these points disappear. The colour of the solution was green but as the

spectra were recorded only to 600 nm, the corresponding band was not measured. Titration with Fe^{2+} gave a very light purple solution and the same remarks as for the case of Cu^{2+} can be made. In conclusion, it is possible that **L1** coordinates weakly to a series of different metal atoms; its donating strength is quite poor. The presence of a six membered chelate ring instead of a five membered one could explain this behaviour. Imines are quite stable when there is an aryl group directly attached to the nitrogen atom. In our case, the absence of a fully delocalised aromatic system in **L1** could explain the metal catalysed hydrolysis. Similar UV-Vis titration experiments have been performed for **L2** with rather different results. As for **L1**, the addition of a Hg^{2+} salt to a ethanolic solution of **L2** did not result on any apparent reaction. Only very small changes in absorbance were observed when the metal was added in excess. The case of Mn^{2+} is comparable to Hg^{2+} although small changes in absorbance already appeared at a metal concentration of 75 μM. The ligand band at 270 nm was then progressively displaced to 285 nm. Ni^{2+}, Co^{2+}, Zn^{2+}, Cd^{2+} and Ag^{+} all present a similar behaviour. The maximum of the ligand band is displaced to 285 nm. The intensity increases at least until the metal concentrations are 75/150 μM and for the most concentrated solution it decreases slightly (Figure 13).

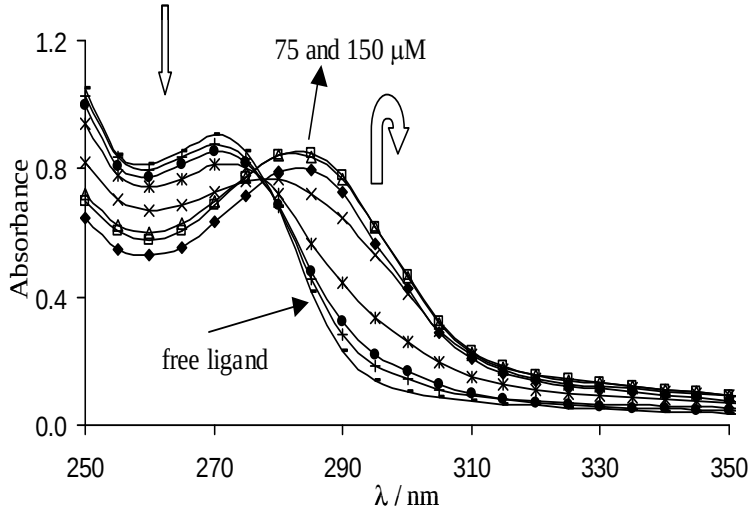

Figure 13. UV spectra of **L2** upon incremental addition of Co(II) in EtOH. Ni(II), Zn(II) and Cd(II) behave in the same manner.

The isosbestic point at 275-80 nm is only poorly defined. The UV-Vis titration experiment of **L2** with Fe^{2+} shows some interesting features (Figure 14).

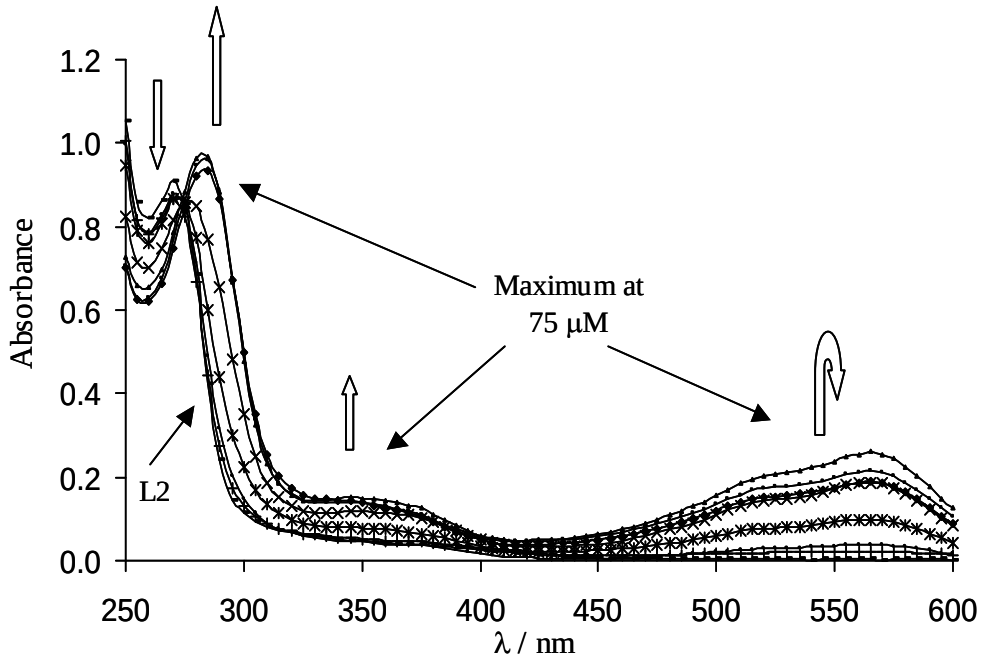

Figure 14. UV spectra of **L2** upon incremental addition of Fe^{2+} in EtOH.

Upon addition of Fe^{2+} the ligand band at 270 nm is gradually displaced to 285 nm with the appearance of an isosbestic at about 275 nm. The intensity of this new band grows until a concentration of 75 μM and then stays almost constant. A second small band appears at about 350 nm following the same behaviour as for the one at 285 nm. Finally, a band appears at 560 nm (the colour of the solution was purple). Its absorption increases until a metal concentration equal to 75 μM and then, the addition of more Fe^{2+} salt leads to a decrease in absorption (that is observed during the measurements by a decrease of the purple colour intensity). Once the concentration of the metal exceeded the concentration of the ligand, one can suggest that a new species is formed. The maximum value of absorbance observed at a metal concentration 75 μM could correspond to a M:L2 ratio of approximately 0.66.

2.2. Coordination behaviour of ligand L3

This ligand was designed with two aims in mind: 1) reducing the flexibility of the central spacer unit and 2) obtaining a fully delocalised aromatic system. In principle, these two parameters should favour the formation of polymers and inhibit the formation of monomers or helical arrangements. Some studies of this ligand have been reported recently. Moriuchi *et al*.[19] have described a palladium binuclear complex and Chakraborty *et al*.[20] have studied the electrochemical properties of a ruthenium complex of **L3**. Several molybdenum complexes have also been reported[21] as well as the use of **L3** ruthenium complexes in catalysis (epoxidation of alkenes)[22-23]. Yoshida *et al*.[7a] have reported a zinc complex, the only one, so far, characterized by X-ray crystallography. In this 1D-polymeric structure, the zinc atoms are coordinated to four N atoms from two ligand molecules and to two DMF molecules.

The ligand **L3** reacts with a large number of metal ions and we have been able to isolate two complexes in a crystalline form: $[Zn_2(L3)I_4]$ (**14**) and $\{[Cd_2(L3)(NO_3)_3(H_2O)_4](NO_3)2H_2O\}_n$ (**15**). UV-Vis titrations have been carried on with different metal ions and the results obtained are described.

2.2.1. Complex $[Zn_2(L3)I_4]$ (14)

The reaction of **L3** with ZnI_2, using diffusion techniques and in dilute conditions, afforded in about a week, very intense red-orange crystals of a centrosymmetric binuclear complex,

$$\textbf{L3}/CH_2Cl_2 \quad + \quad ZnI_2/MeOH \quad \xrightarrow{\text{diffusion}} \quad [Zn_2(L3)I_4]\ \textbf{(14)}$$

$[Zn_2(L3)I_4]$ (**14**).

The IR spectrum of this compound (Table 7) exhibits the characteristic imine, C_{ar}-N and C_{ar}-C_{ar} vibrations slightly shifted to higher frequencies with respect to the IR spectrum of **L3**.

Table 7. IR Data for the ligand **L3** and the complex **14**.

Compound	IR, ν [cm^{-1}]
L3	1619 (s, imine), 1584 (vs), 1563 (s), 1494 (vs), 1462 (vs), 1434 (s), 1353 (m), 1229 (w), 1196 (m), 844 (vs), 773 (s)
$[Zn_2(L3)I_4]$ (**14**)	1624 (w, imine), 1588 (vs), 1563 (m), 1507 (m), 1475 (m), 1442 (w), 1368 (m), 1236 **(**m), 1208 (m), 833 (vs), 777 (s)

The crystal structure consists of discrete binuclear $[Zn_2(L3)I_4]$ molecules, in which each zinc atom achieves a tetrahedral coordination by means of the two nitrogen atoms (one from the pyridine and one from the imine) of each chelating moiety and two terminal iodine atoms.

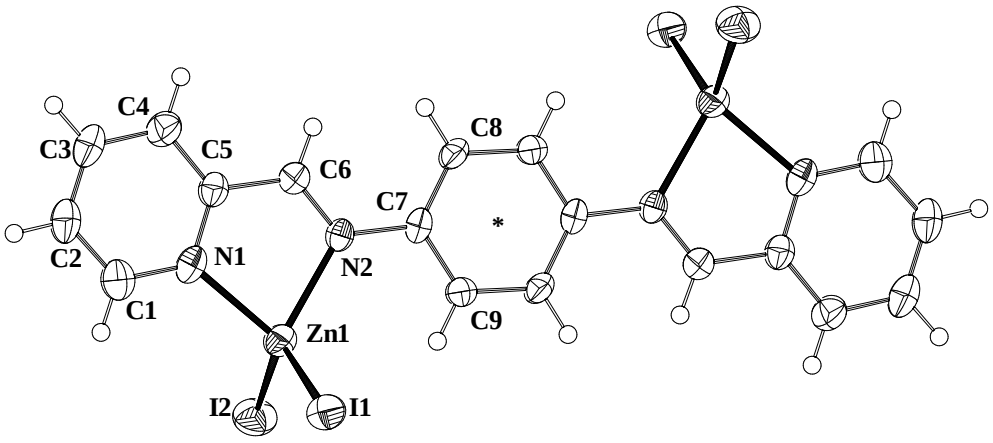

Figure 15. Molecular structure of $[Zn_2(L3)I_4]$ (**14**) showing the crystallographic numbering scheme and thermal ellipsoids at 50% probability level.

The deviation from the ideal geometry is not very important, being mainly reflected in the N1-Zn1-N2 bite angle of 80.9 °, which differs significantly from the theoretic tetrahedral angle of 109 °. In compound **14**, the ligand molecule is almost planar with a dihedral angle between the pyridine and phenyl rings of only 1.8 (5) °.

Table 8. Selected geometric parameters (Å,°) for $[Zn_2(L3)I_4]$ (**14**).

Zn1-Zn1^{i}	8.777(1)	N1-Zn1-N2	80.9(2)
Zn1-N1	2.056(6)	N1-Zn1-I2	112.11(18)
Zn1-N2	2.109(6)	N2-Zn1-I2	114.86(15)
Zn1-I1	2.548(1)	N1-Zn1-I1	111.91(17)
Zn1-I2	2.521(1)	N2-Zn1-I1	112.28(16)
C5-C6	1.470(10)	I2-Zn1-I1	118.78(4)
C6-N2	1.267(9)	C7-N2	1.423(8)

The Zn-N_{im}, Zn-N_{py} and Zn-I bond distances are in good agreement with the standard values[24] of 2.122, 2.116 and 2.574 Å, respectively. In the crystal, symmetry related molecules of **14** are disposed in two intercalated almost perpendicular[#] networks (Figure 16a). A separation of *ca.* 3.7 Å is found between the benzene and pyridine rings indicating weak π-π stacking. As can be seen in Figure 16b, the molecules of **14** are disposed down the c axis in a head to tail manner conferring a *zigzag* shape to the packing.

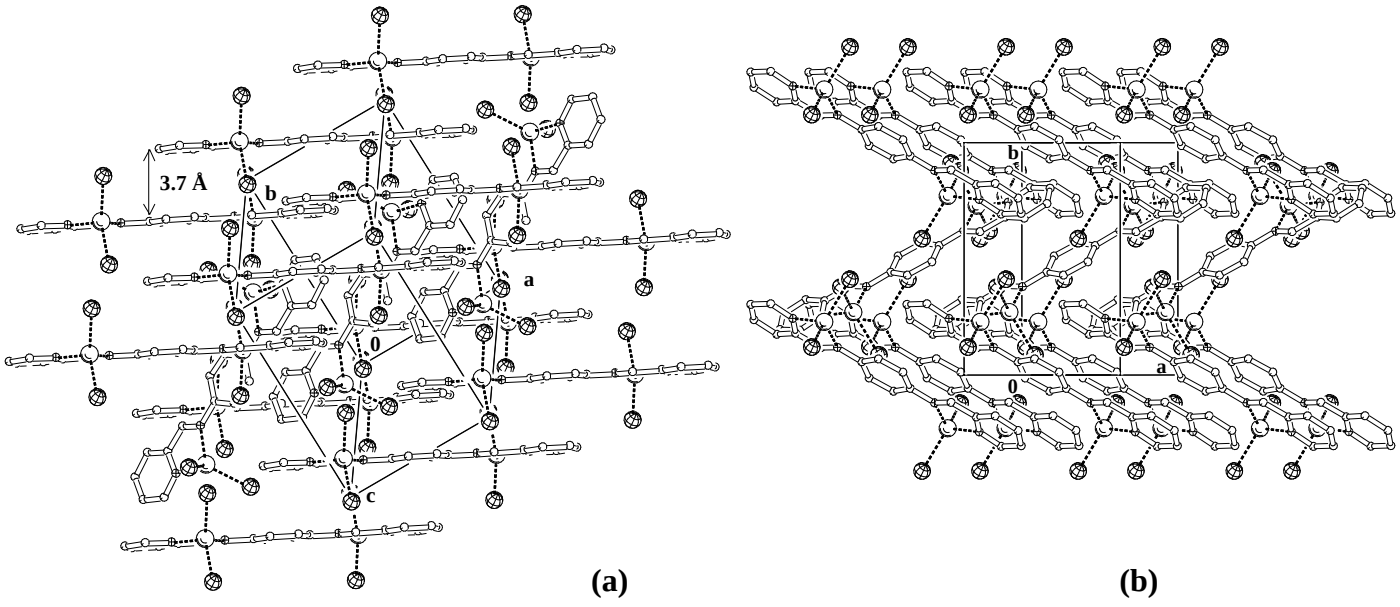

Figure 16. Two views of the crystal packing of $[Zn_2(L3)I_4]$ (**14**). (a) View of the C face direction emphasizing the π-π stacking and (b) *Zigzag* view down the c axis.

[#] The dihedral angle between two molecules belonging each one to one of the networks is 79.6(2) ° (symmetry operation x, -y+3/2, z+1/2)

No disorder was observed in **14** and an empirical absorption correction using DIFABS in PLATON[25] was applied. This compound was insoluble in most common solvents.

2.2.2. Complex {[Cd_2(L3)$(NO_3)_3(H_2O)_4$]·(NO_3)·$2H_2O$}$_n$ (15)

The reaction of **L3** with $Cd(NO_3)_2 \cdot 4H_2O$ using diffusion techniques and in dilute conditions afforded after about one week orange-brown crystals, at the interface between the two solutions, of the polymeric complex, {[Cd_2(L3)$(NO_3)_3(H_2O)_4$]·(NO_3)·$2H_2O$}$_n$ **(15)**.

$$\textbf{L3}/CH_2Cl_2 \; + \; Cd(NO_3)_2 \cdot 4H_2O \,/MeCN \xrightarrow{\text{diffusion}} \{[Cd_2(L3)(NO_3)_3(H_2O)_4]\cdot(NO_3)\cdot 2H_2O\}n \; \textbf{(15)}$$

The IR spectrum of this compound (Table 9) exhibits the characteristic imine, C_{ar}-N and C_{ar}-C_{ar} vibrations slightly shifted to higher or lower frequencies with respect to the IR spectrum of **L3** indicating the coordination of the metal to the ligand. The nitrate vibrations appear as a broad band at 1384-1325 cm^{-1} overlapping with some **L3** bands.

Table 9. IR Data for the ligand **L3** and the complex **15**.

Compound	IR, ν [cm^{-1}]
L3	1619 (s, imine), 1584 (vs), 1563 (s), 1494 (vs), 1462 (vs), 1434 (s), 1353 (m), 1229 (w), 1196 (m), 844 (vs), 773 (s)
15	1633 (m, imine), 1594 (s), 1571 (w), 1493 (m), 1384 (vs), 1325 **(**s), 1197 (m), 1043 (m), 825 (s), 782 (m)

In compound **15** the metal to ligand ratio is 2:1 and the asymmetric unit (Figure 17) consists of one entire repeating unit [Cd_2(L3)$(NO_3)_3(H_2O)_4$]·(NO_3)·$2H_2O$.

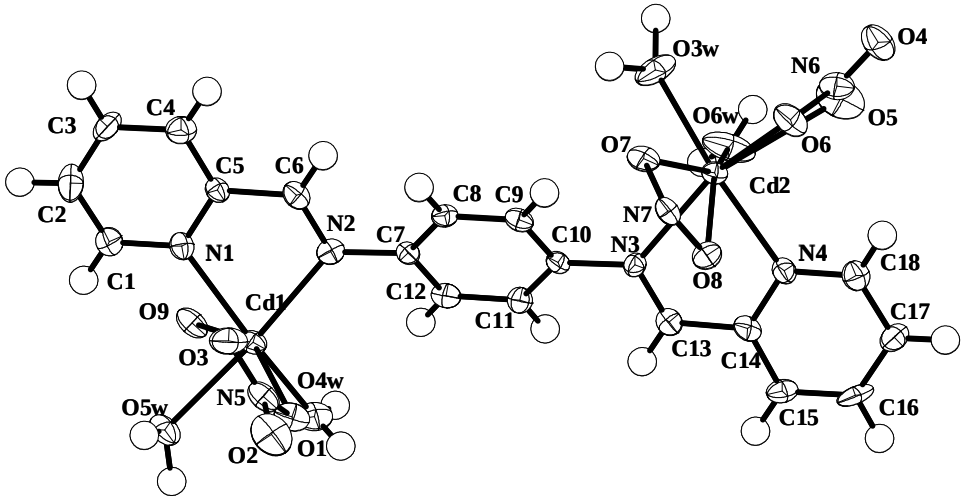

Figure 17. View of the asymmetric unit of the polymer **15** showing the crystallographic numbering scheme and thermal ellipsoids at 50% probability level. The non-coordinated water molecules and nitrate ion have been omitted for clarity.

The crystal structure of complex **15** can be described as a *step-like* one-dimensional polymer where the asymmetric unit is repeated by the symmetry operations: i = x+1/2, -y+1/2, z+1/2 and ii = x-1/2, -y+1/2, z-1/2.

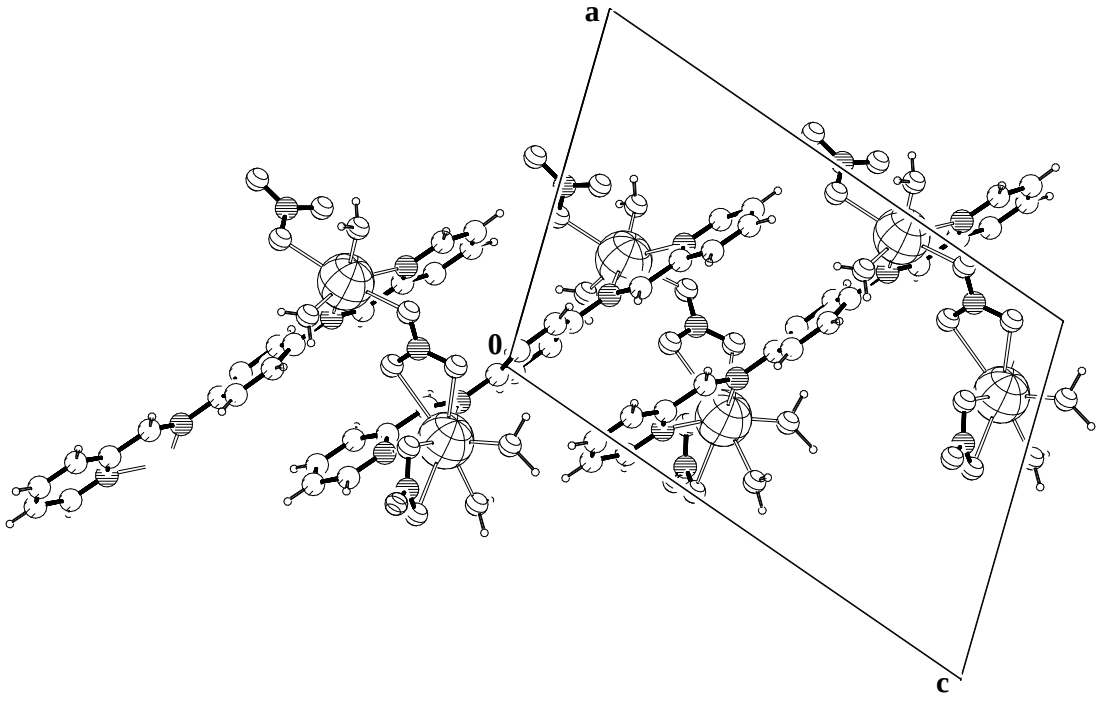

Figure 18. Polymeric structure of complex $\{[Cd_2(L3)(NO_3)_3(H_2O)_4]\cdot(NO_3)\cdot 2H_2O\}_n$ (**15**) viewed down the *b* axis. The non-coordinated water molecules and nitrate ion have been omitted for clarity.

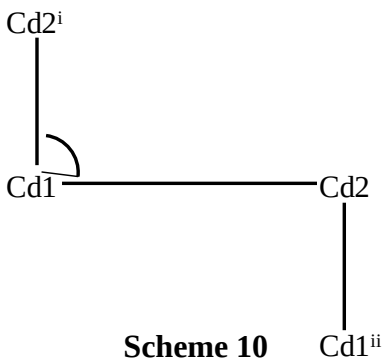

Scheme 10

Scheme 10 illustrates the *step-like* shape of this polymer with a *step-height* of 5.59 Å between metal atoms related by the symmetry operations i or ii. The angles $Cd2^{i}$-Cd1-Cd2 and Cd1-Cd2-$Cd1^{ii}$ differ moderately from 90 °, value for a "perfect" step motif.

This is probably due to the non-planarity of the ligand with dihedral angles between the pyridine and the phenyl rings of 26.62(15) and 31.71(14) °.

Weak π-π stacking can be observed with an average distance of *ca.* 3.8 Å between the pyridine and the phenyl rings of symmetry related molecules although as the ligand is not perfectly planar, the rings are not completely parallel. It is remarkable that the coordination geometry around the two independent cadmium atoms Cd1 and Cd2 is different as showed in Scheme 11.

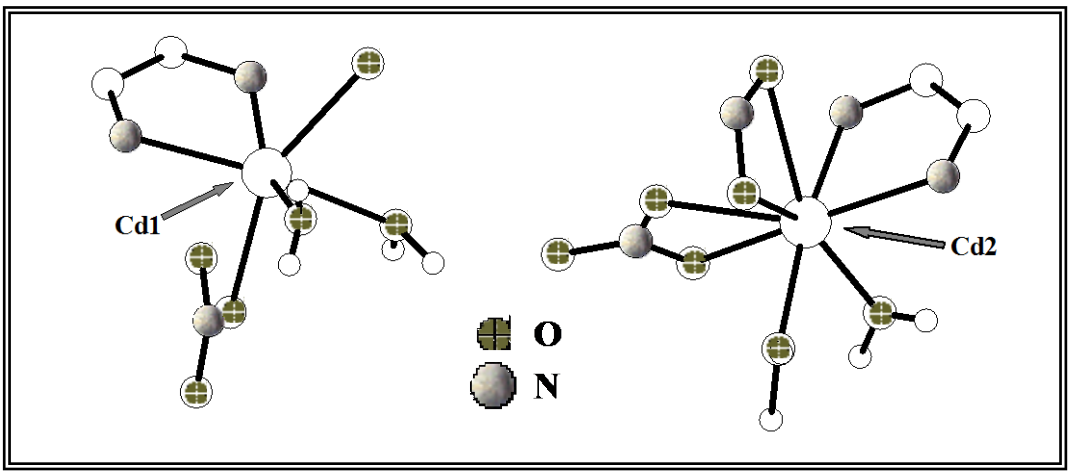

Scheme 11. Coordination sphere of Cd1 and Cd2 in the complex **15**.

The Cd1 is six coordinated with a distorted octahedral geometry and is coordinated to one pyridylimine unit and to four oxygen atoms; two of them water molecules and the other two to two different nitrate anions. The distortion from an ideal octahedral is considerable and is mainly due to the small chelate angle of the pyridylimine unit (Table 10).

Table 10. Some geometric parameters (Å,°) for $\{[Cd_2(L3)(NO_3)_3(H_2O)_4]\cdot(NO_3)\cdot 2H_2O\}_n$ (**15**)
In *italic*, geometric parameters for the imine group.

(a)	Cd1-Cd2	9.299(1)	N1-Cd1-O1	119.19(11)
	Cd1-Cd2^i	5.594(1)	N1-Cd1-N2	73.61(13)
	Cd1-N1	2.286(4)	N1-Cd1-O9	79.08(11)
	Cd1-N2	2.351(3)	O1-Cd1-O9	151.80(9)
	Cd1-O1	2.346(3)	O4w-Cd1-N1	153.63(11)
	Cd1-O9	2.501(3)	O4w-Cd1-N2	108.86(13)
	Cd1-O4w	2.200(3)	O4w-Cd1-O1	84.18(10)
	Cd1-O5w	2.317(3)	O5w-Cd1-O1	80.62(10)
	C5-C6	1.473(6)	O5w-Cd1-N2	163.77(11)
	C6-N2	1.283(5)	O5w-Cd1-O9	74.97(10)
	C7-N2	1.431(6)	*C5-C6-N2-C7*	*-179.5(4)*

(b)	Cd2-N3	2.366(3)	N4-Cd2-O7	121.90(11)	O6w-Cd2-O7	150.32(12)
	Cd2-N4	2.279(4)	N4-Cd2-O5	97.27(13)	O6-Cd2-O8	114.47(12)
	Cd2-O5	2.344(3)	N4-Cd2-N3	73.29(13)	O6-Cd2-O5	49.01(13)
	Cd2-O7	2.584(3)	O5-Cd2-O7	71.37(11)	O7-Cd2-O8	47.57(13)
	Cd2-O3w	2.213(3)	N3-Cd2-O7	89.95(10)	O6-Cd2-O7	118.17(14)
	Cd2-O6w	2.372(3)	O3w-Cd2-O7	72.55(10)	O6-Cd2-O6w	72.74(12)
	Cd2…O6	2.723(3)	O3w-Cd2-N4	165.52(12)	O8-Cd2-O5	72.81(14)
	Cd2…O8	2.756(3)	O3w-Cd2-N3	107.99(14)	O8-Cd2-O3w	120.07(10)
	C13-C14	1.461(6)	N4-Cd2-O6w	85.13(12)		
	C13-N3	1.281(5)				
	C10-N3	1.434(5)	*C13-C14-N3-C10*	-179.5(4)		

Symmetry operation: i = x+1/2, -y+1/2, z+1/2

On the other hand, the Cd2 metal centre (coordination geometry given in Table 10 (b) exhibits a coordination number of eight, relatively rare[26]. It is coordinated to one pyridylimine unit and, this time, to six oxygen atoms, two belonging to water molecules and four to two nitrate anions. In addition, the long bond distances, Cd2-O6 and Cd2-O8, could be considered as a secondary interaction. In this case, the geometric parameters around the Cd2 atom should fit better with an octahedral coordination. However, the bond angles found in the coordination sphere of the Cd2 metal atom are quite far from the ideal and considerably different from those expected for an ideal octahedral angle.

The average Cd-N_{im} bond distance of 2.358 Å is slightly shorter the standard value of 2.399 / 2.457 Å[24]. The same trend is observed for the Cd-N_{py} bond distances (2.282 Å in **15** and 2.381 Å, standard value). The Cd-Ow bond distances in **15** vary from 2.200 to 2.372 Å whereas the standard value is 2.318 Å.

One short and one long Cd-$O_{nitrate}$ bond distances, for each metal atom, are observed (Cd1-O1, Cd2-O5 → short, Cd1-O9, Cd2-O7 → long) plus two very long bonds (Cd2…O6 and Cd2…O8). The standard Cd-$O_{nitrate}$ values are different for a terminal (2.385 Å) or a chelating nitrate (2.460 Å, normally asymmetric). In complex **15** the "short" values are closer to the terminal nitrate value and agree with an asymmetric chelating mode.

A very intricate hydrogen-bonding network that connects the polymeric chains among themselves guarantees the crystal cohesion. These H-bonds are formed between the water molecules (coordinated or not) and the oxygen atoms of the nitrate groups and lead to the formation of a three-dimensional hydrogen-bonded polymer. The following table contains a list of the most representative hydrogen bonds present in compound **15**.

Table 11. Hydrogen-bonding geometry (Å,º) for **15**.

D-H...A	d(D-H)	d(H...A)	d(D...A)	<(DHA)
O1w-H1w1...O5^{iii}	0.82	2.05	2.87(1)	171.7
O1w-H2w1...O10	1.09	1.68	2.76(1)	166.2
O2w-H1w2...O4^{iv}	1.11	1.78	2.87(1)	165.1
O2w-H1w2...O6i^{v}	1.11	2.45	3.33(1)	135.0
O2w-H2w2...O5w^{v}	1.17	1.64	2.78(1)	163.8
O3w-H1w3...O7^{vi}	0.99	1.93	2.91(1)	167.1
O4w-H1w4...O1w^{vii}	0.85	1.85	2.68(1)	166.9
O4w-H2w4...O10	0.79	2.50	3.19(1)	146.7
O5w-H1W5...O12^{viii}	0.86	1.92	2.76(1)	166.0
O5w-H2w5...O2^{viii}	1.04	1.99	3.00(1)	162.0

Symmetry transformations used to generate equivalent atoms:
iii -x-0.5, y-0.5, -z-0.5 iv -x-1, -y+1, -z v -x+0.5, y+0.5, -z+0.5 vi -x, -y+1, -z
vii -x, -y, -z viii -x+1, -y, -z

As for **L1** and **L2**, UV-Vis titration experiments have been recorded at a **L3** concentration of 125 μM and varying the concentration of different metal salts from 0 to 300 μM. The most relevant aspects of a number of cases will be discussed.

The next figure illustrates the changes observed in the UV-Vis spectrum of **L3** when it coordinates to Cd^{2+} in ethanol. Upon addition of increasing quantities of metal ion, the absorbance in the ligand bands at 285 and 360 nm decreases and a shoulder appears at about 425 nm with the formation of an isosbestic point at *ca*. 390-395 nm. The absorption intensity in this region grows while the concentration of the metal does not exceed the concentration of the ligand and then, it slightly decreases.

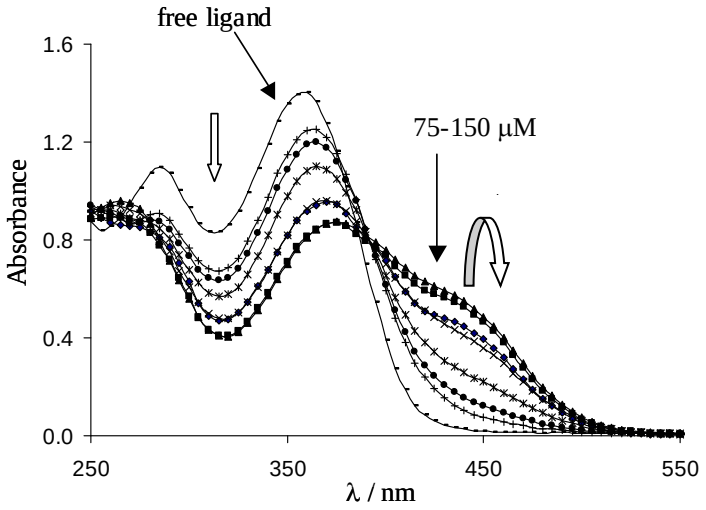

Figure 19. UV spectra of **L3** upon incremental addition of $Cd(NO_3)_2 \cdot 4H_2O$ in EtOH.

By observing this titration experiment, it is difficult to propose any metal to ligand ratio. In any case, we do not observe the Cd:L3 2:1 ratio found in the solid state, complex **15**. This compound **15** can be obtained only by using slow diffusion techniques. The reaction of $Cd(NO_3)_2 \cdot 4H_2O$ with **L3** in a 1:1 or 2:1 ratio in different solvents and at different temperatures always leads to the formation of precipitates either insoluble or only soluble in water (solvent that was not used in order to avoid the hydrolysis of the ligand). In the conditions of very high dilution of the UV-Vis experiments, nothing precipitates.

In general, the UV-Vis experiments performed with ligand **L3** appeared to be quite complicated indicating the presence of several species in many cases. The results of the titration with $AgNO_3$ are presented in Figure 20.

Upon addition of Ag^+ to a **L3** solution several observations can be made. Until a metal concentration of 37.5 μM, isosbestic points at 260, 315 and 385 nm are formed as illustrated in Figure 20, (b). Then, when more Ag^+ is added, these points disappear and the absorbance at 330 and 420 nm reaches a maximum value. Almost the same spectrum is obtained for the last

three concentrations (75, 150 and 300 μM), with almost identical values of absorbance. The significant difference between this three spectra and the rest could come from the stabilization of a second species at $[Ag^+]$:[L3] > *ca*. 0.6.

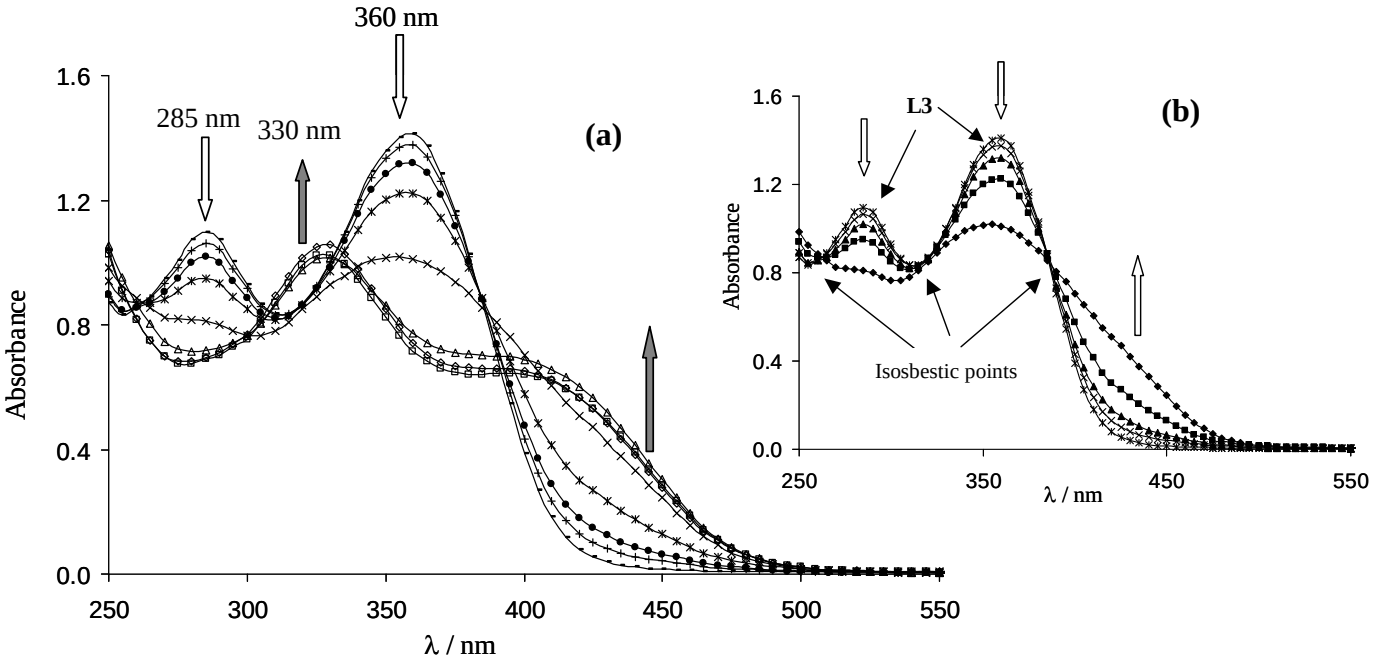

Figure 20. UV spectra of **L3** upon incremental addition of $AgNO_3$ in EtOH. **(a)** full metal concentration range **(b)** from 0 to 37.5 μM

The following figure shows the changes observed in the UV-Vis spectrum of **L3** upon addition of increasing concentrations of CuAcO. Upon addition of Cu^+ to a **L3** solution the ligand bands at 285 and 360 nm suffer a red-shift up to approximately 425 nm. The difference-spectra plot [using the UV-Vis spectrum of **L3** as reference] illustrates the formation of two isosbestic points at 275 and 390-5 nm, suggesting the formation of (principally) one product.

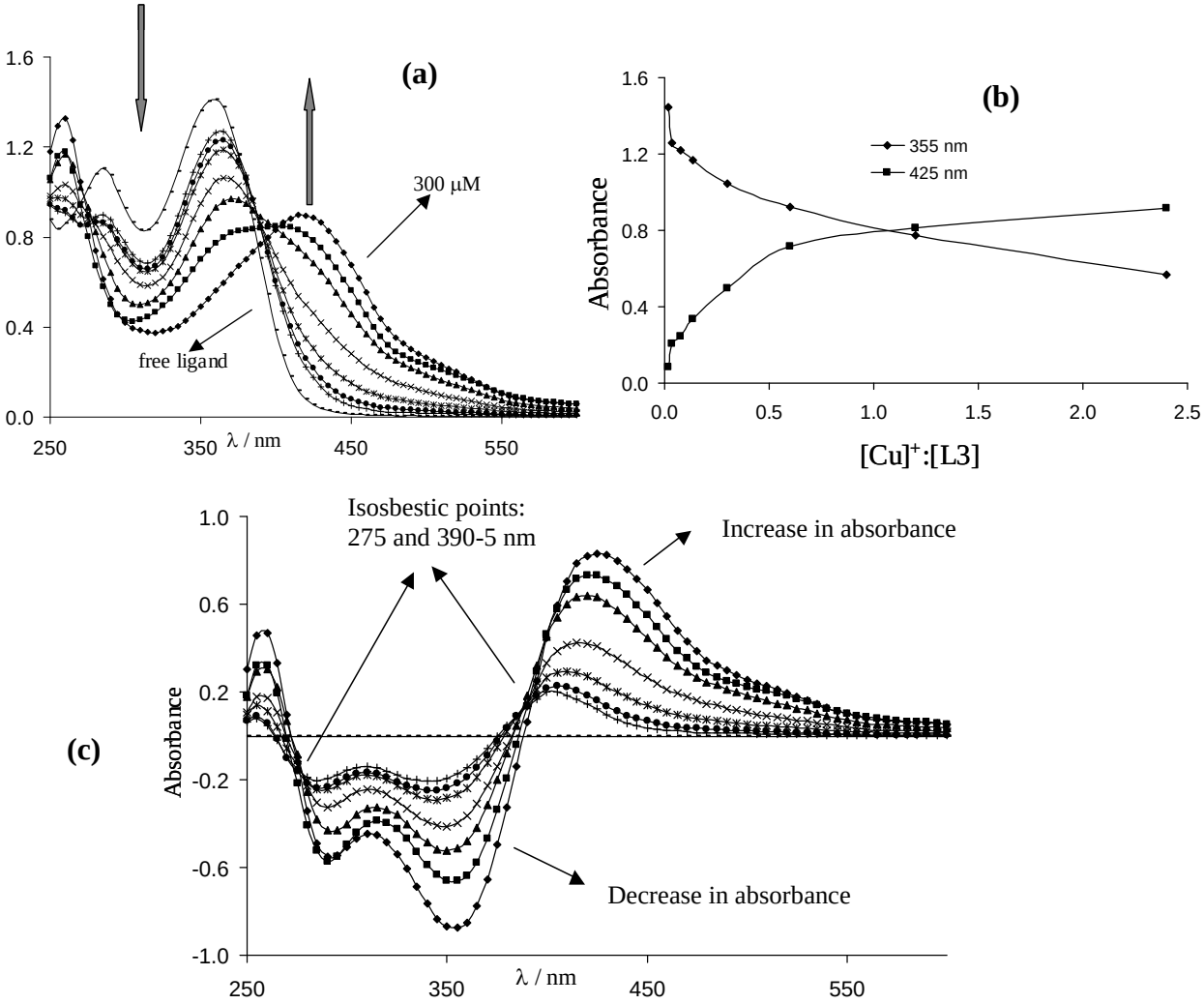

Figure 21. UV spectra of **L3** upon incremental addition of CuAcO in EtOH. **(a)** full concentration range **(b)** ratio plot at 355 and 425 nm and **(c)** difference spectra plot.

As it can be seen in the molecular ratio plot, saturation is not reached, at least under the conditions of the experiment, suggesting that a quantity of complex is still being formed at that concentration. The aspect of this curve is an indication of a relatively small formation constant for this complex. Cu^+ (Ag^+ to some extent) is known for having a marked preference for adopting a tetrahedral geometry. In many cases this "well-coded" information reduces the number of possible species formed and makes it easier to predict the final result. These two metal ions are being largely used in "programmed" self-assembly processes.

In contrast, Cu^{2+} does not have a clear preference for any particular coordination geometry. In many cases it is pentacoordinate (trigonal-bipyramidal or square-pyramidal) but it can also be in octahedral or tetrahedral environments or present irregular geometries. This "flexibility" of Cu^{2+} makes it less used in metal-assisted self-assembly processes [Cu^{2+} could be considered as a *badly* instructed building block].

This behaviour can be observed in the titration of **L3** with $Cu(NO_3)_2 \cdot 3H_2O$, Figure 22. Two plots are presented, (**a**) the UV-Vis spectra for each titration step and (**b**) the difference spectra taking the UV-Vis spectrum of **L3** as the reference (represented as "o" in the graph).

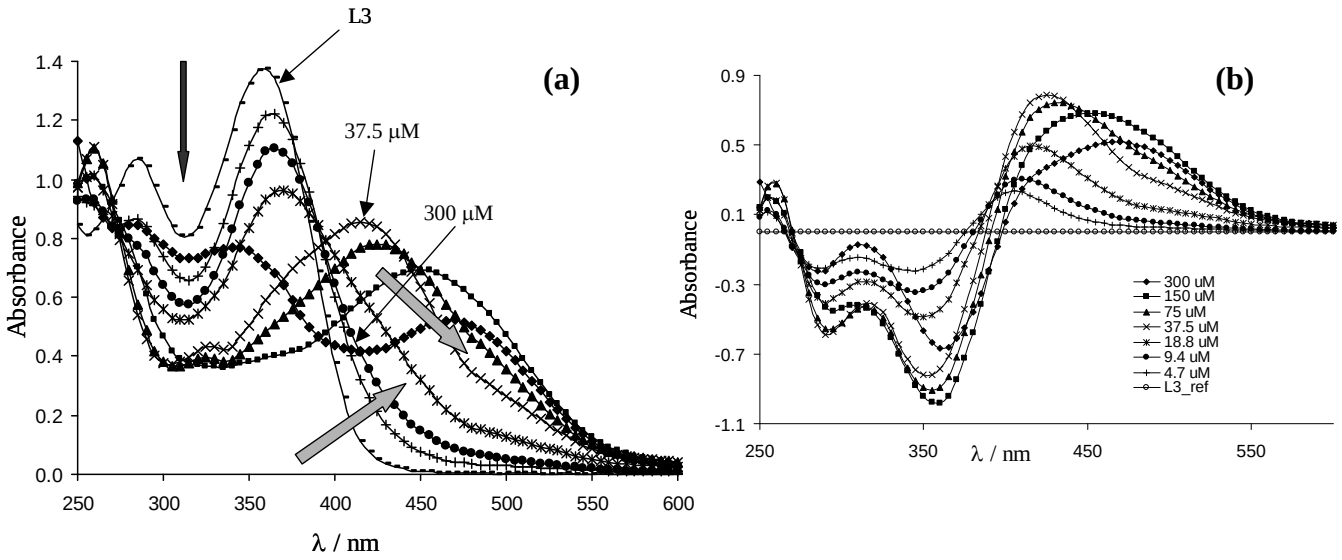

Figure 22. UV-Vis spectra of **L3** upon incremental addition of $Cu(NO_3)_2 \cdot 3H_2O$ in EtOH. **(a)** full concentration range **(b)** difference spectra plot.

In comparison to the titration experiments with Cu^{+}, the results obtained when performing analogous experiments with Cu^{2+} are more complicated. A large red-shift of the ligand bands is observed but in this case isosbestic points do not appear. At a metal concentration equal to 37.5 μM a maximum in absorbance at 415 nm is observed. Then, on continuous addition of Cu^{2+} a decrease in absorption is observed together with the shift of the absorption maximum to 470 nm. Some other metal salts have been tested. Titration of **L3** with Ni^{2+}, Co^{2+} or Zn^{2+}

salts gave very similar results. In all these three cases, the ligand band shows large red-shifts due to coordination (at *ca*. 430, 425, and 420 nm for Ni^{2+}, Co^{2+} and Zn^{2+}, respectively) until a metal concentration equal to 37.5 μM. Then, continuous addition of metal leads to a decrease in absorption with almost no further shift in the maximum of the band. In the case of Fe^{2+} comparable behaviour is observed although this *system* also absorbs at higher wavelengths (maximum *ca*. 575 nm).

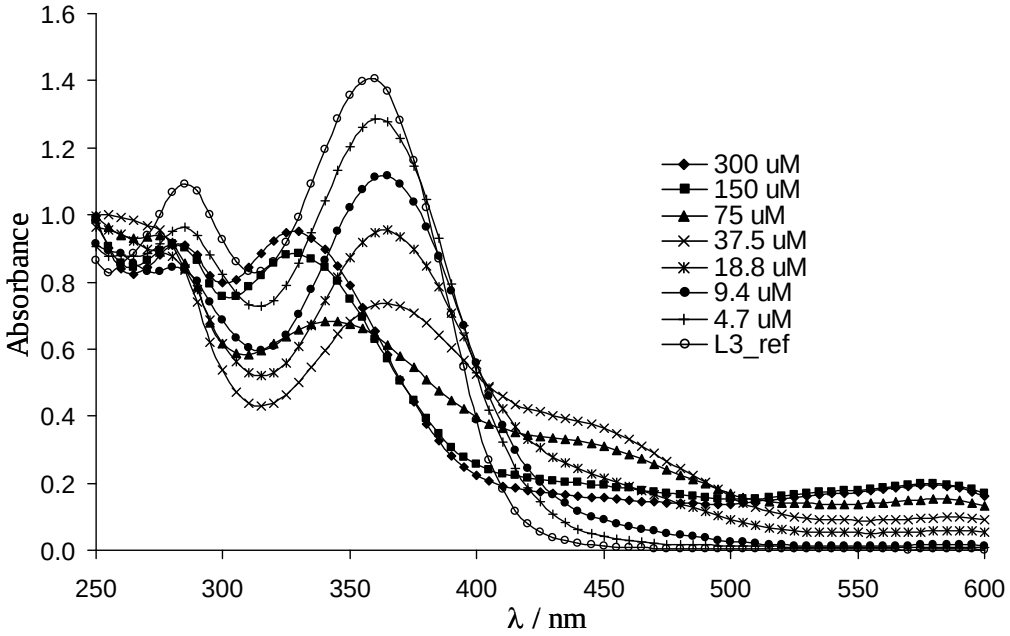

Figure 23. UV-Vis spectra of **L3** upon incremental addition of $Fe(ClO_4)_2 \cdot 4H_2O$ in EtOH.

The colour observed in the solution during the titration experiment[&] was orange-brown. It can be seen in Figure 23 that until a metal concentration of 37.5 μM the maximum in absorbance (in the region 400-600 nm) is located at *ca*. 435 nm then, the maximum is displaced to *ca*. 575 nm (violet colour region) and the absorption at *ca*. 435 nm decreases to approximately half of its maximum value. This suggests the presence of several equilibria in the solution.

[&] The same colour was always observed for the reactions carried out between L3 and different Fe^{2+} salts during the realization of the present work.

2.3. Coordination behaviour of ligand L4

As for **L1** and **L2**, it was impossible to obtain single crystals of metal complexes containing this ligand. The reactions of **L4** with different cadmium, mercury or zinc salts gave sometimes solids. Although they had a crystalline appearance, they did not diffract and appeared to be amorphous. Regardless of this, UV-Vis titrations experiments of the ligand **L4** under the same conditions used for the precedent ligands have been carried out to investigate the reactivity of this ligand towards a series of metal ions. The ligand **L4** is the analogue of the ligand **L3** where the central phenyl spacer has been substituted by a naphthalene group. This makes the ligand even more rigid than **L3**. As previously shown (*Results and Discussion*, p. 27) the crystal structure of **L4** differs quite considerably from that of **L3**. In **L4**, the pyridine rings are significantly inclined with respect to the naphthalene plane whereas the ligand **L3** is almost planar. The difference between the free ligands is also visible with respect to coordination to the metals. As showed in the UV-Vis titration experiments, ligand **L3** reacts quite strongly with almost all the metal salts tested.

The behaviour of ligand **L4** is quite different. Upon addition of VO^{2+}, $Hg^{2+}$and Mn^{2+} salts, the UV-Vis spectrum of **L4** did not change perhaps indicating the absence of reaction or a extremely weak interaction with these metal atoms. The titration experiments with Cd^{2+}, Fe^{2+} or Zn^{2+} salts show only small changes in absorption. The cases of Ni^{2+}, Co^{2+} are comparable. In both cases, the intensity of the ligand bands decreases and at the same time these bands are enlarged and present a queue up to *ca*. 500 nm. An isosbestic point at 420 (for Ni^{2+}) and 425 (for Co^{2+}) nm is also observed during all the titration processes except for the most concentrated solution, 300 μM, for which this point is slightly shifted. The next figure presents the results of the titration with $Ni(ClO_4)_2 \cdot 6H_2O$ divided into two different

wavelength ranges for clarity [the values of absorbance are very different for the UV and for the Visible region].

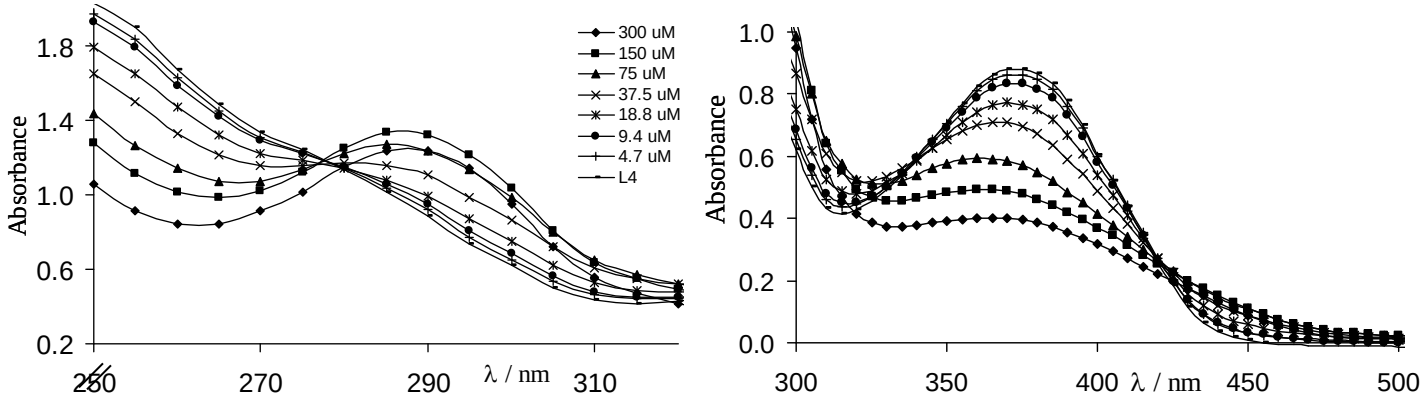

Figure 24. UV-Vis spectra of **L4** upon incremental addition of $Ni(ClO_4)_2 \cdot 6H_2O$ in EtOH. Titration with $Co(BF_4)_2 \cdot 6H_2O$ gave similar results.

The cases of Ag^+ and Cu^+ are also comparable. For Ag^+ three isosbestic points are formed at 275, 335 and 410 nm and two new absorption regions at *ca*. 285 and 440 nm as shown in the difference-spectra plot in Figure 25 (a) [The UV-Vis spectrum of the free ligand has been taken as reference]. Saturation was reached with the three most concentrated solutions, for which we observe almost identical spectra. The case of Cu^+ is quite similar, although the isosbestic point at 410 nm is displaced a little for the concentration 300 μM. Other isosbestic points appear at *ca*. 275-80 and 330 nm and new absorptions in the regions around 285 and 440 nm. In this case saturation is less clearly observed. Only the region 300-500 nm is presented in Figure 25 (b) for clarity.

The colour of both solutions was orange-brown. In general the colours observed during all the titrations experiments were always in the range of the yellows, oranges and browns. No violet colour was observed for Fe^{2+} nor green or blue for Cu^{2+}.

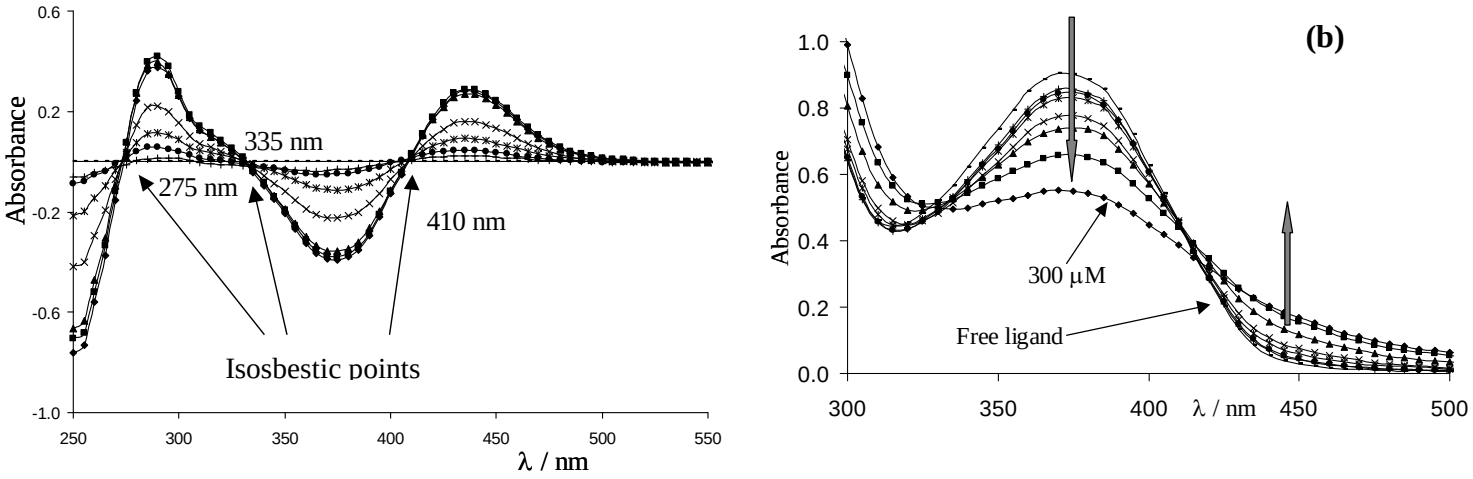

Figure 25. (a) Difference-spectra plot of **L4** upon incremental addition of $AgNO_3$ in EtOH.
(b) UV-Vis spectra of the titration with CuAcO.

Finally, with Fe^{2+} only a very small absorption emerges at *ca.* 440 nm. In any case the disappearance of the ligand bands is much more pronounced that the appearance of new absorptions. Almost the same comments apply to Cu^{2+}. These titrations are more complicated than for other metals because of absence of any clear isosbestic point.

In general it can be said that ligand **L4** coordinates weakly to different metal ions, which could explain why it was not possible to obtain single crystals of **L4** metal complexes. Structural (sterical hindrance) more than electronic reasons could be at the origin of this limitation of **L4** towards coordination to metals.

2.4. Coordination behaviour of ligand L5

This bis-bidentate Schiff base ligand was designed with the idea of modifying the structure of **L3** by moderately increasing its flexibility. In comparison with **L3**, **L5** possesses the same two chelating pyridylimine units linked by a more flexible central spacer that incorporates an oxygen atom between the phenyl rings [instead of the **L3** rigid phenyl group]. This semi-flexible ligand design should prevent the two chelating sites from coordinating to the same metal centre and would favour the formation of helicates, because of its ability to twist [taking into account the metal ion selected for the coordination]. The use of this kind of ligand in diverse domains such as catalysis[27], analysis of drinking water[28] or supramolecular chemistry has been reported[7b,29]. Very recently, Hannon *et al.* have reported some NMR studies on the interactions between a triple helicate and the major groove of DNA[30].

Recent work in the domain of supramolecular chemistry[6c,7a,7c,31] reports coordination compounds having bimetallic triple helical conformations. Different metal ions (transition metals, rare earth, d^{10} metal ions) are involved, as well as a variety of ligands such as diketones, catecholates and pyridylimines. Recently Raymond *et al.*[32] have shown the interesting mechanism of the inter-conversion between a triple-helicate and a tetrahedral cluster using only host-guest interactions with an anthracene backbone ligand.

The coordination behaviour of ligand **L5**[33] with a variety of metal ions has been studied and the complexes $[Ni_2(L5)_3](BF_4)_4 \cdot CH_3OH$ **(16)**[8]**,** $[Co_2(L5)_3](BF_4)_4 \cdot CH_3OH \cdot 0.5H_2O$ **(17)**[8], $\{[Ag(L5)](NO_3)\}_n$ **(18)** and $\{[Ag(L5)](CF_3SO_3) \cdot 0.2H_2O\}_n$ **(18a)**[34] have been synthesized and characterized crystallographically. NMR and ES-MS spectra as well as UV-Vis titrations experiments have also been carried out.

2.4.1. Complexes $[Ni_2(L5)_3](BF_4)_4 \cdot CH_3OH$ **(16)** and $[Co_2(L5)_3](BF_4)_4 \cdot CH_3OH \cdot 0.5H_2O$ **(17)**

These isomorphous complexes of nickel(II) (**16**) and cobalt(II) (**17**) were obtained by refluxing methanolic solutions of 3 equiv. of **L5** and 2 equiv. of $NiCl_2.6H_2O$ or $CoCl_2.6H_2O$, respectively. The complexes were precipitated adding 4 equiv. of $[NH_4][BF_4]$ giving the triple-helicates (**16**) and (**17**). These powders were collected by filtration and then crystallised by slow evaporation of their acetonitrile solutions giving orange (Ni^{2+}) and red-orange (Co^{2+}) crystals suitable for X-ray diffraction analysis.

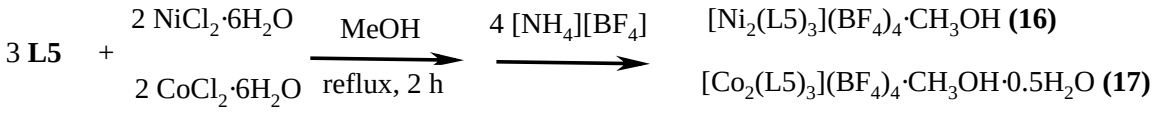

The IR spectra show that the characteristic ligand imine vibration at 1624 cm^{-1} is displaced to 1633 and 1630 cm^{-1} and the pyridine C=N vibration at 1581 cm^{-1} is also displaced to 1596 and 1595 cm^{-1} for compounds **16** and **17** respectively. The ether group absorption bands (1240 and 1198 cm^{-1}) are also displaced (1242, 1201 cm^{-1} for **16** and 1242, 1200 cm^{-1} for **17**). The BF_4^- non-coordinated anions show the expected vibration at 1054 and 1056 cm^{-1} for **16** and **17**, respectively.

Table 12. IR Data for the ligand **L5** and the complexes **16-17**.

Compound	IR, ν [cm^{-1}]
L5	1624 (s, imine), 1581 (s), 1566 (m), 1495 (vs), 1467 (m), 1433 (m), 1344 (w), 1240 (vs), 1198 (s), 993 (m), 776 (s)
16	1633 (m, imine), 1596 (m), 1571 (m), 1494 (s), 1446 (w), 1364 (w), 1242 (m), 1201 (m) 1054 (vs, BF_4), 771 (w)
17	1630 (m), 1595 (m), 1568 (m), 1494 (vs), 1445 (w), 1365 (w), 1308 (m), 1242 (s) 1200 (m) 1056 (vs, BF_4), 773 (w)

The crystal structure (Figure 26) of the isostructural complexes shows the triple-helical geometry of the cations $[M_2(L5)_3]^{4+}$ (M = Ni or Co) with four uncoordinated BF_4^- anions and one molecule of methanol. Half a water molecule of crystallization is also present in the case of compound **17**.

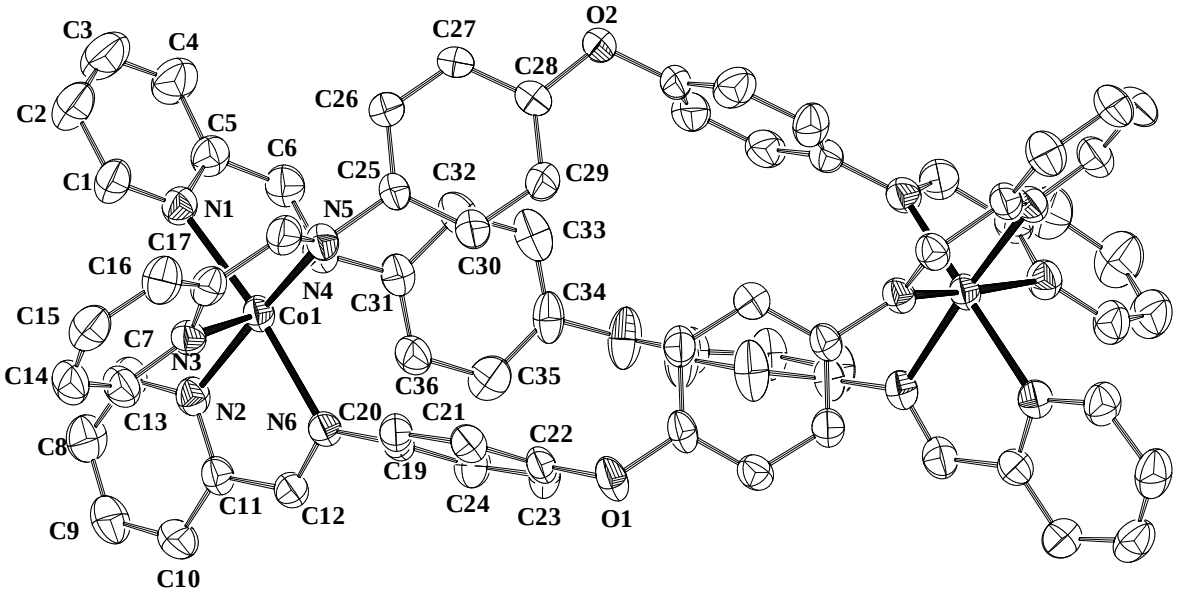

Figure 26. Molecular structure of the cation $[Co_2(L5)_3]^{4+}$ showing the crystallographic numbering scheme and thermal ellipsoids at 50% probability level.

In the binuclear cations the ligand molecules act as bis(bidentate) units bound to the metal atoms, wrapped around the helical axis and leading to a triple–helical structure with a *pseudo*-C_3 axis, defined by the metal atoms which are separated by 11.384 (2) Å for compound **16** and by 11.355 (2) Å for compound **17** [symmetry operation: –x + 1/2, +y, -z + 1/2]. The shortest distance between symmetry related metal centres is in both compounds 10.305 (1) Å, which corresponds to the length of the *b* axis. The coordination sites of the metal atoms in **16** and **17** are very similar and may be described as distorted octahedral geometry with three imine and three pyridine nitrogen atoms occupying the vertices of the octahedron. The chelate pyridylimine bite angles of *ca.* 78.6 (2), for **16** and 77.2 (2) º, for **17**, are significantly smaller than the ideal ones for a regular octahedral geometry and are imposed by the ligand

bis(bidentate) coordination geometry. The average $M–N_{py}$ and $M–N_{im}$ distances of, respectively, 2.094 (4) and 2.104 (4) Å for **16** and of 2.151 (4) and 2.149 (4) Å for **17**, are close to the standard values[24] of 2.122 and 2.051 Å [for Ni^{2+}] and 2.185 and 2.015 Å [for Co^{2+}]. Selected bonds distances and angles are given in Table 13.

Table 13. Selected bond lengths (Å) and angles (º) for compounds **16** and **17**.

	16	**17**
M – M[a]	11.384 (1)	11.355 (1)
M – N1	2.076 (4)	2.185 (4)
M – N2	2.108 (4)	2.126 (4)
M – N3	2.099 (4)	2.141 (4)
M – N4	2.108 (4)	2.168 (5)
M – N5	2.087 (5)	2.126 (4)
M – N 6	2.117 (4)	2.154 (4)
N1 – M – N2	94.09 (17)	95.85 (17)
N1 – M – N3	95.20 (17)	88.82 (17)
N1 – M – N4	78.91 (17)	77.14 (17)
N1 – M – N5	171.35 (18)	172.75 (16)
N1 – M – N6	91.46 (17)	88.28 (16)
N2 – M – N3	91.59 (17)	96.88 (16)
N2 – M – N4	90.65 (17)	92.69 (17)
N2 – M – N5	78.70 (17)	77.10 (16)
N2 – M – N6	168.90 (18)	172.85 (18)
N3 – M – N4	173.84 (17)	163.76 (16)
N3 – M – N5	89.81 (17)	90.31 (16)
N3 – M – N6	78.32 (17)	77.32 (16)
N4 – M – N5	96.26 (17)	104.63 (17)
N4 – M – N6	99.86 (17)	93.92 (16)
N5 – M – N6	96.46 (17)	98.56 (16)

a) M and M[a] are the respective metal centres. Symmetry operation: –x + 1/2, y, -z + 1/2.

On comparing the dihedral angles between all of the aromatic rings in the crystal structures of both the free ligand **L5** and the two helicate complexes, we observe important variations.

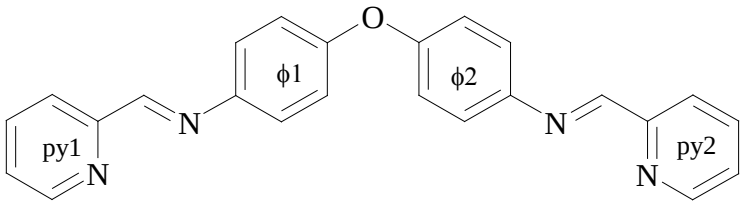

Schema 12. A representation of **L5** showing the labelling used to describe the dihedral angles between aromatic rings.

In **L5** rings ϕ2 and py2 are inclined by only 10.8 º (see Results, page 29) whereas ϕ1 and py1 are tilted by *ca.* 46°. This asymmetry is no longer present in the centrosymmetric complexes **16** and **17** where half of the molecule is generated by the symmetry operation: -x+1/2, y, -z+1/2. In the complexes the twisting between rings (for the three ligand units) is much more important and less uniform (Table 14). In compound **16** the phenyl rings in two of the three ligand molecules (***L2*** and ***L3*** in Table 14) were disordered in two positions and therefore the angles between both ring conformations are given. In **17** the atomic positions of all the three ligand molecules ***L1***, ***L2*** and ***L3*** were well defined.

Table 14. Dihedral angles (º) between aromatic rings for **L5**, **16** and **17**. In compounds **16** and **17**, the three ligand molecules are named ***L1***, ***L2*** and ***L3***.

	L5		**16**		**17**	
py1 - ϕ1	46.36 (6)	***L1***		74.8 (2)	***L1***	41.3 (2)
		L2	72.3 (4),	86.6 (5)	***L2***	69.4 (2)
		L3	75.8 (8),	46.4 (4)	***L3***	70.4 (2)
ϕ1 - ϕ2	67.47 (4)	***L1***		85.5 (2)	***L1***	74.7 (1)
		L2	57.0 (7),	22.3 (7)	***L2***	85.2 (1)
		L3	66.7 (4),	8.1 (2)	***L3***	70.7 (2)
ϕ2 – py2	10.77 (8)	Equal to py1 - ϕ1			Equal to py1 - ϕ1	

Symmetry operation between ϕ1 and ϕ2 in compounds **16** and **17**: –x + 1/2, +y, -z + 1/2

As it can be seen in the space filling representation of **17** (Figure 27), triple helicates are very compact structures due to the wrapping of the ligands and the metal ions are not easily accessible, being very well enveloped by the ligand molecules.

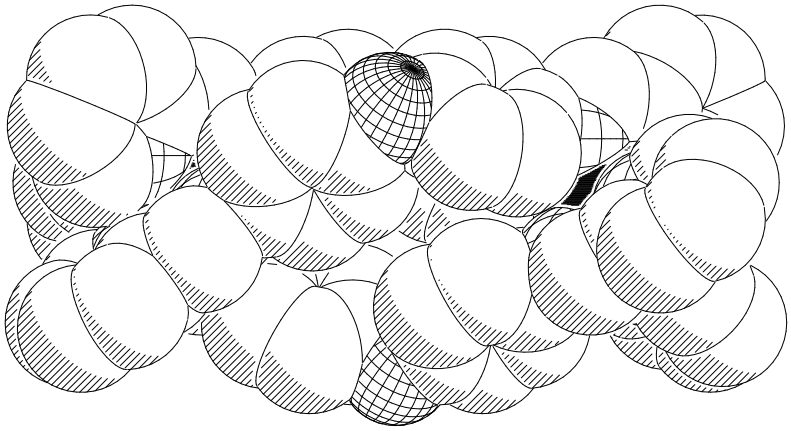

Figure 27. Space filling representation of the cation $[Co_2(L5)_3]^{4+}$ with H atoms omitted.

As for the crystal structure of the non-coordinated ligand, the imine groups possess an *E* configuration. Face-to-face π-stacking interactions cannot be taken into consideration because of the large distances between rings but edge-to-face (CH…π) may have a small effect on the self-assembling processes. However, the main controlling parameter here is the use of octahedral metal ions and a ligand with the adequate structure.

Complexes **16** and **17** crystallize in the centrosymmetric space group A 2/n and the structure is formed by the 1:1 mixture of the two possible helical enantiomers, Δ and Λ. Concerning the crystal structure refinement, several restraints were applied. In both complexes one of the BF_4^- anion molecules was found to be highly disordered and it was refined in two positions with occupations of 0.6 and 0.4, respectively. The B-F and F-F bond distances in disordered BF_4^- molecules were fixed to standard values. The thermal parameters of all the F atoms were

restrained to be equal in the refinement process [B atoms were treated in the same way]. In compound **16** the phenyl rings in two of the three ligand molecules were disordered and have been refined in two positions with occupations of 0.6 / 0.4 or 0.5 / 0.5 depending on the ring.

Complexes **16** and **17** are soluble in acetonitrile and the analysis of their ES-MS spectrum is quite interesting. For both compounds a peak at m/z 313 which corresponds to the formulation $[M_2(L5)_3]^{4+}$ was observed and is consistent with the solid state structure. In the case of Ni^{2+}, a number of peaks at higher m/z values may be assigned to different aggregate species: m/z 423 → $[Ni_2(L5)_3(OH)]^{3+}$, 679 → $[Ni_2(L5)_3(OH)(BF_4)]^{2+}$, 713 → $[(Ni_2(L5)_3)_2(BF_4)_4]^{4+}$, 980 → $[(Ni_2(L5)_3)_2(BF_4)_5]^{3+}$, 1113 → $[(Ni_2(L5)_3)_3(BF_4)_8]^{4+}$and 1513 → $[(Ni_2(L5)_3)_2(BF_4)_9]^{3+}$. The case of Co^{2+}, is quite similar presenting many peaks in common: m/z 423 → $[Co_2(L5)_3(OH)]^{3+}$, 713 → $[(Co_2(L5)_3)_2(BF_4)_4]^{4+}$, 980 → $[(Co_2(L5)_3)_2(BF_4)_5]^{3+}$, 1113 → $[(Co_2(L5)_3)_3(BF_4)_8]^{4+}$and 1513 → $[(Co_2(L5)_3)_2(BF_4)_9]^{3+}$.

Scheme 13 shows the proposed structure of some of the aggregate species observed in the ES-MS spectra [the BF_4^- anions have been omitted as they do not take part in the coordination].

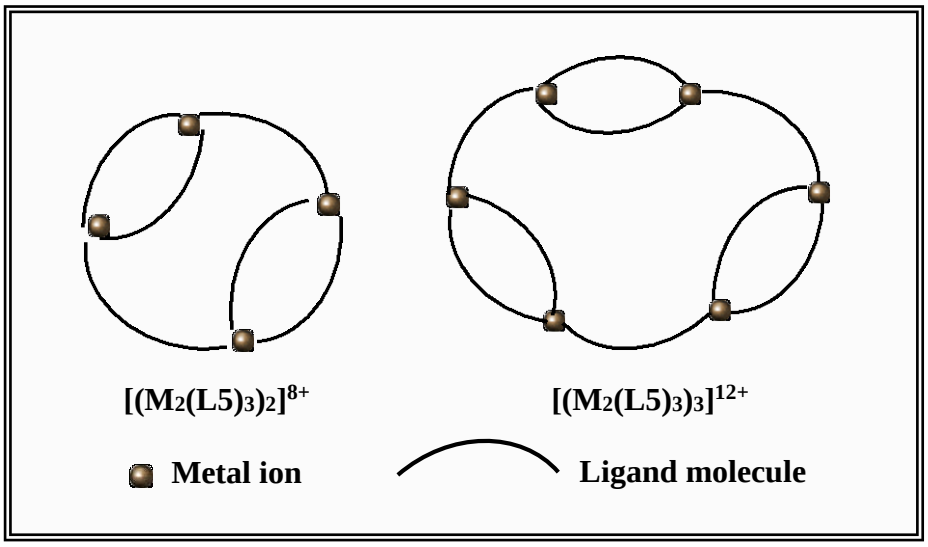

Schema 13

It could be reasonable to conceive these aggregate species as intermediate steps in the self-assembly process of the formation of compounds **16** and **17**.

As for the precedent ligands, UV-Vis titration experiments of **L5** have been carried out at a ligand concentration equal to 125 μM in ethanol and varying the concentration of the metal salt [$Ni(ClO_4)_2 \cdot 6H_2O$ and $Co(BF_4)_2 \cdot 6H_2O$] from 0 to 300 μM. The following figure illustrates the changes observed in the UV-Vis spectrum of the ligand **L5** when it coordinates to Ni^{2+} or Co^{2+} in ethanol.

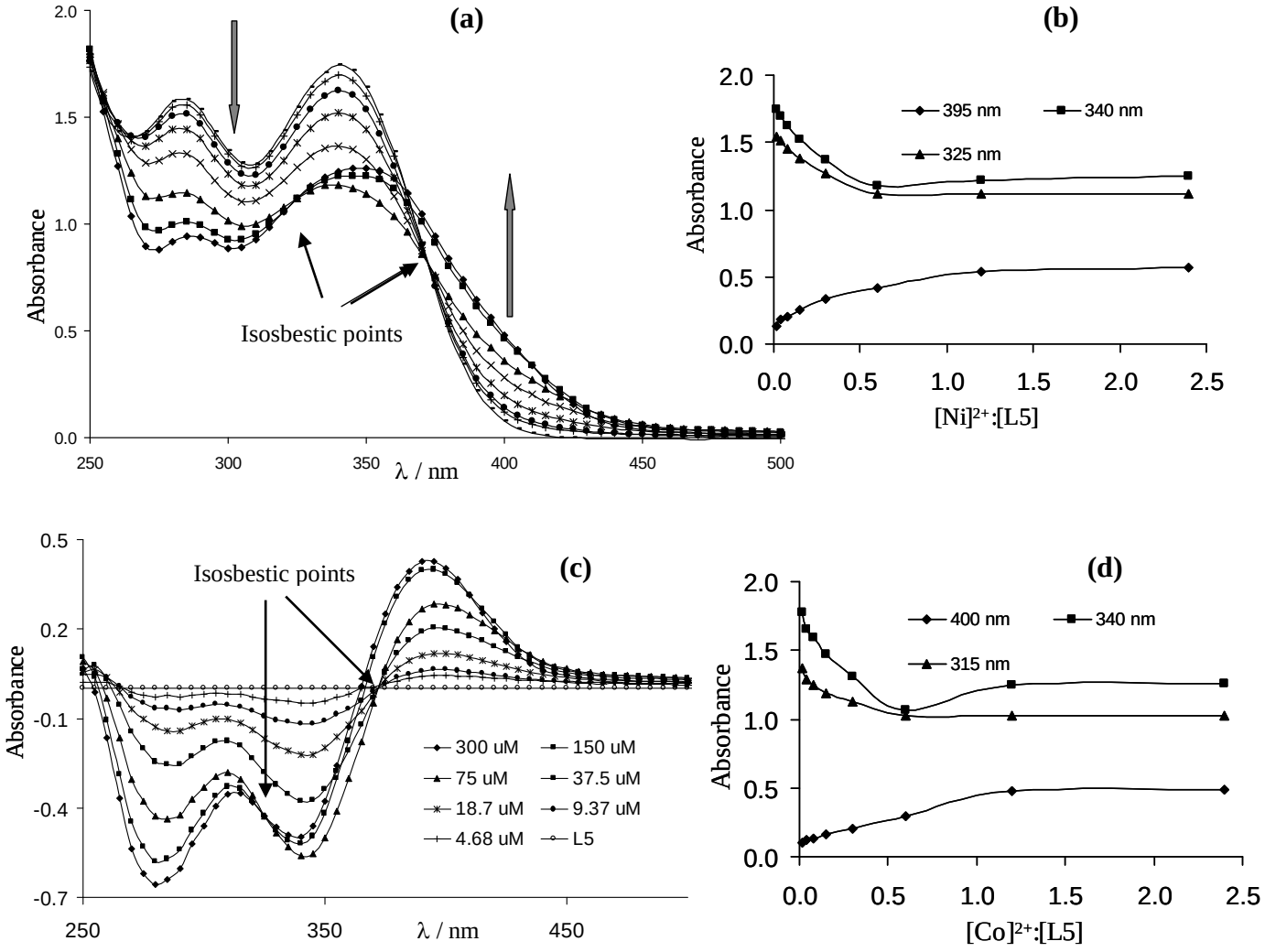

Figure 28. (a) UV spectra of **L5** upon incremental addition of $Ni(ClO_4)_2 \cdot 6H_2O$ in EtOH and **(b)** mole ratio plot at different wavelengths; **(c)** *difference-spectra* plot and **(d)** mole ratio plot of the absorptions at 340 and 400 nm for the titration with Co^{2+}.

It can be seen that upon addition of increasing metal concentration, the intensity of the ligand bands at 285 and 340 nm, progressively decreases. This is accompanied by an enlargement of the band at 340 nm up to around 450 nm. A clear isosbestic point at 370-5 nm is formed until the metal concentration reaches 75 μM. Then, at higher metal concentrations, this point disappears and another at 325 nm is formed. The presence of these isosbestic points suggests the switch between two species. The mole ratio plot of the absorbance values in the second isosbestic point (Figure 28, b) indicates approximately a M:L ratio *ca.* 0.6 for the first species, that is, the one formed at metal concentrations lower than the concentration of the ligand [the same M:L ratio was found in the crystal structure, complex **16**].

In the case of Co^{2+} the same behaviour is observed with the formation of isosbestic points at 380 nm (first) and 315 nm (second). Again, from the observation of Figure 28 (d) specially the absorbance at the second isosbestic point wavelength we could suggest the same behaviour as in the case Ni^{2+}.

Magnetic susceptibility measurements in the temperature range 4-300 K were performed with the aim of investigating the possible magnetic exchange in compounds **16** and **17**. For compound **16**, down to 4K, no maximum was observed in the χ_M versus T curve, indicating a very weak antiferromagnetic coupling. This behaviour was expected due to the large distance between metallic centres, > 11 Å.

The experimental data, fitted for a binuclear nickel compound with S = 1 and $\hat{H} = -2J\Sigma S_i S_j$, gave the best-fit parameters J = -0.21 $cm^{-1}$and g = 2.10.

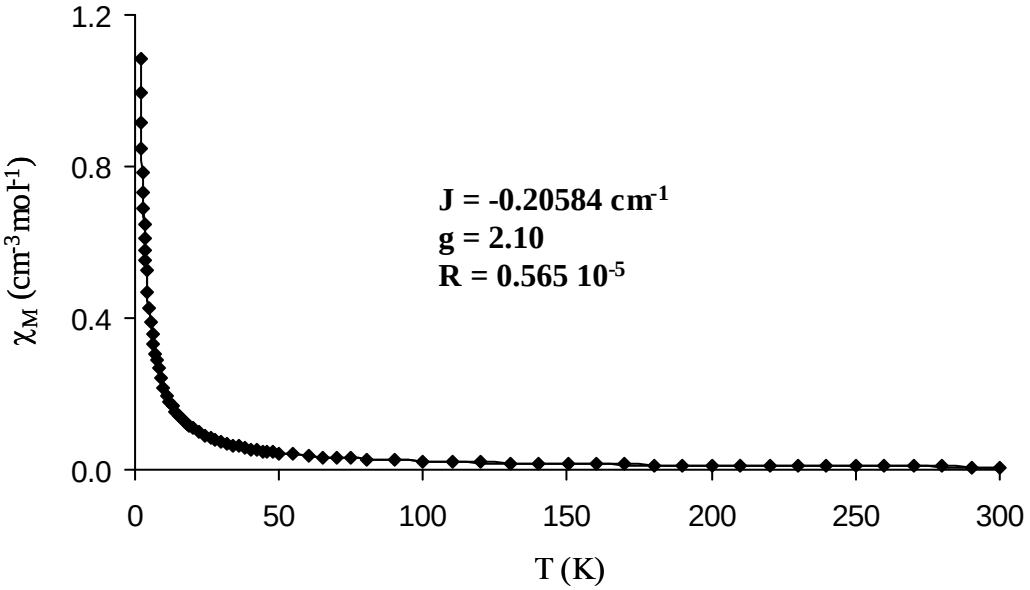

Figure 29. Temperature dependence of the magnetic susceptibility for complex **16**. The solid line represents the best-fit curve.

The magnetic measurements for compound **17** appeared to be more complicated due to the Co^{2+} spin-orbit coupling effect. No attempt was made to interpret the experimental data.

2.4.2. **Complexes** {[Ag(L5)](NO_3)}$_n$ **(18)** and {[Ag(L5)](CF_3SO_3)·0.2H_2O}$_n$ **(18a)**

The reactions [under N_2 and protected from the light] of **L5** with $AgNO_3$ or $AgCF_3SO_3$ in 1:1 ratio lead to the formation of **18** in the form of light yellow crystals from slow evaporation of a methanolic solution or **18a** in the form of yellow-green crystals from an acetonitrile solution.

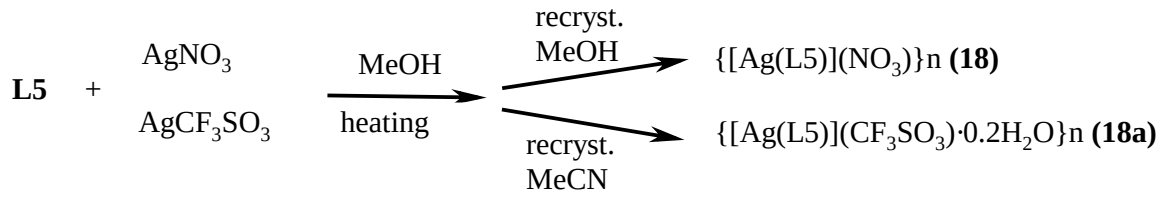

The IR spectra for compounds **18** and **18a** (Table 15) show that the characteristic ligand imine vibration at 1624 cm^{-1} is hardly shifted to 1625 and 1626 cm^{-1}. The pyridine C=N vibration at 1581 cm^{-1} is displaced to 1584 and 1592 cm^{-1} for compounds **18** and **18a** respectively. Bands arising from the ether group (1240 and 1198 cm^{-1}) are very slightly displaced as well at 1245 and 1196 cm^{-1} for **18**. For **18a** these bands are overlapped with the $CF_3SO_3^-$ bands. The NO_3^- and $CF_3SO_3^-$ non-coordinated anions show the expected vibration at 1338 and 1279-1251 cm^{-1} respectively.

Table 15. IR Data for the ligand **L5** and the complexes **18-18a**.

Compound	IR, ν [cm^{-1}]
L5	1624 (s, imine), 1581 (s), 1566 (m), 1495 (vs), 1467 (m), 1433 (m), 1344 (w), 1240 (vs), 1198 (s), 993 (m), 776 (s)
18	1625 (m, imine), 1584 (m), 1561 (w), 1494 (s), 1438 (w), 1338 (vs, nitrate), 1245 (s), 1196 (m), 1155 (m), 836 (m), 777 (w)
18a	1626 (m, imine), 1592 (s), 1561 (m), 1496 (vs), 1441 (m), 1420 (w), 1374 (w), 1279 - 1251 (vs, $CF_3SO_3^-$), 1056 (s), 1029 (s), 837 (m), 775 (m)

The structure of these two isostructural[&] complexes **18** and **18a** consists of a one-dimensional *zigzag* coordination polymer[34] (Figure 30). Similar single-stranded silver polymers have been reported previously[3,35-7]. The first reaction with $AgNO_3$ yielded only very small poor quality crystals and reactions with other counter ions were carried out in order to improve the quality of the crystal structure analysis [for this compound, the number of observed reflections was too small to allow a good refinement. In spite of this, for **18** the unit cell parameters were refined and the silver atom and the backbone atom positions were located. The structure is therefore not presented in detail].

[&] The only difference between compounds **18** and **18a** is the un-coordinated counter-ion.

At the same time, using BF_4^- as counter-ion Cheng *et al.*[8b] have very recently reported the structure of a silver (I) binuclear box-like structure $[Ag_2(L5)_2]^{2+}$. The possibility of obtaining a double-helix was previously postulated by other authors[6a,7c] for a similar ligand where the central ether linkage is replaced by a CH_2 group. In **18**, the Ag-N_{py} and Ag-N_{im} bond distances, of 2.283 (4) and 2.343 (4) Å, respectively, are similar to those observed in the above-mentioned complexes. The chelate bite angle of 72.69 (16) º is also within the expected range.

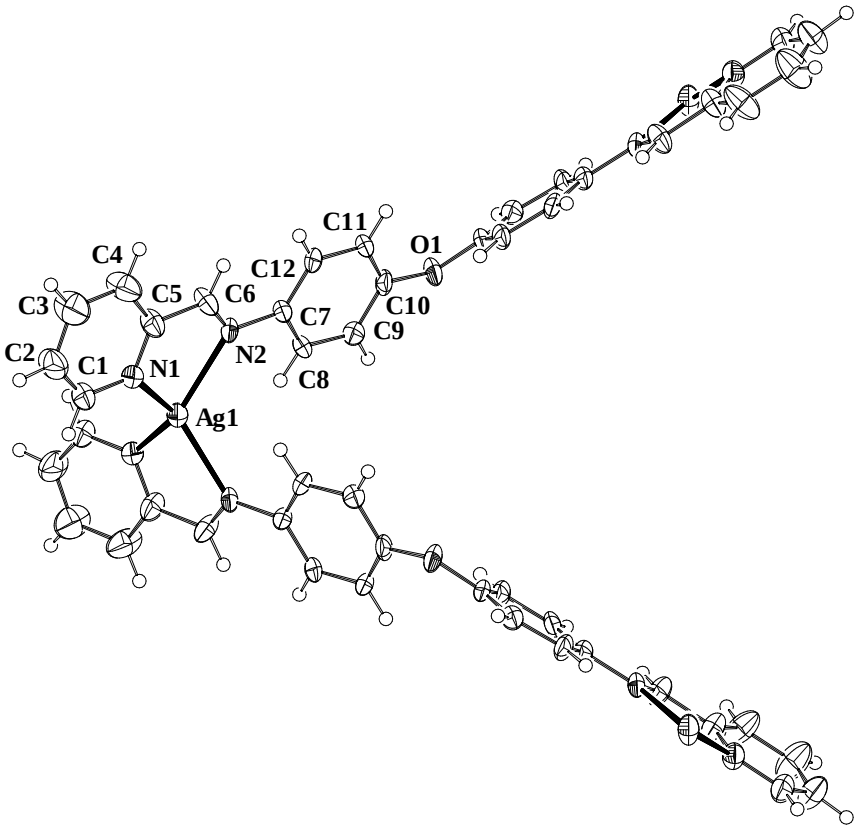

Figure 30. View of the polymeric complex **18a** showing the numbering scheme and thermal ellipsoids at 50% probability level. The disordered $CF_3SO_3^-$ anion and partially occupied water molecules have been omitted for clarity.

The ligand is twisted about the central O atom with the two phenyl rings being inclined by 51.09 (2) º. As was found in compounds **16** and **17**, the two halves of the ligand (related by a

twofold axis) are fairly planar which contrast with the structure of the ligand itself (Results, page 29) where one half of the ligand is much less planar than the other[33]. The best plane through atoms N1,C1-C6/N2,C7-C12 (pyridylimine + phenyl system) is planar to within 0.055 (5) Å and the Ag atom is displaced from this plane by 0.227 (5) Å.

In the crystal, the chains stack up the c axis with a π-π overlap of symmetry related aromatic rings; the shortest intermolecular C…C distance is *ca.* 3.52 (2) Å (Figure 31).

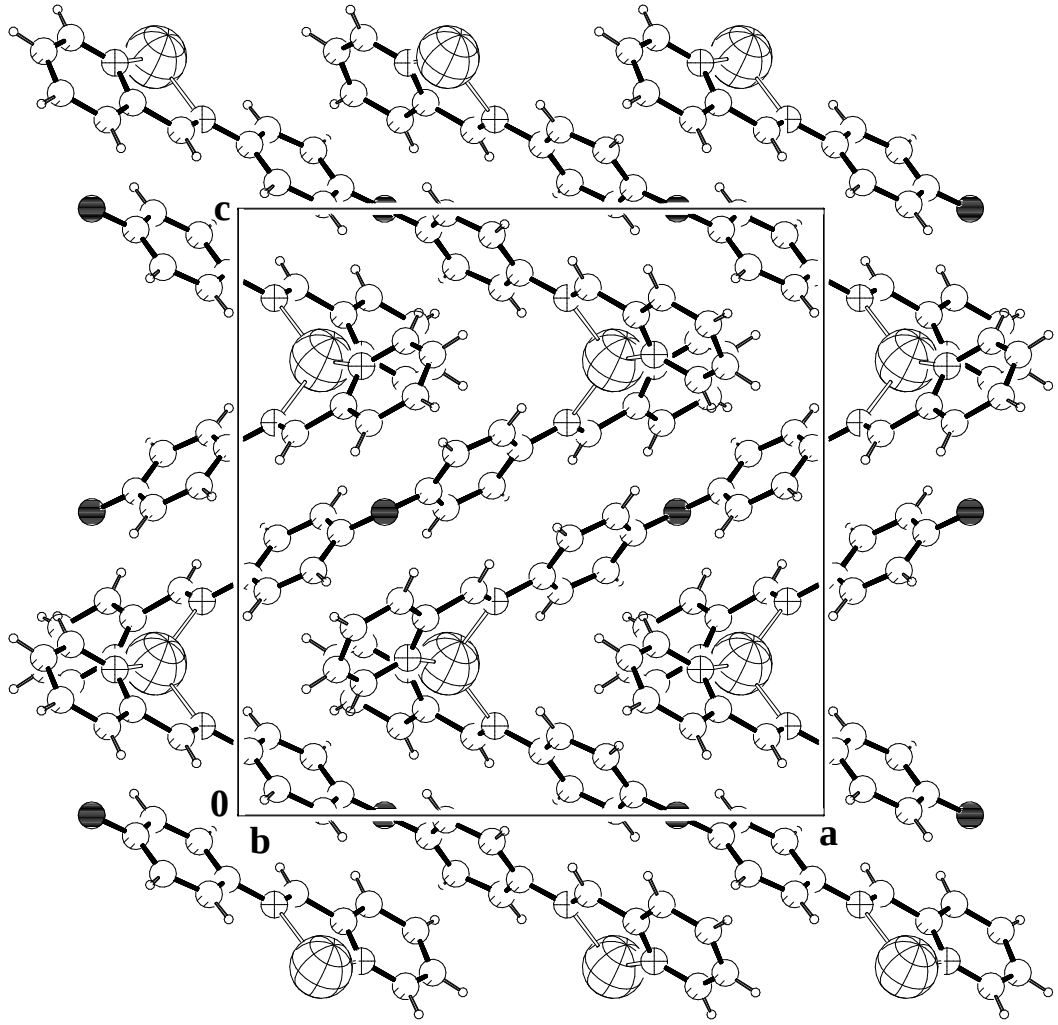

Figure 31. Crystal packing of compound **18a** viewed down the *b* axis showing the π-π interactions.

Compound **18a** crystallizes with one disordered $CF_3SO_3^-$ anion. The sulphur atom is located on a crystallographic inversion centre [with an occupation of 0.5] and therefore each atom of the anion is found in two positions.

Despite the polymeric nature of these two compounds in the solid state, the analysis of their positive ES-MS spectrum in acetonitrile indicates the presence in solution of a peak at *m/z* 486 in both cases, which corresponds to a binuclear complex $[Ag_2(L5)_2]^{2+}$ [consistent with a binuclear box or a double-helix structure]. The peaks at *m/z* 1034 (for **18**) and 1121 (for **18a**) correspond to $[Ag_2(L5)_2X]^+$ where X is the respective anion and confirm the stability in solution of this dimeric compound. Some extra peaks at *m/z* 655 and 865 (compound **18**) were assigned to $[Ag_2(L5)(NO_3)]^+$ and $[Ag(L5)_2]^+$, respectively. Analogues peaks at *m/z* 742 and 865 for compound **18a** correspond to $[Ag_2(L5)(CF_3SO_3)]^+$ and $[Ag(L5)_2]^+$, respectively. For compound **18** several ES-MS spectra have been measured at different voltages (5,10, 20 and 40 V). The peak at *m/z* 486 was always present whereas an increase in the voltage causes a decrease in intensity of other peaks. It is remarkable that the intensity of the peak at *m/z* 655 increases with the voltage suggesting that this species may be formed *in situ* under the conditions of the measurement.

The ^{1}H NMR spectra of compounds **18** and **18a** were also measured and compared with the corresponding spectrum of the free ligand as shown in the following table.

The ^{1}H NMR spectra of the complexes **18** and **18a** display six signals in the aromatic and imine region for the symmetrically coordinated ligand **L5** instead of seven for the free ligand [the signals for the pyridine protons Hc and Hd appear as a multiplet]. The signals are slightly displaced to higher chemical shifts (except for Hg). The largest displacement is found, as

expected, for the imine hydrogen atom, He, signal due to coordination of the N_{imine} atom to the metal.

Table 16. Comparison of ^{1}H NMR Data for **L5** and complexes **18** and **18a**.

	Chemical Shifts (δ, ppm)		
	L5	**18**	**18a**
Ha	8.70 [ddd, 2H]	8.79 [d, Ha, 2H]	8.78 [d, Ha, 2H]
Hb	7.54 [ddd, Hb, 2H]	7.73 [ddd, Hb, 2H]	7.70 [ddd, Hb, 2H]
Hc	8.00 [ddt, Hc, 2H]	8.12-8.19 [m, Hc, Hd, 4H]	8.12-8.14 [m, Hc, Hd, 4H]
Hd	8.24 (td, Hd, 2H]		
He	8.66 (s, imine, 2H)	8.92 [2H, s, imine, 2H]	8.89 [2H, s, imine, 2H]
Hf	7.43 [td, Hf, 4H]	7.50 [4H, td, Hf]	7.50 [4H, td, Hf]
Hg	7.14 [td, Hg, 4H]	7.08 [4H, td, Hg]	7.09 [4H, td, Hg]

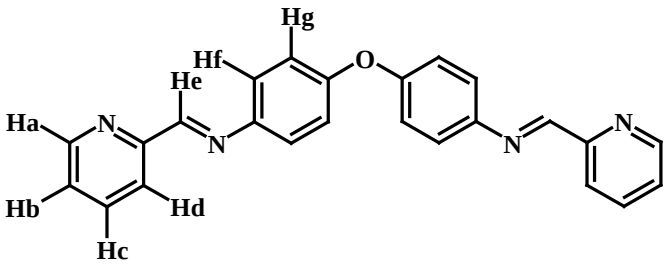

Scheme 14. Representation of **L5** showing the H atoms labelling scheme used for NMR spectra comparison.

UV-Vis titration experiments under the same conditions as for Co^{2+} and Ni^{2+}, were performed using $AgNO_3$ as metal salt. The next figure shows the changes observed in the UV-Vis spectrum of the free ligand upon addition of increasing concentrations of Ag^{+} in ethanol. The following observations can be made: (1) the absorption of the ligand band at 285 nm progressively decreases, (2) the ligand band at 340 nm is gradually displaced to 320 nm with a slight increase in intensity and (3) at the same time, this band broadens considerably (up to *ca*. 450 nm).

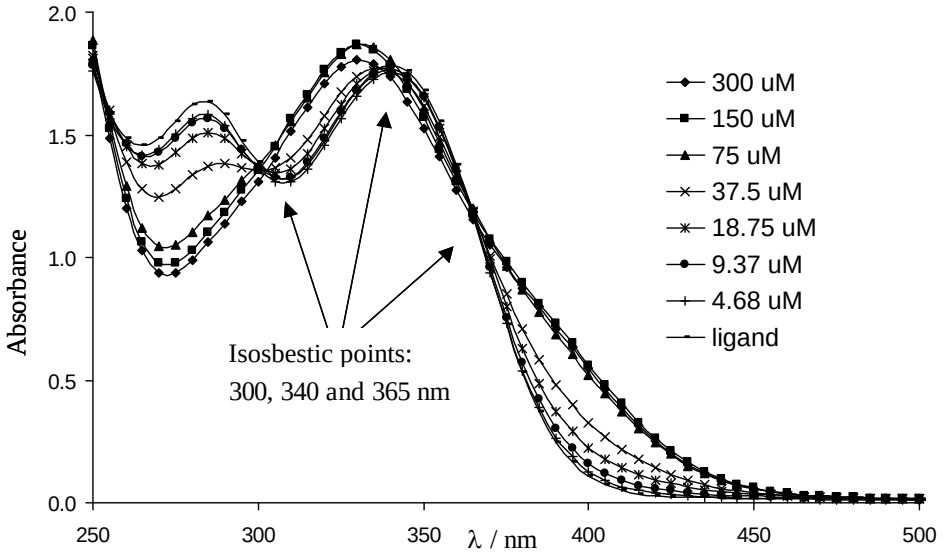

Figure 32. UV-Vis spectra of **L5** upon incremental addition of $AgNO_3$ in EtOH.

From the observation of the molecular ratio plot it is difficult to propose any M:L ratio. However, the presence of isosbestic points can be considered as an indication of the equilibrium between only two species.

UV-Vis titrations with other metal salts allowed us to make some interesting observations. The titration of **L5** with $Zn(ClO_4)_2 \cdot 6H_2O$ gave analogous results as with Co^{2+} or Ni^{2+}, as showed in the next figure. A first isosbestic point at 375 nm appears until a metal concentration equal to 75 μM. The addition of an excess of metal shifts the isosbestic point to 345 nm. As for Ni(II) and Co(II), the mole ratio plot at 345 nm (second isosbestic point) suggest a M:L ratio *ca*. 0.6. In addition, IR spectra of the powder obtained using Zn^{2+} salts show displacements for the imine band at 1636 cm^{-1} and for the pyridine C=N band at 1597 cm^{-1}. Non-coordinated ClO_4^- anions appear at 1091 cm^{-1}.

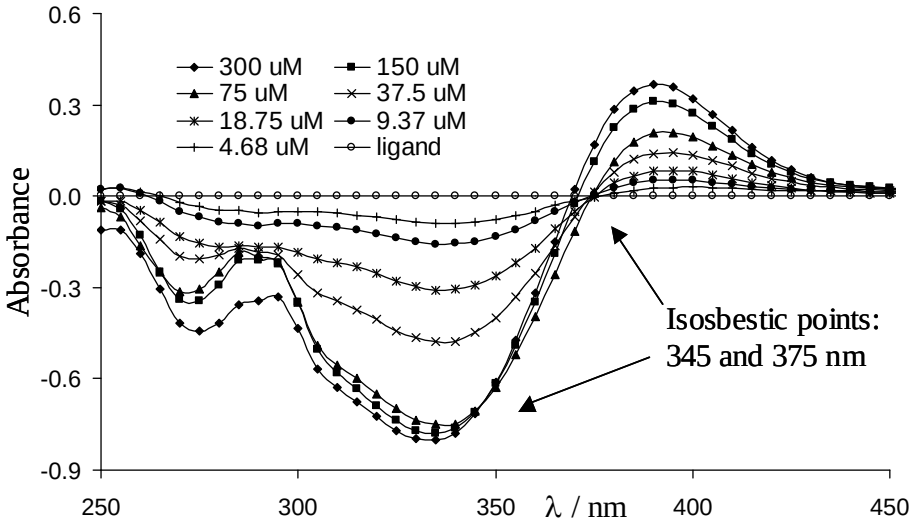

Figure 33. Difference UV-Vis spectra of **L5** upon incremental addition of $Zn(ClO_4)_2 \cdot 6H_2O$.

The ES-MS spectrum in acetonitrile exhibits a peak at m/z 316 that corresponds with the formulation $[Zn_2(L5)_3]^{4+}$. The peaks at higher m/z values can be assigned to aggregate species: m/z 455 → $[Zn_2(L5)_3(ClO_4)]^{3+}$, 732 → $[(Zn_2(L5)_3)_2(ClO_4)_4]^{4+}$, 1009 → $[(Zn_2(L5)_3)_2(ClO_4)_5]^{3+}$, 1148 → $[(Zn_2(L5)_3)_3(ClO_4)_8]^{4+}$ and 1564 → $[(Zn_2(L5)_3)_2(ClO_4)_9]^{3+}$. Unfortunately, it was impossible to obtain X-ray quality crystals of this Zn compound. We think that depending on the metal atom the triple-helical structure can turn more or less about the helical axis during crystal growth. We suppose in the case of Zn that disorder problems [already present in compound **16**] prevent the formation of suitable single crystals.

When $HgCl_2$ was used for the titration experiments, only very insignificant changes in the UV-Vis spectrum of **L5** were observed. In the case of $Mn(ClO_4)_2 \cdot 6H_2O$, the changes are slightly larger but still unimportant. The case of Fe^{2+} is more interesting (Figure 34). The addition of this metal to a solution of **L5** causes a net decrease in the intensity of the ligand bands at 285 and 340 nm, the enlargement of the band at 340 nm up to *ca*. 440 nm and the growth of a new band at about 580 nm. An isosbestic point appears at *ca*. 380 nm. The purple

colour of the solution, characteristic of low-spin iron (II) trispyridylimine compounds, could be consistent with the presence of iron (II) in an octahedral environment, as is the case of a triple helicate.

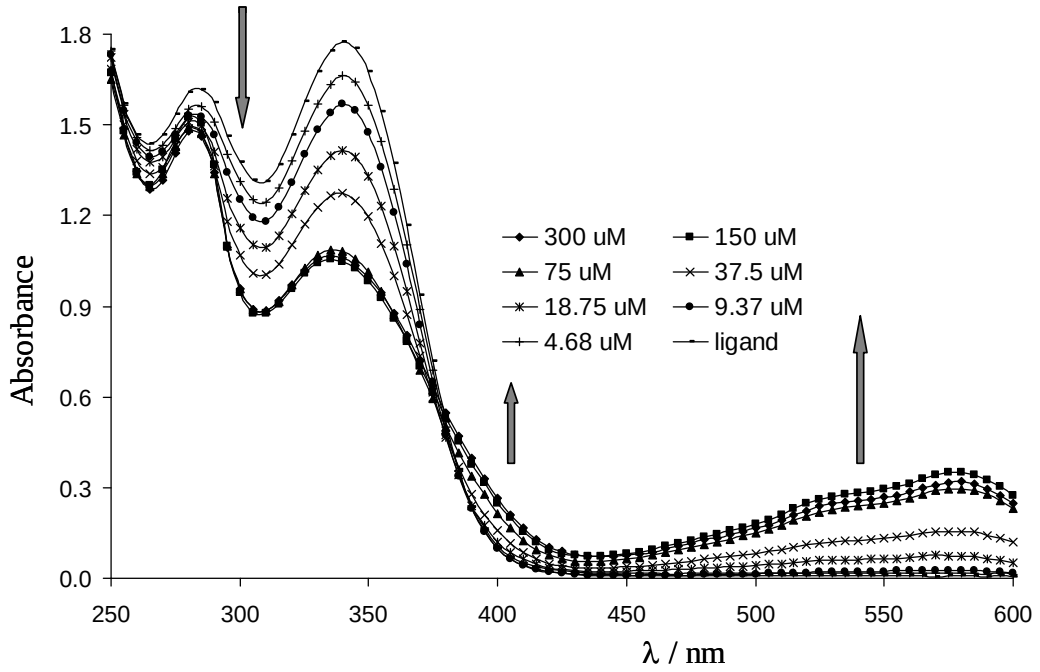

Figure 34. UV-Vis spectra of **L5** upon incremental addition of $Fe(ClO_4)_2 \cdot 6H_2O$ in EtOH.

The reaction of three equiv. of **L5** with two equiv. of $FeCl_2 \cdot 4H_2O$ and, in a second step, four equiv. of $[NH_4][BF_4]$ gave a purple precipitate soluble in acetonitrile. The analysis of the ES-MS spectrum is analogous to those of compounds **16** and **17** and indicates the presence of a peak at m/z 311 that corresponds with the formulation $[Fe_2(L5)_3]^{4+}$. A number of peaks at higher m/z values can be assigned to aggregate species: m/z 710 → $[(Fe_2(L5)_3)_2(BF_4)_4]^{4+}$, 975 → $[(Fe_2(L5)_3)_2(BF_4)_5]^{3+}$, 1109 → $[(Fe_2(L5)_3)_3(BF_4)_8]^{4+}$ and 1507 → $[(Fe_2(L5)_3)_2(BF_4)_9]^{3+}$.

Finally, it is interesting to compare the results obtained with Cu^+ and Cu^{2+}salts. UV-Vis titration of **L5** with CuAcO gave two isosbestic points at 265 and 370 nm, indication of a clean reaction [consistent with the marked geometrical preferences of Cu^+]. As it was the case with other ligands and Cu^+, the saturation was not achieved under the conditions of the

experiment. The ability of Cu^{2+} to adopt different coordination geometries lead to a more complicated UV-Vis titration analysis, as showed in Figure 35 where the results obtained with these two metal ions are illustrated. In this case the new band appears at 365 nm and an isosbestic point emerge at 385-90 nm but only until a metal concentration equal to 18.75 μM (very small with respect to the concentration of the ligand of 125 μM).

(a)

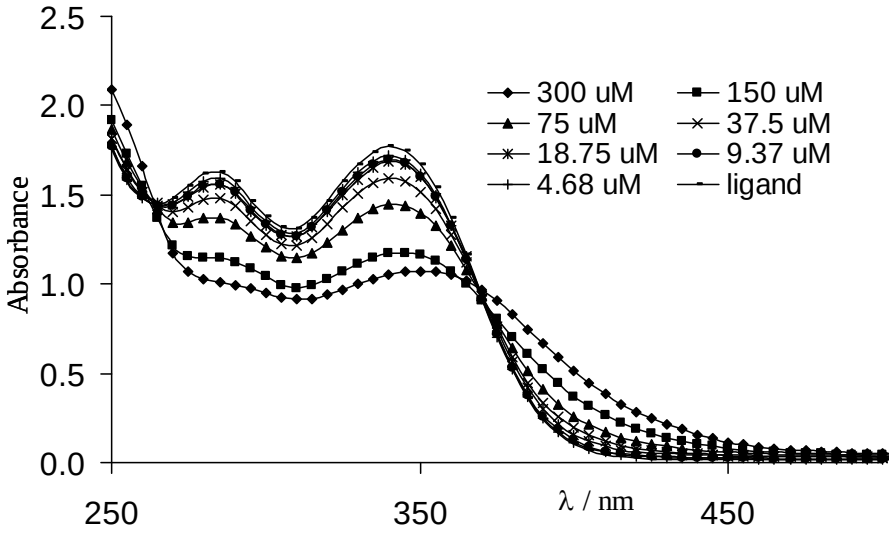

(b)

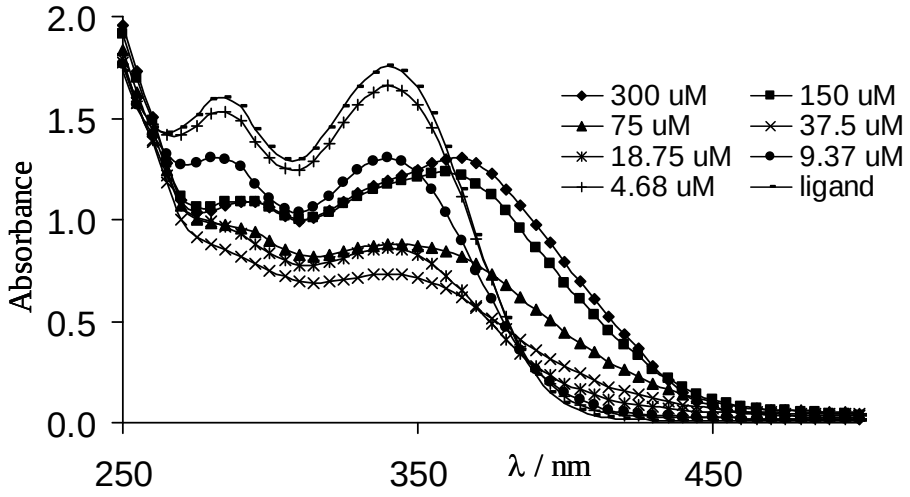

Figure 35. Comparison of UV-Vis spectra of **L5** upon incremental addition of (a) CuAcO and (b) $Cu(NO_3)_2 \cdot 3H_2O$ in EtOH.

2.5. Coordination behaviour of ligand L6

Unfortunately it was impossible to obtain crystals of metal complexes containing this ligand. In spite of this and in order to learn a little about the way in which this ligand reacts with the metal ions, UV-Vis titrations experiments of the ligand **L6** under the same conditions used for the precedent ligands have been carried out. This ligand has a pyrrol instead of a pyridine ring and therefore the chelating group is formed by the N_{pyrrol}-C-C-N_{imine}. The pyrrol NH group must be deprotonated in order to coordinate. Some metals are able to do this spontaneously and the conditions of realization of the titration experiments (no additional base was used) should help to select the best candidates for coordination. The titration with Hg^{2+}, Cd^{2+}, Mn^{2+} and Ag^{+} salts did not lead to any changes in the UV-Vis spectrum of the free ligand indicating that no reaction takes place. In the cases of Zn^{2+}, Ni^{2+} or Co^{2+} (see Figure 36), only small changes were observed. The ligand band at 340 nm decreases in intensity and broadens.

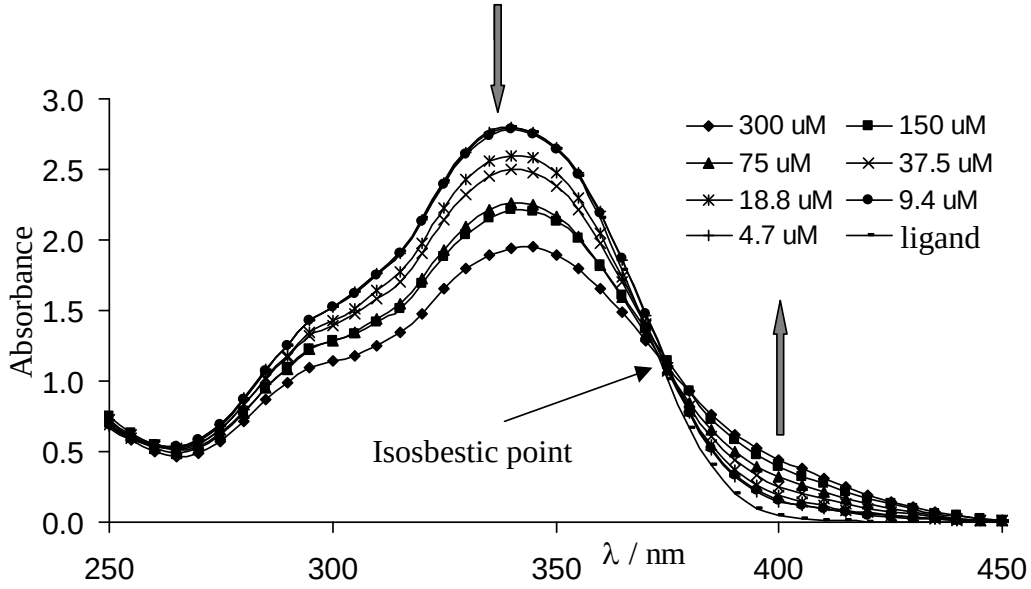

Figure 36. UV-Vis spectra of **L6** upon incremental addition of $Zn(ClO_4)_2 \cdot 6H_2O$ in EtOH. Titrations with $Co(BF_4)_2 \cdot 6H_2O$ and $Ni(ClO_4)_2 \cdot 6H_2O$ gave similar results.

The formation of an isosbestic point at 375 (for Ni^{2+} and Zn^{2+}) or 380 (for Co^{2+}) nm is also observed. The cases of Fe^{2+}, Cu^{2+} and Cu^{+} are more complicated. The ligand **L6** undoubtedly reacts with these three metal ions under the conditions of the experiment (ethanol solution, room temperature and absence of a deprotonating base). In the case of Fe^{2+}, there is a net increase in absorption up to *ca*. 450 nm together with the formation of a clear isosbestic point at 375 nm, as showed in the next figure. The ligand maximum at *ca*. 290 nm, which appears as a shoulder in the spectrum of the ligand, also becomes more pronounced.

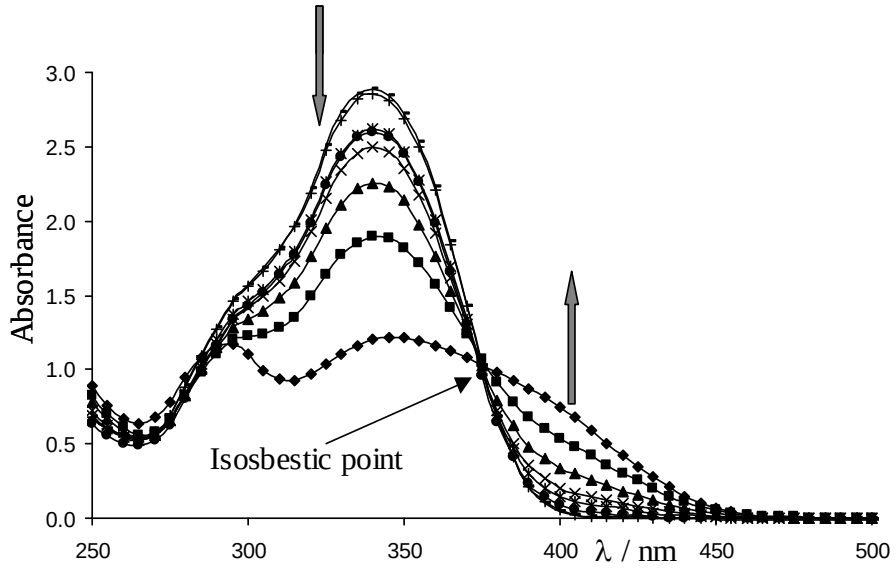

Figure 37. UV-Vis spectra of **L6** upon incremental addition of $Fe(ClO_4)_2 \cdot 6H_2O$ in EtOH.

The titrations with Cu^{2+} and Cu^{+} present some differences. For Cu^{+} an isosbestic point is formed at 365 nm until the metal concentration reaches 75 μM and then, for the two most concentrated solutions, it disappears. At the same time, the ligand band at 340 nm continuously suffers a bathochromic displacement. For Cu^{2+} the isosbestic point at 370 nm remains constant although for the most concentrated solutions it is slightly displaced. In this case the changes in absorbance are quite uniform with respect to the relative metal concentration and the saturation value of absorbance is reached whereas for Cu^{+} the largest changes in absorption occur at the concentrations 150 and 300 μM, when the concentration of

metal exceeds the concentration of the ligand. The following figure shows the main changes observed in the UV-Vis spectrum of **L6** upon addition of Cu^{2+} and Cu^{+}.

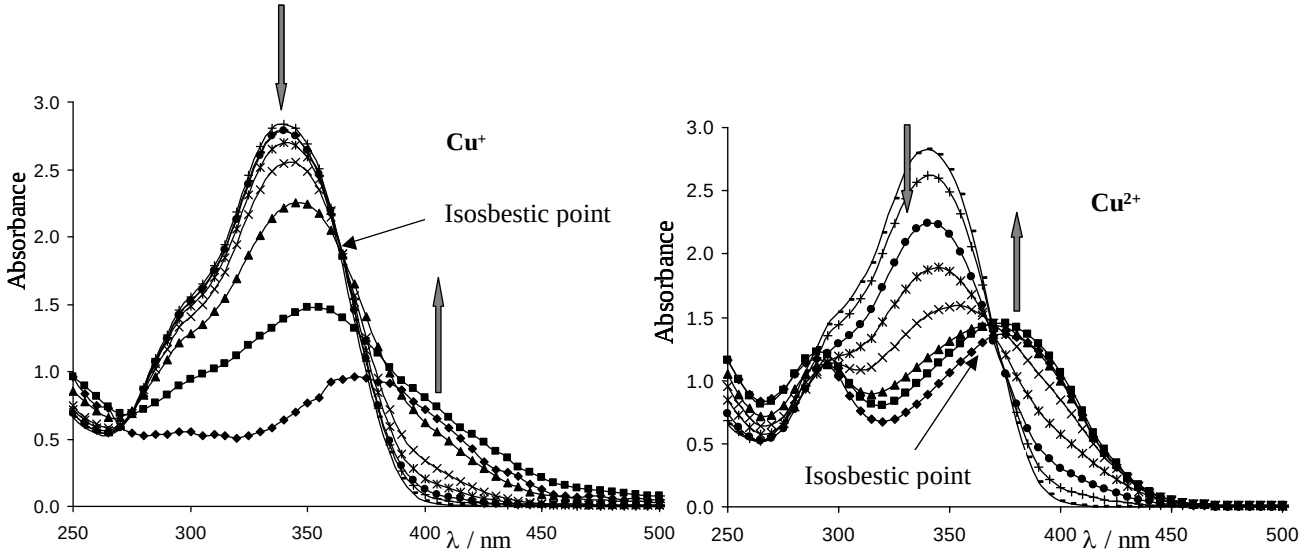

Figure 38. UV-Vis spectra of **L6** upon incremental addition of CuAcO and $Cu(NO_3)_2 \cdot 3H_2O$.

It is interesting to note that the maximum (shoulder) at *ca*. 290 nm for the ligand has disappeared for Cu^{+} but becomes more pronounced and resolved for Cu^{2+}.

For these three cases (Fe^{2+}, Cu^{2+} and Cu^{+}) the colour of the solutions observed during the titration experiments was always orange-brown and never green or purple.

In general, light colours were observed in all the cases perhaps due to the fact that the metal ions were only weakly coordinated. The crystal structures of some metal complexes with ligands containing pyrrol units have been reported[38]. The metals used were Co^{3+}, Zn^{2+}, Cu^{2+} and Ni^{2+}. In some cases only one pyrrol NH group was deprotonated and the coordination sphere of the metal ion was completed by the counter-ions used during the reaction. In our case, the use of a base (NEt_3) to induce the NH group deprotonation leads to the formation of quite insoluble precipitates (for example in the case of silver). Water-soluble bases were avoided to prevent the possible hydrolysis of the ligand.

2.6. Coordination behaviour of ligand L7

The reaction of CdI_2 with **L7** using diffusion techniques, in dilute conditions and at room temperature, afforded in about one week golden crystals of the polymeric complex $[Cd(L7)I_2]_n$ **(19).**

$$\mathbf{L7}/CH_2Cl_2 \quad + \quad CdI_2/MeOH \xrightarrow{\text{diffusion}} [Cd(L7)I_2]_n \ \mathbf{(19)}$$

The IR spectrum of **19** shows the main characteristic signals of **L7** slightly displaced to higher frequencies as given in the following table.

Table 17. IR Data for the ligand **L7** and the complex **19**.

Compound	IR, ν [cm^{-1}]
L7	1622 (m, imine), 1594 (m), 1584 (m), 1572 (m), 1497 (vs), 1428 (m), 1282 (m), 1246 (vs), 1237 (vs), 1197 (m), 834 (s), 757 (s)
$[Cd(L7)I_2]_n$ (**19**)	1637 (m, imine), 1613 (w), 1586 (s), 1557 (w), 1506 (s), 1485 (vs), 1431 (m), 1377 (m), 1344 (s), 1254 (vs), 1226 (s), 1161 (m), 845 (s), 754 (s)

The X-ray structure of this complex is illustrated in Figure 39. It can be described as a single-stranded helical *C_2*-coordination polymer. Several polymeric helices (mainly with silver as metal ion) have been reported previously[35-37]. The solid-state structure of compound **19** is quite unusual in that its asymmetric unit contains two independent and slightly different molecules both of formula $[Cd(L7)I_2]$. Each one of these two molecules generates, upon translations along the *b* axis, an infinite helical chiral species.

The 1:1 mixture of the two possible helical enantiomers (Δ and Λ) ordered in chains of alternating chirality, forms the average structure.

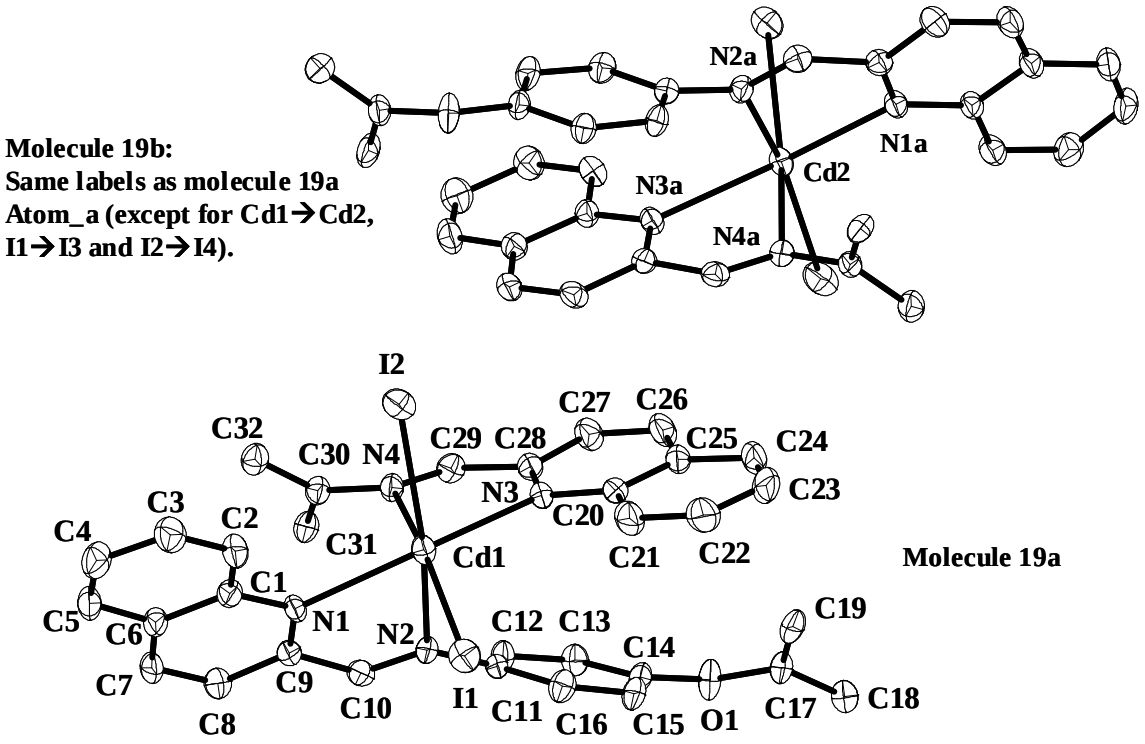

Figure 39. View of the asymmetric unit of the polymer **19** showing the crystallographic numbering scheme for one of the two independent molecules and thermal ellipsoids at 50% probability level.

In **19** the metal atoms in both independent molecules are six coordinate with a distorted octahedral geometry (very similar for Cd1 and Cd2) and are coordinated to two pyridilimine units and to two iodine atoms. The distortions from the ideal octahedron are mainly due to the small bite angle of the pyridilimine units, Table 18. The average Cd-N_{im} bond distance of 2.464 (3) Å is comparable to the standard values of 2.399 / 2.457 Å whereas the average Cd-N_{qui} bond distance of 2.484 (3) Å is slightly longer than the distance of 2.330 Å for the complex reported by Cameron *et al*.[39]. The Cd-I bond distances are within the range of values found in the literature [from 2.702 to 3.000 Å][40]. The imine groups possess the *E* configuration. Selected bond distances and angles are showed in Table 18.

Table 18. Selected bond lengths (Å) and angles (º) for compound **19**. The two independent molecules are named **19a** and **19b**.

	19a	**19b**
Cd1-N1	2.445 (3)	2.474 (3)
Cd1-N2	2.400 (3)	2.412 (3)
Cd1-N3	2.517 (3)	2.499 (3)
Cd1-N4	2.539 (3)	2.506 (3)
Cd1-I1	2.8367 (4)	2.8409 (4)
Cd1-I2	2.8179 (4)	2.8020 (4)
N2-Cd1-N1	69.33(9)	68.77(9)
N2-Cd1-N3	85.83(9)	84.27(9)
N1-Cd1-N3	146.03(9)	144.65(9)
N2-Cd1-N4	72.56(9)	72.63(9)
N1-Cd1-N4	83.18(9)	81.58(9)
N3-Cd1-N4	67.03(9)	68.43(9)
N2-Cd1-I2	161.08(7)	161.50(7)
N1-Cd1-I2	106.09(7)	109.67(7)
N3-Cd1-I2	89.82(6)	88.66(6)
N4-Cd1-I2	88.79(6)	88.88(6)
N2-Cd1-I1	91.59(7)	92.15(7)
N1-Cd1-I1	92.14(6)	90.25(6)
N3-Cd1-I1	111.98(7)	113.96(7)
N4-Cd1-I1	164.12(6)	164.49(6)
I2-Cd1-I1	107.09(1)	106.34(1)

On comparing the crystal structures of both the free ligand **L7** and the complex **19**, important differences are observed. The crystal structure of **L7** is non-centrosymmetric. The two halves of the molecule are quite planar and do not differ significantly, with dihedral angles of 9.73 (2) and 17.85 (1) º between the quinoline and the phenyl rings (see Results, page 33). Compound **19** is centrosymmetric and it exhibits a much larger twist between aromatic rings (see Table 19, p.98). The helical chains run parallel to the crystallographic *b* axis with an intramolecular Cd…Cd^{i} (i = x, y±1, z) distance of 10.9009 (7) Å ≡ length of the *b* axis.

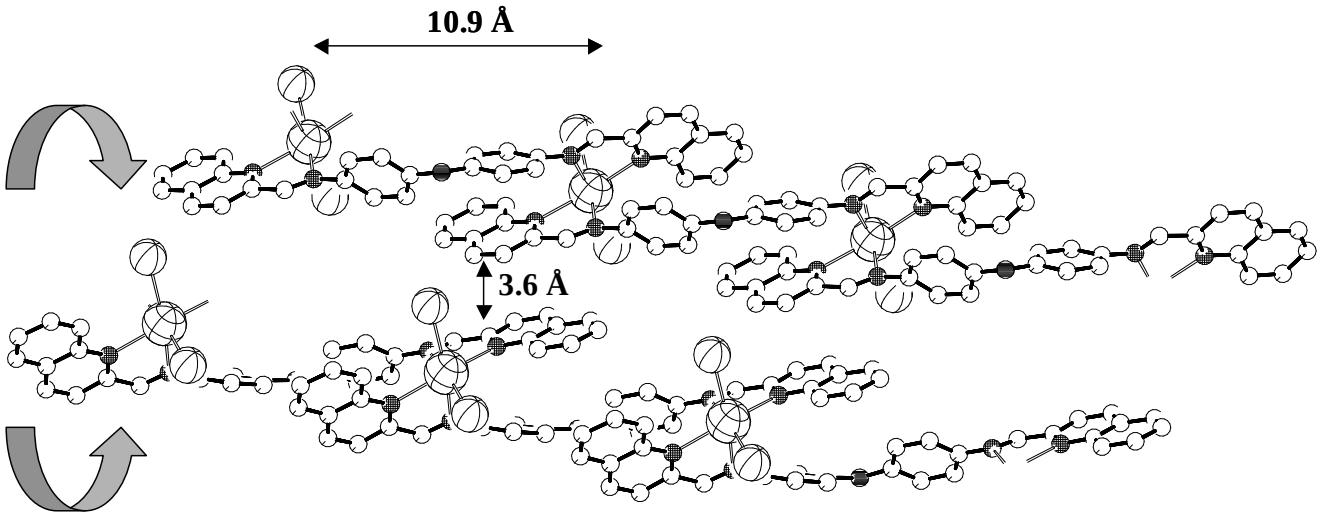

Figure 40. Polymeric structure of the complex $[Cd(L7)I_2]_n$ (**19**). H atoms have been omitted for clarity.

In Table 19, various dihedral angles and distances are compared between the two independent molecules present in compound **19**. It is remarkable that these molecules are not geometrically equivalent, with molecule **19b** being in general more twisted than molecule **19a**. In both molecules the chelating quinoline-imine system is almost planar and the metal atoms are displaced by distances of between 0.041 (7) and 0.493 (6) Å from the mean chelate ring plane.

Although the two helical "enantiomers" generated from the moieties **19a** and **19b** are not identical, each one of them reproduces, by means of a symmetry centre [compound **19** crystallizes in the centrosymmetric space group P 2_1/c], the other conformer and the final result is the 1:1 racemic mixture. Some π-π stacking interactions can be observed with an average distance of *ca*. 3.6 Å between the rings N3-C20-C25-C26-C27-C28 and N3a-C20a-C25a-C26a-C27a-C28a and may have an effect on the self-assembling process.

Table 19. Selected dihedral angles (t, º) and distances (d, Å) for **19**. The two independent molecules are named **19a** and **19b**.

	19a	**19b**
t (q1-che$_1$)	3.59 (22)	4.59 (23)
t (q2-che$_2$)	4.89 (28)	6.77 (26)
d (Cd-che$_1$)	0.4929 (65)	0.0406 (69)
d (Cd-che$_2$)	0.2381 (73)	0.4654 (66)
t (q1 - ϕ_1)	46.17 (8)	60.12 (8)
t (ϕ_1 - ϕ_2)	39.23 (8)	51.91 (9)
t (q1 - q2)	54.55 (7)	63.54 (7)
t (q2 - ϕ_1')	54.65 (9)	64.18 (8)
t (ϕ_1' - ϕ_2')	39.23 (4)	51.91 (9)

Definitions.
For molecule **19a**:**che$_1$**: Cd1-N1-C9-C10-N2; **che$_2$**: Cd1-N3-C28-C29-N4;
q1: N1,C1-C19 ; **q2**: N3, C20-C28, **ϕ_1, ϕ_2, ϕ_1'** and **ϕ_2'**: phenyl groups.
For molecule **19b**: analogue manner.

No disorder was found in compound **19** and an empirical absorption correction using DIFABS in PLATON[25] was applied.

2.7. Coordination behaviour of ligand L8

This ligand can be classified as a *compartmental ligand* using the terminology of Fenton *et al*. who have prepared a series of compartmental Schiff base ligands using pyrrole units and having two dissimilar "N_2O_2" or "N_4" donor sites for metal complexation with different bridges. These ligands were used to study the selective preferences of the metal atom and the effect of the bridge extension[38a]. Recently, an interesting *two-compartmental* receptor ligand capable of moving a metal from one site to another by a change of pH was reported[41]. Bridging amino ether units are commonly used for the formation of macrocyclic ligands[42] but only a few acyclic related compounds are known[38a,43,44]. Lam *et al*[45] have recently described the formation of mono-helical zinc(II) and europium(II) complexes of a similar ligand formed by the reaction of 3-(pyridine-2-yl)pyrazole with the same bridging amino ether unit.

The ligand **L8** reacts with a variety of metal ions and the complexes, $[Ag(L8)](BF_4)$ (**20**), $[Zn_2(L8)Cl_4]$ (**21**), $[Hg_2(L8)Cl_4]$ (**22**), $[Cd_2(L8)I_4]$ (**23**), $[M_2(L8)_3](ClO_4)_4$ with M = Co^{II} (**24**) Fe^{II} (**25**) and Zn^{II} (**26**),and $[Ni_2(L8)_3](BF_4)_4$ **(27)**, have been synthesized and characterized crystallographically.

2.7.1. Complex $[Ag(L8)](BF_4)$ (20)

The reaction of **L8** with $AgBF_4$ in a 1:1 ratio leads to the formation of the mononuclear complex, $[Ag(L8)](BF_4)$ **(20)**.

$$\mathbf{L8} + AgBF_4 \xrightarrow[\text{Reflux, } N_2\text{, no light}]{\text{MeOH}} [Ag(L8)](BF_4)\ \mathbf{(20)}$$

The IR spectrum of compound **20** (Table 20) exhibits the characteristic imine, C_{ar}-N, C_{ar}-C_{ar} (pyridine) and C-O-C vibrations shifted to higher or lower frequencies with respect to the IR spectrum of **L8**. The bands of the BF_4^- anion overlap with the ether bands.

Table 20. IR Data for the ligand **L8** and the complex **20**.

Compound	IR, ν [cm^{-1}]
L8	1651 (s, imine), 1588 (vs), 1568 (m), 1469 (s), 1436 (s), 1353 (m), 1294 (w), 1122 (vs), 993 (m), 776 (s)
[Ag(L8)](BF_4) (**20**)	1660 (m, imine), 1588 (s), 1568 (m), 1473 (m), 1438 (m), 1371 (w), 1308 (m), 1230 (m), 1127-1084-1044 (vs, BF_4), 773 (s)

The structure can be considered as a mono-helical complex where the silver atom is encapsulated by a single ligand molecule, Figure 41.

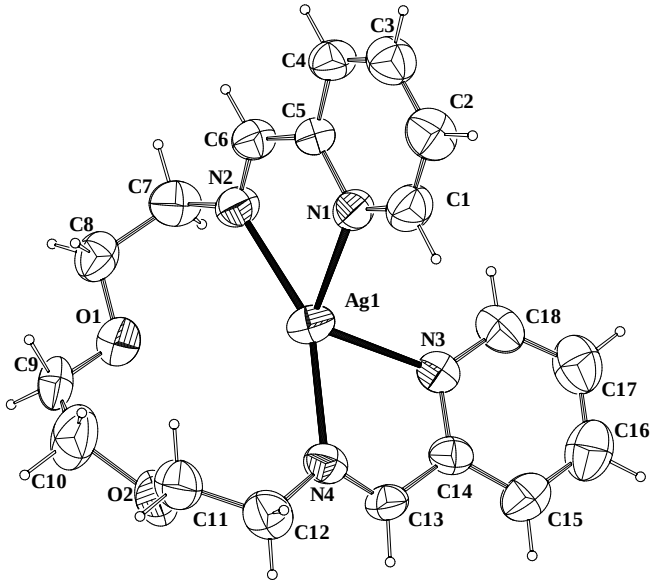

Figure 41. Molecular structure of cation $[Ag(L8)]^+$ (**20**) showing the crystallographic numbering scheme and thermal ellipsoids at 50% probability level.

A number of examples of mono-helical complexes with different ligand molecules have been published[45-49]. The silver atom has a distorted tetrahedral geometry and is coordinated to the

two pyridylimine units of one ligand molecule. Selected bonds distances and bond angles are given in Table 21.

Table 21. Selected geometric parameters (Å,°) for [Ag(L8)](BF_4) (**20**).

Ag1-N1	2.385(5)	Ag1-N3	2.410(6)
Ag1-N2	2.277(5)	Ag1-N4	2.251(5)
N1-Ag1-N2	72.49(17)	N3-Ag1-N4	72.57(17)
N1-Ag1-N3	105.74(45)	N2-Ag1-N4	154.37(17)
N1-Ag1-N4	125.99(16)	N2-Ag1-N3	123.12(17)

The N_{py}-Ag-N_{im} bite angles are very narrow with an average value of 72.5(1)°. The average Ag-N_{py} bond length of 2.398(4) Å is significantly longer than the standard value[24] of 2.299 Å, while the average Ag-N_{im} bond distance of 2.264(4) Å, is considerably shorter than the standard value[24] for Schiff bases, 2.403 Å (see Table 10). The helicity is caused by a twist of **L8** about the very flexible C-O-C-C-O-C chain linking the two pyridylimine units. This twist leads to a dihedral angle between the two pyridine rings (**py_1**, **py_2**) of 74.6 (2)° while the systems **py_1-che_1** and **py_2-che_2**[2] are almost planar with dihedral angles of 1.6 (3) ° and 9.3 (3)° respectively.

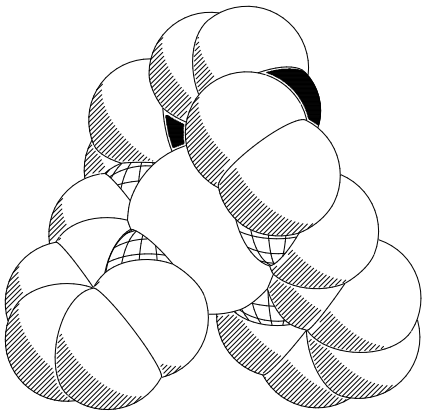

Figure 42 illustrates the space filling representation of the cation $[Ag(L8)]^+$ (BF_4^- anion and H atoms omitted). The flexible ether aliphatic chain of the ligand does not offer available space even for very small molecules.

Figure 42

[2] **che_1:** chelate ring Ag1-N1-C5-C6-N2; **che_2:** chelate ring Ag1-N3-C14-C13-N4.

The complex crystallizes in a non-centrosymmetric space group C c and the average structure is formed by the racemic mixture of the two possible helical enantiomers.

This can be clearly observed in the representation of the molecular packing of the cation $[Ag(L8)]^+$ (Figure 43, H atoms and counter ions omitted for clarity). The crystal selected for the X-ray measurements was a racemic twin, as shown by the refined value of the Flack parameter[50], x = 0.37.

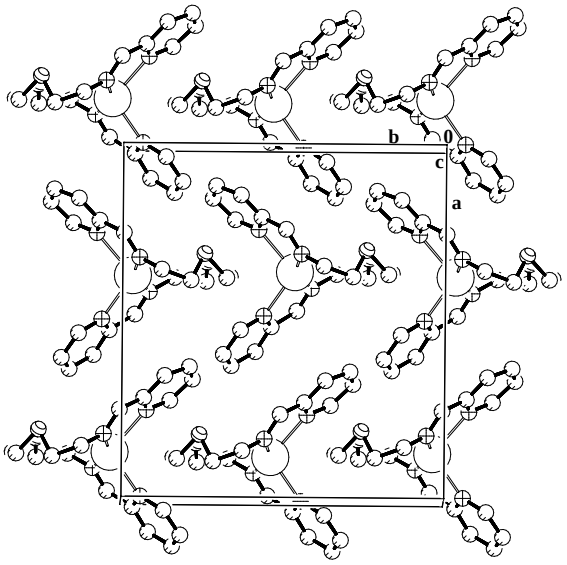

Figure 43

Compound **20** crystallizes with one highly disordered BF_4^- anion with occupancies of 0.5 for all of the fluorine atoms. Part of the ligand was also found to be disordered with occupancies of 0.4 and 0.6 for atoms C9, C10 and $C9^a$, $C10^a$, respectively. The thermal parameters for the fluorine atoms were constrained to be equal in the refinement process.

Apart from the crystallographic analysis, a number of techniques have been employed with the aim of understanding the behaviour of this compound in solution. This complex is soluble in several solvents such as methanol and acetonitrile. The analysis of the positive ES-MS spectrum in acetonitrile indicates the presence of only one peak at *m/z* 435, assigned to $[Ag(L8)]^+$ which corresponds with the solid state compound.

The ^1H NMR spectrum was recorded for **20** and compared with the corresponding spectrum of the free ligand (Table 22). The ^1H NMR spectrum of **20** shows five signals in the aromatic

region for the symmetrically coordinated ligand **L8** and two more resonance sets in the CH_2 region. The signals were slightly displaced to higher or lower chemical shifts depending on the H-atom. The largest displacement was found, as expected, for the imine hydrogen atom, He, signal due to the coordination of the N_{im}-atom to the metal.

Table 22. Comparison of ^{1}H NMR Data for **L8** and Complex [Ag(L8)](BF_4) (**20**).

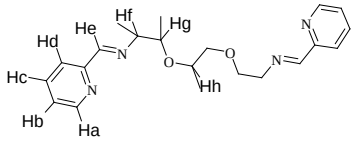 **L8**	Chemical Shifts (δ, ppm)	
		[Ag(L8)](BF_4) (**20**)
Ha	8.62 [ddd, ^{3}J(a,b) = 4.9, ^{4}J(a,c) = 1.7, ^{5}J(a,d) = 1.0, 2H]	8.53 [ddd, ^{3}J(a,b) = 4.8, ^{4}J(a,c) = 1.6, ^{5}J(a,d) = 0.8, 2H]
Hb	7.48 [ddd, ^{3}J(b,c) = 7.5, ^{3}J(b,a) = 4.9, ^{4}J(b,d) = 1.2, 2H]	7.67 [ddd, ^{3}J(b,c) = 7.7, ^{3}J(b,a) = 4.8, ^{4}J(b,d) = 1.2, 2H]
Hc	7.90 [ddt, ^{3}J(c,d) = 7.9, ^{3}J(c,b) = 7.5, ^{4}J(c,a) = 1.7, ^{5}J(c,e) = 0.5, 2H]	8.13 [dt, ^{3}J(c,d) = 7.7, ^{3}J(c,b) = 7.7, ^{4}J(c,a) = 1.6
Hd	8.01 [td, ^{3}J(d,c) = 7.9, ^{4}J(d,b) = 1.2, ^{5}J(d,a) = 1.0, 2H]	7.87 [td, ^{3}J(d,c) = 7.7, ^{4}J(d,b) = 1.2, ^{5}J(d,a) = 0.8, 2H]
He	8.36 (s, broad, 2H)	8.70 (s, broad, 2H)
Hf	3.64 (s, broad, 4H)	3.62 (s, broad, 4H)
Hg,h	3.79 (m, 8H)	3.95 (m, 8H)

Finally, UV-Vis titration experiments of the ligand (125 μM in EtOH) with addition of increasing quantities of silver nitrate solutions ($[Ag]^+$ = 0, 4.7, 9.4, 18.7, 37.5, 75, 150 and 300 μM, in EtOH) have been carried out.

The next figure shows the change in the UV-Vis spectrum (only the significant region from 250 to 350 nm is presented) that occurs when **L8** coordinates to Ag^+ ion in EtOH. Upon addition of Ag^+ ion to the ligand solution, the ligand band at 270 nm is progressively displaced to 280 nm. The *difference-spectra*[&] plot with the free ligand as reference shows that the change in absorption is maximal at 290 nm. The presence of an isosbestic point at 265 nm is the indication of a clean reaction.

(a)

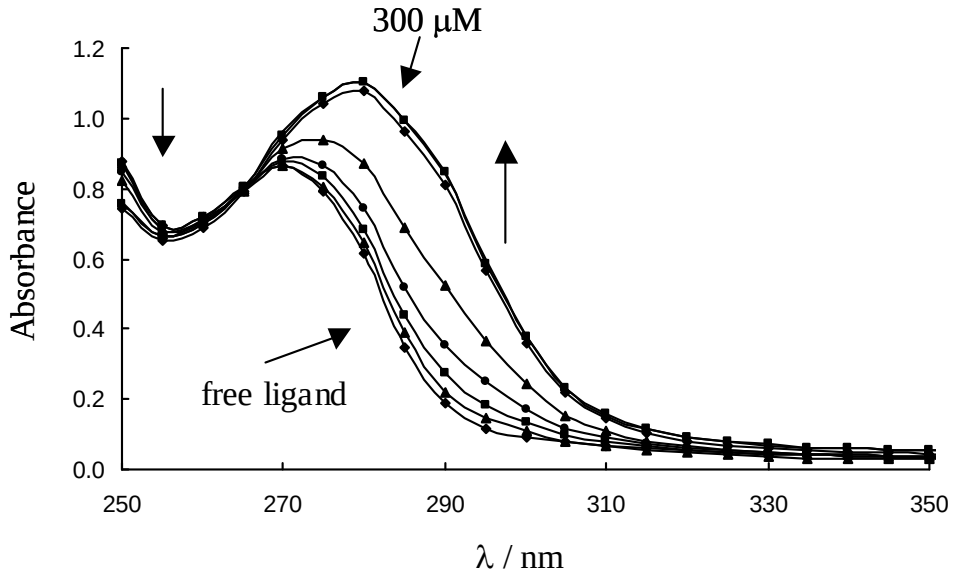

(b)

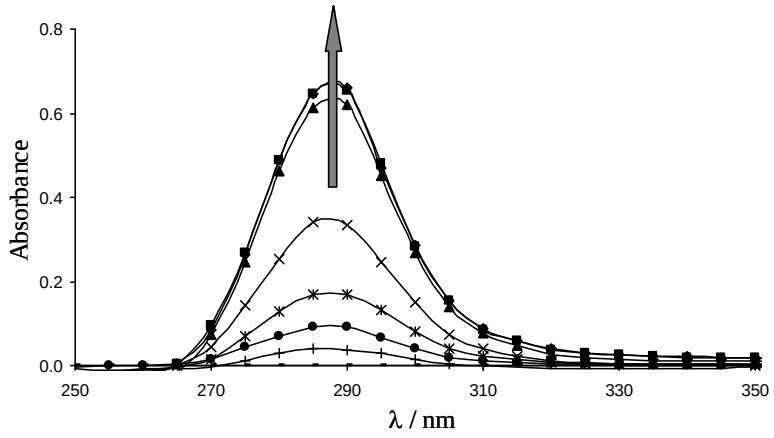

Figure 44. (a) UV spectra of **L8** upon incremental addition of $AgNO_3$ in EtOH, **(b)** *difference-spectra* plot.

[&] Obtained by the subtraction of the UV-Vis spectrum of **L8** to each of the measured spectra.

2.7.2. Complexes $[M_2(L8)X_4]$ where M = Zn^{2+} for (**21**), Hg^{2+} for (**22**) and for Cd^{2+} (**23**); X = Cl^- for (**21**) and (**22**) or I^- for (**23**)

The reaction of **L8** with $ZnCl_2$, $HgCl_2$ and CdI_2, using diffusion techniques and in dilute conditions, gave in a few days, crystals of the centrosymmetric binuclear complexes: $[Zn_2(L8)Cl_4]$ (**21**), $[Hg_2(L8)Cl_4]$ (**22**) and $[Cd_2(L8)I_4]\cdot CH_2Cl_2$ (**23**).

$$\textbf{L8}/CH_2Cl_2 \;+\; \begin{matrix} ZnCl_2/MeOH \\ HgCl_2/MeOH \\ CdI_2/MeOH \end{matrix} \xrightarrow{\text{diffusion}} \begin{matrix} [Zn_2(L8)Cl_4]\ \textbf{(21)} \\ [Hg_2(L8)Cl_4]\ \textbf{(22)} \\ [Cd_2(L8)I_4]\cdot CH_2Cl_2\ \textbf{(23)} \end{matrix}$$

The IR spectrum of compounds **21**, **22** and **23** show clearly the presence of the ligand main vibration bands that are slightly shifted to higher or lower frequencies with respect to the IR spectrum of **L8** due to complexation as it is seen in Table 23.

Table 23. IR Data for ligand **L8** and complexes **21**, **22** and **23**.

Compound	IR, ν [cm^{-1}]
L8	1651 (s, imine), 1588 (vs), 1568 (m), 1469 (s), 1436 (s), 1353 (m), 1294 (w), 1122 (vs), 993 (m), 776 (s)
$[Zn_2(L8)Cl_4]$ (**21**)	1654 (m, imine), 1599 (vs), 1571 (w), 1474 (m), 1445 (s), 1350 (m), 1298 (s), 1222 (m), 1121 (s), 1111 (vs), 1099 (vs), 1091 (s), 1017 (s), 942 (m), 781 (s)
$[Hg_2(L8)Cl_4]$ (**22**)	1658 (s, imine), 1591 (s), 1570 (w), 1472 (m), 1438 (s), 1348 (m), 1299 (s), 1220 (m), 1118 (vs), 1106 (s), 1081 (s), 1025 (m), 1010 (m), 930 (m), 784 (s)
$[Cd_2(L8)I_4]\cdot CH_2Cl_2$ (**23**)	1661 (s, imine), 1594 (vs), 1569 (w), 1476 (m), 1442 (s), 1342 (w), 1302 (s), 1221 (m), 1106 (s), 1091 (vs), 1077 (s), 1012 (m), 934 (m), 925 (m), 779 (s)

The overall structure for these three complexes can be considered as a single-helical-chain, (see Figure 45) although some differences can be found between compounds **21**, **22** and **23**.

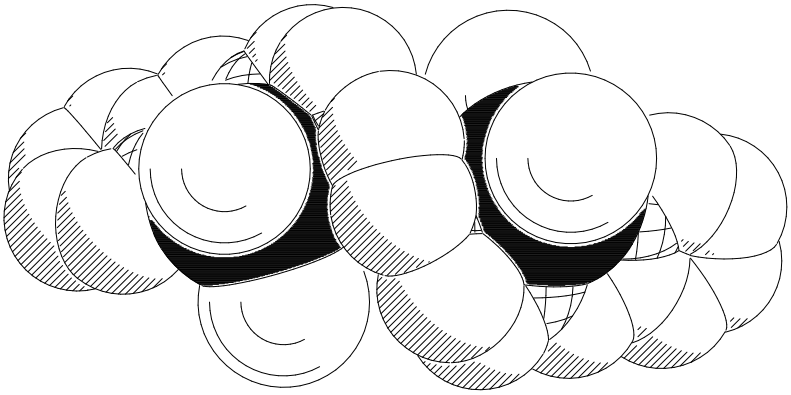

Figure 45. Space filling representation of **23** illustrating its single-helical chain-structure.

In **21** and **22**, which are isomorphous, the metal atoms (Zn^{II} or Hg^{II}) are four coordinate with very distorted tetrahedral geometry and are coordinated to one pyridylimine unit and to two chlorine atoms, Figure 46.

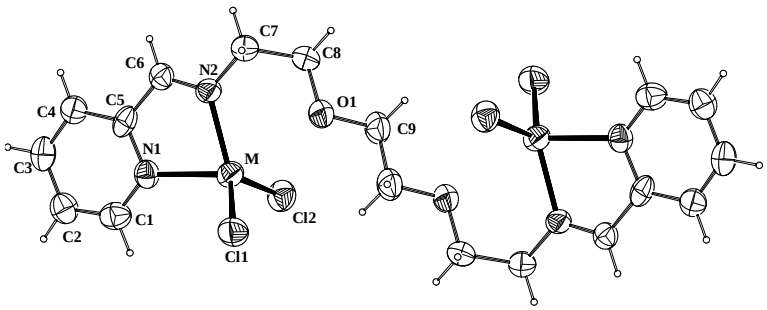

Figure 46. View of the dinuclear isomorphous complexes **21** (M = Zn) and **22** (M = Hg).

Selected bond distances and bond angles for compounds **21-23** are given in Table 24 and select dihedral angles and inter-plane distances in Table 25. The five-membered chelate pyridylimine ring forces the bond angle, N_{py}-M^{2+}-N_{im}, to be almost 70 º, much smaller than the theoretical value of 109 º for an ideal tetrahedron. In **21**, the Zn to O1 distance is very

long, 2.705(5) Å, compared to the typical[24] Zn–O bonding distance of 2.093 Å. In **22** it is reasonable to consider that the O-atom participates in the coordination sphere of the metal as the Hg–O distance of 2.823(10) Å which is comparable to the literature values of 2.825, 2.909 and 2.935 Å[24] for Hg – O distances.

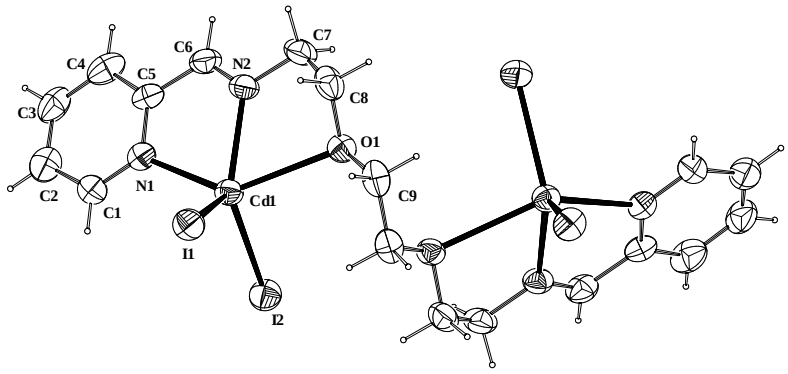

Figure 47. Molecular structure of complex $[Cd_2(L8)I_4]$ (**23**). The solvent molecule of CH_2Cl_2 has been omitted for clarity.

In **23** (Figure 47) the cadmium atom is five coordinate presenting a quite distorted square-pyramidal coordination geometry. Here the Cd-atom adds to its coordination sphere the ether function of the ligand, distance Cd–O is 2.666(5) Å, which is only slightly longer than the standard value of 2.569 Å. The trigonality index τ[51] is 0.18, indicating that the coordination polyhedron around the Cd^{2+} ion can be described as a square-pyramid ($\tau = 0$) with a small trigonal-bipyramid ($\tau = 1$) distortion.

The structures of **21** and **22** differ from that of **23** in their overall conformation as it is shown in their molecular packing representations (Figure 48). In **21** and **22**, the two pyridine rings are strictly parallel while in **23** the bridge is more twisted and the pyridine rings are almost perpendicular to one another, see Table 25.

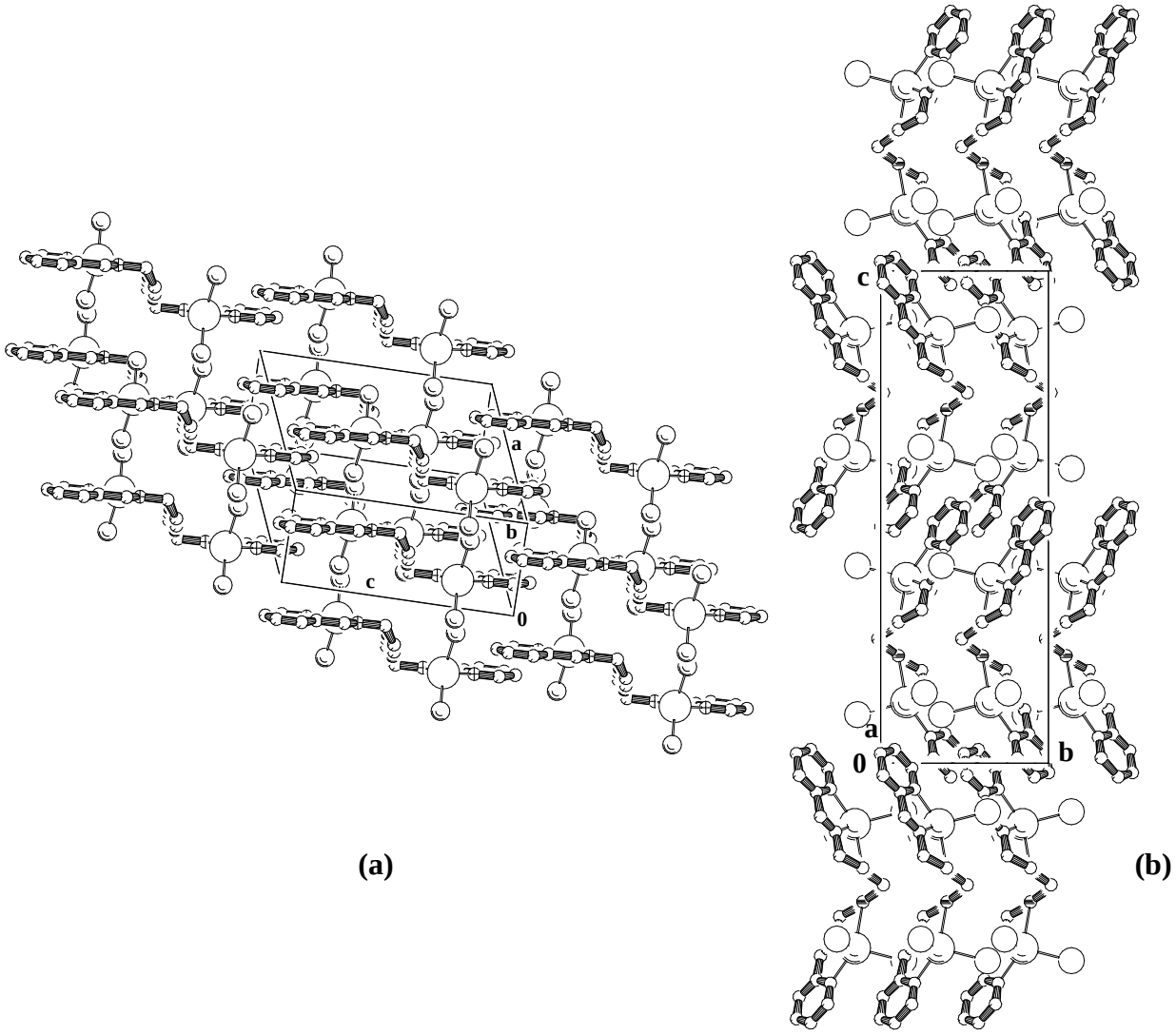

Figure 48. (a) Crystal packing of **21** and **22** and (b) crystal packing of **23** down the *a* axis.

Compound **23** is also more compact than compounds **21** and **23** with the metal centres being separated by 6.645(1) Å in **23** compared to 7.409 (2) Å in **21** and 7.429 (9) Å in **22**. In all three compounds the pyridylimine unit is nearly planar, the pyridine and chelate ring dihedral angles are less than 4 º, and the metal atoms are displaced by less than 0.25 Å from the mean plane of the pyridine ring (Table 25).

Table 24. Comparison of geometric parameters (Å,°) for complexes **21**, **22**, **23**.

	$[Zn_2(L8)Cl_4]$ **(21)**	$[Hg_2(L8)Cl_4]$**(22)**	$[Cd_2(L8)I_4]\cdot CH_2Cl_2$ **(23)**
M-M[a]	7.409(2)	7.429(9)	6.664(1)
M-N1	2.136(7)	2.436(13)	2.373(7)
M-N2	2.054(6)	2.297(11)	2.293(7)
M-X1[b]	2.216(2)	2.381(4)	2.713(1)
M-X2[b]	2.231(2)	2.428(5)	2.714(1)
M…O1	2.705(5)	2.823(10)	2.666(5)
N2-M-N1	78.6(3)	70.5(4)	70.9(2)
N2-M-X1	122.1(2)	121.5(3)	127.1(2)
N1-M-X1	109.4(2)	114.0(3)	99.9(2)
N2-M-X2	115.3(2)	113.4(3)	119.5(2)
N1-M-X2	101.2(2)	99.3(3)	110.2(1)
X1-M-X2	118.5(1)	122.2(2)	112.6(1)
N1-M-O1	147.9(2)	135.1(3)	138.1(2)
N2-M-O1	70.2(2)	66.4(4)	67.4(2)
X1-M-O1	93.8(1)	98.9(2)	101.1(1)
X2-M-O1	85.8(1)	86.8(2)	94.4(1)

a) Symmetry operation for **21** : –x+2, -y+1, -z+2; for **22** : –x+1, -y+2, -z+1; for **23** : –x+1, y, -z+3/2.
b) X = Cl^- for **21** and **22**, X = I^- for **23**.

Table 25. Selected dihedral angles (t, º) and distances (d, Å) for **21**, **22** and **23**.

	21	**22**	**23**
t (py–py[a])	0.0 (4)	0.0 (7)	89.4(3)
t (py-che)	3.7 (3)	3.0 (6)	4.3 (5)
d (py-py[a])	2.61 (4)	3.18(7)	5.53 (4)
d (py-M)	0.18 (1)	0.15 (2)	0.23 (1)
d (py-M[a])	2.44 (3)	3.02 (5)	3.45 (3)

a) Symmetry operations: for **21:** –x+2, –y+1, –z+2; for **22:** –x+1, –y+2, –z+1; for **24:** –x+1, y, –z+3/2. **py** = pyridine ring, **che =** chelate ring M-N1-C5-C6-N2; **M** is the respective metal centre.

Complex **21** was a twinned crystal with more than 40% overlapped reflections. The reflections relating to the major twin component were used for structure analysis. No disorder was observed in compounds **21**, **22** and **23** and an empirical absorption correction using DIFABS in PLATON[25] was applied. One molecule of dichloromethane per molecule of complex was found for structure **23**. Compounds **21**, **22** and **23** were insoluble in all common organic solvents.

To have an idea of the coordination behaviour of **L8** with Cd^{2+}, Zn^{2+} and Hg^{2+}, Uv-Vis titrations were carried out under the same conditions ([L8] = 125 μM, [M^{2+}] = 0, 4.7, 9.4, 18.7, 37.5, 75, 150 and 300 μM) as for compound **20** and using $Zn(ClO_4)_2 \cdot 6H_20$, $Cd(NO_3)_2 \cdot 4H_2O$ and $HgCl_2$ as metal salts. Figure 49 shows the change in the UV-Vis spectrum (250-350 nm region) that occurs when **L8** coordinates to Hg^{2+} ion in EtOH. As for compound **20**, the ligand band at 270 nm is gradually displaced to 280 nm with an increase in intensity. In this case, no clear isosbestic point was observed.

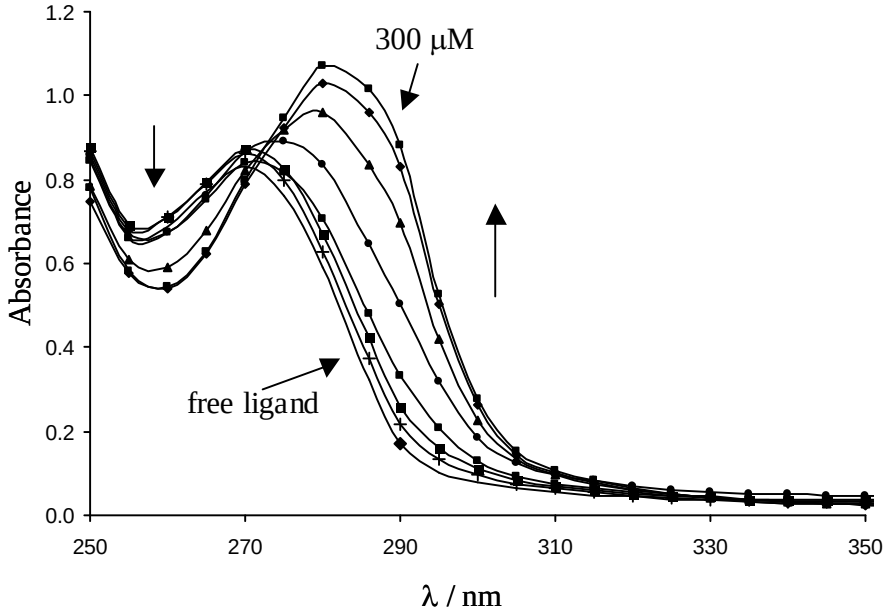

Figure 49. UV spectra of **L8** upon incremental addition of $HgCl_2$ in EtOH.

The results obtained with $Zn(ClO_4)_2 \cdot 6H_20$ will be presented in the next section. Concerning the titration with Cd^{2+}, similar behaviour as for Hg^{2+} was observed with the displacement of ligand band to about 280 nm.

2.7.3. Complexes $[M_2(L8)_3](X)_4$, where M =, Co^{II} for **24**, Fe^{II} for **25,** Zn^{II} for **26** and Ni^{II} for **27** and X = ClO_4^- for **24**, **25** and **26** and BF_4^- for **27.**

These four compounds were obtained either by refluxing a methanolic solution containing three equivalents of **L8** with two equivalents of the correspondent metal salt or by slow diffusion of a methanolic solution of the metal salt into a solution of **L8** in dichloromethane. Complexes **24** - **27** have a metal to ligand ratio of 2:3 and were obtained even when this ratio was varied.

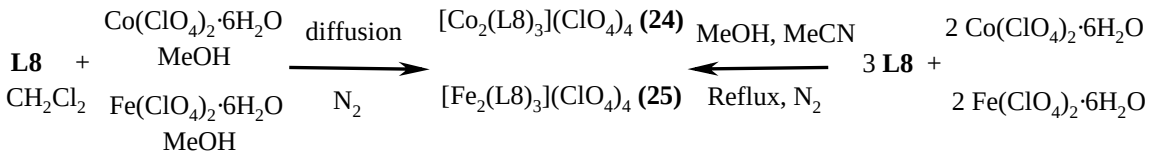

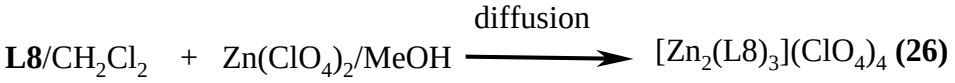

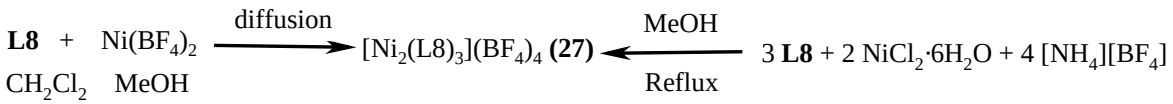

The IR spectra of compounds **24** - **27** show clearly the presence of the ligand main vibration bands that are slightly shifted to higher or lower frequencies with respect to the IR spectrum of **L8** due to complexation as it is illustrated in the following table.

Table 26. IR Data for ligand **L8** and complexes **24** –**27**.

Compound	IR, ν [cm^{-1}]
L8	1651 (s, imine), 1588 (vs), 1568 (m), 1469 (s), 1436 (s), 1353 (m), 1294 (w), 1122 (vs), 993 (m), 776 (s)
$[Co_2(L8)_3](ClO_4)_4$ (**24**)	1645 (m, imine), 1599 (s), 1579 (w), 1480 (m), 1447 (m), 1358 (w), 1309 (m), 1084 (vs, ClO_4), 776 (m)
$[Fe_2(L8)_3](ClO_4)_4$ (**25**)	1615 (m, imine), 1556 (w), 1592 (w), 1474 (m), 1448 (m), 1345 (w), 1302 (m), 1093 (vs, ClO_4), 771 (m)
$[Zn_2(L8)_3](ClO_4)_4$ (**26**)	1652 (m, imine), 1599 (s), 1572 (w), 1482 (m), 1446 (m), 1358 (w), 1310 (m), 1093 (vs, ClO_4), 777 (m)
$[Ni_2(L8)_3](BF_4)_4$ (**27**)	1647 (m, imine), 1599 (s), 1570 (w), 1481 (m), 1448 (m), 1355 (w), 1308 (m), 1058 (vs, BF_4), 777 (m)

The crystal structure of these isomorphous complexes is very interesting. For compound **25**, only a very small crystal was available and it was shown to be isomorphous with compounds **24, 26** and **27**. The number of observed reflections was too small to permit the complete refinement of this compound, nevertheless, the unit cell parameters were refined and the heavy atom and the main backbone atoms positions were located. The structure is not presented in detail.

The overall crystal structure for compounds **24** to **27** combine the two coordination modes observed for complexes **20** to **23**, that is mono-helical (**20**) and single-helical-strand (**21** to **23**), Figure 50. One ligand molecule is wrapped around each metal ion, which in turn are linked by a third ligand molecule. In this way, the metal is coordinated to three pyridine N-atoms and three imine N-atoms.

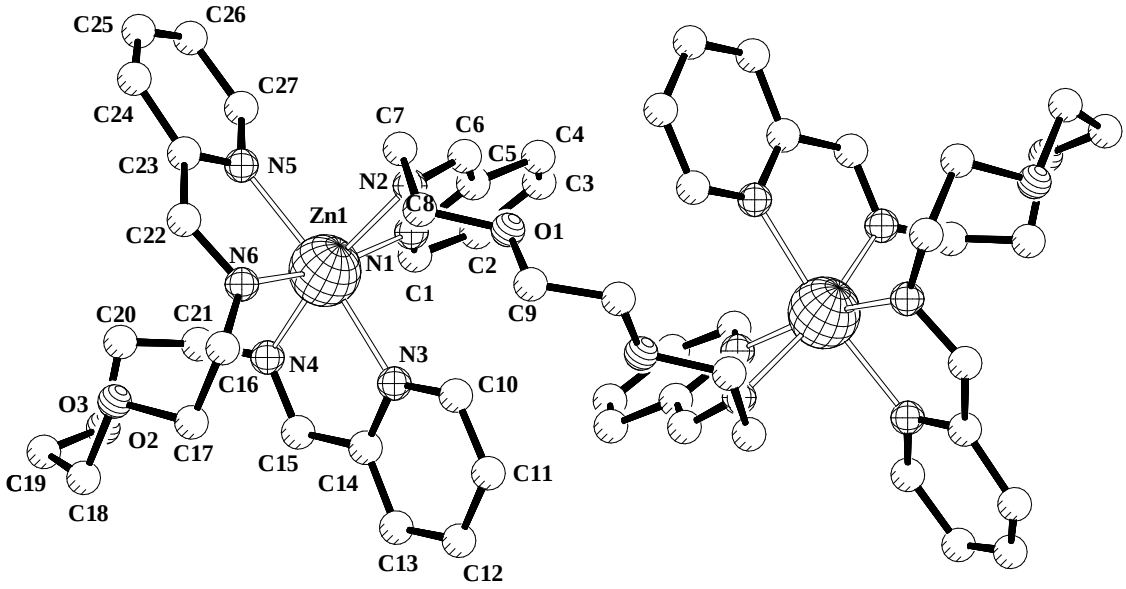

Figure 50. Molecular structure of complex $[Zn_2(L8)_3](ClO_4)_4$ (**26**) with numbering scheme. Hydrogen atoms have been omitted for clarity. Compounds **24**, **25** and **27** are isomorphous.

Selected bond distances and bond angles are given in Table 27 and selected dihedral angles and inter-plane distances in Table 28.

The metals exhibit distorted octahedral geometry. The distortion is essentially due to the narrow N_{py}-M-N_{im} bite angles (*ca.* 77 º) imposed by the ligand. This combination could also be considered as a modification of a binuclear triple helix where the flexibility of the ligand cannot prevent that a ligand molecule wraps itself around one metal atom. The metal centres are separated by distances of between 7.859(2), for **24**, to 8.055(2) Å, for **26**. The overall structure is very compact (like a triple helicate) and the access to the metal ions is very difficult as it can be observed in the space filling representation of **24** (Figure 51) where the ligands envelope almost totally the metallic centres.

Table 27. Selected bond lengths (Å) and bond angles (°) for complexes **24**, **26** and **27**.

	$[Co_2(L8)_3](ClO_4)_4$ **(24)**	$[Zn_2(L8)_3](ClO_4)_4$ **(26)**	$[Ni_2(L8)_3](BF_4)_4$ **(27)**
M-M[a]	7.859(2)	8.055(2)	7.988(2)
M-N1	2.148(5)	2.181(7)	2.108(6)
M-N2	2.148(5)	2.191(6)	2.127(6)
M-N3	2.131(6)	2.177(6)	2.081(7)
M-N4	2.115(5)	2.138(7)	2.067(7)
M-N5	2.116(8)	2.178(8)	2.100(8)
M-N6	2.133(6)	2.161(7)	2.075(7)
N1-M-N2	77.2(2)	76.2(2)	78.0(2)
N1-M-N3	92.2(2)	92.7(2)	91.2(2)
N1-M-N4	91.9(2)	91.1(3)	91.4(3)
N1-M-N5	97.5(3)	95.1(3)	94.5(3)
N1-M-N6	171.9(2)	169.0(3)	170.8(2)
N2-M-N3	98.7(2)	96.5(2)	97.7(2)
N2-M-N4	168.5(2)	166.0(2)	169.0(3)
N2-M-N5	84.6(2)	87.3(2)	86.5(2)
N2-M-N6	96.3(2)	94.8(3)	94.8(2)
N3-M-N4	78.1(2)	77.9(3)	79.2(3)
N3-M-N5	170.2(3)	171.9(3)	173.5(3)
N3-M-N6	93.4(3)	94.7(3)	95.5(3)
N4-M-N5	100.4(2)	99.9(3)	97.5(3)
N4-M-N6	94.9(2)	98.4(3)	95.9(3)
N5-M-N6	77.1(3)	77.9(3)	79.2(3)

[a)] Symmetry operation: –x+1, y, -z+3/2. M and M[a] are the respective metal centres.

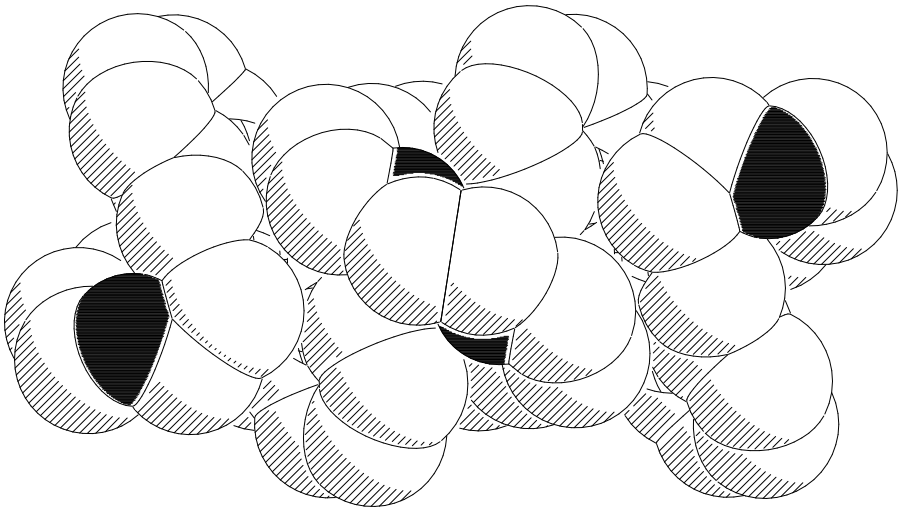

Figure 51. Space filling representation of the cation $[Co_2(L8)_3]^{4+}$ with H atoms omitted.

Table 28. Selected dihedral angles (t, º) and inter-plane distances (d, Å) for **24**, **26** and **27**.

	$[Co_2(L8)_3](ClO_4)_4$ (**24**)	$[Zn_2(L8)_3](ClO_4)_4$ (**26**)	$[Ni_2(L8)_3](BF_4)_4$ (**27**)
t (py_1–py_1^a)	31.0(3)	30.1(3)	29.6(4)
t (py_1-py_2)	82.4(2)	87.8(2)	86.5(2)
t (py_1-py_3)	82.7(6)	86.4(5)	86.6(4)
t (py_2-py_3)	83.5(6)	79.5(5)	81.3(4)
t (py_1-che_1)	2.6(4)	4.1(4)	4.1(4)
t (py_2-che_2)	7.1(3)	3.5(4)	5.4(5)
t (py_3-che_3)	3.1(1.5)	3.2(1.5)	2.2(1.2)
d (py_1–M)	0.09(1)	0.17(1)	0.15(1)
d (py_1-M^a)	5.20(1)	4.95(1)	4.98(1)
d (py_2-M)	0.32(1)	0.16(1)	0.23(1)
d (py_2-M^a)	5.04(1)	5.18(1)	5.13(1)
d (py_3-M)	0.09(3)	0.14(3)	0.11(2)
d (py_3-M^a)	4.80(8)	5.22(9)	4.92(6)

[a] Symmetry operation: –x+1, y, -z+3/2

When disorder was present, only the mean values are reported.

In compounds **24, 26** and **27**, one ligand (one pyridine ring and the ether chain) molecule presents conformational disorder. The disordered atomic positions were refined with occupancies of 0.56 for **24,** 0.44 for **26** and 0.47 for **27**, and their thermal parameters were constrained to be equal in the refinement process. The two perchlorate anions were also highly disordered. The thermal parameters for the disordered oxygen atoms were constrained to be equal. The Cl–O bond distances as well as some of the N_{im}-C distances, were constrained to their theoretical values. In compound **27** the BF_4^- anions were highly disordered and were refined with occupancies of 0.5 for the F atoms.

These complexes are moderately soluble in methanol and acetonitrile. The analysis of the positive ES-MS spectra in acetonitrile (compounds **25** and **26**) or in a mixture methanol/acetonitrile (compounds **24** and **27**) appears to be more complicated than for compound **20**. Each spectrum is composed of several peaks of different intensity. In all of them the peak corresponding to the mononuclear species $\{[M(L8)](ClO_4)\}^+$ can be clearly identified (*m/z* 484 for **24**, 481 for **25**, 489 for **26** and 483 for **27**[*]). This could be seen as a 1st step in the formation of the solid-state species. That is, perhaps a mono-helical complex, where the metal is coordinated to the four nitrogen atoms of the ligand and the two remaining positions (needed for achieving an octahedral geometry) could be occupied by two oxygen atoms. In the case of **24** and **26**, this mononuclear species is the most stable one (stronger peak) under the conditions of the measurement. The peaks at *m/z* 634 and 634 for **27** and at 644 for **25** are assigned to $\{[Ni_2(L8)_3](BF_4)_2\}^{2+}$ and $\{[Fe_2(L8)_3](ClO_4)_2\}^{2+}$, respectively, species which correspond to the solid state structures. In **24** the same aggregate species incorporates a methoxy group instead of one perchlorate (*m/z* 612). In **25** and **27** peaks at m/z 807 and 797, respectively, have been assigned to 1:2 (M:L) species with a ClO_4^- or BF_4^-

[*] For compound **27** the ClO_4^- anion comes from the $NaClO_4$ used during the diffusion reaction.

anion. This could be considered as the second step in the formation of the M_2L_3 species. A medium intensity peak at m/z 1083 in **26** was assigned to a binuclear species $\{[Zn_2(L8)_2](ClO_4)_3\}^+$.

As for other metals, UV-Vis titration experiments of the ligand (125 μM in EtOH) with addition of increasing quantities of metal salt* solutions ($[M]^+$ = 0, 4.7, 9.4, 18.7, 37.5, 75, 150 and 300 μM, in EtOH) were carried out. In the case of **25**, supplementary measurements were carried out with the aim of studying this compound in more detail as it presented some interesting features. The next figures show the changes in the UV-Vis spectrum (from 250 to 350 nm) that occur when **L8** coordinates to Ni^{2+} (Figure 52), Co^{2+} (Figure 53) and Zn^{2+} (Figure 54) ions in EtOH. Upon addition of Ni^{2+} ion to the ligand solution, the ligand band at 270 nm is progressively displaced to 285 nm. The saturation was achieved for the two most concentrated solutions. The presence of an isosbestic point at about 270 nm is not as clear as for **20**.

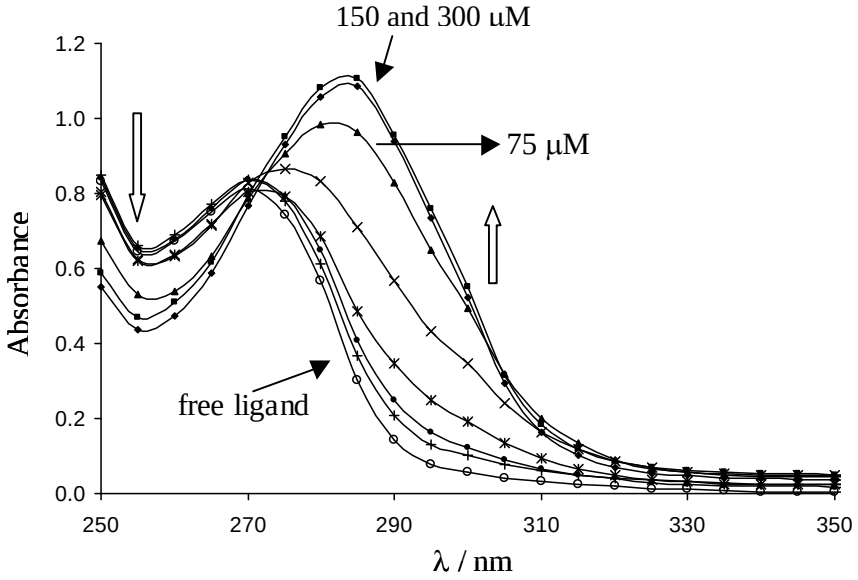

Figure 52. UV spectra of **L8** upon incremental addition of (a) Ni^{2+}.

* Metal salts employed: $Co(BF_4)_2 \cdot 6H_2O$, $Fe(ClO_4)_2 \cdot 6H_2O$, $Zn(ClO_4)_2 \cdot 6H_2O$ and $Ni(ClO_4)_2 \cdot 6H_2O$.

In the case of Co^{2+}, the band due to complexation appears at 280 nm and the same behaviour as for Ni^{2+} is observed.

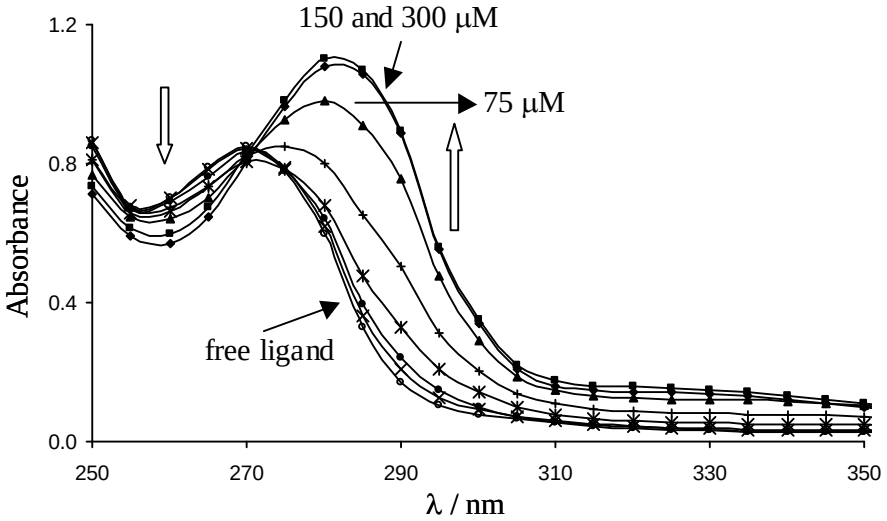

Figure 53. UV spectra of **L8** upon incremental addition of Co^{2+}.

In the case of Zn^{2+}, the ligand band is displaced to 285 nm on complexation and approximately the same behaviour as for Ni^{2+} and Co^{2+} is observed.

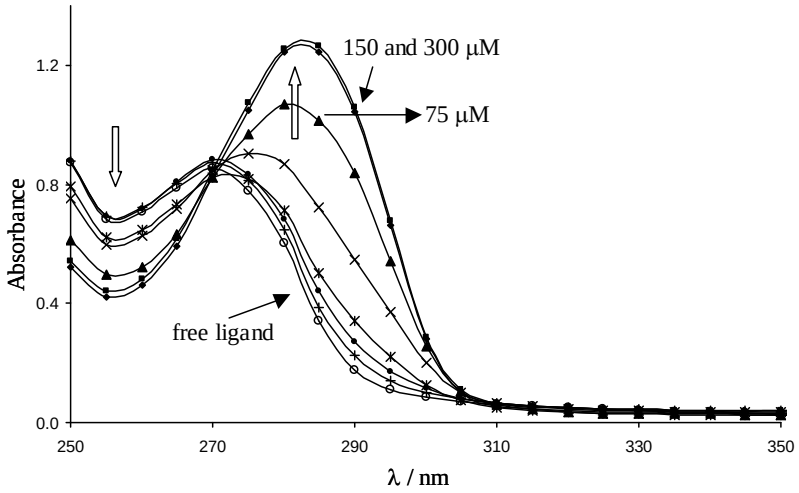

Figure 54. UV spectra of **L8** upon incremental addition of Zn^{2+}. Ratio plot at 285 nm.

In these three cases, the isosbestic point at about 270 nm is only poorly defined and a mole ratio plot using the changes in absorbance cannot be used in order to propose a M:L ratio for the complex(es) formed.

It is interesting to notice that in all three cases, the maximum value of absorption occurs when the concentration of the metal is 150 μM, that is, in slight excess with respect to the ligand concentration (125 μM). The addition of an excess of metal does not increase the absorption value or the amount of product formed. The M:L 2:3 species (solid state form) is possibly not fully achieved at the theoretical ratio of 0.66. It appears that a larger concentration of metal ion is necessary, perhaps due to a non-quantitative reaction (relatively small stability constant).

The UV-Vis titration experiments of **L8** with $Fe(ClO_4)_2 \cdot 6H_2O$ present some interesting differences. In a first approach, the titration experiment was performed under the same conditions as for the other three cases (Ni^{2+}, Co^{2+} and Zn^{2+}) and in view of the remarkable features that had been already observed; we have decided to carry out more detailed measurements.

The concentration of the ligand was constant and equal to 125 μM and the metal was added in different concentrations varying from 0 to 1 mM in 31 steps [In each step the metal concentration was multiplied by a factor 1.25]. The absorbance of each curve has been measured each 3 nm instead of each 5 nm as in the first experiment. The new spectra have been obtained in the wavelength range from 250 to 750 nm. In the first titration experiment, the maximum metal concentration used was 300 μM, therefore, the new measurements are not only more detailed but the metal concentration range is much larger and includes cases with large metal excess.

The complete results from the experiment are presented in Figure 55. This figure includes the full range of metal concentrations.

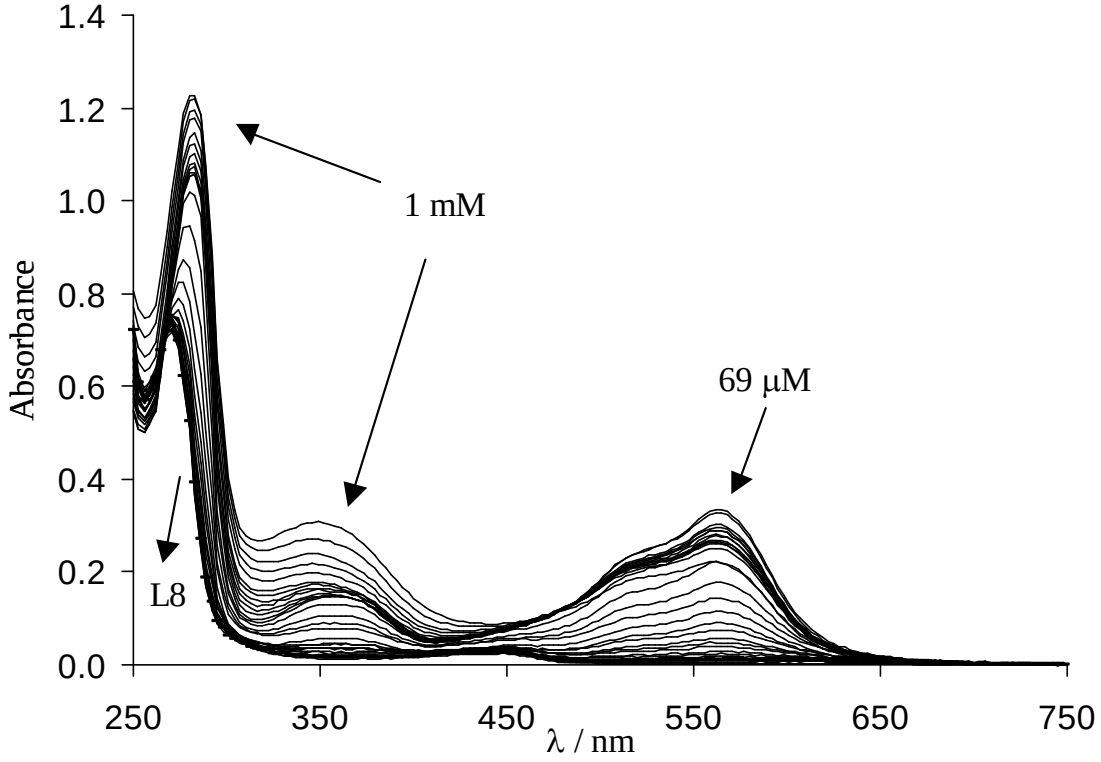

Figure 55. UV spectra of **L8** upon incremental addition of Fe^{2+} in EtOH.

It can be seen that upon addition of Fe^{2+} to **L8**:

1. The ligand band at 270 nm is progressively displaced to 280 nm. Its intensity grows continuously as the concentration of Fe^{2+} increases but not proportionally.
2. A new band appears at 349 nm. It gets more intense with increasing amounts of Fe^{2+}.
3. Finally, a band emerges at 562 nm. The absorption increases until a metal concentration equal to 69 μM is reached and then continuous addition of Fe^{2+} leads to a decrease in absorption.

This case is more difficult to visualize than those of Zn^{2+}, Ni^{2+} or Co^{2+} and for this reason the UV-Vis spectrum has been divided into several sub-ranges according to the observed features of Fe^{2+} with the ligand (Figures 56 and 57).

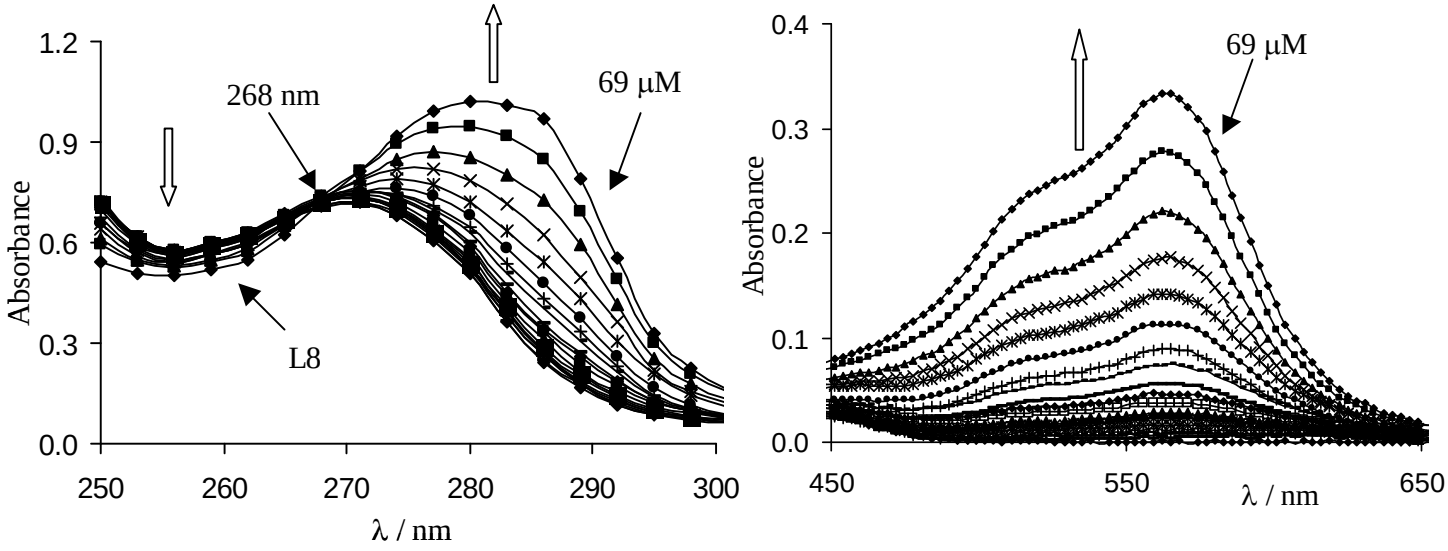

Figure 56. UV spectra of **L8** upon incremental addition of Fe^{2+}. Only concentrations from 0 to 69 μM have been represented in two different wavelength domains.

Figure 56 illustrates the change in the UV-Vis spectrum of **L8** upon addition of increasing quantities of Fe^{2+} (until a $[Fe^{2+}]$ = 69 μM). The presence of a clear isosbestic point at 268 nm is the confirmation of the formation of only one product, at least until that metal concentration. In the region of 450 to 650 nm, the band at 562 nm grows parallel to $[Fe^{2+}]$ with a maximum value at 69 μM which correspond to a M:L ratio of approximately 2:3, which is the same M:L ratio observed in the deep purple species found in the solid state. When the metal is in excess with respect to the ligand, that is, at Fe^{2+} concentrations higher than 69 μM and which correspond to a M:L ratio of at least 1:1, a new species with a weaker absorption appears and displaces the former one. This fact was clearly observed during the realization of the experiment. The intensity of the purple colour obtained upon addition of Fe^{2+} decreased once the metal concentration exceeded the concentration of the ligand.

Figure 57 illustrates what happens in this range of concentrations.

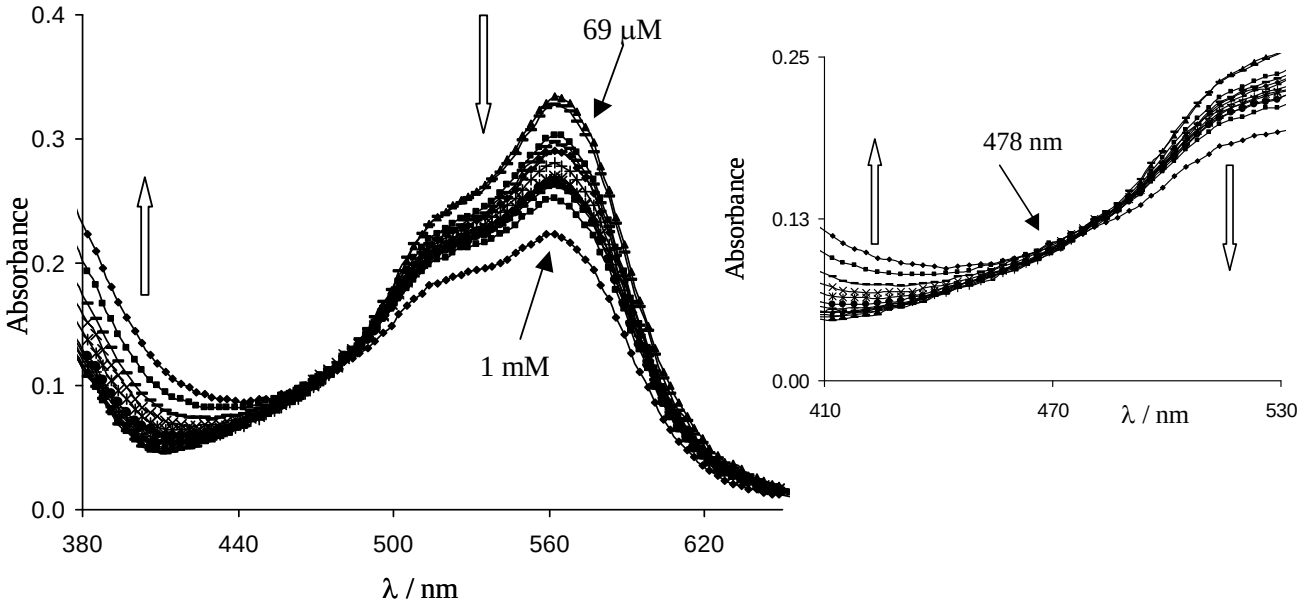

Figure 57. UV spectra of **L8** upon incremental addition of Fe^{2+}: concentration range from 69 μM to 1 mM. The region from 410 to 530 nm has been enlarged.

The band at 562 nm decreases gradually starting from the concentration 69 μM. For the next metal concentration, 86 μM, the value of absorbance decreases only slightly. The diminution becomes more pronounced for concentrations greater than 108 μM. The isosbestic point at 268 nm disappears and a new one appears at 478 nm as it can be seen in the enlargement of figure 57. Taking into account all of this information the following solution equilibria may be proposed:

$$2\ Fe^{2+} + 3\ L8 \rightleftharpoons [Fe_2(L8)_3]^{4+} + Fe^{2+} \rightleftharpoons 3\ [Fe(L8)]^{2+}$$

Using the Lambert-Beer equation: **A = ε.c.l** (where A = absorption, ε = molar extinction coefficient [$L \cdot mol^{-1} \cdot cm^{-1}$], c = concentration [$mol \cdot L^{-1}$] and l = path [cm]), and admitting that the concentration of the species $[Fe_2(L8)_3]^{4+}$ is $3.45 \cdot 10^{-5}$ (half of 69 μM) and a l = 0.5 cm, it is possible to obtain an ε value of approximately 19400 at λ = 562 nm. If we take into account

that the compound contains two Fe^{2+} atoms (two chromophore groups), the value of 19400:2 = 9700 per Fe^{2+} can be compared with the value ε = 11100 at 508 nm for the mononuclear complex tris-phenanthroline-Fe^{2+} and therefore, it is reasonable to suppose that the Fe^{2+} in the complex $[Fe_2(L8)_3]^{4+}$ is in a low-spin state.

This contradicts the fact that the ^1H NMR spectrum of the complex **25** (purple crystals dissolved in CD_3OD) was poorly resolved. This could be explained by the presence of a high-spin species, $[Fe(L8)]^{2+}$, for example. The gradual lightening of the purple colour upon addition of Fe^{2+} in excess is a sign of the formation of a high-spin Fe^{2+} complex. As the solution was, for all metal concentrations, still slightly purple, it is possible that the two species co-exist in solution.

General considerations

It can be seen from Tables 25 and 28 that in complexes **21** to **27**, the metal atoms are only slightly displaced from the best plane through the pyridine rings, and that the pyridine and chelate rings are almost perfectly co-planar, with the dihedral angles varying from 2.6 to 7.1º. For compounds **20** to **27**, the average $C{=}N_{im}$ bond distance of 1.266(4) Å, is close to the standard value[24] of 1.279 Å for a Schiff base system. The average C_{py}-C_{im} bond distance, 1.469(4) Å, is close to the standard value[24] of 1.476 Å found for a conjugated system. The N_{py}-M-N_{im} bite angles vary from 70.5(4) to 79.2(3)º.

In Table 29 the standard values[24] for Metal-N_{py} and Metal-N_{im} bond distance are compared with the values found in complexes **20**-**27**. In the case of complexes **20** to **23** it is interesting to note that the observed M-N_{py} bond distances are longer than the standard values and that

this trend is reversed for the M-N_{im} bond distances except for compound **22**. For the first row transition metal complexes, **24**, **25** and **27**, and for compound **26** the M-N_{py} and the M-N_{im} bond distances for individual complexes are very similar. For the same series of compounds it can be seen that the M-N_{py} bond distances are shorter than the standard values while the M-N_{im} bond distances are either similar or longer than the standard values. This difference, in the relative M-N bond distances with respect to the standard values, of compounds **20** to **23** compared to compounds **24** to **27**, is possibly due to steric overcrowding in the latter.

Table 29. A comparison of **M-N_{py}** and **M-N_{im}** bond distances (Å) for compounds **20-27** with standard values, given in parentheses.

	M-N_{py}	**M-N_{im}**
Ag (**20**)	2.385, 2.410 (2.299)	2.251, 2.277 (2.403)
Zn (**21**)	2.136 (2.116)	2.054 (2.122)
Hg (**22**)	2.436 (2.164)	2.297 (2.158)
Cd (**23**)	2.373 (2.381)	2.293 (2.399, 2.457)
Co (**24**)	2.116, 2.131, 2.148 (2.185)	2.115, 2.133, 2.148 (2.015)
Fe (**25**)[a]	1.945, 1.965, 2.000 (1.969, 1.961)	1.907, 1.911, 2.030 (1.958)
Zn (**26**)	2.177, 2.178, 2.181 (2.116)	2.138, 2.161, 2.191 (2.122)
Ni (**27**)	2.081, 2.100, 2.108 (2.122)	2.067, 2.075, 2.127 (2.051)

[a] approximate values only as the crystal was of poor quality. Standard values are given for Fe(II) compounds in their low-spin state. For M-N_{py}, the value reported corresponds to the compound tris-phenanthroline-Fe^{2+} (1.969 Å) and to Fe-N_{bipy} (1.961 Å).

To sum up, as expected, the ligand **L8** is found to be very flexible and reacts readily with transition metals. Two different coordination modes of the ligand are possible; mono-helical and single-helical-strand. Depending on the geometrical preferences of the metal these coordination modes can either be observed separately or combined in the same complex. With

silver(I) a mono-helical complex **20** was formed rather than a polymeric structure. With zinc(II), mercury(II) and cadmium(II) the complexes, **21**, **22** and **23**, can be considered to be single-helical-strands. Finally with the first row transition metals, which favour octahedral coordination, that is, complexes **24** to **27**, both mono-helical and single-helical-strand coordination modes are present. This result was surprising as frequently binuclear complexes of this type of ligand, with a M:L ratio of 2:3 and with metals having predilection for octahedral geometry, form triple helical arrangements[6-8]. The flexibility of the central spacer obviously plays an important role here and it also appears that the type of complex formed depends upon the counter-ion used for the reaction. In the case of Zn^{II}, two different complexes, **21** and **26,** were obtained using chloride or perchlorate, respectively, as counter-ions. The chloride atoms prefer to coordinate to the metal centre while with $Zn(ClO_4)_2$ the metal prefers to coordinate with the N-atoms only, with an octahedral geometry. Interestingly the mono-helical zinc(II) complex obtained by Lam *et al.*[45] was synthesized using anhydrous $ZnCl_2$ but $NaClO_4$ was later added to the refluxed solution in absolute ethanol. There the zinc atoms are also coordinated to the ether O-atoms with typical Zn-O bond distances of 2.203-2.211 Å.

2.8. Coordination behaviour of ligand L9

The ligand **L9** is analogous to ligand **L5**, the only difference being the central spacer group (NH group instead of O atom). The design of this ligand should, as **L5**, favour the formation of helical species. The NH group could act as a donor group either for coordinating to a metal or to form hydrogen-bonding networks. The ligand **L9** reacts with a large number of metal ions as indicate by the UV-Vis titrations carried out with different metal salts.

The reaction of HgI_2 with **L9** using diffusion techniques, in dilute conditions and at room temperature, afforded in a few days dark red-orange crystals of the binuclear complex $[Hg_2(L9)I_4]$ **(28)**

$$\textbf{L9}/CH_2Cl_2 \quad + \quad HgI_2/MeOH \xrightarrow{\text{diffusion}} [Hg_2(L9)I_4]\ \textbf{(28)}$$

The IR spectrum of **28** shows the main characteristic absorption bands of **L9** slightly displaced to higher or lower frequencies with respect to the IR spectrum of the free ligand as shown in the following table.

Table 30. IR Data for the ligand **L9** and the complex **28**.

Compound	IR, ν [cm^{-1}]
L9	3242 (NH, w), 1621 (m, imine), 1593 (s), 1572 (vs), 1520 (s), 1499 (s), 1468 (m), 1325 (vs), 1168 (m), 839 (s), 775 (m)
$[Hg_2(L9)I_4]$ **(28)**	3341 (NH, m), 1618 (m, imine), 1587 (s), 1551 (w), 1529 (vs), 1485 (m), 1473 (m), 1371 (m), 1350(m), 1242 (m), 1174 (m), 1153 (w), 819 (m), 780 (w)

The shift of the stretching vibration band ν(N-H) from 3242 to 3341 cm^{-1} upon coordination is remarkable. The lower wave number value observed for the free ligand suggests that the amine is hydrogen bonded. In the complex, this hydrogen bond has disappeared as was confirmed by the X-ray structure analysis [#].

$[Hg_2(L9)I_4]$ **(28)** is a centrosymmetric binuclear complex in which two mercury centres are bridged by a ligand molecule coordinating in a bis-bidentate manner, resulting in a $Hg…Hg^i$ distance of 11.763 (1) Å. The tetrahedral geometry about each metal ion is completed by two iodine ions. The distortion from the ideal tetrahedral geometry is the result of the very small bite angle N1-Hg1-N2 of 71.0 (3) º.

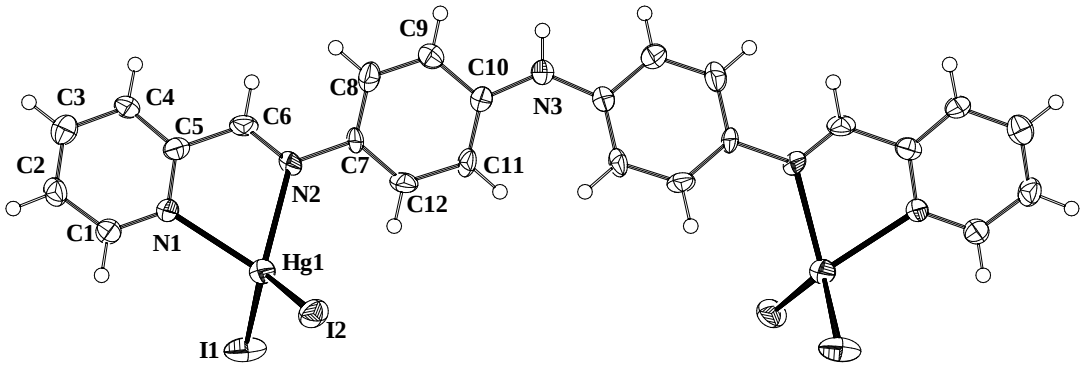

Figure 58. Molecular structure of the binuclear complex $[Hg_2(L9)I_4]$ **(28)** showing the numbering scheme and thermal ellipsoids at 50% probability level.

In complex **28** the ligand is twisted about the central NH group with the two phenyl rings being inclined by 25.7 (4) º. The two halves of the molecule (related by a twofold axis) are not planar either, as it was found in compounds **16** and **17,** but not in compound **18a**. The aromatic rings N1/C1-C6/ and C7-C12 (pyridine and phenyl rings) are inclined to one another

[#] No single crystals suitable for X-ray analysis of **L9** have been obtained.

by 26.5 (4) º and the Hg atom is displaced from the chelate plane by only 0.088 (2) Å. In the crystal, the molecules stack up the *b* axis with a π-π overlap of symmetry related aromatic rings; the shortest intermolecular C…C distance is *ca.* 3.57 (2) Å (Figure 59). A good overlap is possible because the dihedral angle between the rings exhibiting this stacking, for instance, N1,C1-C5 and $C7^{ii}$-$C12^{ii}$, is only 4.6 (6) º [the rings are almost parallel]. (ii = x, -y+1, z+1/2).

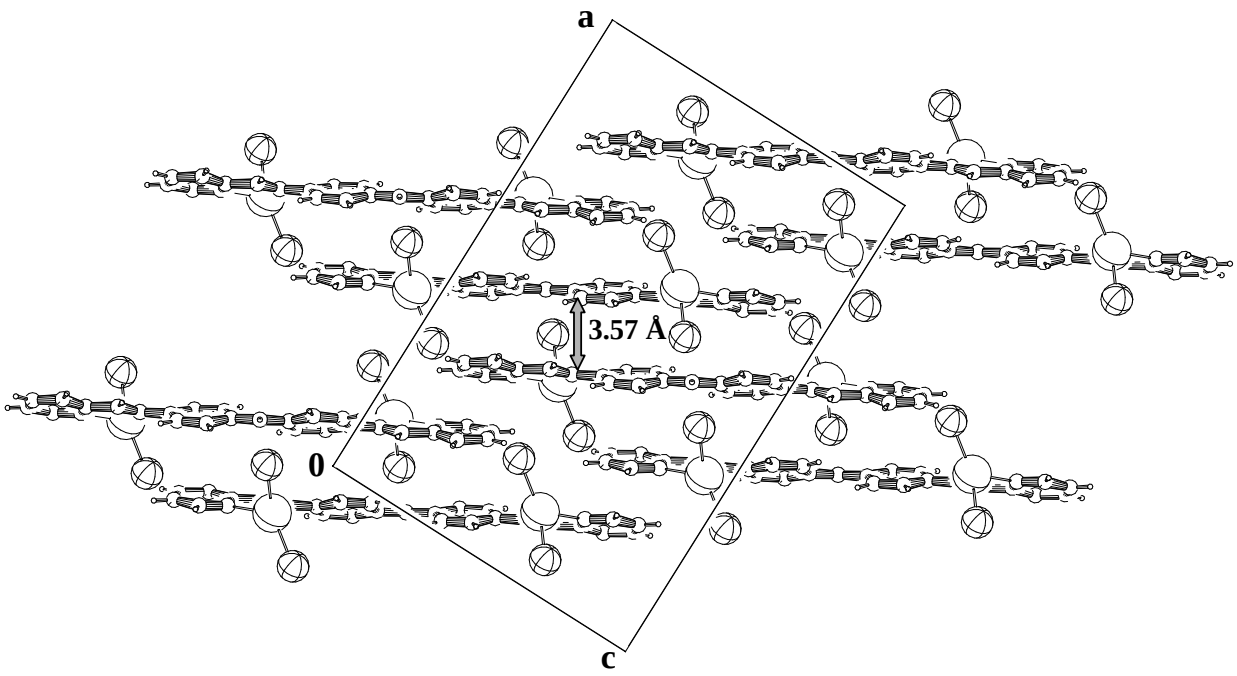

Figure 59. Crystal packing of compound **28** viewed down the *b* axis and showing the π-π interactions.

The Hg–N_{py} and Hg–N_{im} distances of 2.373(9) and 2.389(9) Å are longer than the standard values[24] of 2.164 and 2.158 Å whereas the Hg-I distances of 2.6676(8) and 2.6879(9) Å are very close to the standard value of 2.702 Å. The imine group has an *E* configuration [the torsion angle C5-C6-N2-C7 is equal to –175.9(10) º] with a C=N bond distance of 1.270 (14) Å, indicative of a double bond, and distances of 1.495 (16) and 1.438 (13) Å for C5-C6 and N2-C7 respectively, standard values for single C-C and C-N bonds.

Selected bonds distances and angles are given in Table 31.

Table 31. Selected geometric parameters (Å,°) for $[Hg_2(L9)I_4]$ **(28)**.

Hg1-Hg1^{i}	11.763(1)	C7-N2	1.438(13)
Hg1-N1	2.373(9)	N1-Hg1-N2	71.0(3)
Hg1-N2	2.389(9)	N1-Hg1-I2	125.9(2)
Hg1-I2	2.6676(8)	N2-Hg1-I2	111.18(19)
Hg1-I3	2.6879(9)	N1-Hg1-I3	98.9(2)
C5-C6	1.495(16)	N2-Hg1-I3	118.9(2)
C6-N2	1.270(14)	I2-Hg1-I3	121.21(3)

Symmetry operation: –x, y, -z-1/2

As for the other ligands, UV-Vis titrations with a number of metal ions have been carried out. Titration of **L9** with Co^{2+}, Ni^{2+}, Zn^{2+} or Cd^{2+} salts gave very similar results. In all of these four cases, hypochromic effect of the ligand bands at 270 and 420 nm as the concentration of the metal increases to 75 μM was observed. On increasing metal concentration two new bands appeared at *ca*. 285 and 465 nm. Several isosbestic points appear during the titration (see Table 32). In Figure 60, the case of Zn(II) is presented. Titrations with $Co(BF_4)_2 \cdot 6H_2O$, $Ni(ClO_4)_2 \cdot 6H_2O$ and $Cd(NO_3)_2 \cdot 4H_2O$ gave similar results. Saturation was achieved for the two most concentrated solutions.

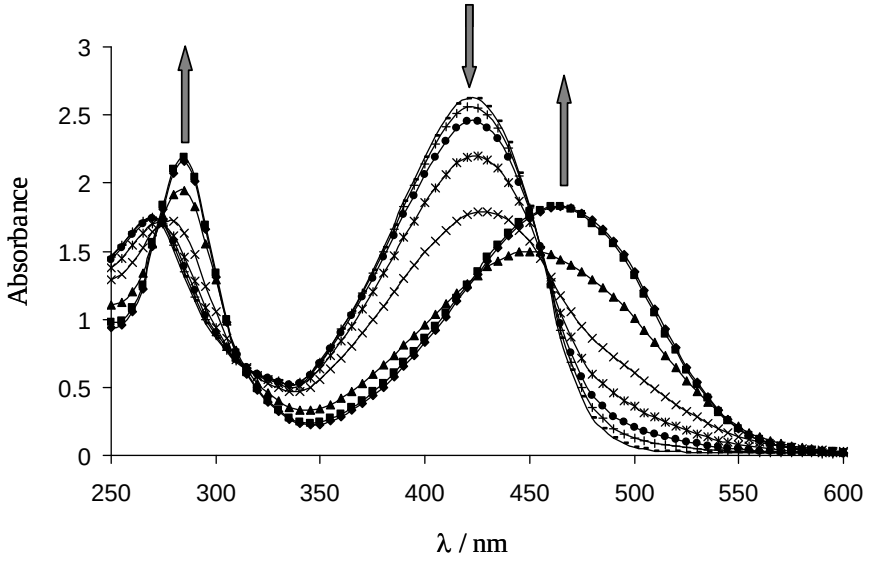

Figure 60. UV-Vis spectra of **L9** upon incremental addition of $Zn(ClO_4)_2 \cdot 6H_2O$ in EtOH.

As observed for the triple helicates **16** and **17**, the first isosbestic point formed at *ca.* 460 nm suffers a hypsochromic shift when the concentration of the metal is greater than 75 μM.

The titrations with Ag^+ and Cu^+ (Figure 61) afforded some information due to the presence of several clear isosbestic points and two new bands. The isosbestic points do not shift during all of the titration experiments supporting the formation of only one species. The saturation in absorbance is reached for the most concentrated solutions [although this was better observed for Ag^+ than for Cu^+].

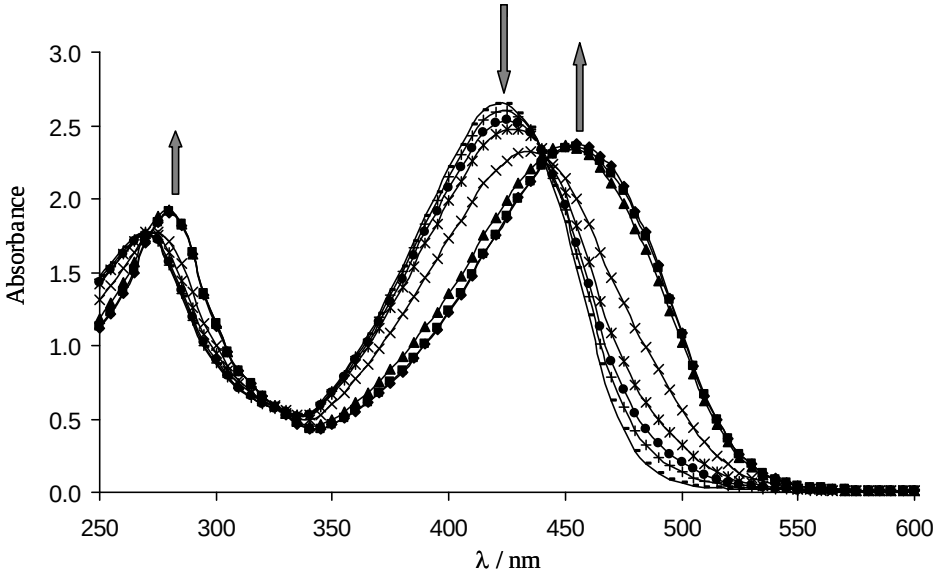

Figure 61. UV-Vis spectra of **L9** upon incremental addition of $AgNO_3$ in EtOH.

For Cu^{2+} similar behaviour to that of Fe^{2+} with **L8** was observed. In this case the measurements were carried out from 250 to 750 nm (Figure 62), in order to measure the maximum of the band at 680 nm (the colour of the solution was green). The intensity of the green colour obtained upon addition of Cu^{2+} decreases once the metal concentration exceeded the concentration of the ligand. The maximum value of this band is obtained at a metal concentration of 75 μM. This gradual lightening of the green colour is possibly the sign of the transformation of one species into another.

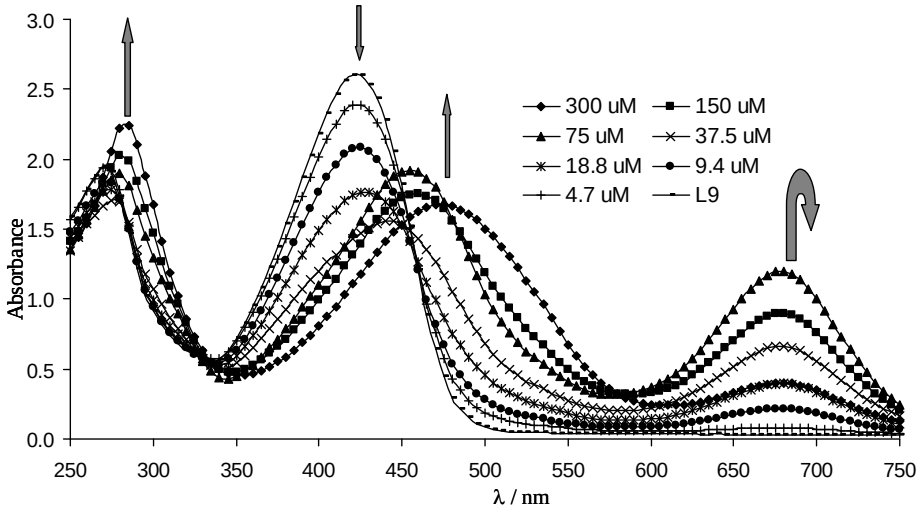

Figure 62. UV-Vis spectra of **L9** upon incremental addition of $Cu(NO_3)_2 \cdot 3H_2O$ in EtOH.

Finally, titrations with Hg^{2+} and Mn^{2+} have also been performed leading to smaller (compared with other metal ions) changes in the **L9** UV-Vis spectrum, although in both cases the reaction is clean (only one product formed). This agrees with the long Hg-N bond distances found in the complex **28**, indicating that the metal coordinates only weakly to the ligand. The next table contains a resume of the most important UV-Vis titration data. During the reaction of **L9** with $MnCl_2 \cdot 4H_2O$, a reddish powder was formed. Its ES-MS spectrum shows a peak at m/z 467 that corresponds with the formulation $[Mn_2(L9)_2Cl_2]^{2+}$ and a small peak at m/z 425 that can be assigned to a triple helix formulation $[Mn_2(L9)_3Cl]^{3+}$.

Table 32. Uv-Vis spectra relevant data.

Metal ion	Isosbestic Points	New Maxima
Co^{2+}	275, 320 and 460 nm	285 and 465 nm
Ni^{2+}	275 and 460 nm	285 and 465 nm
Zn^{2+}	270-5, 310-5 and 455 nm	285 and 465 nm
Cd^{2+}	270-5, 315 and 450 nm	285 and 465 nm
Ag^{+}	270-5, 325-30 and 440-5 nm	280 and 455 nm
Cu^{+}	445-50 nm	450 nm
Cu^{2+}	335 nm (not clear)	285, 455 and 680 nm
Mn^{2+}	455-60 nm	485 nm
Hg^{2+}	450-5 nm	490 nm

2.9. Coordination behaviour of ligand bptz

Some aspects of the coordination chemistry of this ligand have been briefly investigated. A number of studies of this ligand have already been reported. Recently, it was reported that this ligand leads to the formation of molecular squares or pentagons[52]. Roche *et al*.[53] have studied the electrochemical properties of a **bptz** binuclear ruthenium complex. Kaim *et al*.[54] have published numerous EPR, electrochemical and electronic studies of several **bptz** complexes. **bptz** reacts with several metal ions and we have been able to isolate the following compounds in crystalline form: $[Ag_2(bptz)_3](SbF_6)_2$ **(29)**, $[Ag_2(bptz)_3](PF_6)_2$ **(29a)**, $\{[Cd(bptz)I_2]\cdot CH_2Cl_2\}_n$ **(30)**, $[Cd(bptz)(NO_3)_2]_n$ **(31),** $[Zn(bptz)(NO_3)_2]_n$ **(32),** $[Hg_2(bptz)Cl_4]_n$ **(33)**, [Hg(bptz2)Cl_2] (**33a**), $[Hg(bptz)Br_2]_n$ **(34),** $[Hg_2(bptz)I_4]_n$ **(35),** $[Cu(bptz1)Cl_2]_n$ **(36)**[55]**,** [Mn(bptz2)$Cl_2\cdot CH_3OH$] **(37)** and bptz3 **(38).** In compounds **36**-**38** the ligand has suffered a transformation due perhaps to the catalytic effect of certain metal atoms in the presence of air oxygen or water [the tetrazine ring is not very stable and **bptz** can loose a N_2 molecule].

2.9.1. Complexes $[Ag_2(bptz)_3](SbF_6)_2$ (29) and $[Ag_2(bptz)_3](PF_6)_2\cdot 0.2H_2O$ (29a)

The reactions [under N_2 and protected from the light] of **bptz** with $AgSbF_6$ or $AgPF_6$ in 1:1 ratio lead, upon slow evaporation of the acetonitrilic solution, to the formation of **29** in the form of red-violet crystals, or to **29a** in the form of red-blue crystals.

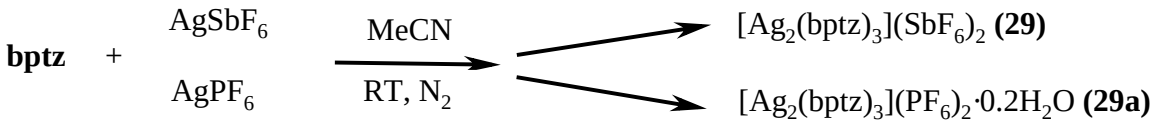

The IR spectra for compounds **29** and **29a** (Table 33) show the characteristic bands of the ligand. Evidence for coordination is provided by the shift to higher or lower wave numbers of

the stretching frequencies arC-arC, arC-arN and arN-arN compared to the free ligand. In compound **29a** the PF_6^- band appears at 838 cm^{-1}.

Table 33. IR Data for the ligand **bptz** and the complexes **29-29a**.

Compound	IR, ν [cm^{-1}]
bptz	1640 (b, w), 1582 (s), 1479 (w), 1444 (m), 1391 (vs), 1130 (m), 994 (m), 799 (s), 745 (m), 733 (m), 597 (vs)
29	1632 (b, w), 1588 (m), 1451 (w), 1391 (s), 1258 (m), 1139 (m), 1000 (m), 932 (m), 791 (s), 745 (m), 658 (vs), 595 (s)
29a	1636 (b, m), 1593 (m), 1452 (w), 1389 (s), 1263 (m), 1137 (m), 932 (m), 838 (vs, PF_6^-), 787 (w), 738 (w), 596 (m), 557 (s)

Compound **29** crystallizes in the centrosymmetric trigonal space group $R\bar{3}$. The structure of complex **29** is quite unusual and consists of discrete, propeller-like, $[Ag_2(bptz)_3]^{2+}$ dimeric cations with two SbF_6^- anions per cation molecule. The molecule has C_3 symmetry with the two silver ions lying on the 3-fold axis. One of SbF_6^- anions has C_3 symmetry and the other anion is split over two different sites both with C_{3i} symmetry. The two silver centres are bridged by three ligand molecules coordinating in a bis-bidentate manner leading to an octahedral geometry for the metal atoms. The Ag…Ag distance is 4.426 (1) Å. As the chelating angles are very small, the octahedron around the silver atoms is quite distorted (Figure 63).

Compound **29a** is isomorphous with compound **29** the only difference being the presence of PF_6^- instead of SbF_6^- as counter-anions. For compound **29a**, only a small crystal was available, too small to permit the complete refinement of this compound and, therefore, the structure is not presented in detail.

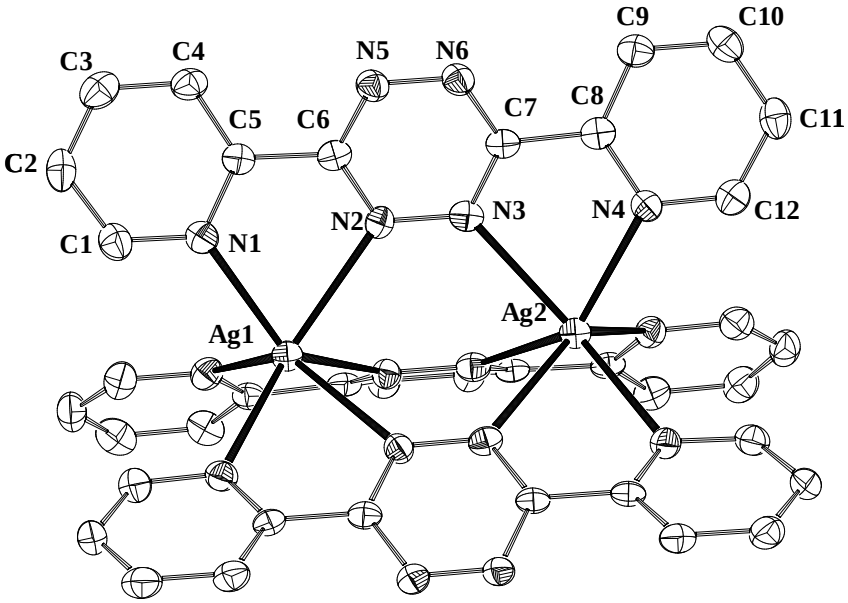

Figure 63. Molecular structure of the binuclear complex **29** showing the numbering scheme and thermal ellipsoids at 50% probability level. H-atoms and counter-ions omitted.

Although the most frequent coordination geometry associated with silver is tetrahedral, some complexes containing N ligands and silver atoms in octahedral environments have been also reported[56].

In the complex **29**, the ligand molecules are distorted from planarity. The dihedral angles between the pyridine and tetrazine rings are, 20.6 (1) º for N1,C1-C5 / N2-N6 and 18.1 (1) º for N2-N6 / N4,C8-C12. The two Ag atoms are displaced from the chelate rings by 0.286 (7) and 0.180 (7) Å for Ag1 and Ag2, respectively. In the crystal, the molecules stack up the *c* axis with a good π-π overlap of the symmetry related aromatic rings (symmetry operation –x+2/3, -y+1/3, -z+1/3); the shortest intermolecular C…C distance is *ca*. 3.50 (1) Å (see Figure 64). Selected bond distances and angles are given in the following table. The asymmetric unit contains one third of the $[Ag_2(bptz)_3](SbF_6)_2$ unit and only the geometrical parameters of the asymmetric unit are presented.

Table 34. Selected geometric parameters (Å,°) for $[Ag_2(bptz)_3](SbF_6)_2$ (**29**).

Ag1-Ag2	4.426(1)		
Ag1-N1	2.435(3)	Ag2-N3	2.568(3)
Ag1-N2	2.549(3)	Ag2-N4	2.432(3)
N1-Ag1-N2	67.58(10)	N4-Ag2-N3	66.66(10)
$N1^{i}$-Ag1-N1	97.26(10)	$N4^{i}$-Ag2-N4	98.29(10)
$N1^{ii}$-Ag1-N2	123.12(9)	$N4^{ii}$-Ag2-N3	124.95(9)
$N1^{i}$-Ag1-N2	137.56(9)	$N4^{i}$-Ag2-N3	135.04(9)
$N2^{ii}$-Ag1-N2	87.39(10)	$N3^{ii}$-Ag2-N3	87.17(10)

Symmetry transformations used to generate equivalent atoms:
i = -y+1,x-y,z ii = -x+y+1,-x+1,z

The mean Ag–N_{py} bond distance of 2.433(3) Å is longer than the standard value[24] of 2.299 Å and the same trend is observed for the mean Ag-N_{tz} bond distance. In the absence of a standard value in the crystallographic tables, in this case, the observed value of 2.558(3) Å is compared with the Ag-$N_{pyridazine}$ mean value of 2.338 Å [range from 2.20 to 2.56 Å] obtained using the program VISTA together with the CSD[9].

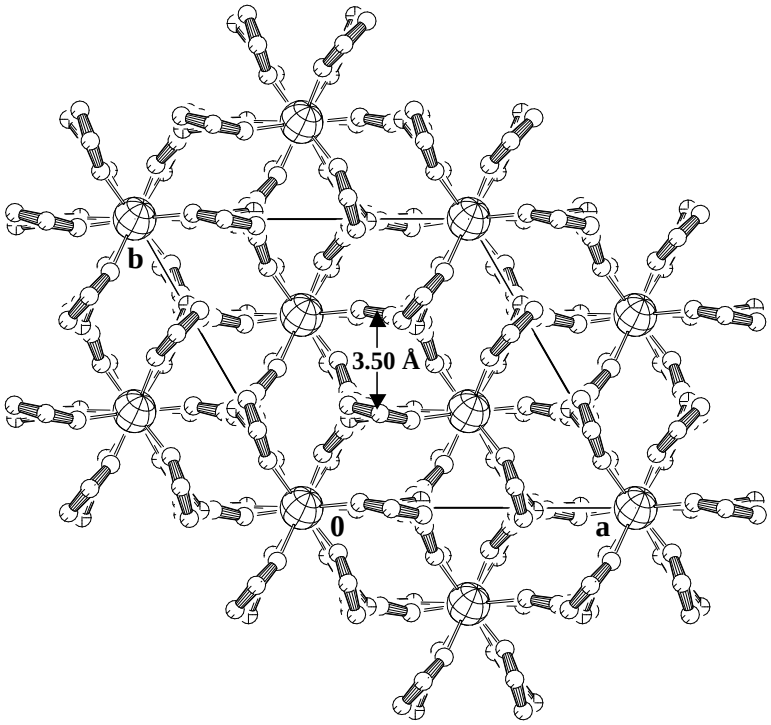

Figure 64. Crystal packing of compound **29** viewed down the *c* axis showing the π-π interactions and a honeycomb motif.

The analysis of their positive ES-MS spectrum in acetonitrile exhibits peaks at *m/z* 343, 462 and 580 which may be attributed to the species $[Ag_2(bptz)_2]^{2+}$, $[Ag_2(bptz)_3]^{2+}$and $[Ag(bptz)_2]^{+}$, respectively. The peaks at *m/z* 922 (for **29**) and 832 (for **29a**) correspond to $[Ag_2(bptz)_2X]^{+}$ where X is the respective counter-anion. Very weak peaks at *m/z* 1158 (for **29**) and 1069 (for **29a**) may be assigned to $[Ag_2(bptz)_3X]^{+}$ species. As it was suggested for compound **18** (Results, p 85) the peak at *m/z* 580 may be formed *in situ* under the conditions of the measurement with the loss of a silver atom. The two main species found in these spectra, $[Ag_2(bptz)_2]^{2+}$ (Ag in a tetrahedral environment) and $[Ag_2(bptz)_3]^{2+}$ (solid state compound), present comparable relative abundance and it is reasonable to suppose that π-π stacking effects as well as a gain in symmetry play a role in the crystallization of only the second species in both cases.

2.9.2. Complex $\{[Cd(bptz)I_2]\cdot CH_2Cl_2\}_n$ (30)

The reaction of **bptz** with CdI_2 using diffusion techniques yielded, after a few days, dark-red crystals of the polymeric complex $\{[Cd(bptz)I_2]\cdot CH_2Cl_2\}_n$ **(30)**.

$$\textbf{bptz}/CH_2Cl_2 \quad + \quad CdI_2/MeOH \xrightarrow{\text{diffusion}} \{[Cd(bptz)I_2]\cdot CH_2Cl_2\}_n \textbf{ (30)}$$

The IR spectrum of **30** shows the ligand characteristic vibrations shifted due to coordination.

Table 35. IR Data for the ligand **bptz** and the complex **30**.

Compound	IR, ν [cm^{-1}]
bptz	1640 (b, w), 1582 (s), 1479 (w), 1444 (m), 1391 (vs), 1130 (m), 994 (m), 799 (s), 745 (m), 733 (m), 597 (vs)
$\{[Cd(bptz)I_2]\cdot CH_2Cl_2\}_n$ **(30)**	1637 (w), 1594 (m), 1442 (w), 1394 (vs), 1255 (m), 1158 (m), 1139 (s), 1010 (m), 789 (m), 742 (m), 592 (s)

The crystal structure can be described as a *zigzag* or *step-like* (see Figure 66) one-dimensional polymer in which the Cd ions are bridged by bis-bidentate **bptz** molecules. The intra- and inter-chain[&] Cd…Cd distances are 7.645 (1) and 8.053 (1) Å, respectively. The asymmetric unit consists of one half of the $[Cd(bptz)I_2]\cdot CH_2Cl_2$ repeating unit and the polymer is generated by the symmetry operation x±n0.5, ±y, z. The coordination geometry around the cadmium atom is octahedral and arises from the coordination to two pyridine and two tetrazine nitrogen atoms plus two terminal iodine ions. The distortion from a perfect octahedral is essentially due to the small chelate angle of 66.44 (9) º.

The mean Cd-I and Cd–N_{py} bond distances of 2.7816(4) and 2.403(3) Å are comparable with the standard value[24] of 2.750 and 2.381 Å. No standard value is available for the Cd-N_{tz} but in any case the observed value, 2.528(3) Å, is longer than the standard values for Cd-N_{ar} (*ar* = aromatic ring containing N atoms) of *ca*. 2.35 Å.

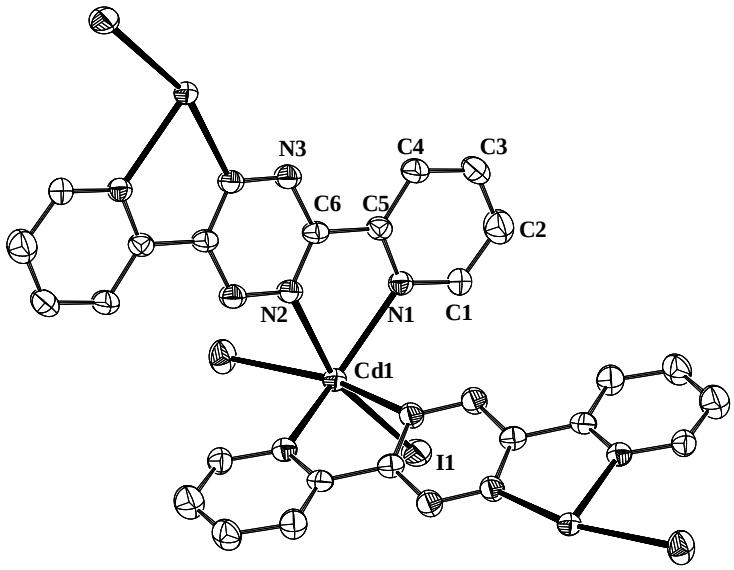

(a)

Cd1-Cd1^{i}	7.645(1)
Cd1-Cd1^{ii}	8.053(1)
Cd1-N1	2.403(3)
Cd1-N2	2.528(3)
Cd1-I1	2.7816(4)
N1-Cd1-N2	66.44(9)
N1-Cd1-I1	96.68(7)
N2-Cd1-I1	162.80(7)
N1^{iii}-Cd1-N1	135.93(13)
N1^{iii}-Cd1-N2	82.51(10)
N2-Cd1-N2^{iii}	90.14(14)
N1^{iii}-Cd1-I1	109.67(7)
N2^{iii}-Cd1-I1	84.09(7)
I1-Cd1-I1^{iii}	105.76(2)

i = -x,-y,z ii = -x+1/2,-y+1/2, -z+1/2
iii = -x+1/2, y, -z

(b)

Figure 65. **(a)** Molecular structure [H-atoms and solvent molecule omitted] and **(b)** some selected geometric parameters (Å,°) of complex **30**.

[&] Symmetry operation: -x+1/2, -y+1/2, -z+1/2

π-π stacking with a good overlap (rings parallel) can be observed with an average distance of *ca*. 3.78 (1) Å between the aromatic rings of symmetry related molecules (symmetry operation.: -x+1/2, -y+1/2, -z+1/2). In this complex the **bptz** molecules are rather planar with a dihedral angle between the pyridine and tetrazine rings of 11.8(2) º and the Cd atom is displaced from the chelate ring by 0.458 (7) Å.

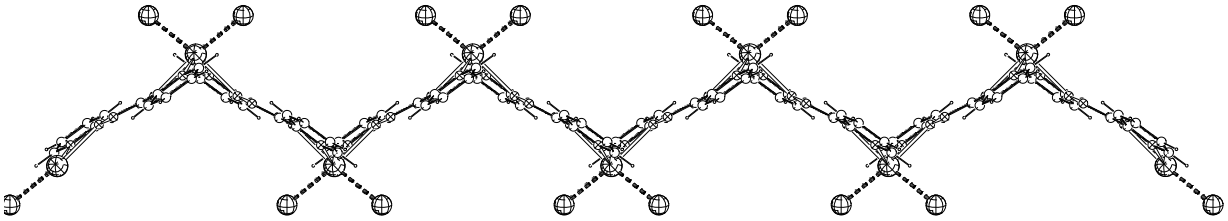

Figure 66. Zigzag structure of the complex $[Cd(bptz)I_2]_n$ **(30)** (CH_2Cl_2 molecule omitted).

No disorder was observed in this compound and an empirical absorption correction using DIFABS in PLATON[25] was applied.

2.9.3. Complexes $[Cd(bptz)(NO_3)_2]_n$ (31) and $[Zn(bptz)(NO_3)_2]_n$ (32)

The reaction of **bptz** with $Cd(NO_3)_2 \cdot 4H_2O$ or $Zn(NO_3)_2 \cdot 4H_2O$ using diffusion techniques yielded, after a few days, bright orange crystals of the polymeric complex $[Cd(bptz)(NO_3)_2]_n$ **(31)** and intense orange micro-crystals of the polymer $[Zn(bptz)(NO_3)_2]_n$ **(32)**. Compound **31** has been analysed by single crystal diffraction.

As compound **32** was obtained only in microcrystalline form, it was analysed by X-ray powder diffraction. Both compounds are isostructural [they present the same structure but have different unit cell parameters; see Table 38].

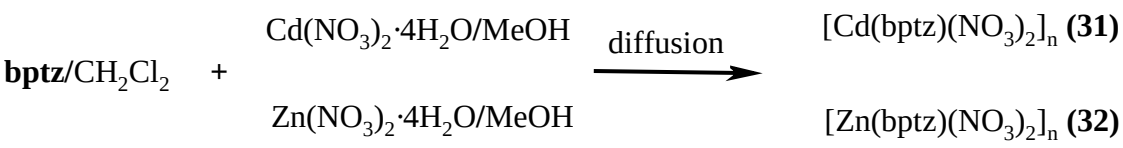

Apart from the typical imprint of the ligand, the most significant feature observed in the IR spectra of compounds **31** and **32** is the presence of the nitrate. In the case of the polymer **31** this vibration appears, as a broad band, together with the **bptz** band at 1394 cm^{-1}, whereas in compound **32** two clear bands at 1399 and 1384 cm^{-1} can be assigned to **bptz** and the nitrate vibrations, respectively.

Table 36. IR Data for the ligand **bptz** and the complexes **31** and **32**.

Compound	IR, ν [cm^{-1}]
bptz	1640 (b, w), 1582 (s), 1479 (w), 1444 (m), 1391 (vs), 1130 (m), 994 (m), 799 (s), 745 (m), 733 (m), 597 (vs)
$[Cd(bptz)(NO_3)_2]_n$ **(31)**	1596 (m), 1450 (s), 1394 (b, vs), 1306 (s), 1162 (w), 1138 (m), 1034 (m), 1017 (m), 946 (m), 797 (m), 601 (s)
$[Zn(bptz)(NO_3)_2]_n$ **(32)**	1600 (m), 1495 (w), 1462 (s), 1399 (vs), 1384 (vs), 1319 (s), 1143 (w), 1043 (m), 1020 (s), 952 (m), 795 (m), 604 (s).

The structure of both compounds, as in compound **30**, consists of a one-dimensional polymer in which the metal ions are bridged by bis-bidentate **bptz** molecules. In this case the shape of the chains cannot be described as a *zigzag* but as an almost planar strand in which the nitrate ions occupy the two axial positions of the metal coordination sphere.

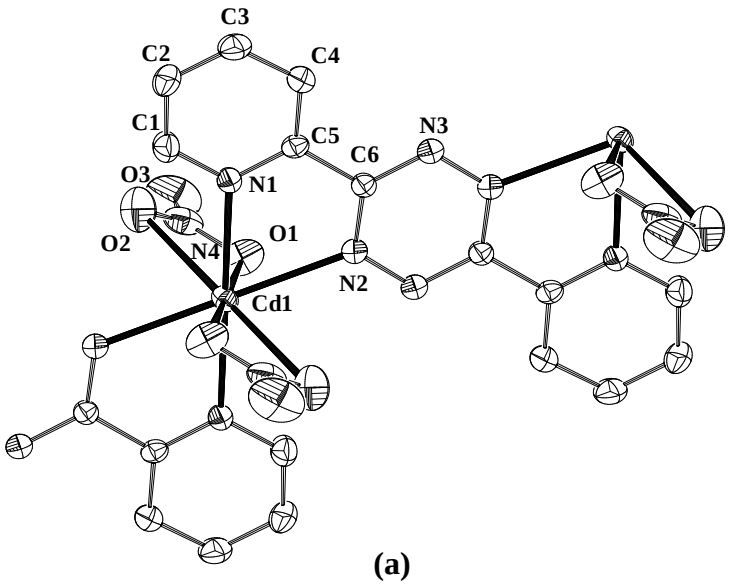

(a)

(b)

Cd1-Cd1^{i}	7.564(1)
Cd1-N1	2.325(2)
Cd1-N2	2.446(2)
Cd1-O1	2.349(2)
Cd1-O2	2.692(3)
N1-Cd1-O1	96.55(8)
N1-Cd1-N2	68.87(8)
O1-Cd1-N2	78.79(9)
O2-Cd1-O1	49.66(8)
O2-Cd1-N1	74.40(8)
O2-Cd1-N2	110.77(8)
N1^{ii}-Cd1-N1	180.00(16)
N1^{ii}-Cd1-O1	83.45(8)
O1-Cd1-O1^{ii}	180.00(15)
N1-Cd1-N2^{ii}	111.13(8)
O1-Cd1-N2^{ii}	101.21(9)
N2^{ii}-Cd1-N2	180.00(12)

i = x-1, y, z ii = -x+2, -y, -z

Figure 67. **(a)** Molecular structure [H-atoms omitted] and **(b)** selected geometric parameters (Å,°) of complex $[Cd(bptz)(NO_3)_2]_n$ (**31**).

In compound **31** the cadmium can be described as being eight coordinate although the long distance Cd1-O2 may better be considered as a secondary interaction and the coordination geometry would then correspond to a distorted octahedron. In general, the bond distances are in good agreement with standard values. The ligand is almost planar with a dihedral angle of 3.7 (1) º between the pyridine and the tetrazine rings and the cadmium ion is displaced by only 0.155 (5) Å from the binding unit mean plane. As in compound **30**, weak π-π interactions of *ca*. 3.8 Å between symmetry related (i = 1-x, -y, 1-z) molecules are observed. The polymeric chains are connected by weak C-H…O interactions [C2…O2^{i} = 3.212 Å and C2^O2^{i} 129.9 º with i = -x, -y, 1-z] that have an effect on the final crystal organization, forcing the ligands to be almost parallel with respect to its neighbours. The planar

arrangement of the 1D polymeric structure of this complex can be clearly visualized in the next figure.

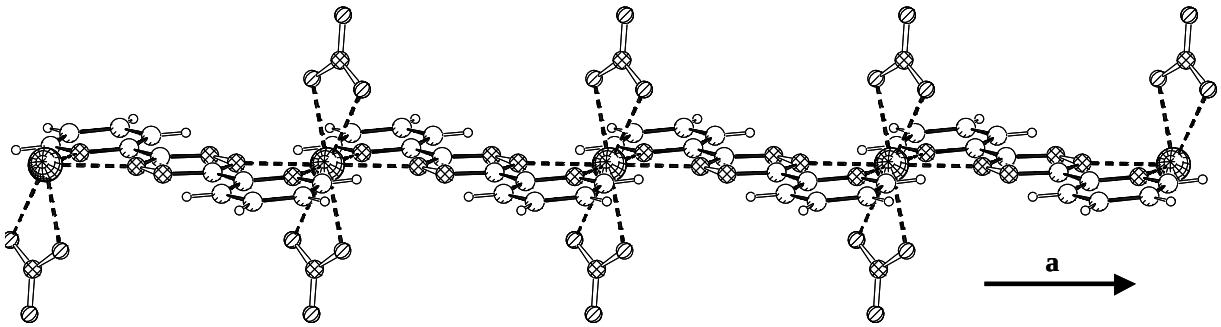

Figure 68. Polymeric structure of the complex $[Cd(bptz)(NO_3)_2]_n$ **(31).**

The structure of compound **32** differs from that of compound **31** mainly in the manner in which the nitrate ions coordinate to the metal. In **32** the distances Zn1-O1 and Zn1-O2 are very different and it is clear that atom O2 does not take part in coordination. The Zn1-O1 bond distance is close to the standard value of 2.179 Å for $Zn\text{-}O_{nitrate}$ where the nitrate acts in a non-chelating manner, whereas the Zn-N distances are slightly longer than the standard values [$Zn\text{-}N_{py}$ 2.116 Å, $Zn\text{-}N_{heterocycle}$ < 2.2 Å].

Table 37. Selected geometric parameters (Å,°) for $[Zn(bptz)(NO_3)_2]_n$ **(32)**.

$Zn1\text{-}Zn1^{i}$	7.166	O1-Zn1-N2	94.60(24)
Zn1-N1	2.153(6)	$N1^{ii}$-Zn1-N1	180.00(0)
Zn1-N2	2.255(3)	$N1^{ii}$-Zn1-O1	97.00(24)
Zn1-O1	2.103(6)	$O1\text{-}Zn1\text{-}O1^{ii}$	180.00(0)
Zn1-O2	3.114(6)	$N1\text{-}Zn1\text{-}N2^{ii}$	103.09(25)
N1-Zn1-O1	83.00 (23)	$O1\text{-}Zn1\text{-}N2^{ii}$	85.40(24)
N1-Zn1-N2	76.91(25)	$N2^{ii}$-Zn1-N2	180.00(0)

As in compound **31** weak π-π interactions of *ca*. 3.8 Å between symmetry related molecules are observed in **32**. Some C-H…N and C-H…O short interactions, that are different to those found for compound **31**, guarantee the crystal cohesion and influence the packing motif,

forcing the ligand molecules to be in the same plane. The shortest distances are found for the couples C1…N3 3.405 Å, C1^N3 144.13 °; C2…O3 3.240 Å, C2^O3 143.71 ° and C4…O3 3.281 Å, C4^O3 127.02 ° (see Figure 69).

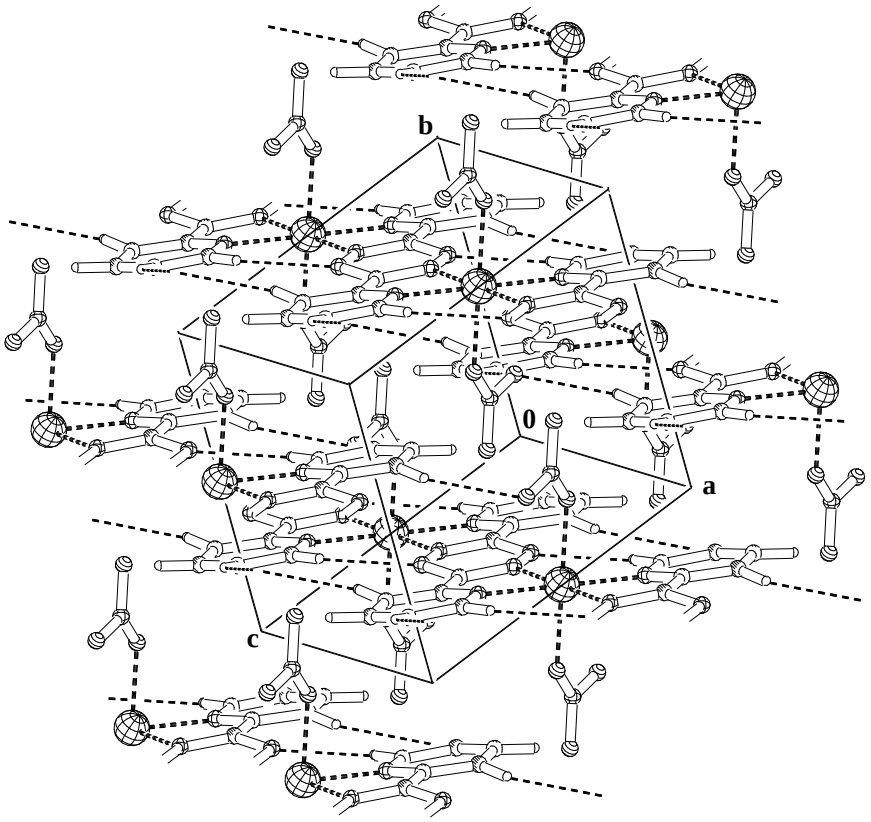

Figure 69. Polymeric structure of the complex $[Zn(bptz)(NO_3)_2]_n$ **(32)** emphasizing the C-H…O and C-H…N short interactions. It can also be clearly observed the monodentate way in which the nitrate ions are coordinated.

Table 38. Unit cell dimensions for $[Cd(bptz)(NO_3)_2]_n$ **(31)** and $[Zn(bptz)(NO_3)_2]_n$ **(32)**

	a	**b**	**c**	**α**	**β**	**γ**	**V**
31	7.5644(8)	7.8640(9)	8.1179(9)	66.143(12)	67.702(12)	63.301(12)	382.83
32	7.1756(1)	7.6770(2)	8.4978(2)	113.507(2)	92.530(1)	117.002(1)	367.66

No disorder was observed in compounds **31** and **32** and an empirical absorption correction using DIFABS in PLATON[25] was applied for compound **31**.

2.9.4. Complexes $[Hg_2(bptz)Cl_4]_n$ (33), $[Hg(bptz2)Cl_2]$ (33a), $[Hg(bptz)Br_2]_n$ (34) and $[Hg_2(bptz)I_4]_n$ (35)

The reaction, either by diffusion or at reflux, of **bptz** with different mercury salts afforded crystals of the polymeric complexes $[Hg_2(bptz)Cl_4]_n$ **(33)**, $[Hg(bptz)Br_2]_n$ **(34)** and $[Hg_2(bptz)I_4]_n$ **(35)**. The appearance of the crystalline material was different depending on the reaction method. When diffusion techniques were applied, a very thin hair-like crystalline material was obtained whereas when the two reactants were mixed and refluxed, block-like crystals were obtained. Except for **35**, the crystals selected for the measurements were obtained by the second method. The IR spectra and, in the case of compound **33**, the powder diffraction pattern, showed that the compounds obtained by both methods were identical.

$$\textbf{bptz} + HgCl_2{\cdot}2H_2O \xrightarrow[\text{or diffusion}]{\text{MeOH, reflux}} [Hg_2(bptz)Cl_4]_n\ \textbf{(33)} \xrightarrow{\text{solvent evaporation}} [Hg(bptz2)Cl_2]\ \textbf{(33a)}$$

Compound **33a** was obtained by allowing the solution that remained after taking off the crystals of compound **33** to stand for more than 1 month and **bptz2** is the result of a transformation of the ligand **bptz**.

$$\textbf{bptz} + HgBr_2 \xrightarrow[\text{or b) diffusion}]{\text{a) MeCN, reflux}} [Hg(bptz)Br_4]_n\ \textbf{(34)}$$

$$\textbf{bptz}/CH_2Cl_2 + HgI_2/MeOH \xrightarrow{\text{diffusion}} [Hg_2(bptz)I_4]_n\ \textbf{(35)}$$

The IR spectra of compounds **33**, **34** and **35** show clearly the presence of the ligand main vibration bands that are slightly shifted to higher or lower frequencies with respect to the IR spectrum of **bptz** due to complexation, as is seen in Table 39.

Table 39. IR Data for the ligand **bptz** and the complexes **33**, **34** and **35**.

Compound	IR, ν [cm^{-1}]
bptz	1640 (b, w), 1582 (s), 1479 (w), 1444 (m), 1391 (vs), 1130 (m), 994 (m), 799 (s), 745 (m), 733 (m), 597 (vs)
$[Hg_2(bptz)Cl_4]_n$ **(33)**	1629 (w), 1589 (m), 1447 (w), 1391 (vs), 1260 (m), 1136 (m), 1003 (m), 787 (s), 743 (m), 590 (s)
$[Hg(bptz)Br_2]_n$ **(34)**	1622 (w), 1584 (s), 1442 (m), 1385 (vs), 1259 (m), 1151 (m), 1124 (m), 999 (m), 799 (s), 745 (m), 592 (s)
$[Hg_2(bptz)I_4]_n$ **(35)**	1683 (m), 1589 (m), 1468 (m), 1444 (m), 1389 (vs), 1132 (m), 1067 (m), 1003 (m), 783 (s), 744 (m), 591 (s).

Complexes **33-35** crystallize as one-dimensional polymers in which the mercury atoms are bridged by **bptz** ligand molecules coordinating in a bis-mono or bis-bidentate manner.

In compound **33** the coordination geometry around the mercury atom can be described as a square-based pyramid with a τ value[51] equal to 0. The distance Hg1-N2 (2.94 (3) Å) is too long to be taken as part of the coordination sphere of the metal ion. The Hg(II) ion is displaced by 0.357(9) Å out of the basal plane, defined by the atoms Cl1, Cl2, $Cl1^i$ and $Cl2^i$ (i = x+1, y, z), towards the N1 axial donor.

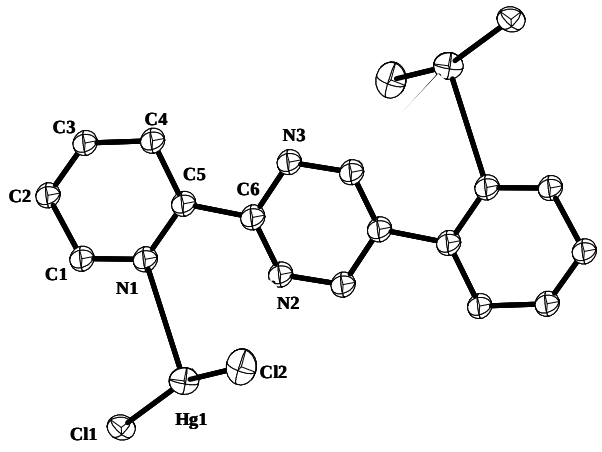

Figure 70. Molecular structure of the complex **33** showing the numbering scheme and thermal ellipsoids at 50% probability level. H-atoms have been omitted.

Apart from the **bptz** ligand molecules, the mercury ions are connected by means of an asymmetric chloride bridge where all of the four Hg-Cl bond distances are different, as depicted in Scheme 15.

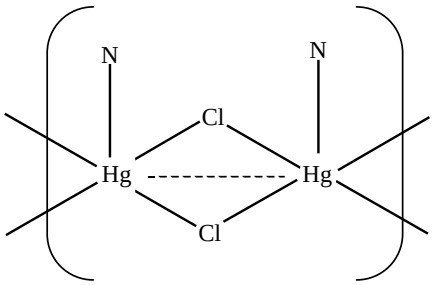

Scheme 15

Table 40. Selected geometric parameters (Å,°) for **33**.

Hg1-Hg1^{iii}	8.321(3)	Hg1-Hg1^{i}	3.989(1)
Hg1-Cl1	2.339(10)	Hg1-Hg1^{ii}	4.343(3)
Hg1-Cl2	2.332(10)	Cl1-Hg1-N1	93.0(9)
Hg1-Cl1^{i}	3.165(10)	Cl2-Hg1-N1	102.5(9)
Hg1^{i}-Cl2	3.075(11)	Cl1^{i}-Hg1-N1	75.8(7)
Hg1-N1	2.65(3)	Cl2^{i}-Hg1-N1	86.1(9)
Hg1…N2	2.94(3)	Cl2-Hg1-Cl1	162.3(4)

Symmetry operations: i x+1,y,z ii –x,-y,1-z iii -x,-y,-z

In complex **33** the ligand molecules are relatively planar with a dihedral angle of 16.00 (4.11)° between the pyridine and the tetrazine ring mean planes. As in some of the **bptz** polymers already presented weak π-π interactions of 3.9895(6) Å [distance that corresponds to the length of the *a* axis] between symmetry related chains are observed in **33**, as well as C-H…Cl weak interactions [C2…Cl1^{i} 3.719 Å and C2^Cl1^{i} 164.51 °] that link the one-dimensional chains to form, to some extent, a two dimensional network (Figure 71).

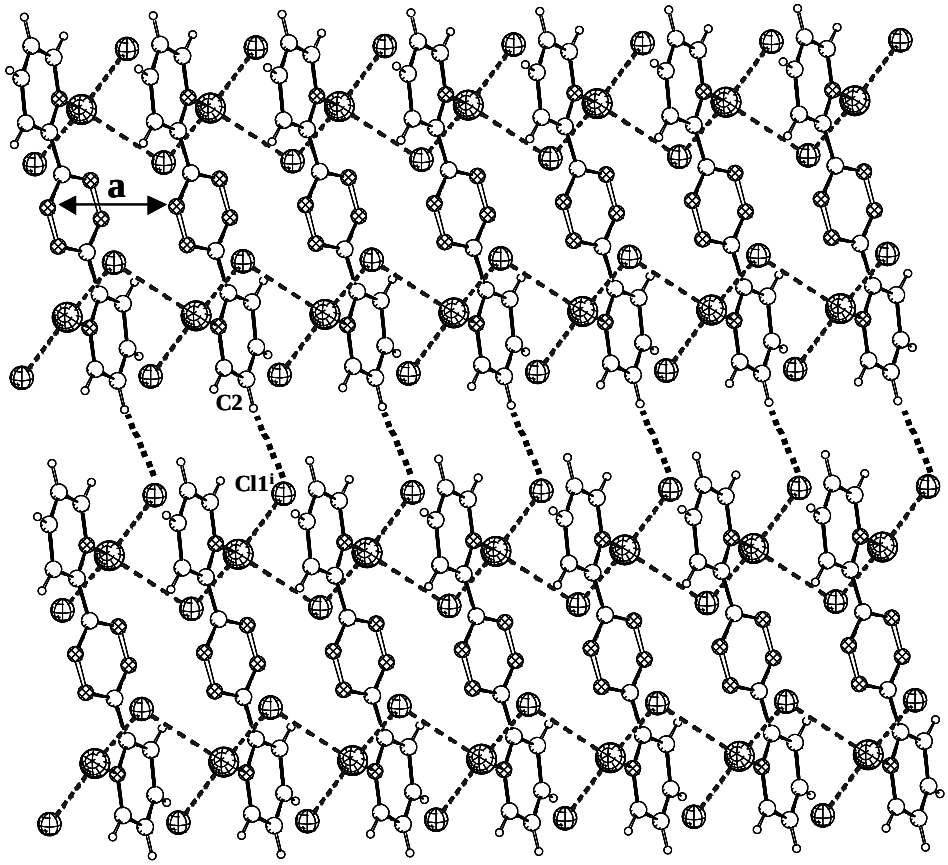

Figure 71. Polymeric structure of the complex $[Hg_2(bptz)Cl_4]_n$ **(33)**.

A very high R(int) value, probably due to the poor quality of the crystal, resulted in a poor refined structure. An empirical absorption correction using DIFABS in PLATON[25] was applied but it did not improve the accuracy of the refined structure.

Colourless crystals of the mononuclear complex **33a** were obtained as a degradation product from the former reaction. Within approximately one-month, the strong pink solution remaining after picking out the crystals of compound **33**, progressively became colourless and crystals of compound **33a** were formed and measured. The crystal structure is showed in the following figure and consist of discrete [Hg(bptz2)Cl_2] monomeric units.

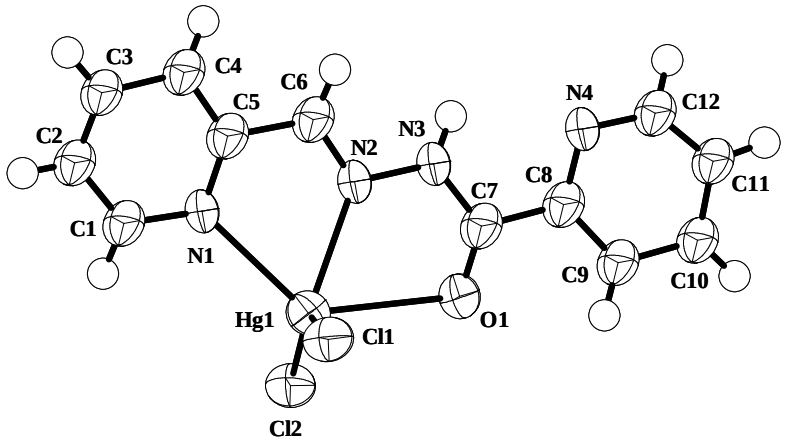

Figure 72. Molecular structure of the complex [Hg(bptz2)Cl_2] **(33a)** showing the numbering scheme and thermal ellipsoids at 50% probability level.

The asymmetric unit consists of four independent molecules, which differ only slightly in bond lengths and angles. The mercury atom is pentacoordinate. The *new* ligand molecule, **bptz2**, coordinates in a tridentate manner resulting in the formation of two nearly coplanar five-membered rings. Two terminal chloride atoms occupy the remaining positions. The polyhedron around the mercury atom could be described as an almost perfect square-based pyramid with a τ value varying from 0 to 0.11 for the four independent molecules. A comparison of the main bond distances and angles for the four independent molecules in **33a** is given in the next table.

The crystal was refined as a racemic twin with a Flack parameter[50] of 0.61(7).

Table 41. Selected geometric parameters (Å,°) for **33a**.

	Molecule 1	**Molecule 2**	**Molecule 3**	**Molecule 4**
Hg1-N1	2.53(3)	2.42(4)	2.46(4)	2.40(3)
Hg1-N2	2.37(4)	2.42(4)	2.46(4)	2.47(4)
Hg1-O1	2.67(3)	2.70(3)	2.63(3)	2.70(3)
Hg1-Cl1	2.400(12)	2.398(12)	2.373(14)	2.365(13)
Hg1-Cl2	2.351(13)	2.356(13)	2.334(12)	2.354(13)
Cl2-Hg1-Cl1	137.5(5)	129.8(6)	133.6(5)	130.8(6)
Cl2-Hg1-N1	112.6(9)	113.3(8)	115.0(9)	115.9(10)
Cl1-Hg1-N1	95.3(9)	99.8(8)	93.6(10)	98.9(10)
Cl2-Hg1-N2	120.7(10)	111.6(9)	115.8(10)	109.1(10)
Cl1-Hg1-N2	99.3(10)	115.5(8)	108.0(10)	115.4(10)
N1-Hg1-N2	66.3(11)	67.8(12)	69.4(12)	69.2(12)
Cl2-Hg1-O1	88.7(8)	87.3(8)	85.4(8)	89.0(8)
Cl1-Hg1-O1	96.8(8)	99.6(8)	102.3(9)	94.2(8)
N1-Hg1-O1	130.8(1.0)	130.0(1.1)	131.9(11)	130.1(1.1)
N2-Hg1-O1	64.7(1.1)	62.3(1.1)	62.5(11)	61.7(1.0)

The whole ligand molecule is almost planar. The atoms N1,C1-C5,C6,N2-3,C7,O1 lie in the same plane [mean deviation: 0.0326 Å] and the dihedral angle between this plane and the mean plane of the pyridine N4,C8-C12 varies from 0.5 to 6.1 °. The discrete mononuclear molecules are connected via a hydrogen-bonding network.

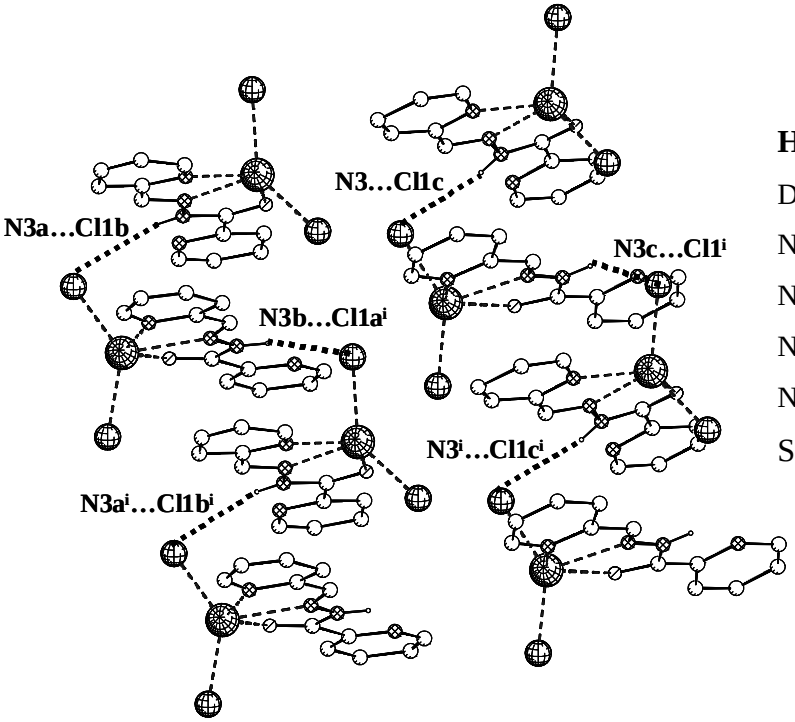

Hydrogen-bonding geometry (Å,º)

D-H...A	d(H...A)	d(D...A)	(D^A)
N3-H3...Cl1C	2.959	3.615	134.65
N3A-H3A...Cl1B	2.792	3.567	150.63
N3B-H3B...Cl1A^{i}	2.710	3.388	136.73
N3C-H3C...Cl1^{i}	2.763	3.512	146.41

Symmetry operation: i = x+1,y,z

Figure 73. Diagram showing the hydrogen bonding motif in [Hg(bptz1)Cl_2] **(33a)**.

In the crystal packing of **33a**, the hydrogen bonding connections give rise to one-dimensional chains that run parallel with the crystallographic *a* axis, as depicted in Figure 73.

Compound **34** can be described as a one-dimensional polymeric chain in which the Hg ions are bridged by bis-bidentate **bptz** molecules leading to a intra-chain Hg…Hg distance of 8.2912(2) Å. The asymmetric unit consists of half of the [Hg(bptz)Br_2] repeating unit and the polymer is generated by the symmetry operation x, y-1, z-1. The coordination geometry around the mercury atom is octahedral (Figure 74) and arises from the coordination to two pyridine and two tetrazine nitrogen atoms plus two terminal *trans* bromide ions. The distortion from a perfect octahedral is essentially due to the very small chelate angle of 58.9(1) º. The Hg-Br bond distance of 2.4610(8) Å is shorter than the standard value of 2.539 Å whereas the Hg-N bond distances are much longer (> 2.71 Å) than, for instance, the standard value for Hg-N_{py} of 2.164 Å. The N atoms can therefore be considered as weakly coordinated, see below.

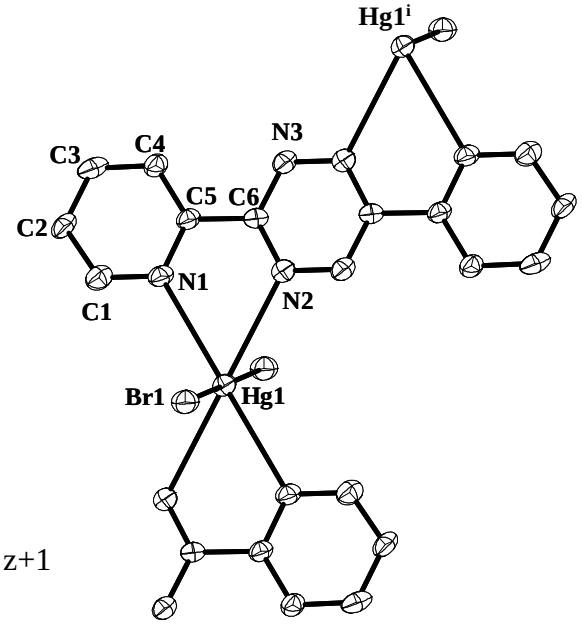

Hg1-Hg1^{i}	8.2912(2)
Hg1-N1	2.712(5)
Hg1-N2	2.824(5)
Hg1-Br1	2.4610(8)
N1-Hg1-N2	58.9(1)
N1-Hg1-Br1	88.3(1)
N2-Hg1-Br1	94.4(1)
Br1-Hg1-Br1^{ii}	180.0
N1-Hg1-Br1^{ii}	91.7(1)
N1-Hg1-N1^{ii}	180.0
N2-Hg1-Br1^{ii}	85.57(1)
N2-Hg1-N2^{ii}	180.0

i : -x+1,-y-1,-z ii : -x+1,-y,-

Figure 74. **(a)** Molecular structure [H-atoms omitted] and **(b)** selected geometric parameters (Å,°) of complex **34**.

In this polymer the **bptz** molecules are almost perfectly planar with a dihedral angle between the pyridine and tetrazine ring mean planes of 6.8(9) º and the Hg atom is displaced from the chelate ring by 0.71 (1) Å. Weak inter-chain π-π stacking is found between the aromatic rings of symmetry related molecules (-x, -y-1, -z) with an average distance of *ca*. 3.75 (1) Å.

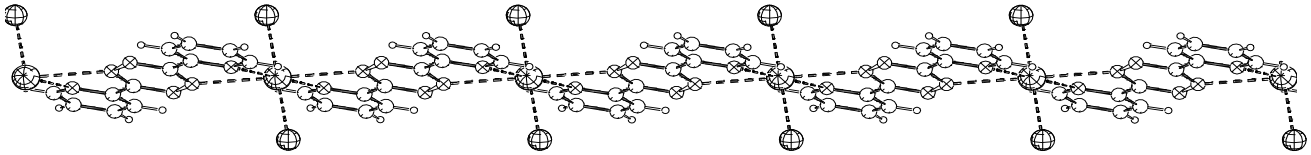

Figure 75. Polymeric structure of the complex $[Hg(bptz)Br_2]_n$ **(34)**.

Finally, the crystal structure of complex **35** can be also described as a one-dimensional polymeric *zigzag* chain. The repeated structural moiety consists of $[Hg_2(bptz)I_4]$ units that are related to one another by translations of the length of the crystallographic *c* axis with intra- (i = -x+1,-y,-z+1) and inter- (ii = -x+1,-y,-z) molecular Hg…Hg distances of 8.1905(14) and 4.0246(12) Å, respectively.

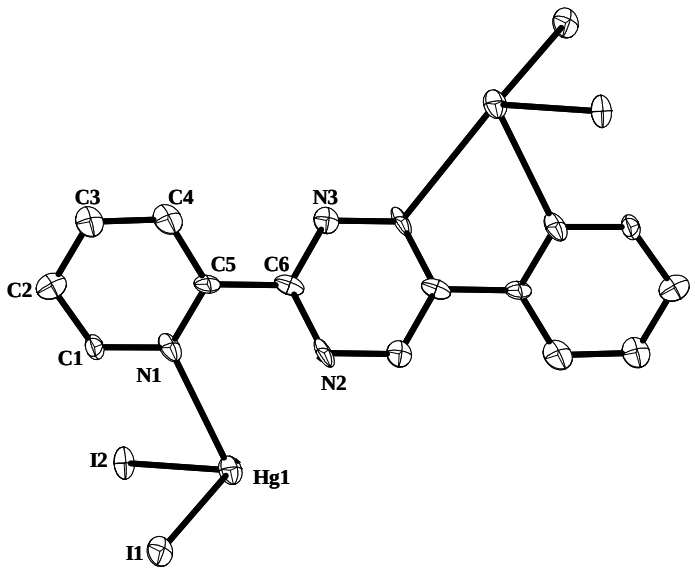

Hg1-Hg1^{i}	8.1905(14)
Hg1-Hg1^{ii}	4.0246(12)
Hg1-N1	2.489(10)
Hg1-N2	2.893(10)
Hg1-I1	2.6538(10)
Hg1-I2	3.1028(9)
Hg1-I2^{ii}	2.6854(10)
N1-Hg1-I1	95.4(2)
N1-Hg1-I2	84.7(2)
I1-Hg1-I2	107.25(3)
N1-Hg1-I2^{ii}	121.8(2)
I1-Hg1-I2^{ii}	139.65(3)
I2^{ii}-Hg1-I2	92.21(3)

i : -x+1,-y,-z+1 ii -x+1,-y,-z

Figure 76. **(a)** Molecular structure [H-atoms omitted] and **(b)** selected geometric parameters (Å,°) of complex **35**.

The mercury atom is in a distorted tetrahedral environment provided by the pyridine nitrogen atom and three iodine ions; one of them is terminal and the other two are involved in an asymmetrical bridge. As for compound **33**, the distance Hg1-N2 of 2.893(10) Å is too long for it to be considered as part of the coordination sphere of the metal ion. While in compound **33** the four Hg-Cl bridging bond distances were different, in this case the iodine bridge has a symmetry centre and therefore, there are only two different Hg-I distances. In complex **35** the ligand molecules are less planar than in compound **33** with a dihedral angle of 30.9(7) ° between the pyridine and the tetrazine ring mean planes. This is probably due to the steric hindrance caused by the presence of the larger iodine instead of the smaller chloride ions. Weak π-π interactions of 3.71(2) Å between symmetry related chains [symmetry operation: -x, 1-y, 1-z] are observed in **35** but no H-bonds.

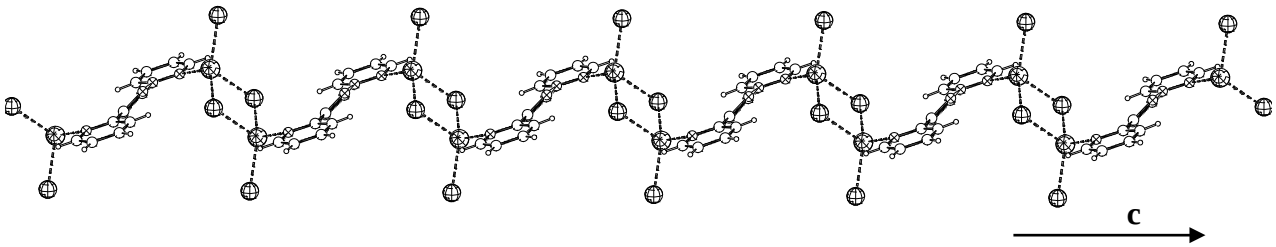

Figure 77. Polymeric structure of the complex $[Hg_2(bptz)I_4]_n$ **(35)**

2.9.5. **Compounds** $[Cu(bptz1)Cl_2]_n$ **(36)** $[Mn(bptz2)Cl_2 \cdot CH_3OH]$ **(37)** and bptz3 **(38)**

During the realization of the complexation reactions with the ligand **bptz** the unexpected products $[Cu(bptz1)Cl_2]_n$ **(36)** $[Mn(bptz2)Cl_2 \cdot CH_3OH]$ **(37)** and bptz3 **(38)** were obtained.

Compound **36** had already been reported[55]. This compound was obtained by the reaction of the ligand (1,3,4-oxadiazole-2,5-diyl)dipyridine, **odp** with $CuCl_2 \cdot 2H_2O$ whereas in our case, the same result was obtained using the ligand **bptz** which under the conditions of the

experiment is transformed into **bptz1** = **odp**. During the reaction of **bptz** with $CuCl_2 \cdot 2H_2O$ two products were always formed. A purple insoluble powder precipitate appeared almost instantaneously and was filtered off. After several weeks green crystals of compound **36** were formed from the remaining solution. From the analysis of the IR spectra signals of both products it is reasonable to suppose that the purple powder (**X**) is a complex, probably a polymer of un-transformed **bptz** [the main **bptz** vibrations can be identified in the IR spectrum of X]. The IR spectrum of compound **36** does not present the normal absorption bands of this ligand.

Table 42. Compared IR Data for the ligand **bptz** and the complexes **X** and **36**.

Compound	IR, ν [cm^{-1}]
bptz	1640 (b, w), 1582 (s), 1479 (w), 1444 (m), 1391 (vs), 1130 (m), 994 (m), 799 (s), 745 (m), 733 (m), 597 (vs)
Purple powder **(X)**	1640 (b, w), 1596 (m), 1460 (w), 1446 (m), 1391 (vs), 1134 (m), 1025 (m), 940 (m), 809 (m), 595 (m).
$[Cu(bptz1)Cl_2]_n$ **(36)**	1614 (m), 1545 (s), 1469 (s), 1425 (vs), 1314 (m), 1288 (m), 1253 (m), 1148 (s), 1094 (m), 1051 (m), 1022 (m), 806 (vs), 707 (s).

Compound **36** can be described as a linear $[Cu(bptz1)Cl_2]_n$ chain in which the Cu(II) atoms are bridged by a bis-bidentate **bptz1** molecule with a Cu…Cu distance of 5.522 (1) Å. Two terminal chloride ions complete the distorted octahedral coordination around the copper atom.

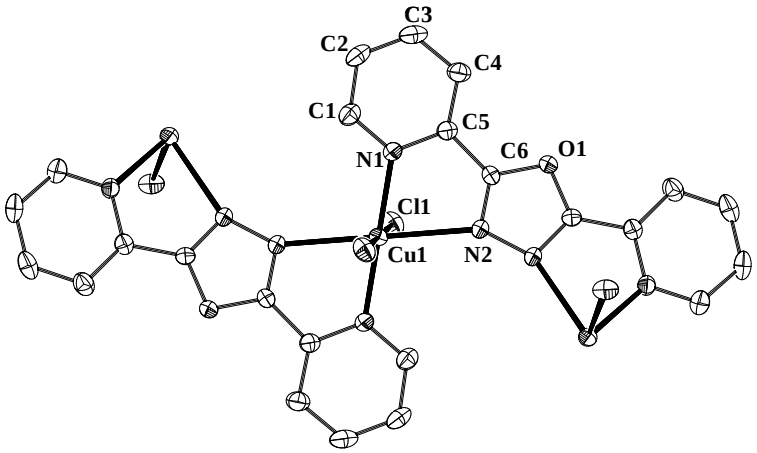

All the crystallographic data for **36** are in agreement with the already published structure[55].

Figure 78. Crystal structure of the complex $[Cu(bptz1)Cl_2]n$ **(36)** with numbering scheme.

The second unexpected product [Mn(bptz2)Cl_2·CH_3OH] **(37)** was obtained in the form of brown crystals after *ca*. 3 weeks, from the reaction between **bptz** and $MnCl_2·4H_2O$ in MeOH. Very small orange crystals were also formed during this reaction.

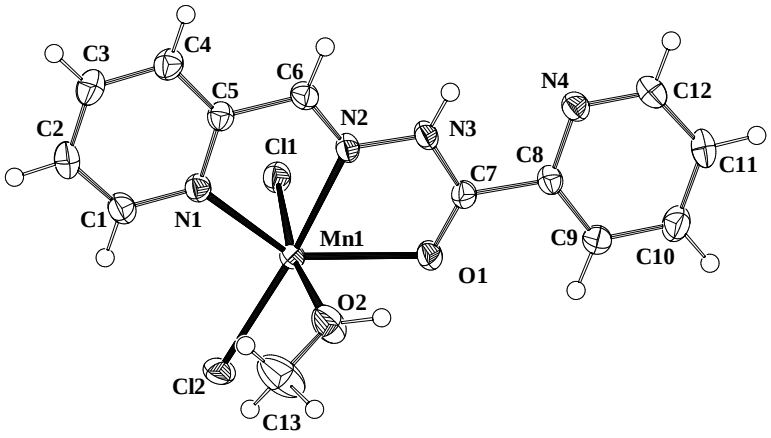

Figure 79. Molecular structure of the complex [Mn(bptz2)Cl_2·CH_3OH] **(37)** showing the numbering scheme and thermal ellipsoids at 50% probability level.

Compound **37** consists of discrete monomeric [Mn(bptz2)Cl_2·CH_3OH] units in which the ligand **bptz** has suffered the same transformation found in compound **33a**. The *new* ligand molecule, **bptz2**, coordinates in a tridentate manner and the manganese distorted octahedral geometry is completed by means of two terminal *cis* chloride ions and one methanol molecule.

Table 43. Selected geometric parameters (Å,°) for **37**

Mn1-N1	2.2972(14)	N2-Mn1-O1	68.73(4)
Mn1-N2	2.2536(14)	N1-Mn1-O1	138.69(5)
Mn1-O1	2.3402(12)	O2-Mn1-Cl2	87.66(4)
Mn1-O2	2.2277(13)	N2-Mn1-Cl2	171.20(4)
Mn1-Cl1	2.5016(5)	N1-Mn1-Cl2	101.63(4)
Mn1-Cl2	2.4053(5)	O1-Mn1-Cl2	118.42(3)
		O2-Mn1-Cl1	169.77(4)
O2-Mn1-N2	88.62(5)	N2-Mn1-Cl1	87.04(4)
O2-Mn1-N1	92.02(6)	N1-Mn1-Cl1	95.26(4)
N2-Mn1-N1	70.53(5)	O1-Mn1-Cl1	89.25(4)
O2-Mn1-O1	80.54(5)	Cl2-Mn1-Cl1	97.874(17)

As observed in compound **33a**, the ligand molecule is almost perfectly planar. The atoms N1,C1-C5,C6,N2-3,C7,O1 lie in the same plane [mean deviation: 0.0156 Å] and the dihedral angle between this plane and the mean plane of the pyridine N4,C8-C12 is 9.0 (1) °. As for compound **33a**, intermolecular hydrogen-bonding interactions link the mononuclear complexes to form a 2D hydrogen-bonded network.

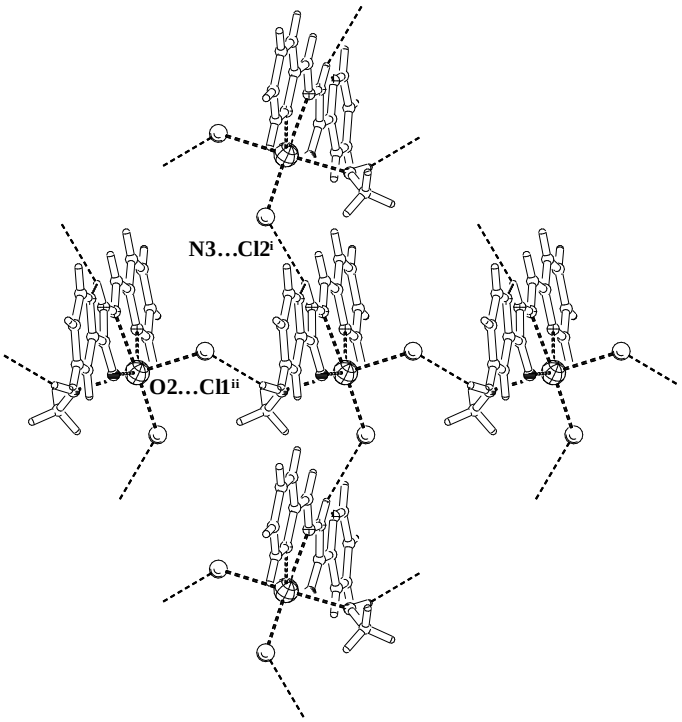

Hydrogen-bonding geometry (Å,º)

D-H...A	d(D-H)	d(H...A)	d(D...A)	(D^A)
N3-H3N...Cl2^{i}	0.870	2.604	3.356	145.22
O2-H2O...CL1^{ii}	0.940	2.293	3.113	145.37

Symmetry operations:

i -x+1/2,y-1/2,-z+3/2 ii x+1,y,z

Figure 80. Diagram showing the hydrogen bonding motif in [Mn(bptz2)Cl_2·CH_3OH] **(37)**

Finally, product **bptz3 (38)** was obtained in the form of orange-brown crystals by slow diffusion of **bptz** in MeOH over $Mn(ClO_4)_2$·$6H_2O$ in H_2O in a glass tube. Its structure is very interesting combining the forms **bptz-H** (the tetrazine central ring has been transformed into a 1,4-dihydro-tetrazine) and **bptz2** together in one single molecule as shown in the following figure.

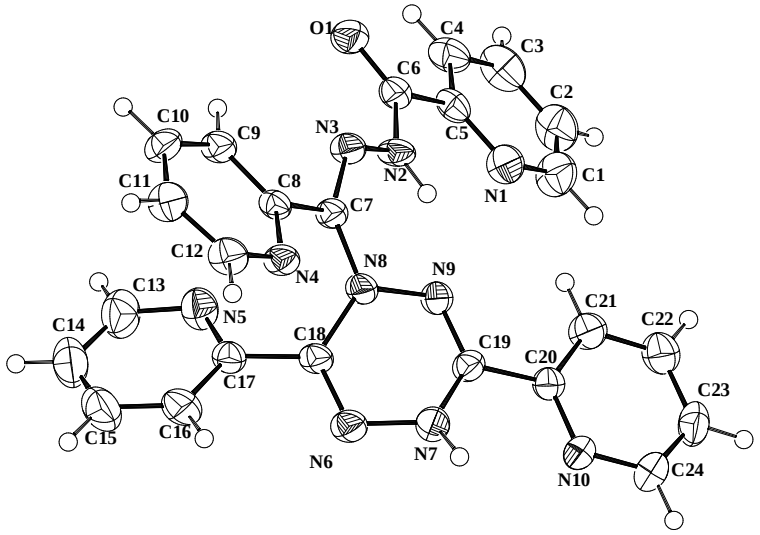

C5-C6	1.502(5)
C6-O1	1.219(4)
C6-N2	1.345(5)
C7-N3	1.295(4)
C7-N8	1.385(5)
C17-C18	1.474(5)
C18-N6	1.271(5)
C18-N8	1.410(5)
C19-N9	1.281(5)
C19-N7	1.388(5)
C19-C20	1.485(5)
N2-N3	1.383(4)
N6-N7	1.412(4)
N8-N9	1.432(4)

Figure 81. Molecular structure and selected bond distances (Å) for compound **38**.

The bond distances are in agreement with the observed structure with double bond distances for the bonds C19-N9, C18-N6 and C6-O1 and a delocalised path from atom C6 to atom C7. The pyridine and hydro-tetrazine rings are considerably twisted one with respect to the other as shown in the next table. All the pyridine rings are almost perfectly planar as expected for an aromatic ring whereas the hydro-tetrazine ring is not; the largest atomic deviation from the mean ring plane being 0.1761 Å.

Table 44. Some dihedral angles (t, º) and distances (d, Å) for **38**.

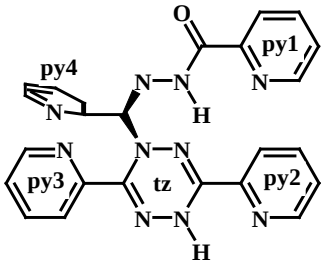

t(py1-py2)	25.6(2)	d(py1)	0.0035
t(py2-tz)	19.0(1)	d(py2)	0.0048
t(tz-py3)	38.0(1)	d(py3)	0.0128
t(py3-py4)	45.1(1)	d(py4)	0.0098
		d(tz)	0.1761

The distance d is a measure of the planarity of the rings.

The crystal packing of compound **38** is determined by the presence of some weak intra- and inter- molecular hydrogen bonds that link symmetry related molecules. A packing diagram and the hydrogen bond geometry are given in the next figure and table.

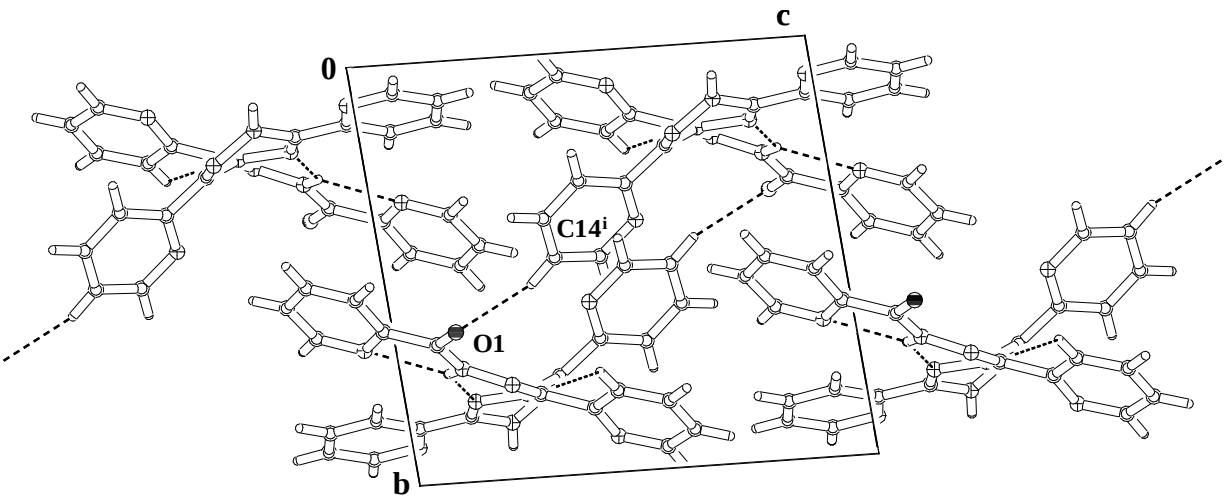

Figure 82. Crystal packing showing the H-bond motif for compound **38**.

Table 45. Hydrogen-bonding geometry **(Å,º)** for **38**.

D-H...A	d(D-H)	d(H...A)	d(D...A)	(D^A)
C21-H21...N1	0.94	2.64	3.55(1)	162.3
N2-H2A...N1	0.87	2.29	2.67(1)	106.4
N2-H2A...N9	0.87	2.04	2.69(1)	131.5
$C14^{i}$-$H14^{i}$...O1	0.94	2.35	3.25(1)	161.4

Symmetry operation: i –x,1-y,1-z

As observed in compounds **33a**, **36**, **37** and **38**, the ligand **bptz**, under certain conditions, can undergo diverse structural modifications. Three different forms (Scheme 16) of this ligand have been found, either in metal complexes (**33a**, **36** and **37**) or as a pure organic compound (**38**).

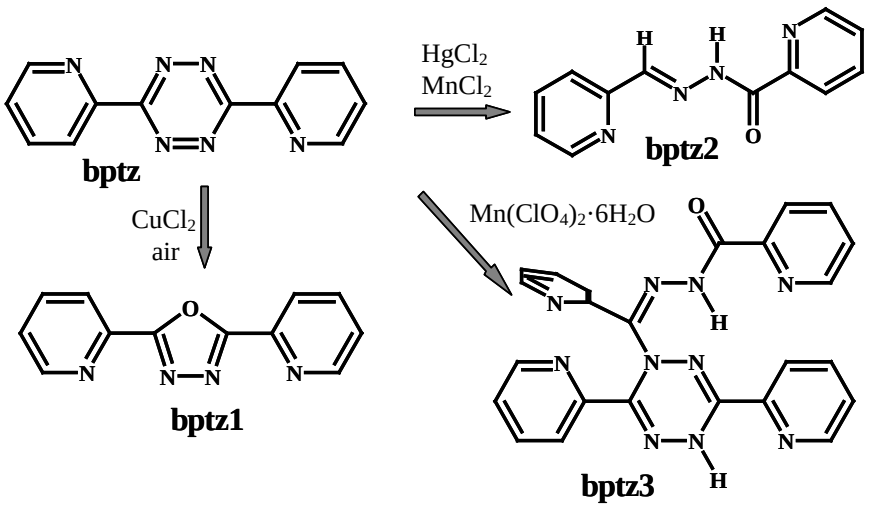

Scheme 16

Several studies on base-catalysed reactions of 3,6-disubstituted tetrazines have been reported[57] and they provide an idea of the most probable mechanism for the formation of these three compounds. In these studies, KOH in alcoholic solution has been used to form the analogous molecules to **bptz1** and **bptz2**. In our case, during the reaction of **bptz** with different metal salts, no base was added. However, the presence of water together with the perhaps catalytic action of the metal itself, could favour the formation of these products. A hypothetical mechanism is proposed in the following scheme.

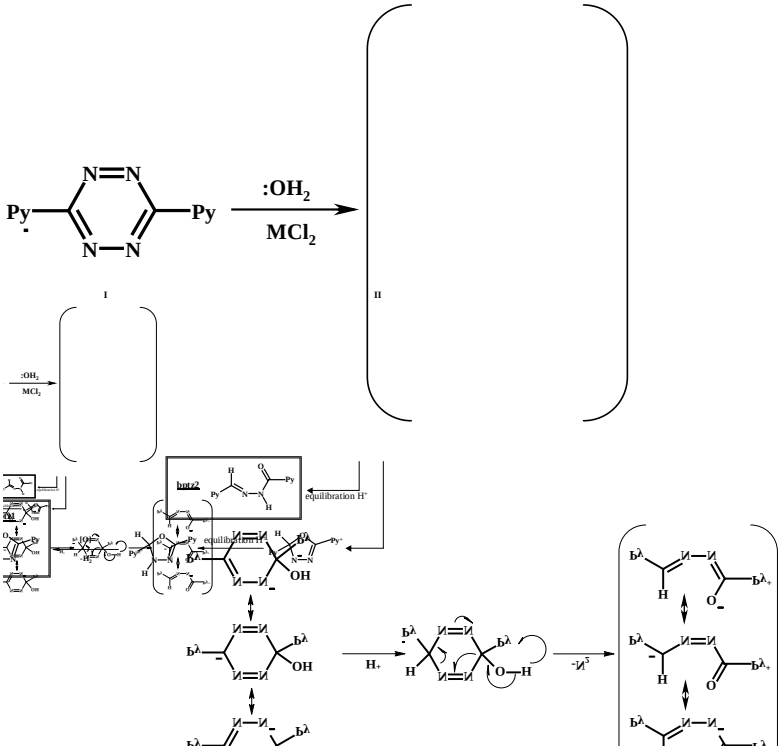

Scheme 17

It is reasonable to suppose that the metal atom (Hg^{2+}, Mn^{2+} or Cu^{2+} in our case) interacts with the ligand making it more electrophilic, hence, making it more susceptible to nucleophilic attack from the oxygen of a water molecule. These water molecules may come either from the solvent or from the metal salts used (all were hydrated). Once this attack [favoured by the formation of a resonant transition state, **I** in Scheme 17] takes place; **bptz** can easily loose one N_2 molecule leading, through the formation of a second transition state, **II**, to the formation of

bptz2, found in compounds **33a** and **37**. A second pathway from the transition state **II**, an intramolecular reaction followed by oxidation by the air could occur to form **bptz1**, as found in compound **36**. In the case of compound **bptz3**, we believe that, as for **bptz1** and **bptz2**, under the conditions of the reaction the same transition state **II** is formed. Then, while a certain quantity of **bptz** remains unchanged, one of the resonant forms of **II** could attack a molecule of **bptz**, in the manner shown in the following scheme, leading, after charge equilibration and transposition of one H from the carbon to the nitrogen [according to the crystal structure], to the compound **bptz3**.

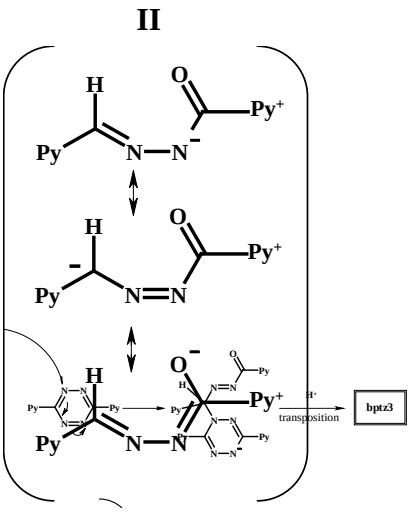

Scheme 18

The mechanisms shown in both Schemes 17 and 18 are simple hypothesis. More exhaustive studies, which exceed the aims of this work, would be necessary to be able to affirm exactly how these transformations actually take place.

2.10. Coordination behaviour of ligand tma

The coordination chemistry of this substituted pyrazine ligand was studied and two complexes have been isolated in the form of single crystals: [Cd(tma)I_2] **(39)** and [Zn(tma)Cl_2]·CH_2Cl_2 **(40)**. Another compound tma2 **(41)** was formed during the complexation reaction of this ligand with several metal salts.

2.10.1. Complexes [Cd(tma)I_2] (39) and [Zn(tma)Cl_2]·CH_2Cl_2 (40)

The reaction of **tma** with CdI_2 using diffusion techniques, or in MeOH at RT with $ZnCl_2$ afforded, in a few days, the mononuclear isostructural complexes [Cd(tma)I_2] **(39)** and [Zn(tma)Cl_2]·CH_2Cl_2 **(40)**.

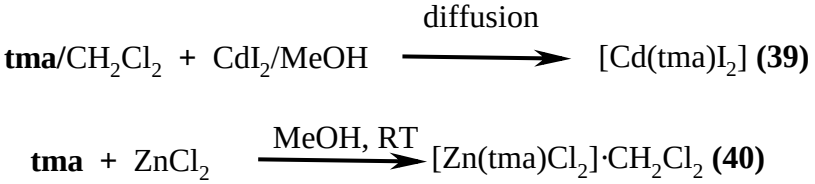

The main ligand peaks are observed in the IR spectra of complexes **39** and **40**. The peaks corresponding to the arC-arC and arC-arN vibrations at 1601 and 1508 cm^{-1} appear almost at the same position whereas other peaks are more displaced.

Table 46. IR Data for the ligand **tma** and the complexes **39-40**.

Compound	IR, ν [cm^{-1}]
tma	2926 (w), 1601 (s), 1508 (vs), 1446 (m), 1377 (m), 1366 (m), 1313 (m), 1257 (m), 1212 (m), 1117 (w), 745 (s), 689 (m)
[Cd(tma)I_2] **(39)**	2922 (m), 1599 (vs), 1507 (s), 1497 (s), 1376 (w), 1173 (m), 1120 (m), 751 (s), 694 (s)
[Zn(tma)Cl_2]·CH_2Cl_2 **(40)**	2909 (w), 1599 (vs), 1507 (s), 1451 (m), 1363 (s), 1257 (m), 1171 (m), 1033 (m), 920 (m), 746 (s), 691 (s)

The crystal structure of compounds **39** and **40** consists of discrete mononuclear [Cd(tma)I_2] are [Zn(tma)Cl_2] molecules, respectively. In compound **39** the asymmetric unit contains half a [Cd(tma)I_2] molecule whereas in compound **40** it contains one full complex molecule (for simplicity we have used the same labelling scheme in both halves with subscript *a* for the second half) plus one CH_2Cl_2 molecule. These compounds are *isostructural* and not *isomorphous* because, although the chemical structure is the same, they crystallize in different crystal systems. In both compounds the ligand coordinates in a monotridentate manner. Two terminal iodine (for **39**) and chloride (for **40**) atoms complete the coordination sphere of the metal atoms. This leads to a slightly distorted square-pyramidal geometry (τ = 0.14) for **39** and to what can be described as a square-based pyramid with a trigonal-bipyramid distortion (τ = 0.30) for **40**[&].

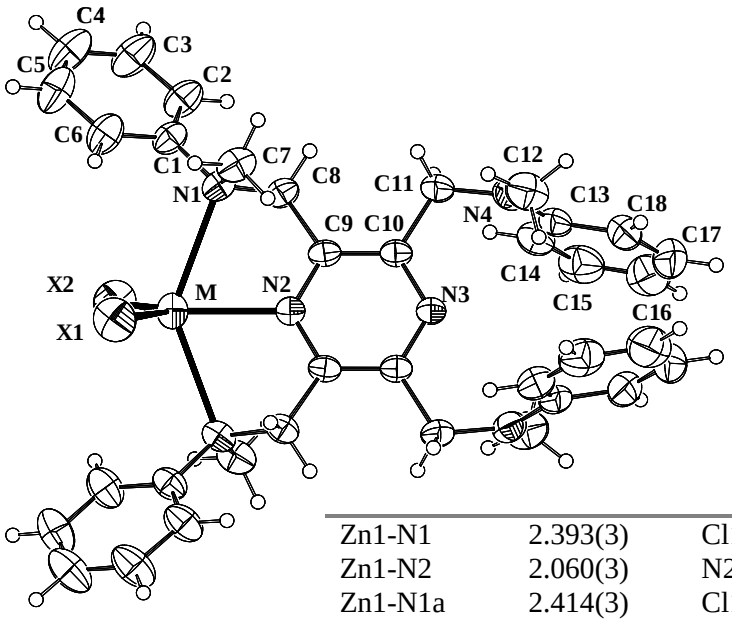

Cd1-N1	2.599(3)
Cd1-N2	2.294(3)
Cd1-I1	2.7038(3)
N2-Cd1-N1	69.65(6)
N2-Cd1-I1	114.551(10)
N1-Cd1-I1	101.29(6)
N1-Cd1-$N1^i$	139.30(12)
N1-Cd1-$I1^i$	95.35(6)
$N1^i$-Cd1-$I1^i$	101.29(6)
$I1^i$-Cd1-I1	130.90(2)
where i: -x+3/2,y,-z	

Zn1-N1	2.393(3)	Cl1-Zn1-Cl2	131.14(4)
Zn1-N2	2.060(3)	N2-Zn1-N1	74.93(11)
Zn1-N1a	2.414(3)	Cl1-Zn1-N1	98.05(7)
Zn1-Cl1	2.2257(9)	Cl2-Zn1-N1	95.70(8)
Zn1-Cl2	2.2419(10)	N2-Zn1-N1a	74.26(11)
		Cl1-Zn1-N1a	93.09(7)
N2-Zn1-Cl1	113.98(8)	Cl2-Zn1-N1a	98.38(7)
N2-Zn1-Cl2	114.86(8)	N1-Zn1-N1a	149.16(10)

Figure 83. Crystal structure and selected geometric parameters (Å,°) of complexes [Cd(tma)I_2] **(39)** and [Zn(tma)Cl_2]·CH_2Cl_2 **(40) [**M = Cd, Zn and X = I, Cl].

[&] Remark: it was not possible to coordinate metals in both coordination sites of the ligand, even when an excess of metal salt was used for the reactions.

The distances M-X are very close to the standard values. The M-N_{pz} distances are shorter than the standard values with 2.393 and 2.114 Å for Cd-N_{pz} and Zn-N_{pz}, respectively whereas the M-N_{amine} distance can be considered, for both compounds, as a weak interaction. The structures of **39** and **40** differ only slightly in their overall conformation as is shown by the similarity of the dihedral angles among the pyrazine and the four phenyl rings (Table 47). However, the molecular packing is quite different, mainly due to the presence in compound **40** of a CH_2Cl_2 molecule that changes the space filling distribution [as well as the space group and crystal system].

Table 47. Selected dihedral angles (t, º) for [Cd(tma)I_2] (**39**) and [Zn(tma)Cl_2]·CH_2Cl_2 (**40**).

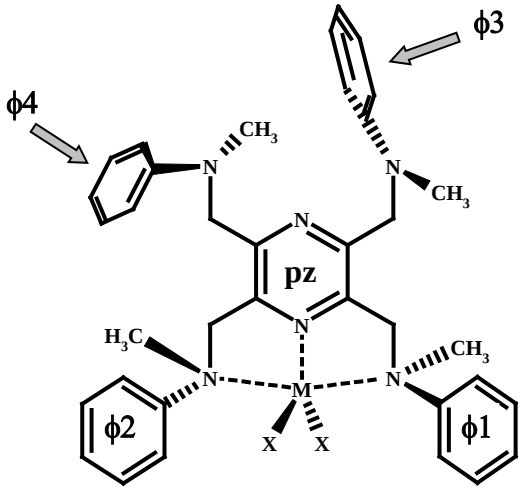

	39	**40**
t (ϕ1-ϕ2)	38.0(2)	26.9(2)
t (pz-ϕ2)	41.7(2)	34.7(2)
t (ϕ1-pz)	42.1(2)	35.3(2)
t (ϕ1-ϕ3)	54.0(1)	53.9(2)
t (ϕ3-ϕ4)	24.9(1)	18.3(3)
t (ϕ3-pz)	86.0(1)	87.6(1)
t (pz-ϕ4)	86.2(1)	74.3(1)

It is remarkable that in both compounds the two halves of the molecule, the coordinated and the uncoordinated one, are quite different. The phenyl rings ϕ3 and ϕ4 are almost perpendicular to the pyrazine ring mean plane while the dihedral angles t (ϕ1-pz) and t (pz-ϕ2) are much smaller due to coordination [the N atom lone pair electrons points towards the metal atom and influences the conformation of these phenyl rings]. In both compounds the metal atom is displaced by approximately 1 Å from the chelate ring [0.967 (5) and 0.987 (6) Å for **39** and **40**, respectively].

The next two figures show the differences observed in the packing motif of compounds **39** and **40**. The hydrogen atoms and the CH_2Cl_2 molecule in compound **40** have been excluded for clarity. In **39** the metal atoms are located in special positions and the *order* seems to be higher (higher symmetry; monoclinic *versus* triclinic system) than in **40**.

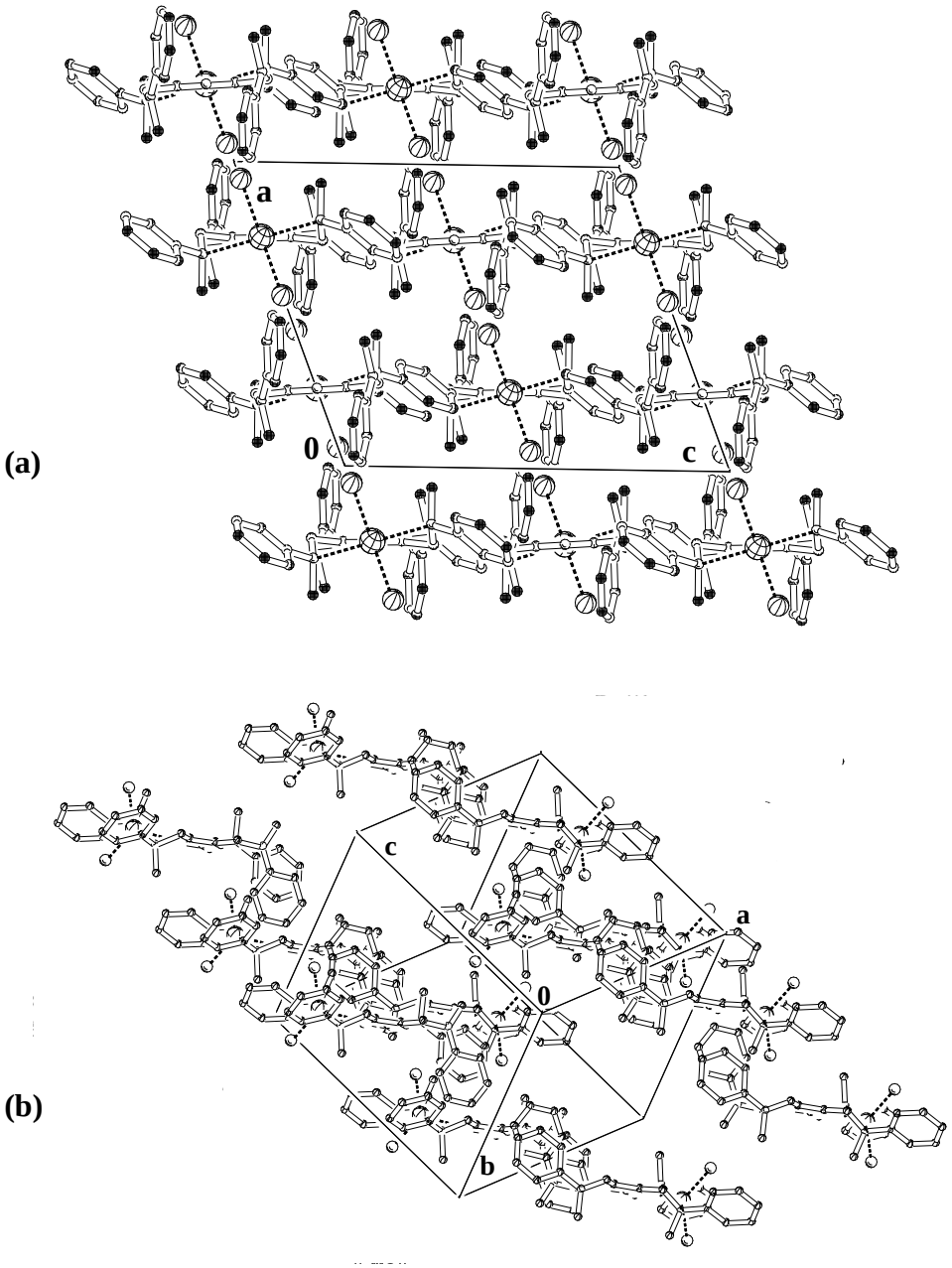

Figure 84. Molecular packing of complexes (**a**) $[Cd(tma)I_2]$ **(39)** and (**b**) $[Zn(tma)Cl_2]\cdot CH_2Cl_2$ **(40)**.

2.10.2. Compound tma2 (41)

During the reactions of the ligand **tma** with different metal salts such as $Zn(ClO_4)_2$, $MnCl_2{\cdot}4H_2O$ and $Ni(AcO)_2{\cdot}4H_2O$, pale yellow crystals of this new organic compound were obtained. The reactions with $MnCl_2{\cdot}4H_2O$ and $Ni(AcO)_2{\cdot}4H_2O$ were performed in mild conditions using diffusion techniques while with $Zn(ClO_4)_2$ the reaction was done in a mixture of CH_2Cl_2/MeOH at 40 °C and using a large excess of metal salt. The molecular structure and some selected geometrical parameters are given in Figure 85 and Table 48, respectively.

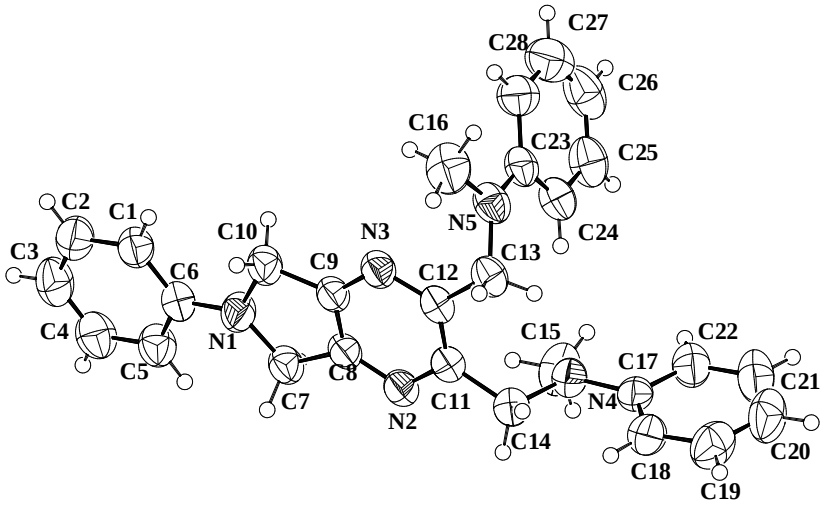

Figure 85. Crystal structure of compound tma2 **(41)**.

The crystal structure of **41** shows that the original ligand **tma** has been transformed. In the presence of at least Ni^{2+}, Mn^{2+} and Zn^{2+} metal salts, one of the four arms plus the methyl group of a second arm are lost with the formation of a five-member ring by the nucleophilic attack of one $:NR_2$ group (N1) to one CH_2 group (for instance, C10). The system formed by the pyrazine and the five-member ring plus the phenyl C1-C6 ring is almost perfectly planar with a deviation of only 0.055 Å from its mean plane equation. The two arms are mutually

perpendicular and also perpendicular with respect to the pyrazine ring, with dihedral angles of 89.5 (1) º in both cases.

Table 48. Selected geometric parameters (Å, º) for compound **41**.

C6-N1	1.374(3)	N1-C7-C8	102.22(16)
C7-N1	1.453(2)	N1-C10-C9	102.24(17)
C7-C8	1.498(3)	C8-C9-C10	111.26(19)
C8-N2	1.328(3)	C9-C8-C7	110.5(2)
C8-C9	1.377(3)	N2-C8-C9	123.17(19)
C9-N3	1.333(2)	N2-C8-C7	126.32(18)
C9-C10	1.483(3)	N3-C9-C8	122.8(2)
C10-N1	1.463(2)	N3-C9-C10	125.93(18)
C11-C14	1.515(3)	N3-C12-C13	115.36(19)
C12-C13	1.527(3)	N2-C11-C14	115.81(19)

The crystal packing of compound **41** is influenced by the presence of weak π-π stacking interactions of *ca*. 3.8 Å between the planar moieties of symmetry related molecules (symmetry operation: 1-x, 2-y, -z).

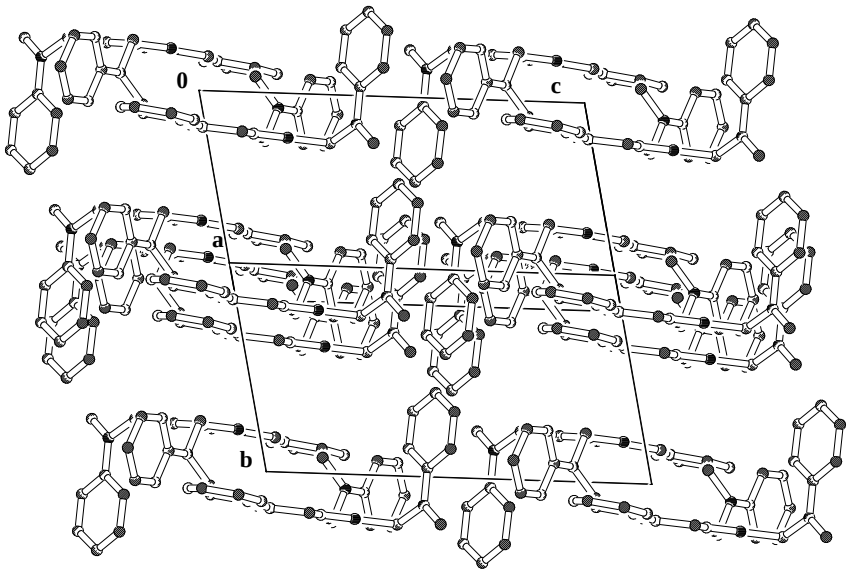

Figure 86. Crystal packing of compound tma2 **(41)** showing the weak π-π interactions.

A possible mechanism for the formation of **tma2** is showed in the next scheme. The interaction of the metal with a **tma** molecule [probably in only one of the two tridentate units, as observed in the complexes **39** and **40**], makes this part of the ligand more electrophilic and one of the non-coordinated nitrogen atoms of the other tridentate moiety is involved in a nucleophilic attack on one of the CH_2 groups. This could be favoured by the formation of a five-member ring. Then, the negatively charged leaving group may attack the molecule formed with the transfer of a methyl group leading to the formation of compound **tma2**.

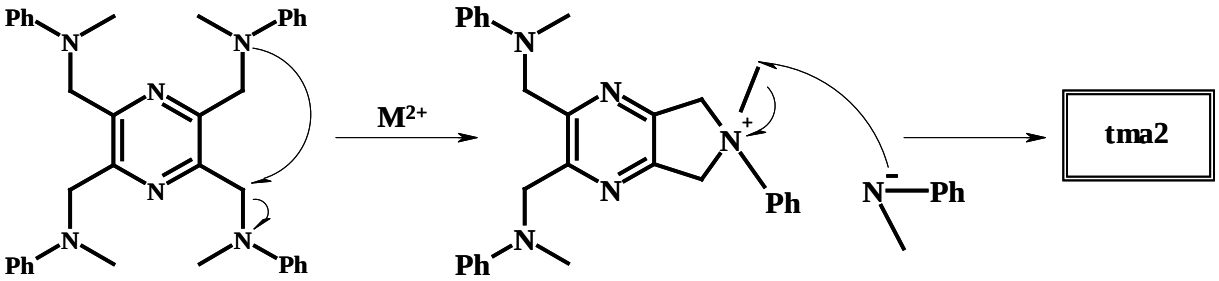

Scheme 19

We believe that once this molecule is formed, it is not possible to repeat the same reaction on the other side of the molecule, because the chelating environment for the metal is no longer available.

The mechanism for the transformation of ligand **tma** is tentative. Further investigations, beyond the scope of this work, would be necessary to prove or disprove this hypothesis.

III. CONCLUSIONS AND PERSPECTIVES

The synthesis of the ligands **L1** to **L9** has been accomplished with no special difficulty. The solvents used were sometimes varied depending on the solubility of the reactants. In the case of **L6**, the reaction time needed was longer as is usual in syntheses involving pyrrol-carboxaldehyde. The yields obtained were always very high and, for this reason, together with the simplicity and low toxicity of these reactions, the imino-based ligands can be considered as good building blocks for supramolecular chemistry. Most of these ligands are air- and light- stable (**L6** is hygroscopic). A general outlook of their spectroscopic characteristics has been given in Table 3a (*Results and discussion*, p. 37). It was not possible to obtain single crystals for two of the ligands, **L6** and **L9**. The presence of a NH function, in both ligands, may play a role in the troublesome crystallization process, perhaps through formation of hydrogen bonds [although H-bonding could probably give a very regular structure and hence, lead to crystals]. In the case of **L9**, this phenomenon can be observed in the IR spectra of the free and complexed ligand. For **L6** the NH vibration appears in the region expected for a free NH group. In Table 3b (*Results and discussion*, p. 38) a resume of the most important geometrical parameters of this series of ligands has been given. An *E* imine configuration was always observed in the solid state, indicative of the lower sterical hindrance of this isomer, when an extended delocalised and ideally planar π-system is imposed [at least for the chelating moiety]. The next two schematic drawings illustrate the two extreme situations for the ligand **L3**.

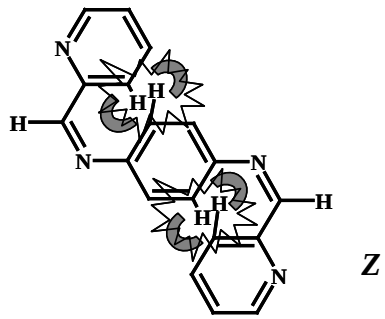

Z

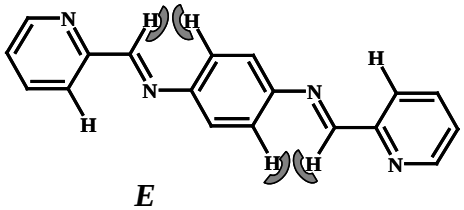

E

Aliphatic imines are normally too unstable to be isolated but aromatic imine ligands are more stable. In Table 49, a comparison of several structural features of the free imine based ligands with their metal complexes is presented. Upon coordination, slight changes in the bond distances involving the coordinating atoms [in particular, for parameters **b** and **d**] could be expected. The lone pairs of electrons from both the imine and the pyridine/quinoline nitrogen atoms participate in the creation of the coordinative bonds and are directed towards the metal ion. As a consequence, the electronic properties of the ligand are modified.

Table 49. A comparison of bond distances (Å) and angles (°) for the imine base ligands and their complexes. The parameters have been defined as for Table 3b (*Results and discussion*, p 38) and **d** represents the distance arC-N in the pyridine or quinoline ring. The average is reported when more than one value for the same parameter is found in the molecule.

	a	**b**	**c**	**d**	**ϕ**	**φ**
L3	1.471	1.258	1.420	1.335	178.1	11.1
14	1.470	1.267	1.423	1.343	178.5	1.79
15	1.467	1.282	1.433	1.350	179.5	26.62, 31.71
L5	1.473	1.263	1.417	1.340	175.5	10.77, 67.47, 46.35
16	1.456	1.277	1.439	1.347	176.7	74.8, 85.5[#] 79.4, 39.6 61.1, 37.3
17	1.464	1.275	1.430	1.341	176.5	41.3, 74.7[#] 69.4, 85.2 70.4, 70.7
18a	1.477	1.249	1.435	1.344	178.7	7.91, 51.09
L7	1.470	1.271	1.419	1.323, 1.376	175.6	17.85, 9.73
19*	1.475	1.275	1.422	1.328, 1.373	176.5	46.17, 39.23 60.12, 51.91
L8: no crystal structure						
20	1.461	1.272	1.460	1.337	177.5	74.6
21	1.498	1.255	1.463	1.348	179.0	2.61
22	1.490	1.280	1.474	1.330	179.4	3.18
23	1.497	1.237	1.476	1.327	179.9	5.53
24	1.457	1.279	1.479	1.340	176.7	82.9
26	1.448	1.288	1.480	1.340	176.5	84.5
27	1.452	1.277	1.472	1.340	176.1	83.9
L9: no crystal structure						
28	1.495	1.270	1.438	1.330	175.9	26.5, 25.7
Standard[&]	1.476	1.279	1.465	1.341 (py)	178.5	-

[#] values for the three ligand molecules; * two independent molecules

[&] International Tables for Crystallography vol. C, (1995).

Several observations can be made. The *E* configuration and the double bond character of the C=N bond of the imine group are retained in all of the complexes obtained. For the bond distances, no remarkable changes were observed. In some cases the values for the parameters **b** or **d** in the complexes are slightly longer but a general trend cannot be observed. The dihedral angles between the aromatic rings differ but this is more likely due to the 3D structure of the complex [crystal packing requirements] and not to the complexation itself.

Table 50. A comparison of the **M-N$_{ar}$** and **M-N$_{im}$** bond distances (Å) and chelate angles (º) in the complexes obtained with ligands **L1**-**L9**.

	17 (M = Co)	**24** (M = Co)	**16** (M= Ni)	**27** (M = Ni)	**14** (M = Zn)	**21** (M = Zn)	**26** (M = Zn)
M-N$_{ar}$	2.185(4) 2.126(4) 2.141(4)	2.148(5) 2.148(5) 2.131(6)	2.076(4) 2.108(4) 2.099(4)	2.108(6) 2.127(6) 2.081(7)	2.056(6)	2.136(7)	2.181(7) 2.191(6) 2.177(6)
Standard	2.185		2.122		2.116		
M-N$_{im}$	2.168(5) 2.126(4) 2.154(4)	2.115(5) 2.116(8) 2.133(6)	2.108(4) 2.087(5) 2.117(4)	2.067(7) 2.100(8) 2.075(7)	2.109(6)	2.054(6)	2.138(7) 2.178(8) 2.161(7)
Standard	2.015		2.051		2.122		
N$_{im}$-M-N$_{ar}$	77.1(2) 77.1(2) 77.3(2)	77.2(2) 78.1(2) 77.1(3)	78.9(2) 78.7(2) 78.3(2)	78.0(2) 79.2(3) 79.2(3)	80.9(2)	78.6(3)	76.2(2) 77.9(3) 77.9(3)

	20 (M = Ag)	**18a** (M= Ag)	**15** (M= Cd)	**19** (M= Cd)	**23** (M = Cd)	**22** (M = Hg)	**28** (M= Hg)
M-N$_{ar}$	2.385(5) 2.410(6)	2.283(4)	2.286(4) 2.279(4)	2.445 (3) 2.517 (3) 2.474 (3) 2.499 (3)	2.373(7)	2.436(13)	2.373(9)
Standard	2.299		2.381			2.164	
M-N$_{im}$	2.277(5) 2.251(5)	2.343(4)	2.351(3) 2.384(3)	2.400 (3) 2.539 (3) 2.412 (3) 2.506 (3)	2.293(7)	2.297(11)	2.389(9)
Standard	2.403		2.399			2.158	
N$_{im}$-M-N$_{ar}$	72.49(17) 72.57(17)	72.7(2)	79.1(1) 73.3(1)	69.33(9) 68.77(9) 67.03(9) 68.43(9)	70.9(2)	70.5(4)	71.0(3)

In Table 50, selected structural parameters of the complexes **14**-**28**, together with the standard values for the **M-N$_{ar}$** and **M-N$_{im}$** bond distances are summarized. The observed **M-N$_{ar}$** bond distances are longer than the standard values for the compounds containing Ag(I), Hg(II) and for compound $[Cd(L7)I_2]_n$ **(19)**. For the rest of complexes, they are either similar or slightly shorter than the standard values. The trend observed for the **M-N$_{im}$** bond distances is slightly different. The experimental values are longer than the standard ones for Hg(II), Co(II) and for compound **19** whereas, for the rest, they are quite similar. The largest variation is found for compound $[Ag(L8)](BF_4)$ (**20**).

As expected, the different structural features of these ligands and the electronic and geometrical preferences of the metal ions used, have lead to a **diversity** of **structural motifs** including monomers, dimers, single-helical polymeric chains, triple helicates and one-dimensional polymers. It has been possible to analyse all of these compounds by X-ray crystallography.

IR spectroscopy has been used as a characterization technique (*fingerprint*) and as a guide to check if complexation had taken place [shift of the free-ligand vibrations to higher or lower frequencies upon complexation].

Beside the ligand and the metal, the **counter-ion** used in the complexation reactions has been found to have an influence on the final structure of the complex. For instance, it was possible to tune the formation of different motifs by simply employing different counter-ions. Anions with weak coordinating tendency like ClO_4^-, BF_4^- or $CF_3SO_3^-$ will mainly give cationic complexes uniquely formed by the metal and the ligand and where the anion just equilibrates the charges [for example, compounds **16**-**17** or **24**-**27**]. Other anions such as NO_3^- or the halides easily coordinate to the metal leading to, in most of the cases, neutral species as dimers or polymers. The same argument can be applied for the use of different **solvents**. For

example, water or acetonitrile molecules can easily coordinate to the metals whereas hexane or dichloromethane cannot.

Before starting the second part of this work (p. 50) we have explained the methodology used to carry out the UV-Vis measurements. We have decided to perform a general screening of almost all of the ligands and a series of metal salts. The aim was to get an impression of the coordination chemistry of these ligands to see:

1. Whether they react with a large number of metals or if they are rather selective and if so, to which metals.
2. To have an idea of the complexity of the reactions: is only one product (complex) formed or does the reaction consist of several simultaneous equilibria?

The disadvantage of this approach is that it is difficult both to determine the most probable metal to ligand ratio and to propose a concrete structure for the species in solution.

The experiments performed show that some of the ligands coordinate better than others. In some cases (i.e. **L1** or **L2**), only very slight changes in the UV-Vis spectra of the ligands were observed. In other cases, i.e. **L3**, the ligand seems to complex with high affinity with most of the metal salts tested, although the attainment of single crystals proved to be quite difficult [perhaps due to the coexistence of several species in solution]. **L3** has a significantly delocalised π-conjugate system and the π-π* band shows a large red-shift up to about 450 nm in many cases due to metal coordination. This phenomenon was also observed in the case of ligand **L9** were the magnitude of the red-shift is about 100 nm. In general, the complexes show intense transitions in the UV region due to ligand-based π-π* transitions and MLCT or

LMCT (Metal-to-Ligand or Ligand-to-Metal Charge-Transfer) bands in the Visible region. This type of ligand induces high *ligand fields* around the metal (they coordinate strongly) and hence the metals are expected to be mainly in their **low-spin state**. The blue-violet colour observed for many of the Fe(II) complexes with the Schiff-base ligands used in this work, indicates the presence of a low-spin Fe(II) in an octahedral environment. With some of the ligands (i. e. **L3**), it appears difficult, from a steric point of view, to complete an octahedron by means of only imino-ligand molecules and solvent molecules or counter-ions occupy the remaining positions (as in compound **15**). Under these conditions, the colour of the Fe(II) solutions was not violet. This could be due to the presence of **high-spin species**.

Taking into account the UV-Vis studies and the information obtained from analytical techniques, such as NMR, IR and ES-MS, together with the crystal structures obtained for related complexes makes it possible in some cases to *extrapolate* and propose a three dimensional structure for the complex formed.

This chemistry is far from being finished and many possibilities for further investigations are possible. Different reaction conditions, solvents and techniques of crystallization could be used in order to obtain new single crystals or at least microcrystalline materials that could be then analysed by powder diffraction. Depending on the metal, magnetic measurements could be also carried out to analyse the magnetic M-M coupling.

Concerning the UV-Vis titrations, one possibility would be to select several interesting cases and perform this time more precise measurements. It would then be possible to calculate the equilibrium constants and the distribution of the species in solution. It would be very interesting to find a ligand selective (or at least presenting a high preference) for *only* one

metal atom and leading directly to the formation of a single product (*clean reaction*). In such a case, if it is possible to follow the reaction of small amounts of that metal with the ligand by the formation of a strong band in the visible region [highly *sensitive* reaction], this could lead to the development of a new **photochemical sensor** for that particular metal atom in solution. The **luminescence** properties of some of the systems used in this work could be also explored. Ligands **L4** and **L7** contain, respectively, naphthalene and quinoline groups and **L9** have been shown to give very strongly coloured solutions upon complexation with most of the metal salts tested. As a suggestion for further investigations, the coordination behaviour of these ligands with M(III) salts as well as with lanthanide ions could be considered.

It would also be interesting to **reduce** the imine function to an amine in order to eliminate the problem of the possible hydrolysis of this function and to explore and compare the coordination chemistry of these new ligands. This reduction reaction has been carried out with some of the ligands (see compound **L2r**), using $NaBH_4$ as reducing agent, and the reactions appear to work very well. Some preliminary attempts of complexation have also been carried out and gave rise to, for the moment, strongly coloured oils or powders.

The coordination chemistry of the ligand **bptz** was briefly studied and it has turned out to be very interesting. It has been possible to obtain single crystals of complexes of this ligand only with d^{10} metals although transition metal ions have also been tested. In all of these complexes (**29**-**35**), the M-N distances (Table 51) have been found to be significantly longer than the standard values* indicating that the metal:ligand interaction is very weak.

* In some cases the M-Ntz standard value was not available and a M-Nar mean value or a range of M-Nar values have been used as reference.

Table 51. A comparison of **M-N$_{py}$** and **M-N$_{tz}$** bond distances (Å) and chelate angles (º) in the complexes obtained with **bptz**.

	29 (M = Ag)	**30** (M = Cd)	**31** (M= Cd)	**32** (M = Zn)	**33** (M = Hg)	**34** (M = Hg)	**35** (M = Hg)
M-N$_{py}$	2.435(3) 2.432(3)	2.403(3)	2.325(2)	2.153(6)	2.65(3)	2.712(5)	2.49(1)
Standard	2.299	2.381		2.116	2.164		
M-N$_{tz}$	2.549(3) 2.568(3)	2.538(3)	2.446(2)	2.255(3)	2.94(3)	2.824(5)	2.89(1)
Standard	2.338	*ca.* 2.35		< 2.2	2.16-2.65		
N$_{py}$-M-N$_{tz}$	67.6(1) 66.7(1)	66.4(1)	68.87(8)	76.9(2)	58.8(9)	58.9(1)	61.6(2)

The ligand **bptz** is itself highly coloured and during the complexation experiments carried out with different metals, very deep colours have been observed. It would therefore be interesting to explore the electronic properties of this ligand. The transition metals are more reactive than the d^{10} metal ions and some examples where the original ligand has been involved in a transformation have been observed. The use of completely dry solvents and metal salts, anaerobic conditions and mild reaction conditions might decrease the possibility of the degradation of **bptz** [although some authors[53] have carried out reactions with **bptz** in H_2O without degradation of the ligand]. However, these transformations merit some attention and they could also be systematically studied, in an attempt to understand the role played by the metal and to know if any of these processes could be used, for instance, in catalysis. For the ligand **tma** similar considerations can be applied. To date, only mononuclear complexes have been obtained. It has not been possible to take advantage of the full donor capacity of this ligand. Furthermore, on several occasions the original ligand has been transformed leading to the formation of the product **tma2**. As it has been mentioned for the transformations of **bptz**, it would also be interesting to investigate this reaction in more detail.

IV. OVERVIEW OF SYNTHESIZED PRODUCTS ANALYSED CRYSTALLOGRAPHYCALLY

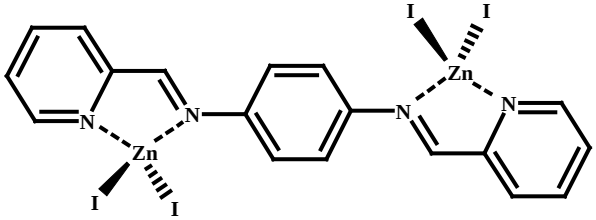

$[Zn_2(L3)I_4]$ (**14**)

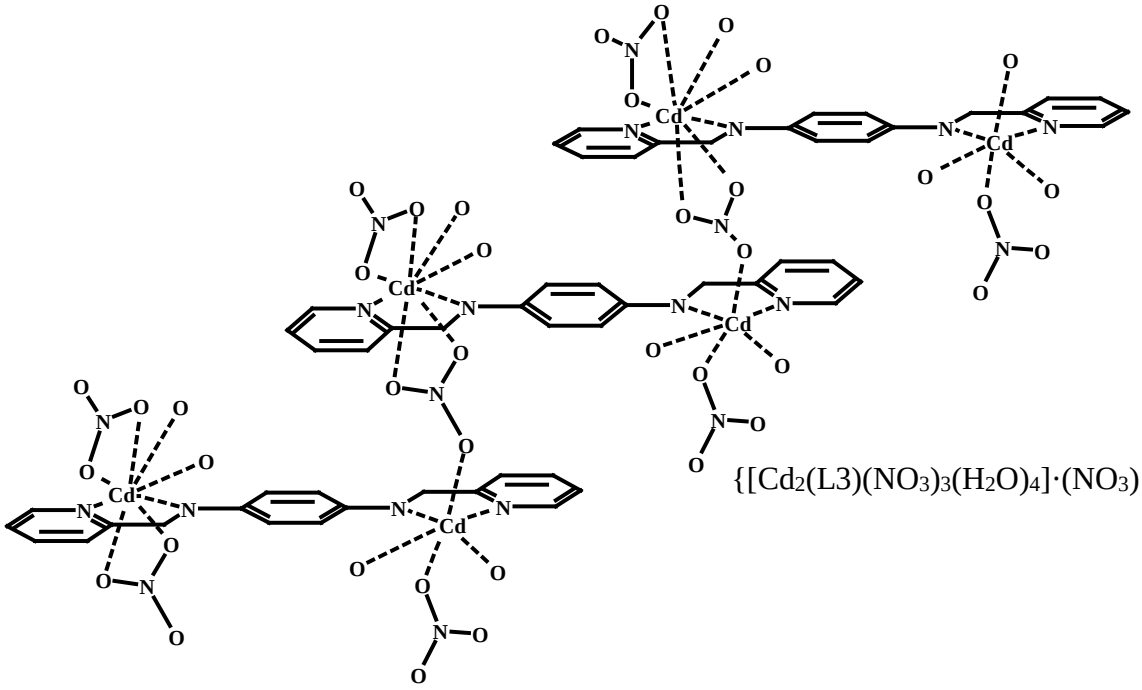

$\{[Cd_2(L3)(NO_3)_3(H_2O)_4]\cdot(NO_3)\cdot 2H_2O\}_n$ **(15)**

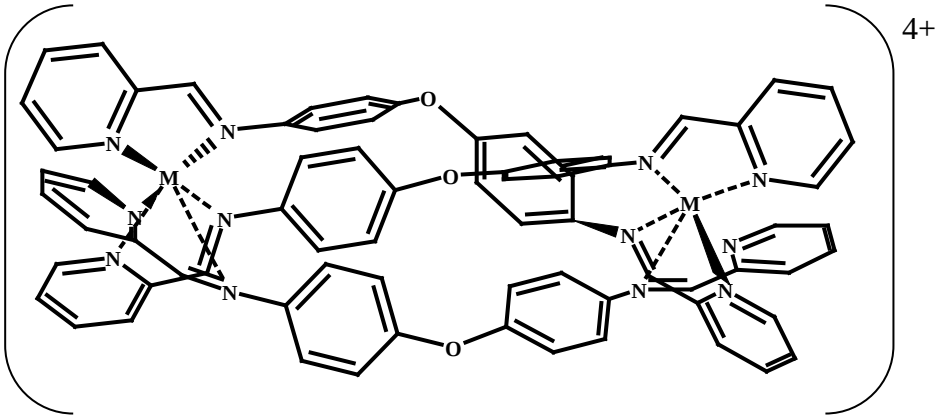

$[Ni_2(L5)_3](BF_4)_4\cdot CH_3OH$ **(16)**
$[Co_2(L5)_3](BF_4)_4\cdot CH_3OH\cdot 0.5H_2O$ **(17)**

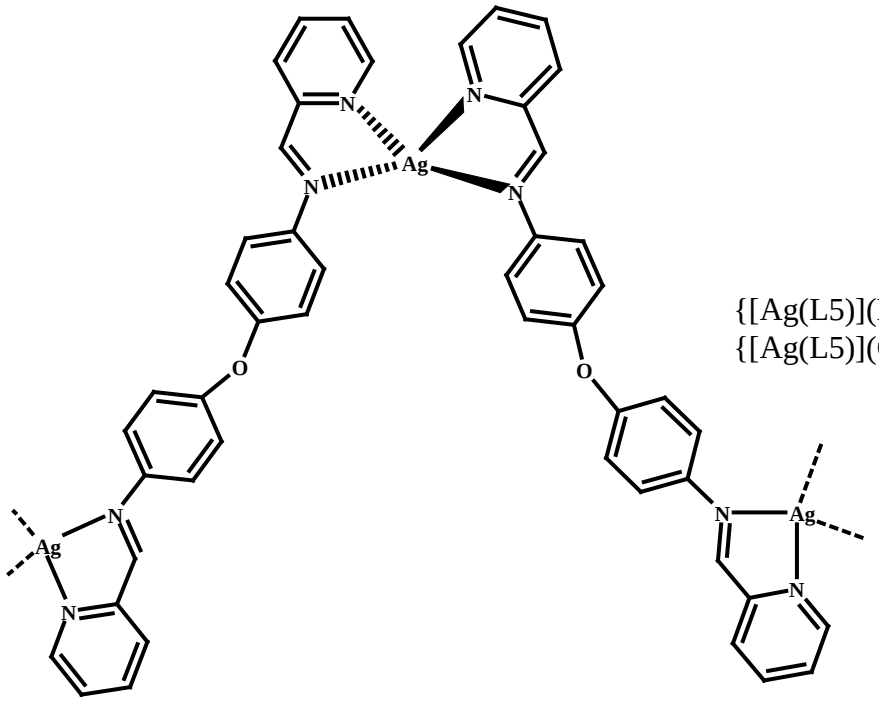

{[Ag(L5)](NO$_3$)}$_n$ **(18)**
{[Ag(L5)](CF$_3$SO$_3$)·0.2H$_2$O}$_n$ **(18a)**

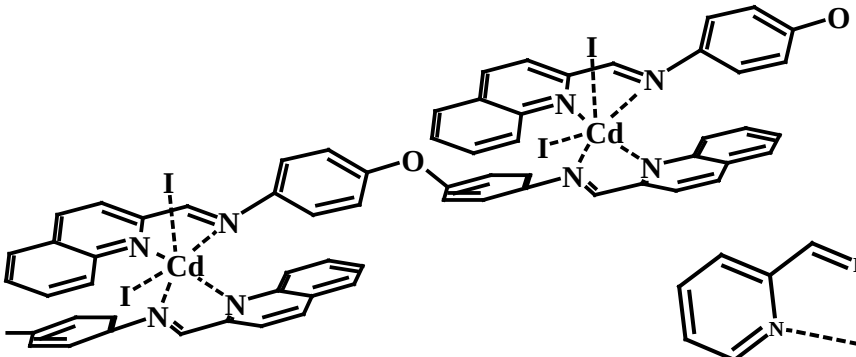

[Cd(L7)I$_2$]$_n$ **(19)**

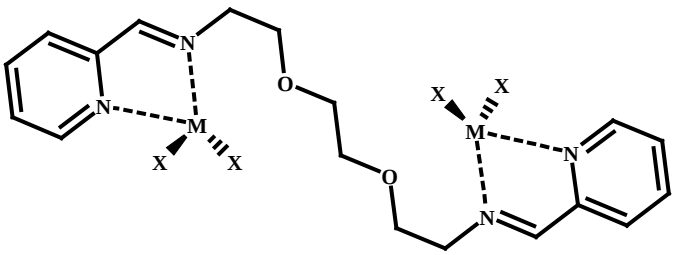

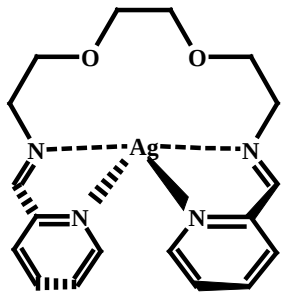

[Zn$_2$(L8)Cl$_4$] (**21**), [Hg$_2$(L8)Cl$_4$] (**22**)

[Ag(L8)](BF$_4$) (**20**)

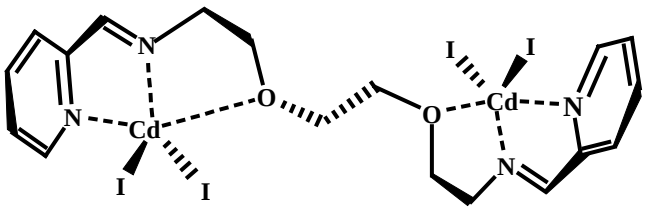

[Cd$_2$(L8)I$_4$] (**23**)

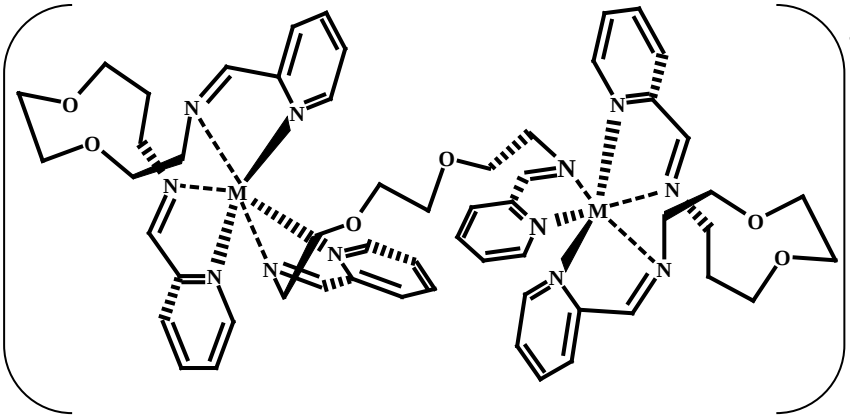

$[M_2(L8)_3](ClO_4)_4$ with M = Co^{II} (**24**) Fe^{II} (**25**) and Zn^{II} (**26**),and $[Ni_2(L8)_3](BF_4)_4$ **(27)**

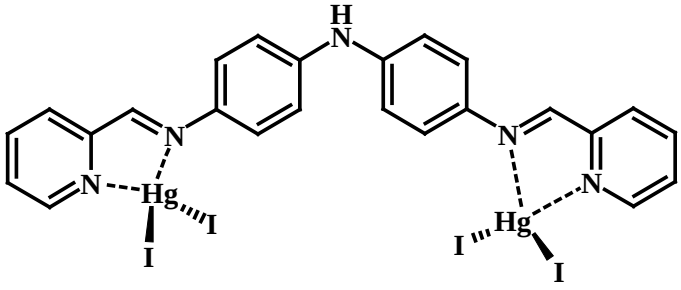

$[Hg_2(L9)I_4]$ **(28)**

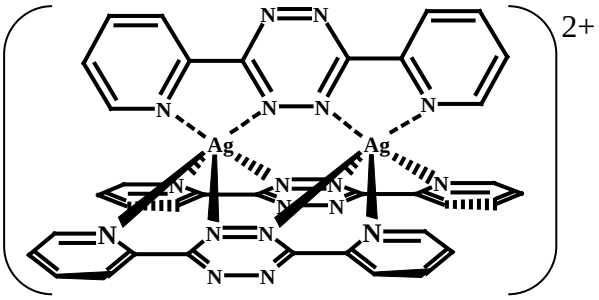

$[Ag_2(bptz)_3](SbF_6)_2$ **(29)**
$[Ag_2(bptz)_3](PF_6)_2$ **(29a)**

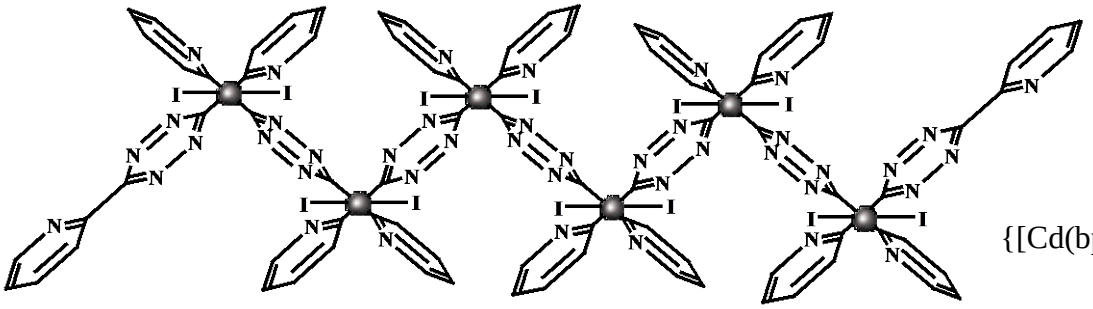

$\{[Cd(bptz)I_2]\cdot CH_2Cl_2\}_n$ **(30)**

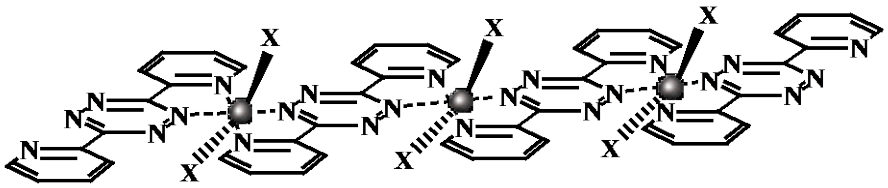

where ● represents the metal atom and X the counter-ion (nitrate for compounds **31** and **32** and bromine for compound **34**.
$[Cd(bptz)(NO_3)_2]_n$ **(31)**, $[Zn(bptz)(NO_3)_2]_n$ **(32)** and $[Hg(bptz)Br_2]_n$ **(34)**

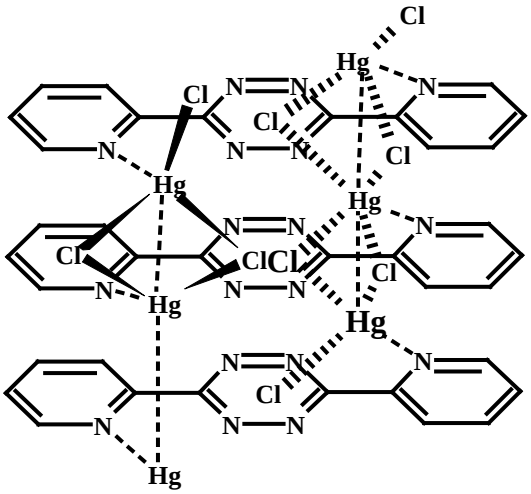

$[Hg_2(bptz)Cl_4]_n$ **(33)**

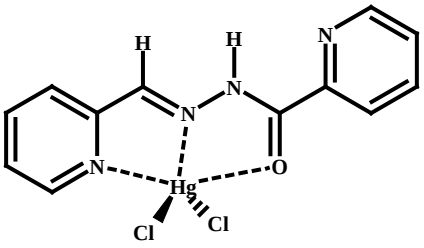

$[Hg(bptz2)Cl_2]$ (**33a**)

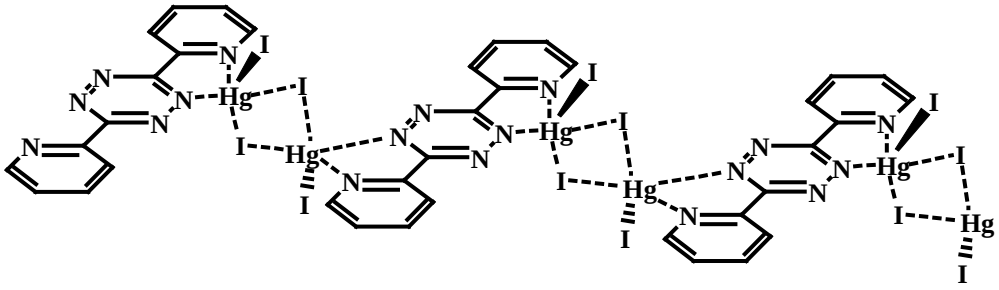

$[Hg_2(bptz)I_4]_n$ **(35)**

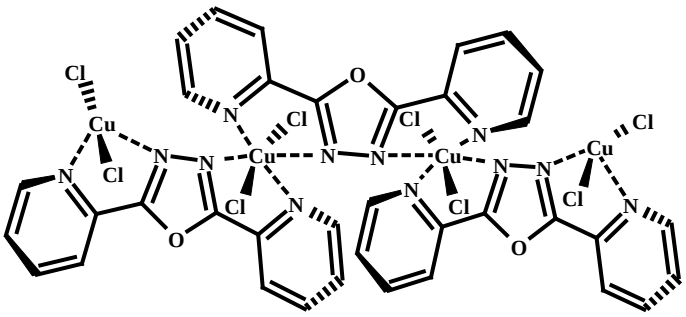

$[Cu(bptz1)Cl_2]_n$ **(36)**

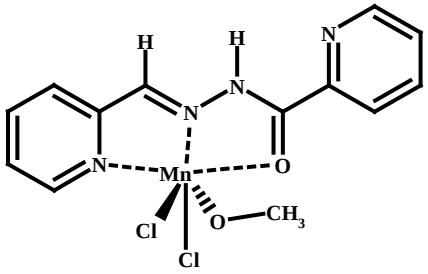

[Mn(bptz2)Cl_2·CH_3OH] **(37)**

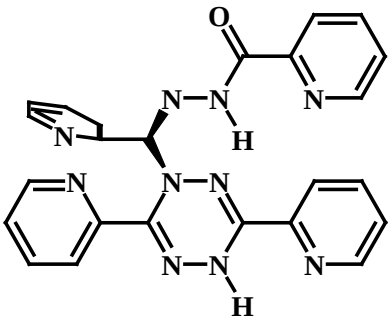

bptz3 **(38)**

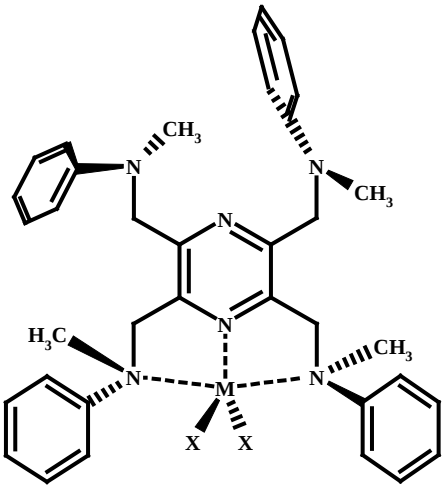

[Cd(tma)I_2] **(39)**
[Zn(tma)Cl_2]·CH_2Cl_2 **(40)**

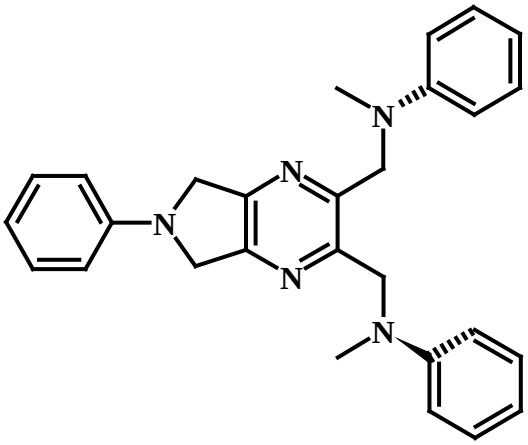

tma2 **(41)**

V. EXPERIMENTAL PART

1. GENERALITIES

All chemicals employed were commercially available reagent grade materials from Aldrich Chemicals Co. and Fluka Chemie AG and were used as received, without further purification. TLC was carried out on silica gel (Alugram Sil G/UV_{254}). Perchlorate salts with organic ligands are potentially explosive and should be handled with the necessary precautions.

1.1. Physical Measurements

Elemental analyses were performed by the ISF Hochschule für Technik Fribourg, Abteilung Chemie, Fribourg. Compounds containing perchlorate anions as well as heavy metals have not been analysed by this technique. IR spectra were obtained on a PERKIN-ELMER FT-IR 1720X spectrometer using KBr pellets. The absorption bands are given in cm^{-1} and all spectra were taken in the range between 4000 and 400 cm^{-1}. The abbreviations for the described intensities are: b (broad), w (weak), m (medium), s (strong) and vs (very strong). The NMR spectra of all compounds were recorded on a VARIAN GEMINI 200 (200 MHz) or on a BRUKER AMX-400 (400 MHz) spectrometer. Chemical shifts (δ) are reported in ppm values relative to TMS and $CDCl_3$, DMSO-d_6, CD_3OD or D_2O were used as solvents depending on the solubility of the compounds. The abbreviations used are: s (singlet), d (doublet), t (triplet), m (multiplet) and b (broad). Electron impact (EI) mass spectra were obtained using a DELSI-NERMAG R30-10 system. Electrospray (ESI) mass spectra were performed by the MS-Service UNI Fribourg using a BRUKER FTMS 4.7T BioAPEX II system. The magnetic susceptibility was measured on polycrystalline samples in the 300-1.8 K temperature range with a Quantum Design MPMS superconducting SQUID magnetometer, operating at a field

strength of 1KOe. The diamagnetic corrections were estimated from the Pascal's tables. The measurements were performed by the Department of Chemistry and Biochemistry of the University of Bern. UV-Vis titration measurements were performed in 96-well microtitre plates monitored in a Spectramax-250 plate reader at the Department of Chemistry and Biochemistry of the University of Bern. The results were analysed using SoftmaxPro 2.2.1 and then treated with Excel2000 Worksheets. General conditions: 1) Metal salts tested: $VOSO_4$, $CrCl_2$, $Mn(ClO_4)_2 \cdot 6H_2O$, $Fe(ClO_4)_2 \cdot 6H_2O$, $Co(BF_4)_2 \cdot 6H_2O$, $Ni(ClO_4)_2 \cdot 6H_2O$, $Cu(NO_3)_2 \cdot 3H_2O$, CuAcO, $AgNO_3$, $Zn(ClO_4)_2 \cdot 6H_2O$, $Cd(NO_3)_2 \cdot 4H_2O$ and $HgCl_2$. All of them were used in ethanolic solution. 2) Concentrations: Ligands→ 125 μM and Metals → 300, 150, 75, 37.5, 18.75, 9.37, 4.68 and 0 μM. Solutions also in ethanol.

1.2. X-Ray structure analysis

Intensity data were collected on either a STOE AED2 four circle diffractometer or a STOE IPDS imaging plate diffractometer both using graphite monochromated MoKα radiation (λ = 0.71073). The structures were solved using direct methods or Patterson heavy-atom syntheses with SHELXS-97[1]. The refinement of all structures was done using SHELXL-97[2]. The H atoms (except those from water molecules) were included in the geometrically calculated positions and allowed to ride on their parent atoms with $U_{iso} = xU_{eq}$ (C,N) $Å^2$, where x = 1.5 for methyl H atoms and x = 1.2 for all other H atoms. The data collection was mostly carried out at 153 ± 2 K and for some crystals at room temperature. Figures were drawn using the program PLUTON/PLATON-97[3] and SCHAKAL-97[4].

1.3. X-Ray Powder Crystallography

Compound $[Zn(bptz)(NO_3)_2]_n$ **(32)** could only be obtained in micro-crystalline form. Therefore, X-ray powder diffraction data were measured in transmission mode (0.3 mm

rotating capillary) on a high-resolution laboratory powder diffractometer (Stoe STADIP) using copper $K_{\alpha 1}$ radiation (1.5406 Å) and a curved germanium monochromator. Eight equivalent data sets were collected, each from 4 to 90° in 2θ with steps of 0.1° and a counting time of 1005 sec. per step using a linear position sensitive detector (PSD). No decomposition was observed during the measurement. The indexing procedure using ITO[5] reveals a triclinic unit cell with a=7.166, b=7.666, c=7.166Å and α=113.49, β=92.55 and γ=117.00°, V=366.02. 580 peaks were extracted from the profile using the program EXPO[6]. With EXPO the heavy atom position of the zinc atom could be identified. All lighter atoms such as carbon, nitrogen and oxygen atoms were derived from difference Fourier maps using SHELXL-97[2]. The obtained structural model was refined in GSAS[7] using the profile over the range 4° < 2θ < 90°. After the initial refinement of the scale, background and unit cell constants, the atomic positions were refined using soft constraints consisting of C-C, C-N and C-H bond distances and bond angles. Hydrogen atoms were included in calculated positions to give better final agreement factors. Final refinement was carried out with low weighted soft constraints. The constraints could not be removed completely without reducing the stability of the refinement. All atoms were refined isotropically. In the final cycles of refinement the shifts in all parameters were less than their estimated standard deviations. Neutral scattering factors were used for all atoms. The final Rietveld plot is given together with the synthesis of **32**.

2. SYNTHESIS OF THE LIGANDS

2.1. Synthesis of L1 *N,N'-Bis[2-(2-pyridinylethyl)-amino]-terephthalalimine* **(1)**

To a solution of methanol (50 ml) containing terephthalaldehyde (2 mmol, 0.2683 g), was added drop by drop 2-(2-aminoethyl)pyridine (4 mmol, 0.48868 g, 0.4758 ml). The mixture was heated at reflux, with stirring, for 5 h. Removal of solvent under vacuum yielded **L1** as a

yellow powder which was dried afterwards under high vacuum for several hours (yield: 0.675 g, 98.5 %). Suitable crystals for crystallographic analysis were obtained by slow diffusion of cyclehexane into a solution of the ligand in ethylacetate.

^{1}H RMN ($CDCl_3$, 200 MHz, ppm): 8.55 [td, Ha, ^{3}J(a,b) = 4.8, ^{4}J(a,c) = 1.8, ^{5}J(a,d) = 0.8, 2H], 8.22 (s,2H, imine, Hg), 7.55 [td, Hc, ^{3}J(c,b) = 7.6, ^{4}J(c,d) = 4.8, ^{5}J(c,a) = 1.8, 2H], 7.27 (s, Hh, 2H), 7.19 (m, Hb, Hd, 4H), 4.04 [t, He, ^{3}J(e,f) = 7.3, 4H], 3.20 [t, Hf, ^{3}J(f,e) = 7.3, 4H] ^{13}C RMN ($CDCl_3$, 400 MHz, ppm): 161.02, 159.57, 149.20, 137.88, 136.10, 128.10, 123.62, 121.18, 61.10, 39.44. IR (KBr pellet, cm^{-1}): 2910 (w), 2875 (m), 2849 (m), 1642 (s), 1588 (s), 1567 (m), 1476 (m), 1465 (w), 1437 (m), 1370 (w), 1299 (w), 1159 (w), 1033 (m), 1014 (m), 989 (m), 963 (m), 830 (s), 769 (s), 616 (m), 512 (m). MS (EI, 70 eV), m/z (%): 342 (M, 10.1), 236 (64.1), 117 (5.9), 106 (100.0) Anal. For $C_{22}H_{22}N_4 \cdot 1/5H_2O$(Mr = 342.45 g/mol Calc. (%): C: 76.36 H: 6.52 N: 16.20 Found (%): C: 76.26 H: 6.53 N: 16.54

2.2. Synthesis of L2 *N,N'-Bis(2-pyridinylmethylene)-1,4-diamino-p-xylene* **(2)**

To a solution of methanol (100 ml) containing α,α'-diamino-p-xylene (15.9 mmol, 2.166 g), was added drop-by-drop pyridine-2-carboxaldehyde (31.81mmol, 3 ml). The mixture was heated at reflux, with stirring, for 5 h. Removal of solvent under vacuum yielded **L2** as a green-yellow powder which was dried afterwards under high vacuum for several hours (yield: 4.85 g, 97.0 %). Slow diffusion of acetonitrile into a solution of the ligand in chloroform afforded light yellow crystals suitable for crystallographic analysis.

^{1}H RMN ($CDCl_3$, 200 MHz, ppm): 8.64 [td, Ha, ^{3}J(a,b) = 4.9, ^{4}J(a,c) = 1.8, ^{5}J(a,d) = 1.0, 2H], 8.48 (s, He, 2H, imine), 8.06 [td, Hd, ^{3}J(d,c) = 8.0, ^{4}J(d,b) = 1.2, ^{5}J(d,a) = 1.0, 2H], 7.74 [dt, Hc, ^{3}J(c,d) = 8.0, ^{4}J(c,b) = 7.1, ^{5}J(c,a) = 1.8, 2H], 7.34-7.29 (m, Hb, 2H), 7.26 (s, Hg, 4H), 4.88 (s, Hf, 4H, CH2) ^{13}C RMN ($CDCl_3$, 400 MHz, ppm): 162.73, 154.51, 149.35, 137.57, 136.51, 128.42, 124.77, 121.30, 64.61. IR (KBr pellet, cm^{-1}): 2889 (w), 2850 (w), 1640 (s),

1587 (s), 1565 (s), 1469 (s), 1434 (s), 1360 (m), 1324 (m), 1044 (m), 1015 (s), 849 (vs), 777 (vs), 512 (m). MS (EI, 70 eV), m/z (%): 314 (M, 0.9), 222 (9.8), 208 (100.0), 93 (69.6) Anal. For $C_{20}H_{18}N_4$ (Mr = 314.39 g/mol) Calc. (%) C: 76.41 H: 5.57 N: 17.82 Found (%) C: 76.44 H: 5.86 N: 17.73

2.3. Synthesis of L2R *N,N'-Bis(2-pyridinylmethyl)-1,4-diamino-p-xylene* **(3)**

To a solution of **L2** (1.6 mmol, 0.5 g) in 100 ml of dry EtOH, $NaBH_4$ (10.6 mmol, 0.4 g) was added in portions at 0 °C (ice bath). The colour of the solution changed from yellow-green to orange. The mixture was stirred at RT for 1 hour, then heated to about 40 °C and finally refluxed, everything within 3 hours. Then 5 ml H_2O were added to the solution to react with the $NaBH_4$ in excess to give a white precipitate. This solution was stirred at RT for about 1 hour, cooled with ice, filtered and then solvent was evaporated under vacuum. The residue was dissolved in water (30 ml) and then extracted with CH_2Cl_2 (5 x 25 ml), dried over anhydrous $CaCl_2$ and after filtration, evaporated to dryness to yield, after drying under vacuum for several hours, 0.45 g (88% yield) of an orange oil, **L2R**.

^{1}H RMN ($CDCl_3$, 200 MHz, ppm): 8.56 [dd, Ha, ^{3}J(a,b) = 4.8, ^{4}J(a,c) = 1.8, 2H], 7.64 [td, Hc, ^{3}J(c,d) = 7.7, ^{3}J(c,b) = 7.6, ^{4}J(c,a) = 1.8, 2H], 7.29 [m, 6H], 7.16 [ddd, Hb, ^{3}J(b,c) = 7.6, ^{4}J(b,a) = 4.8, ^{5}J(b,d) = 1.8, 2H], 3.92 (s, He, 4H, CH2), 3.83 (s, Hg, 4H, CH2), 2.12 (s, Hf, 2H, amine). ^{13}C RMN ($CDCl_3$, 400 MHz, ppm): 159.56, 149.19, 138.70, 136.41, 128.30, 122.34, 121.90, 54.31, 53.11. IR (KBr pellet, cm^{-1}): 3054 (m), 3012 (m), 1593 (vs), 1570 (s), 1514 (w), 1475 (m), 1456 (w), 1435 (s), 1361 (m), 1116 (m), 1050 (w), 841 (m), 762 (vs). MS (ESI, m/z): 319 (MH^+), 223, 94. Anal. For $C_{20}H_{22}N_4$ (Mr = 318.43 g/mol) Calc. (%) C: 75.44 H: 6.96 N: 17.59 Found (%) C: 75.04 H: 6.54 N: 17.33

2.4. Synthesis of L3 *N,N'-Bis(2-pyridylmethylene)-1,4-diaminobenzene* **(4)**

To a solution of methanol (40 ml) containing 1,4-phenylendiamine (5.23 mmol, 0.565 g), was added drop-by-drop pyridine-2-carboxaldehyde (10.45 mmol, 1 ml). The mixture was heated at reflux, with stirring, for 8 h. Removal of solvent under vacuum yielded **L3** as a brown-green powder which was dried under high vacuum for several hours (yield: 1.40 g, 97.9 %). Slow diffusion of cyclehexane into a solution of the ligand in ethylacetate afforded light yellow-brown crystals suitable for crystallographic analysis.

^{1}H RMN (DMSO-d_6, 400 MHz, ppm): 8.74 [ddd, Ha, ^{3}J(a,b) = 4.9, ^{4}J(a,c) = 1.7, ^{5}J(a,d) = 1.0, 2H], 8.67 (s, 2H, imine), 8.19 [td, Hd, ^{3}J(d,c) = 7.6, ^{4}J(d,b) = 1.2, ^{5}J (d,a) = 1.0, 2H], 7.98 [ddt, Hc, ^{3}J(c,d) = 7.6, ^{4}J(c,b) = 1.5, 2H], 7.55 [ddd, Hb, ^{3}J(b,c) = 7.5, ^{3}J(b,a) = 4.9, ^{4}J(b,d) = 1.2, 2H], 7.46(s, 4H, ph). ^{13}C RMN (DMSO-d_6, 400 MHz, ppm): 161.34, 154.91, 150.61, 149.85, 137.97, 126.55, 123.24, 122.16 IR (KBr pellet, cm^{-1}): 3048 (w), 3000 (w), 2918 (w), 1619 (s), 1584 (vs), 1563 (s), 1494 (vs), 1462 (vs), 1434 (s), 1416 (w), 1353 (m), 1229 (w), 1196 (m), 1086 (m), 992 (m), 844 (vs), 773 (s), 563 (s). MS (ESI, m/z): 287 (MH+), 208, 182. Anal. For $C_{18}H_{14}N_4$ (Mr = 286.23 g/mol) Calc. (%) C: 75.50 H: 4.92 N: 19.56 Found (%) C: 75.30 H: 5.01 N: 19.51

2.5. Synthesis of L4 *N,N'-Bis(2-pyridylmethylene)-1,5-diamino-naphthalene* **(5)**

To a solution of methanol (40 ml) containing 1,5-diaminonaphthalene (5.233 mmol, 0.828 g), drop-by-drop pyridine-2-carboxaldehyde (10.466 mmol, 1 ml) was added with immediately apparition of a precipitate. The mixture was heated at reflux, with stirring, for 2 h. After cooling in an ice bath, the yellow precipitate was filtered off, washed with some methanol, and dried under high vacuum for several hours to give 1.58 g (yield: 96.0 %) of **L4**. Suitable crystals for crystallographic analysis were obtained by slow diffusion of methanol into a solution of the ligand in dichloromethane.

^{1}H RMN ($CDCl_3$, 400 MHz, ppm): 8.75 (s, 2H, imine), 8.44 (d, 2H), 8.33 (d, 2H), 8.00 (td, 2H), 7.93 (dt, 2H), 7.56 (m, 2H), 7.45 (ddd, 2H), 7.24 (dd, 2H). ^{13}C RMN ($CDCl_3$, 400 MHz, ppm): 161.23, 155.15, 150.11, 148.39, 137.18, 129.81, 126.49, 125.68, 123.00, 122.41, 113.96 IR (KBr pellet, cm^{-1}): 3055 (w), 1622 (s), 1584 (m), 1566 (m), 1467 (m), 1438 (m), 1402 (m), 1352 (w), 1150 (w), 1044 (w), 994 (m), 927 (m), 799 (vs), 780 (s), 743 (m), 623 (m), 494 (m). MS (EI, 70 eV), m/z (%): 337.1 (MH+), 258, 169 Anal. For $C_{22}H_{16}N_4 \cdot 1/3H_2O$ (Mr = 336.4 g/mol) Calc. (%): C: 77.20 H: 4.90 N: 16.36 Found (%) C: 77.81 H: 4.80 N: 16.51

2.6. Synthesis of L5 *N,N'-Bis(2-pyridylmethylene)-1,4-diamino-diphenyl ether* **(6)**

To a solution of tetrahydrofurane (50 ml) containing 4,4'-diaminophenyl ether (10.465 mmol, 2.096 g), was added drop-by-drop pyridine-2-carboyaldehyde (20.930 mmol, 2 ml). The mixture was heated at reflux, with stirring, for 6 h. Removal of solvent under vacuum yielded **L5** as a yellow powder which was dried under high vacuum for several hours (yield: 3.87 g, 98.0 %). Suitable crystals for crystallographic analysis were obtained by slow diffusion of hexane into a solution of the ligand in dichloromethane.

^{1}H RMN (CD_3OD, 400 MHz, ppm): 8.70 [ddd, Ha, ^{3}J(a,b) = 4.9, ^{4}J(a,c) = 1.7, ^{5}J(a,d) = 0.9, 2H], 8.66 (s, imine, 2H), 8.24 (td, Hd, ^{3}J(d,c) = 7.9, ^{4}J(d,b) = 1.2, ^{5}J(d,a) = 0.9, 2H], 8.00 [ddt, Hc, ^{3}J(c,d) = 7.9, ^{4}J(c,b) = 7.5, ^{5}J(c,a) = 1.7, 2H], 7.54 [ddd, Hb, ^{3}J(b,c) = 7.5, ^{4}J(b,a) = 4.9, ^{5}J(b,d) = 1.2, 2H], 7.43 [td, Hf, ^{3}J(f,g) = 8.9, ^{5}J(f,e) = 2.7, 4H], 7.14 [td, Hg, ^{3}J(g,f) = 8.9, ^{5}J(g,e) = 2.7, 4H]. ^{13}C RMN (CD_3OD, 400 MHz, ppm): 159.27, 156.92, 154.46, 149.57, 146.49,137.78, 125.87, 122.97, 122.38, 119.62 IR (KBr pellet, cm^{-1}): 3047 (w), 2905 (w), 1624 (s), 1581 (s), 1566 (m), 1495 (vs), 1467 (m), 1433 (m), 1344 (w), 1240 (vs), 1198 (s), 993 (m), 859 (s), 832 (s), 776 (s), 542 (m). MS (EI, 70 eV), m/z (%): 379 (MH+), 197, 182,

169 Anal. For $C_{24}H_{18}N_4O$ (Mr = 378.43 g/mol) Calc. (%) C: 76.17 H: 4.80 N: 14.80 Found (%) C: 75.90 H: 4.86 N: 14.83

2.7. Synthesis of L6 *N,N'-Bis(2-pyrrolidinmethylene)-1,4-diamino-diphenyl ether* **(7)**

To a solution of THF (10 ml) containing 4,4'-diaminophenyl ether (2.5 mmol, 0.500 g), was added drop by drop a solution of pyrrol-2-carboyaldehyde (5 mmol, 0.475 g) in THF (15 ml). The mixture was heated at reflux under N_2 atmosphere with stirring, for 8 h. Removal of solvent under vacuum yielded **L6** as yellow powder that was washed with THF and dried afterwards under high vacuum for several hours to afford 0.75 g (yield: 86.0 %).

^{1}H RMN (DMSO-d_6, 400 MHz, ppm): 11.74 (b, 2H, NH), 8.33 (s, 2H, imine), 7.24 [td, ph, ^{3}J(a,b) = 8.8, ^{3}J(a,d) = 3.3, ^{4}J(a,c) = 2.1, 4H], 7.04 (m, 6H, Hc and ph), 6.69 (m, 2H, Ha), 6.21 (s, 2H, Hb). ^{13}C RMN (DMSO-d_6, 400 MHz, ppm): 155.25, 150.79, 148.42, 131.47, 124.60, 123.10, 120.10, 117.14, 110.55. IR (KBr pellet, cm^{-1}): 3413 (vs), 2959 (w), 2889 (w), 1617 (vs), 1549 (w), 1499 (vs), 1452 (m), 1421 (s), 1332 (w), 1282 (m), 1260 (s), 1240 (m), 1196 (s), 1082 (s), 1008 (w), 882 (m), 836 (vs), 728 (vs), 666 (m), 532 (m). MS (ESI, m/z), m/z: 355 (MH+), 278, 211 Anal. For $C_{22}H_{18}N_4O \cdot 1/3H_2O$ (Mr = 360.41 g/mol) Calc. (%): C: 73.32 H: 5.22 N: 15.54 Found (%): C: 73.50 H: 5.46 N: 14.76.

2.8. Synthesis of L7 *N,N'-Bis(2- quinolidin methylene)-1,4-diamino-diphenyl ether* **(8)**

To a suspension of ethanol (40 ml) containing 4,4'-diaminophenyl ether (0.87 mmol, 0.1757 g), quinoline-2-carboxaldehyde (1.75 mmol, 0.2759 g) was added drop-by-drop. In minutes, a deep yellow precipitate appeared. The mixture was heated at reflux, with stirring, for 2 h. After cooling in an ice bath, the yellow precipitate was filtered off, washed with ethanol, and dried under high vacuum for several hours to give 0.38 g (yield: 90.0 %) of **L7**. Suitable

crystals for crystallographic analysis were obtained by slow diffusion of methanol into a solution of the ligand in dichloromethane.

^{1}H RMN ($CDCl_3$, 200 MHz, ppm): 8.86 [d, Hg, 2H, imine], 8.40 (d, Hf, 2H, qui), 8.29 (d, He, 2H, qui), 8.20 (d, 2H, qui), 7.91 (dd, 2H, qui), 7.80 (dtd, 2H, qui), 7.64 (dt, 2H, qui), 7.45 [td, Hh, ^{3}J(h,i) = 8.8, 4H, phe], 7.16 [td, Hi, ^{3}J(i.h) = 8.8, 4H, phe] ^{13}C RMN ($CDCl_3$, 400 MHz, ppm): 160.23, 156.87, 155.35, 148.41, 146.49, 137.07, 130.37, 130.10, 129.30, 128.19, 128.11, 123.39, 120.00, 119.05, 118.12, 116.68. IR (KBr pellet, cm^{-1}): 3034 (w), 1622 (m), 1594 (m), 1584 (m), 1572 (m), 1560 (w), 1497 (vs), 1428 (m), 1301 (w), 1282 (m), 1246 (vs), 1237 (vs), 1197 (m), 954 (m), 898 (w), 885 (w), 872 (w), 834 (s), 757 (s), 549 (w). MS (EI, 70 eV), m/z (%): 479 (MH+), 380, 340. Anal. For $C_{32}H_{22}N_4O$·1/2MeOH (Mr = 494.02 g/mol) Calc. (%) C: 78.93 H: 4.89 N: 11.33 Found (%) C: 78.95 H: 4.61 N: 11.35

2.9. Synthesis of L8 *N,N'-Bis(2-pyridylmethylene)-2,2'-(ethylenedioxy)bis(ethylamine)* **(9)**

To a solution of methanol (50 ml) containing 2,2'-(ethylenedioxy)bis(ethylamine) (10.46 mmol, 1.53 ml), was added drop by drop pyridine-2-carboxaldehyde (20.93 mmol, 2 ml). The mixture was heated at reflux, with stirring, for 5 h. Removal of solvent under vacuum yielded **L8** as a yellow-brown oil which was dried under high vacuum for several hours (yield: 3.34 g, 98.0 %).

^{1}H RMN (CD_3OD, 400 MHz, ppm): 8.62 [ddd, Ha, ^{3}J(a,b) = 4.9, ^{4}J(a,c) = 1.7, ^{5}J(a,d) = 1.0, 2H]; 7.48 [ddd, Hb, ^{3}J(b,c) = 7.5, ^{3}J(b,a) = 4.9, ^{4}J(b,d) = 1.2, 2H] ; 7.90 [ddt, Hc, ^{3}J(c,d) = 7.9, ^{3}J(c,b) = 7.5, ^{4}J(c,a) = 1.7, ^{5}J(c,e) = 0.5, 2H]; 8.01 [td, Hd, ^{3}J(d,c) = 7.9, ^{4}J(d,b) = 1.2, ^{5}J(d,a) = 1.0, 2H]; 8.36 (s, He, broad, 2H)**;** 3.64 (s, Hf, broad, 4H); 3.79 (m, Hg and Hh, 8H).

^{13}C RMN (CD_3OD, 400 MHz, ppm): 163.65, 154.11, 149.28, 137.66, 125.65, 121.79, 70.51, 70.24, 60.65. IR (KBr pellet, cm^{-1}): 2863 (vs), 1651 (s), 1588 (vs), 1568 (m), 1469 (s), 1436 (s), 1353 (m), 1294 (w), 1122 (vs), 993 (m), 776 (s), 618 (m). MS (EI, 70 eV), m/z (%): 349.3

(MNa+), 327.4 (MH+), 238.3, 219.1, 175.1, 134.1, 106.2. Anal. for $C_{18}H_{22}N_4O_2$(326.39 g/mol) Calc. (%) C 66.24 H 6.80 N 17.16 Found (%) C 66.00 H 7.09 N 17.17

2.10. Synthesis of L9 *N,N'-Bis(2-pyridylmethylene)-1,4-diamino-diphenylamine* **(10)**

To a solution of methanol (50 ml) containing 4,4'-diaminodiphenylamine sulfate (2.614 mmol, 0.7786 g), KOH (5.229 mmol, 0.2982 g) was added in solid at RT. The color of the solution changed from black to purple. The mixture was heated to reflux for about 1 hour then pyridine-2-carboyaldehyde (5.229 mmol, 0.5 ml) was added drop-by-drop. The solution was heated at reflux, with stirring, for another 4 h. After cooling in an ice bath, the solution was filtered off to eliminate the amine that did not react and the solvent was removed under vacuum. The residue was extracted into CH_2Cl_2 (50 ml), washed with water (4 x 20 ml), dried over anhydrous $CaCl_2$ and then evaporated to dryness after filtration to yield, after drying under vacuum for several hours, 0.69 g (70% yield) of a bright brown solid, **L9**.

^{1}H RMN (DMSO-d_6, 400 MHz, ppm): 8.70 [ddd, ^{3}J(a,b) = 4.4, ^{4}J(a,c) = 1.6, ^{5}J (a,d) = 1.0, Ha, 2H], 8.66 (s, He, 2H, imine), 8.15 [td, Hd, ^{3}J(d,c) = 7.7, ^{4}J(d,b) = 1.1, ^{5}J(d,a) = 1.0, 2H], 7.93 [ddt, Hc, ^{3}J(c,d) = 7.7, 4J(c,b) = 7.3, 5J(c,a) = 1.6, 2H], 7.41 [ddd, Hb, ^{3}J(b,c) = 7.3, ^{4}J(b,a) = 5.1, ^{5}J(b,d) = 1.1, 2H], 7.32 [d, Hf, ^{3}J(f,g) = 8.9, 4H, phe], 7.10 [d, Hg, ^{3}J(g,h) = 8.9, 4H, phe], 4.10 (b, 2H, amine) ^{13}C RMN (DMSO-d_6, 400 MHz, ppm): 157.64, 155.46, 150.47, 143.41, 142.93, 137.80, 123.81, 121.50, 118.11, 80.17, 79.83, 79.50. IR (KBr pellet, cm^{-1}): 3242 (w), 1621 (m), 1593 (s), 1572 (vs), 1520 (s), 1499 (s), 1468 (m), 1325 (vs), 1168 (m), 1115 (w), 998 (m), 839 (s), 816 (m), 775 (m), 546 (m). MS (EI, 70 eV), m/z: 379 (MH^+), 273, 196. Anal. For $C_{24}H_{19}N_5 \cdot 1/3H_2O$ (Mr = 383.43 g/mol) Calc. (%): C: 75.18 H: 5.17 N: 18.26 Found. (%): C: 75.11 H: 5.14 N: 17.95

2.11. Synthesis of tma *2,3,5,6-Tetrakis(N-methylanilin-methyl)pyrazine* **(11)**

A solution of 2,3,5,6-tetrakis(bromomethyl)pyrazine (0.4530 g, 1 mmol) in 35 ml CH_3CN was added drop by drop to a suspension of N-methylaniline (1.2 ml, 10 mmol) and Na_2CO_3 (5.3 g, 50 mmol) in 25 ml CH_3CN. The colour changed immediately from light to deep yellow. The mixture was refluxed for about 2 hours, followed by TLC and then cooled to RT. The white precipitate (NaBr and excess Na_2CO_3) was filtered off and the filtrate was evaporated under vacuum. The residue was dissolved in hexane and the insoluble yellow powder obtained was recovered, washed with more hexane and then dried to yield 0.335 g (60 %) of **tma**.

^{1}H RMN ($CDCl_3$, 200 MHz, ppm): 7.14 (t, 8H, ph), 6.68 (m, 12H, ph), 4.58 (s, 8H, CH_2), 2.79 (s, 12H, CH_3). ^{13}C RMN (CD_3OD, 400 MHz, ppm): 149.64, 149.31, 128.94, 116.92, 113.17, 54.75, 39.46. IR (KBr pellet, cm^{-1}): 2926 (w), 1601 (s), 1508 (vs), 1446 (m), 1377 (m), 1366 (m), 1313 (m), 1257 (m), 1212 (m), 1117 (w), 993 (w), 820 (w), 745 (s), 689 (m). MS (EI, 70 eV), m/z: 594 (MK^+), 374, 291. Anal. for $C_{36}H_{40}N_6$(556.7 g/mol) Calc. (%) C 77.66 H 7.24 N 15.09 Found (%) C 76.82 H 7.19 N 15.07

2.12. Synthesis of tda *2,3,5,6-Tetrakis(dimethylaminomethyl)pyrazine* **(12)**

A large excess of dimethyl amine hydrochloride in water is neutralized with NaOH in an ice bath. The Me_2NH formed *in situ* is a gas and is directly condensed in a round bottom flask in an acetone/liquid N_2 bath at about –60 ºC using a weak vacuum. Once a sufficient quantity of liquid amine was formed, a solution of 2,3,5,6-tetrakis(bromomethyl)pyrazine (0.4530 g, 1 mmol, 50 ml CH_2Cl_2) was added dropwise at low temperature (about –30 ºC). The reaction was left for about 4 hours letting the temperature rise to rt. The excess amine was allowed to evaporate off before the solvent was gassed off. The residue was dissolved in 40 ml MeOH and passed through a resin column (15 g of Dowex 1 X8) previously charged with OH^- ions in order to exchange the HBr molecules, still attached to the ligand, by H_2O molecules. About

150 ml were used as eluent. Solvent evaporation yielded 0.27 g (87 %) of a light yellow powder, **tda**.

^{1}H RMN ($CDCl_3$, 200 MHz, ppm): 3.65 (s, 8H, CH_2), 2.15 (s, 12H, CH_3). ^{13}C RMN (D_2O, 400 MHz, ppm): 152.16, 62.53, 46.54. IR (KBr pellet, cm^{-1}): 2974 (s), 2942 (s), 2854 (m), 2820 (vs), 2772 (vs), 1635 (b), 1456 (s), 1414 (m), 1348 (s), 1259 (s), 1204 (m), 1168 (m), 1027 (vs), 987 (m), 841 (s). MS (EI, 70 eV), m/z: 310 (MH^+), 264, 178. Anal. for $C_{16}H_{32}N_6$ (308.5 g/mol) Calc. (%) C 62.30 H 10.46 N 27.24 Found (%) C 61.86 H 10.73 N 27.50

3. SYNTHESIS OF THE COMPLEXES

3.1. Complexes with L3

$[Zn_2(L3)I_4]$ (14)

A very diluted solution of **L3** in 10 ml CH_2Cl_2 was introduced into a glass tube and layered with about 2 ml MeOH as a buffer zone. Then a dilute solution of ZnI_2 in MeOH was slowly added to avoid possible mixing. The glass tube was sealed and left at RT. After less than one week red-orange crystals were obtained at the interface between the two solutions. IR (KBr pellet, cm^{-1}): 3060 (w), 1624 (w), 1611 (w), 1588 (vs), 1563 (m), 1507 (m), 1475 (m), 1442 (s), 1426 (w), 1368 (m), 1236 (m), 1208 (m), 1102 (m), 1024 (s), 992 (m), 833 (vs), 777 (s), 650 (m), 636 (m), 545 (m) Anal. for $[Zn(L3)I_4]\cdot MeOH$ (Mr = 956.73 g/mol) Calc. C: 23.85 H: 1.90 N: 5.86 Found. C: 24.34 H: 1.69 N: 5.74 %.

$\{[Cd_2(L3)(NO_3)_3(H_2O)_4]\cdot(NO_3)\cdot 2H_2O\}_n$ (15)

A very dilute solution of **L3** in 10 ml CH_2Cl_2 was introduced into a glass tube and layered with about 2 ml MeCN as a buffer zone. Then a dilute solution of $Cd(NO_3)_2\cdot 4H_2O$ in MeCN

was slowly added to avoid possible mixing. The glass tube was sealed and left at RT. After about one week orange-brown crystals were obtained at the interface between the two solutions. IR (KBr pellet, cm^{-1}): 3106 (w), 2395 (w), 1633 (m), 1594 (s), 1571 (w), 1493 (m), 1384 (vs), 1325 (s), 1197 (m), 1156 (w), 1106 (w), 1043 (m), 1016 (m), 913 (w), 825 (s), 782 (m), 640 (w), 630 (w), 570 (m).

3.2. Complexes with L5

$[Ni_2(L5)_3](BF_4)_4 \cdot CH_3OH$ (16) and $[Co_2(L5)_3](BF_4)_4 \cdot CH_3OH \cdot 0.5H_2O$ (17)

Both complexes are obtained by mixing methanolic solutions of 3 equiv. (0.3 mmol, 0.113 g, 20 ml MeOH) of **L5** and 2 equiv. (0.2 mmol, 10 ml MeOH) of $NiCl_2 \cdot 6H_2O$ or $CoCl_2 \cdot 6H_2O$ and heating at reflux during 2 hours. The complexes were precipitated by adding 4 equiv. of $[NH_4][BF_4]$ giving the triple-helicates of formulation $[M_2(L5)_3](BF_4)_4$ ($M = Ni^{2+}$, Co^{2+}), with a high yield (>80%). These powders were collected by filtration and then recrystallized by slow evaporation of acetonitrile solutions of the residues giving orange (Ni^{2+}) and orange-red (Co^{2+}) crystals suitable for X-ray diffraction analysis. IR (KBr pellet, cm^{-1}) for $[Ni_2(L5)_3](BF_4)_4$: 2921 (m), 2852 (w), 1633 (m), 1596 (m), 1571 (m), 1494 (s), 1446 (w), 1364 (w), 1242 (m), 1201 (m), 1054 (vs), 771 (w). For $[Co_2(L5)_3](BF_4)_4$: 1630 (m), 1595 (m), 1568 (m), 1494 (vs), 1445 (w), 1365 (w), 1308 (m), 1242 (s), 1200 (m), 1056 (vs), 773 (w). *Anal.* for $[Ni_2(L5)_3](BF_4)_4$ (Mr = 1599.93 g/mol) : Calc. C, 54.05; H, 3.40; N 10.50. Found C, 53.7; H, 3.36; N, 10.46 %, for $[Co_2(L5)_3](BF_4)_4$ (Mr = 1600.38 g/mol) : Calc. C, 54.04; H, 3.40; N, 10.50 Found C, 53.82; H, 3.34; N, 10.52 %. MS (ESI) for $[Ni_2(L5)_3](BF_4)_4$ m/z: 1112, $\{[Ni_2(L5)_3]_3(BF_4)_8\}^{4+}$; 979, $\{[Ni_2(L5)_3]_2(BF_4)_5\}^{3+}$; 712, $\{[Ni_2(L5)_3]_2(BF_4)_4\}^{4+}$; 423 $\{[Ni_2(L5)_3](OH^-)\}^{3+}$ and 313 $[Ni_2(L5)_3]^{4+}$. MS (ESI) for $[Co_2(L5)_3](BF_4)_4$ m/z: 1113,

$\{[Co_2(L5)_3]_3(BF_4)_8\}^{4+}$; 980, $\{[Co_2(L5)_3]_2(BF_4)_5\}^{3+}$; 713, $\{[Co_2(L5)_3]_2(BF_4)_4\}^{4+}$; 423 $\{[Co_2(L5)_3](OH^-)\}^{3+}$ and 313 $[Co_2(L5)_3]^{4+}$.

$\{[Ag(L5)](NO_3)\}_n$ (18)

To a solution protected from the light and kept under nitrogen of $AgNO_3$ (0.1 mmol, g) in 10 ml of dry MeOH, a solution of **L5** (0.1 mmol, 0.376 g) in dry MeOH was added dropwise. The mixture was refluxed with stirring for 2 h and then filtered to avoid any impurities. The resulting yellowish solution was allowed to slowly evaporate at room temperature, still light protected. After about 3 weeks, light yellow crystals were formed. IR (KBr pellet, cm^{-1}): 3435 (w), 1625 (m), 1584 (m), 1561 (w), 1494 (s), 1438 (w), 1338 (vs), 1245 (vs), 1196 (m), 1155 (m), 836 (m), 777 (w), 583 (w). MS (ESI) m/z: 1034, $[Ag_2(L5)_2(NO_3)]^+$; 865, $[Ag(L5)_2]^+$; 656, $[Ag_2(L5)(NO_3)]^+$ and 486, $[Ag_2(L5)_2]^{2+}$. ^1H NMR [DMSO-d^6]: 7.08 (4H, dt, Ph), 7.50 (4H, dt, Ph), 7.73 (2H, m, py), 8.15 (4H, dd, py), 8.79 (2H, d, py), 8.92 (2H, s, C=N). Anal. for $[Ag(L5)](NO_3)$ (Mr = 548.30 g/mol) Calc. C: 52.57 H: 3.31 N: 12.77 Found C: 53.57 H: 3.50 N: 12.20 %.

$\{[Ag(L5)](CF_3SO_3)\cdot 0.2H_2O\}_n$ (18a)

A methanolic solution of $AgCF_3SO_3$ (1 equiv., 0.1 mmol, 0.0257 g/15 ml) was slowly added to a methanolic solution of **L5** (1 equiv., 0.1 mmol, 0.0378 g/10 ml) under N_2 and protected from the light. The colour of the mixture changed to deep yellow and a precipitate appeared. The mixture was heated to *ca.* 40°C with stirring for 2 hours, cooled to room temperature and filtered. The yellow solid obtained was dissolved in acetonitrile and left undisturbed in the dark for *ca.* two weeks, whereupon yellow-green crystals were formed. IR (KBr pellet, cm^{-1}): 3468, 3067, 1626, 1592, 1561, 1496, 1441, 1420, 1251, 1056, 1029, 1008, 837, 775.Anal. for $[Ag(L5)](CF_3SO_3)\cdot 2H_2O$(623.41 g/mol): Calc. C 48.17, H 3.71, N 8.98; Found C 48.43, H

3.36, N 8.20 %. MS (ESI) m/z: 1121, $[Ag_2(L5)_2(CF_3SO_3)]^+$; 865, $[Ag(L5)_2]^+$; 742, $[Ag_2(L5)(CF_3SO_3)]^+$ and 486, $[Ag_2(L5)_2]^{2+}$. ^{1}H NMR [DMSO-d^6]: 7.09 (4H, d, Ph), 7.50 (4H, d, Ph), 7.70 (2H, m, py), 8.13 (4H, dd, py), 8.78 (2H, d, py), 8.89 (2H, s, C=N).

3.3. Complex with L7

$[Cd(L7)I_2]_n$ (19)

A very dilute solution of **L7** (0.014 g, 0.03 mmol) in 8 ml CH_2Cl_2 was introduced into a glass tube and layered with about 2 ml MeOH as a buffer zone. Then a diluted solution of CdI_2 (0.022 g, 0.06 mmol) in 8 ml MeOH was slowly added to avoid possible mixing. The glass tube was sealed and left at room temperature. After about one week bright golden crystals were obtained at the interface between the two solutions. IR (KBr pellet, cm^{-1}): 3041 (w), 1637 (m), 1613 (w), 1586 (s), 1557 (w), 1506 (s), 1485 (vs), 1431 (m), 1377 (m), 1344 (s), 1296 (m), 1254 (vs), 1226 (s), 1161 (m), 1143 (m), 1008 (w), 989 (m), 931 (m), 845 (s), 754 (s), 629 (m).

3.4. Complexes with L8

$[Ag(L8)](BF_4)$ (20)

To a methanolic (5 ml) solution of **L8** (1 equiv, 0.1704 mmol, 0.5 ml of a solution 0.341 M), $AgBF_4$ (1 equiv., 0.1704 mmol, 0.0332 g) in MeOH (15 ml) was slowly added under N_2 and protected from the light. The colour of the reaction mixture changed immediately to yellow. The solution was refluxed during 2h and then left undisturbed in the dark for at least two weeks, whereupon yellow-green crystals were formed. IR (KBr pellet, cm^{-1}): 1660 (m), 1588 (s), 1473 (m), 1438 (m), 1371(w), 1308 (m), 1230 (m), 1127-1084-1044 (vs), 930 (w), 773

(s), 628 (w). Anal. for $[Ag(L8)](BF_4)\cdot 2H_2O$(635.01 g/mol): Calc. C 38.81, H 4.70, N 10.06; Found C 38.85, H 4.10, N 9.75 %. ^{1}H RMN (CD_3OD, 400 MHz, ppm): 8.53 [ddd, Ha, ^{3}J(a,b) = 4.8, ^{4}J(a,c) = 1.6, ^{5}J(a,d) = 0.8, 2H]; 7.67 [ddd, Hb, ^{3}J(b,c) = 7.7, ^{3}J(b,a) = 4.8, ^{4}J(b,d) = 1.2, 2H] ; 8.13 [dt, Hc, ^{3}J(c,d) = 7.7, ^{3}J(c,b) = 7.7, ^{4}J(c,a) = 1.6, 2H]; 8.01 [td, Hd, ^{3}J(d,c) = 7.7, ^{4}J(d,b) = 1.2, ^{5}J(d,a) = 0.8, 2H]; 8.70 (s, He, broad, 2H)**;** 3.62 (s, Hf, broad, 4H); 3.95 (m, Hg and Hh, 8H). MS (ESI) m/z: 435, $[Ag(L8)]^+$.

$[Zn_2(L8)Cl_4]$ (21)

A very dilute solution of **L8** (*ca.* 0.1 mmol in 10 ml CH_2Cl_2) was introduced into a glass tube and layered with about 2 ml MeOH as a buffer zone. Then a dilute solution of $ZnCl_2$ (*ca.* 0.25 mmol in MeOH) was added very slowly to avoid possible mixing. The glass tube was sealed and left at room temperature. After about 2 days pale yellow plate-like crystals were obtained at the interface between the two solutions. IR (KBr pellet, cm^{-1}): 1654 (s), 1599 (vs), 1474 (m), 1445 (s), 1298 (s), 1222 (m), 1121 (s), 1111 (vs), 1099 (vs), 1091 (s), 1017 (s), 942 (m), 781 (s), 642 (m). Anal. for $[Zn_2(L8)Cl_4]\cdot CH_2Cl_2\cdot 0.5MeOH$ (699.93 g/mol): Calc. C 33.10, H 3.84, N 7.94; Found C 33.53, H 3.67, N 8.24 %.

$[Hg_2(L8)Cl_4]$ (22)

A very dilute solution of **L8** (*ca.* 0.1 mmol in 10 ml CH_2Cl_2) was introduced into a glass tube and layered with about 2 ml MeOH as a buffer zone. Then a dilute solution of $HgCl_2$ (*ca.* 0.25 mmol in 10 ml MeOH) was added very slowly to avoid possible mixing. The glass tube was sealed and left at room temperature. After about 2 days light yellow plate-like crystals were obtained at the interface between the two solutions.

IR (KBr pellet, cm^{-1}): 1658 (s), 1591 (s), 1472 (m), 1438 (s), 1299 (s), 1220 (m), 1118 (vs), 1106 (s), 1081 (s), 1025 (m), 1010 (m), 930 (m), 784 (s), 636 (m).

$[Cd_2(L8)I_4]\cdot CH_2Cl_2$ (23)

A very dilute solution of **L8** (*ca.* 0.1 mmol in 10 ml CH_2Cl_2) was introduced into a glass tube and layered with *ca.* 2 ml MeOH as a buffer zone. Then a dilute solution of CdI_2 (*ca.* 0.25 mmol in 10 ml MeOH) was added slowly to avoid possible mixing. The glass tube was sealed and left at room temperature. After about 2 days light yellow plate-like crystals were obtained at the interface between the two solutions. IR (KBr pellet, cm^{-1}): 1661 (s), 1594 (vs), 1476 (m), 1442 (s), 1302 (s), 1221 (m), 1106 (s), 1091 (vs), 1077 (s), 1012 (m), 934 (m), 925 (m), 779 (s), 638 (m).

$[M_2(L8)_3](ClO_4)_4$, where M = Co, Fe, Zn

Co^{II} complex (24)

A methanolic solution of 3 equiv. (0.423 mmol, 3 ml of a solution 0.141 M) of **L8** was slowly added, under N_2, to a solution of $Co(ClO_4)_2\cdot 6H_2O$ (0.282 mmol, 0.1031 g) in 10 ml MeOH. The colour of the reaction mixture changed immediately to deep orange-red and a precipitate appeared in some minutes. 10 ml MeCN were then added in order to dissolve the precipitate. The orange-red clear solution obtained was heated at reflux during 2 h and $NaClO_4$ in 10 ml MeOH was added in excess (0.211 mmol, 0.03 g). The solution was refluxed for another 2 h. Slow evaporation yielded orange-red rod-like crystals. The same compound was obtained by slow diffusion of a methanolic solution containing a mixture of $Co(ClO_4)_2\cdot 6H_2O$ and $NaClO_4$ over a solution of **L8** in CH_2Cl_2. The addition of $LiClO_4$ or $KClO_4$ did not give any crystal.
IR (KBr pellet, cm^{-1}): 1645 (m), 1599 (s), 1480 (m), 1447 (m), 1309 (m), 1084 (vs), 776 (m), 623 (s). MS (ESI) m/z: 612, $[Co_2(L8)_3(ClO_4)(MeO)]^{2+}$ and 484, $[Co(L8)(ClO_4)]^{+}$.

Fe^{II} complex (25)

A methanolic solution of **L8** (3 equiv, 0.341 mmol, 1 ml of a solution 0.341 M) was slowly added, under N_2, to a solution of $Fe(ClO_4)_2 \cdot 6H_2O$ (2 equiv., 0.227 mmol, 0.0082 g) in 50 ml MeOH. The colour of the reaction mixture changed immediately to deep purple. The solution was refluxed during 2 h, filtered to avoid any impurity, diluted with more MeOH and allowed to evaporate slowly. After about 2 weeks, purple needle-like crystals were obtained. The same compound was also obtained by slow diffusion of $Fe(ClO_4)_2 \cdot 6H_2O$ in MeOH over $NaClO_4$, also in MeOH and **L8** in CH_2Cl_2 in a glass tube under N_2. IR (KBr pellet, cm^{-1}): 1615 (m), 1599 (w), 1474 (m), 1448 (m), 1302 (m), 1093 (vs), 771 (w), 623 (m). MS (ESI) m/z: 807, $[Fe(L8)_2(ClO_4)]^+$; 644, $[Fe_2(L8)_3(ClO_4)_2]^{2+}$ and 481, $[Fe(L8)(ClO_4)]^+$.

Zn^{II} complex (26)

A very diluted solution of **L8** in about 10 ml CH_2Cl_2 was introduced into a glass tube and layered with about 2 ml MeOH as a buffer zone. Then a dilute solution of $Zn(ClO_4)_2$ in MeOH was slowly added to avoid possible mixing. The glass tube was sealed and left at room temperature. After about 2 weeks light yellow small needle-like crystals were obtained at the interface between the two solutions. IR (KBr pellet, cm^{-1}): 1652 (m), 1599 (s), 1482 (m), 1446 (m), 1310 (m), 1093 (vs), 777 (m), 624 (s). MS (ESI) m/z: 1082, $[Zn_2(L8)_2(ClO_4)_3]^+$; 828, $[Zn(L8)_2(ClO_4)]^+$ and 489, $[Zn(L8)_2(ClO_4)]^+$

$[Ni_2(L8)_3](BF_4)_4$ (27)

A solution of **L8** (3 equiv, 0.341 mmol, 1 ml of a solution 0.341 M, 30 ml MeOH) was added 0.054 g of $NiCl_2 \cdot 6H_20$ (2 equiv., 0.227 mmol). The colour of the reaction mixture changed immediately to light orange. The solution was refluxed for 2 h. 0.0476 g of $[NH_4][BF_4]$ (4 equiv., 0.454 mmol) were then added. The clear solution obtained was heated for a further 2h,

cooled and filtered to avoid any impurity and allowed to slowly evaporate. After about one week, light orange needle-like crystals of the complex were obtained. The same compound was also obtained by slow diffusion of $Ni(BF_4)_2$ in MeOH over $NaClO_4$ in MeOH and **L8** in CH_2Cl_2 in a glass tube. IR (KBr pellet, cm^{-1}): 1647 (m), 1599 (s), 1481 (m), 1448 (m), 1308 (m), 1058 (vs), 777 (m), 643 (w). Anal. for $[Ni_2(L8)_3](BF_4)_4 \cdot H_2O$ (1461.8 g/mol): Calc. C 43.83 H: 4.77 N: 11.36; Found C 43.89 H: 4.25 N: 10.86 %. MS (ESI) m/z: 797, $[Ni(L8)_2(BF_4)]^+$; 634, $[Ni_2(L8)_3(BF_4)_2]^{2+}$ and 483, $[Ni(L8)(BF_4)]^+$.

3.5. Complex with L9

$[Hg_2(L9)I_4]$ (28)

A very diluted solution of **L9** in 10 ml CH_2Cl_2 was introduced into a glass tube and layered with about 2 ml MeOH as a buffer zone. Then a dilute solution of HgI_2 in MeOH was slowly added to avoid possible mixing. The glass tube was sealed and left at room temperature. After a few days orange crystals were obtained at the interface between the two solutions.

IR (KBr pellet, cm^{-1}): 3341 (m), 1618 (m), 1587 (s), 1551 (w), 1529 (vs), 1499 (m), 1473 (m), 1371 (m), 1350 (m), 1242 (m), 1174 (m), 1153 (w), 819 (m), 780 (w), 535 (m).

3.6. Complexes with bptz

$[Ag_2(bptz)_3](SbF_6)_2$ (29)

To a solution of **bptz** (1 equiv, 8.7 mg, 0.04 mmol, 5 ml CH_3CN), $AgSbF_6$ (1 equiv., 12.7 mg, 0.04 mmol) in MeCN (10 ml) was slowly added under N_2 and protected from the light. The violet solution was stirred at RT during 2h and then left undisturbed in the dark for less than one week, whereupon red-violet crystals were formed. IR (KBr pellet, cm^{-1}): 1632 (w), 1588

(m), 1451 (w), 1391 (s), 1258 (m), 1139 (m), 1067 (w), 1000 (m), 932 (m), 791 (s), 745 (m), 658 (vs), 595 (s). Anal. for $[Ag_2(bptz)_3](SbF_6)_2$ (1395.94 g/mol): Calc. C 30.98 H 1.73 N 18.06 Found C 28.0 H 1.57 N 14.78 %. MS (ESI) m/z: 1160, $[Ag_2(bptz)_3(SbF_6)]^+$; 922, $[Ag_2(bptz)_2(SbF_6)]^+$; 580, $[Ag(bptz)_2]^+$, 462, $[Ag_2(bptz)_3]^{2+}$, 343, $[Ag_2(bptz)_2]^{2+}$.

$[Ag_2(bptz)_3](PF_6)_2$ (29a)

To a solution of **bptz** (1 equiv, 5.4 mg, 0.02 mmol, 5 ml CH_3CN), $AgPF_6$ (1 equiv., 5.8 mg, 0.02 mmol) in CH_3CN (5 ml) was slowly added under N_2 and protected from the light. The violet solution was stirred at RT during 3h and then left undisturbed in the dark for about one week, whereupon red-blue crystals were formed. IR (KBr pellet, cm^{-1}): 2922 (w), 1636 (m), 1593 (m), 1452 (w), 1389 (s), 1263 (m), 1137 (m), 932 (m), 838 (vs), 787 (w), 738 (w), 596 (s), 557 (s). Anal. for $[Ag_2(bptz)_3](PF_6)_2$ (1214.38 g/mol): Calc. C 35.61 H 1.99 N 20.76 Found C 28.0 H 1.57 N 14.78 %. MS (ESI) m/z: 1069, $[Ag_2(bptz)_3(PF_6)]^+$; 832, $[Ag_2(bptz)_2(PF_6)]^+$; 580, $[Ag(bptz)_2]^+$, 462, $[Ag_2(bptz)_3]^{2+}$, 343, $[Ag_2(bptz)_2]^{2+}$

$\{[Cd(bptz)I_2]\cdot CH_2Cl_2\}_n$ (30)

A very dilute solution of **bptz** (*ca.* 0.1 mmol, 0.024 g in 10 ml CH_2Cl_2) was introduced into a glass tube and layered with *ca.* 2 ml MeOH as a buffer zone. Then a dilute solution of CdI_2 (*ca.* 0.1 mmol, 0.036 g, in 10 ml MeOH) was added slowly to avoid possible mixing. The glass tube was sealed and left at room temperature. After a few days, dark-red crystals in a branch shape were formed in the interphase of the two solutions IR (KBr pellet, cm^{-1}): 3060 (m), 1637 (w), 1594 (m), 1442 (w), 1394 (vs), 1255 (m), 1158 (m), 1139 (s), 1071 (w), 1010 (m), 789 (m), 742 (m), 592 (s).

[Cd(bptz)(NO$_3$)$_2$]$_n$ (31)

A very dilute solution of **bptz** (*ca.* 0.1 mmol, 0.024 g, in 10 ml CH_2Cl_2) was introduced into a glass tube and layered with *ca.* 2 ml MeOH as a buffer zone. Then a dilute solution of $Cd(NO_3)_2 \cdot 4H_2O$ (*ca.* 0.1 mmol, 0.031 g, in 10 ml MeOH) was added slowly to avoid possible mixing. The glass tube was sealed and left at room temperature. After a few days, bright orange crystals were formed in the interphase of the two solutions. IR (KBr pellet, cm^{-1}): 3101 (w), 1596 (m), 1450 (s), 1394 (vs), 1306 (s), 1162 (w), 1138 (m), 1076 (w), 1034 (m), 1017 (m), 946 (m), 797 (m), 601 (s).

[Zn(bptz)(NO$_3$)$_2$]$_n$ (32)

A very dilute solution of **bptz** (*ca.* 0.1 mmol, 0.024 g, in 10 ml CH_2Cl_2) was introduced into a glass tube and layered with *ca.* 2 ml MeCN as a buffer zone. Then a dilute solution of $Zn(NO_3)_2 \cdot 4H_2O$ (*ca.* 0.1 mmol, 0.026 g, in 10 ml MeCN) was added slowly to avoid possible mixing. The glass tube was sealed and left at room temperature. After a few days, intense orange micro-crystals were formed in the interphase of the two solutions. This compound was analysed by X-ray powder diffraction. IR (KBr pellet, cm^{-1}): 3079 (w), 2343 (w), 1600 (m), 1570 (w), 1495 (w), 1462 (s), 1399 (vs), 1384 (vs), 1319 (s), 1161 (w), 1143 (w), 1053 (m), 1043 (m), 1020 (s), 952 (m), 795 (m), 604 (s). Anal. for [Zn(bptz)(NO$_3$)$_2$] (425.6 g/mol): Calc. C 33.86 H: 1.89 N: 26.33; Found C 34.33 H: 2.02 N: 25.72 %.

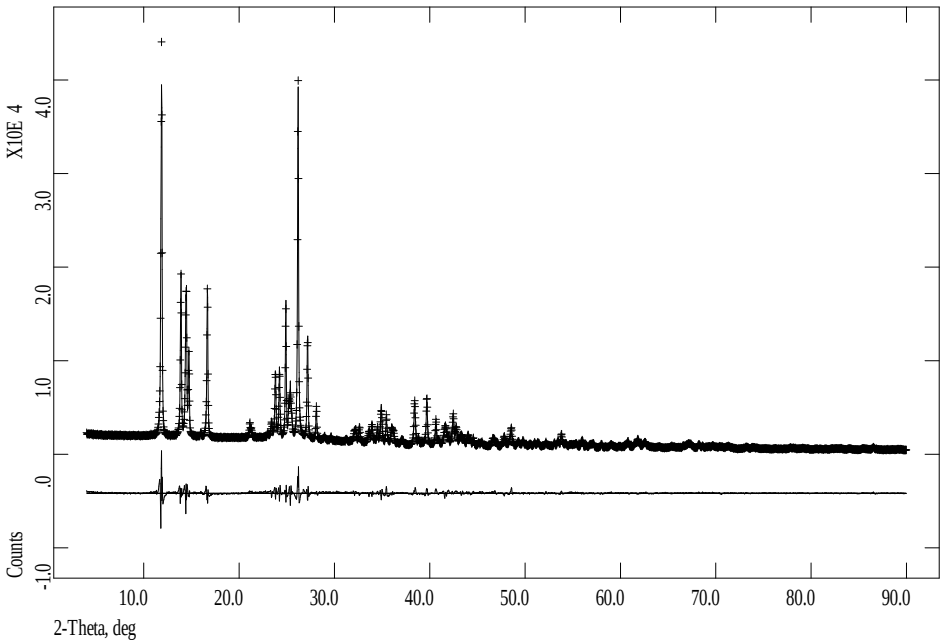

Final Rietveld plot for compound $[Zn(bptz)(NO_3)_2]_n$ (**32**).

$[Hg_2(bptz)Cl_4]_n$ (33)

To a solution of $HgCl_2 \cdot 2H_2O$ (0.1 mmol, 0.031 g) in 10 ml dry MeOH, a solution of **bptz** (0.1 mmol, 0.024 g, 10 ml dry MeOH) was added under nitrogen. The mixture was stirred at reflux for 3 hours without any significant colour change. The clear dark pink solution obtained was cooled, filtered to avoid any impurity and allowed to slowly evaporate. After about 1 month pink block-like crystals were obtained. The same compound was also obtained by slow diffusion of $HgCl_2 \cdot 2H_2O$ in MeCN over **bptz** in CH_2Cl_2 in a glass tube. The shape of the crystals was different (hair-like) but the IR spectrum and the powder diffractogram were identical for both products. IR (KBr pellet, cm^{-1}): 1629 (w), 1589 (m), 1575 (w), 1447 (w), 1391 (vs), 1260 (m), 1159 (w), 1136 (m), 1066 (w), 1049 (m), 1003 (m), 930 (w), 787 (s), 743 (m), 590 (s). By allowing the former solution to stand for more than 1 month, another compound was formed in the form of colourless crystals that appeared to be $[Hg(bptz2)Cl_2]$ (**33a**) were **bptz2** results from a transformation of the ligand **bptz**.

$[Hg(bptz)Br_2]_n$ (34)

To a solution of $HgBr_2$ (0.1 mmol, 0.036 g) in 10 ml MeCN, a solution of **bptz** (0.1 mmol, 0.024 g, 10 ml MeCN) was added. The solution was stirred at reflux for 4 hours without any significant colour change. The clear dark pink solution was cooled to room temperature, filtrated to avoid any impurity and allowed to evaporate slowly. After about 3 weeks pink block-like crystals were obtained. As for $[Hg_2(bptz)Cl_4]_n$, hair-like crystals were obtained by slow diffusion of $HgBr_2$ in MeCN over **bptz** in CH_2Cl_2 in a glass tube. The IR spectra of both crystalline samples were identical. IR (KBr pellet, cm^{-1}): 3059 (w), 1622 (w), 1584 (s), 1570 (w), 1442 (m), 1385 (vs), 1259 (m), 1151 (m), 1124 (m), 1065 (m), 1043 (w), 999 (m), 922 (w), 799 (s), 745 (m), 592 (s).

$[Hg_2(bptz)I_4]_n$ (35)

A very dilute solution of **bptz** (*ca.* 0.1 mmol, 0.024 g, in 10 ml CH_2Cl_2) was introduced into a glass tube and layered with *ca.* 2 ml MeOH as a buffer zone. Then a dilute solution of HgI_2 (*ca.* 0.1 mmol, 0.045 g, in 10 ml MeOH) was added slowly to avoid possible mixing. The glass tube was sealed and left at room temperature. After more than 1 month, intense pink block-like crystals were formed. IR (KBr pellet, cm^{-1}): 1683 (m), 1589 (m), 1508 (m), 1468 (m), 1444 (m), 1389 (vs), 1258 (w), 1155 (m), 1132 (m), 1067 (m), 1047 (w), 1003 (m), 926 (w), 783 (s), 744 (m), 591 (s).

$[Cu(bptz1)Cl_2]_n$ (36)

A very dilute solution of **bptz** (*ca.* 0.1 mmol, 0.024 g, in 10 ml CH_2Cl_2) was introduced into a glass tube and layered with *ca.* 2 ml MeOH as a buffer zone. Then a dilute solution of $CuCl_2 \cdot 2H_2O$ (*ca.* 0.1 mmol, 0.017 g in 10 ml MeOH) was added slowly to avoid possible mixing. The glass tube was sealed and left at room temperature. A purple solid was formed

immediately in the interphase of the two solutions. After about 1 week this powder was recovered and the remaining solution was allowed to slowly evaporate giving finally green crystals of $[Cu(bptz1)Cl_2]_n$. IR (purple compound) (KBr pellet, cm^{-1}): 3055 (w), 1596 (m), 1460 (w), 1446 (m), 1391 (vs), 1263 (m), 1158 (m), 1134 (m), 1052 (w), 1025 (m), 940 (m), 809 (m), 595 (m). IR for [Cu(bptz1)Cl_2]n (KBr pellet, cm^{-1}): 3054 (m), 1614 (m), 1545 (s), 1481 (w), 1469 (s), 1425 (vs), 1314 (m), 1288 (m), 1253 (m), 1148 (s), 1094 (m), 1051 (m), 1022 (m), 806 (vs), 753 (m), 707 (s). Anal. for $[Cu(bptz1)Cl_2]_n$ (358.66 g/mol): Calc. C 40.18 H 2.25 N 15.62 Found C 40.83 H 2.57 N 15.78 %.

[Mn(bptz2)Cl_2·CH_3OH] (37)

To a solution of $MnCl_2·4H_2O$ (0.2 mmol, 0.040 g) in 10 ml MeOH a **bptz** solution (0.1 mmol, 0.024 g, 10 ml CH_2Cl_2) was added. The solution was stirred at reflux for 4 hours with any significant colour change. The clear dark pink solution was then cooled, filtered to avoid any impurity and allowed to slowly evaporate. In a few days, the colour changed to orange and after approximately 3 weeks a few orange and brown crystals were obtained. The X-ray analysis of the brown crystals resulted in compound **37**.

bptz3 (38)

This decomposition product was obtained by slow diffusion of **bptz** in MeOH over $MnClO_4·6H_2O$ in H_2O in a glass tube.

3.7. Complexes with tma

[Cd(tma)I_2] (39)

About 10 ml of a very dilute CH_2Cl_2 solution of **tma** were introduced into a glass tube and

layered with *ca.* 2 ml MeOH as a buffer zone. Then, 10 ml of a dilute methanolic solution of CdI_2 were added slowly to avoid possible mixing. The glass tube was sealed and left at room temperature. The colour of the interphase changed immediately to deep yellow and in hours to green. After a few days, green crystals were formed. IR (KBr pellet, cm^{-1}): 2922 (m), 1599 (vs), 1507 (s), 1497 (s), 1455 (w), 1376 (w), 1173 (m), 1120 (m), 751 (s), 694 (s).

$[Zn(tma)Cl_2]\cdot CH_2Cl_2$ (40)

To a solution of $ZnCl_2$ (0.1 mmol, 0.014 g) in 5 ml MeOH a solution of **tma** (0.05 mmol, 0.028 g, 5 ml CH_2Cl_2) was added. The solution was stirred at RT for 2 hours without any significant colour change. The clear light green solution obtained was filtrated to avoid any impurity and allowed to evaporate slowly. In a few days, yellow crystals were obtained. These crystals were recovered and the light green solution yielded after some days green crystals that appeared to be the ligand. IR (KBr pellet, cm^{-1}): 2909 (w), 1599 (vs), 1573 (w), 1507 (s), 1451 (m), 1412 (w), 1363 (s), 1257 (m), 1171 (m), 1096 (w), 1033 (m), 920 (m), 746 (s), 691 (s) Anal. for $[Zn(tma)Cl_2]\cdot 1/3CH_2Cl_2$ (749.6 g/mol): Calc. C 60.50 H: 5.68 N: 11.65; Found C 60.66 H: 5.78 N: 11.93 %.

tma2 (41)

This decomposition product was obtained several times by reacting the ligand **tma** with different metal salts such as $Zn(ClO_4)_2$ (in excess), $MnCl_2\cdot 4H_2O$ and $Ni(AcO)_2\cdot 4H_2O$.

1. REFERENCES INTRODUCTION

1. Graddon, D.P. *"An Introduction to Coordination Chemistry"* **1961**, Ed. Pergamon Press.
2. Cotton F.A. and Wilkinson G. *"Advanced Inorganic Chemistry: A comprehensive text"* 3rd Ed. **1972**, Interscience Publishers, John Wiley & Sons.
3. Lehn, J.-M. *Pure Appl. Chem.* **1978**, *50*, 871.
4. a) Lehn, J.-M. *"Supramolecular Chemistry: Concepts and perspectives"* VCH, Verlagsgeselleshaft, Weinheim, Germany, **1995** b) Several authors in *"Comprehensive Supramolecular Chemistry: Templating, Self-assembly and Self-organization"*, volume 9 Atwood, J.L., Davies, J.E.D., MacNicol, D.D. and Vögtle, F. **1996** c) Ribas Gispert, J. *"Química de coordinación"* Universitat de Barcelona Ed. Omega, S.A., **2000** d) Constable, E.C. *Prog. Inorg. Chem.*, **1994**, *42*, 67 e) Williams, A.F., Floriani, C., Merbach, A.E., *"Perspectives in Coordination Chemistry"*, VHCA Verlag Helvetica Chimica Acta, Basel and VCH Verlagsgeselleschaft, Weinheim, Germany, **1992** f) Caulder, D.L. and Raymond, K., N. *J. Chem. Soc. Dalton Trans.* **1999**, 1185 g) Robson, R. J. *Chem. Soc. Dalton. Trans.* **2000**, 3735.
5. Piguet, C., Bernardinelli, G. and Hopfgartner, G. *Chem.Rew*. **1997**, *97*, 2005-62.
6. Swiegers, G.F.; Malefetse, T.J.; *Chem. Rew*. **2000**, *100*, 3483-537.

Helices: Single-helices
7. Vögtle, F. and Weber, E., *Angew. Chem. Int. Ed. Engl*. **1979**, *18*, 753.
8. Goedken, V.L. and Christoph, G.G. *Inorg. Chem.* **1973**, *12*, 2316.
9. a) Wester, D. and Palenik, G.J. *J. Chem. Soc. Chem. Commun.* **1975**, 74 b) Wester, D. and Palenik, G.J. *Inorg. Chem.* **1976**, *15*, 755.
10. Constable, E.C., Martínez Manez, R., Cargill Thompson A.M.W. and Walker, J.V. J. *Chem. Soc. Dalton Trans.* **1994**, 1585.
11. Deuschel-Cornioley, C., Stoeckli-Evans, H. and von Zelewsky, A. *J. Chem. Soc. Chem. Commun.* **1990**, 121.
12. Fu, Y., Sun, J., Li, Q., Chen, Y., Dai, W., Wang, D., Mak, T.C.W., Tang, W. and Hu, H. *J. Chem. Soc. Dalton Trans.* **1996**, 2309.
13. Youinou, M.T., Ziessel, R. and Lehn, J.-M. *Inorg. Chem.* **1991**, *30*, 2144.
14. Lam, M.H.W., Lee, D.Y.K., Chiu, S.S.M., Man K.W. and Wong, W.T. *Eur. J. Inorg. Chem*. **2000**,1483.
15. Bowyer, P.K., Porter, K.A., Rae, A.D., Willis, C. and Wild, S.B. *Chem. Commun.*, **1998**, 1153.
16. Carlucci, L., Ciani, G., Proserpio, D. M. and Sironi, A. *Inorg. Chem.* **1998**, *37*, 5941.
17. Suzuki, T., Kotsuki, H., Isobe, K., Moriya, N., Nakagawa, Y. and Ochi, M. *Inorg. Chem.* **1995**, *35*, 530.
18. Withersby, M.A., Blake, A.J., Champness, N.R., Hubberstey, P., Li, W.S. and Schöder, M. *Angew.Chem. Int. Ed. Engl.* **1997**, *36*, 21, 2327.
19. Bermejo M.R., Fondo, M., González, A.M., Hoyos, O.L., Sousa, A., McAuliffe, C.A., Hussain, W., Pritchard, R. and Novotorsev, V.M., *J. Chem. Soc. Dalton Trans.*, **1999**, 2211.

Double-helices
20. Berl, V.; Huc, I.; Khoury, R.G.; Krische, M. J. and Lehn, J.-M. *Nature* **2000,** *407*, 720.
21. Rüttimann, S.; Piguet, C.; Bernardellini, G.; Bocquet, B. and Williams, A.F. *J. Am. Chem. Soc.* **1992**, *114*, 4230.
22. Constable, E.C., Edwards, A.J., Hannon, M.J. and Raithby, P.R. *J. Chem. Soc. Chem. Commun*. **1994**, 1991.

23. Bin Silong, S., Kildea, J.D., Patalinghung, C., Skelton, B.W. and White, A.H. *Aus. J. Chem*, **1994**, *47*, 1545.
24. Hasenknopf, B., Lehn, J.-M., Baum, G. and Fenske, D., *Proc. Natl. Acad. Sci. U.S.A.* **1996**, *93*, 1397.
25. a) Constable, E.C., Hannon, M.J., Martin, A., Raithby, P.R. and Tocher, D.A. *Polyhedron* **1992**, *11*, 2967 b) Constable, E.C., Elder, S.M., Hannon, M.J., Martin, A., Raithby, P.R. and Tocher, D.A. *J. Chem. Soc. Dalton Trans.* **1996**, 2423.
26. Zarges, W., Hall, J., Lehn, J.-M. and Bolm, C. *Helv. Chim. Acta* **1991**, *74*, 1843.
27. a) Kramer, R., Lehn, J.-M. and Marquis-Rigault, A. *Proc. Natl. Acad. Sci. U.S.A* **1993**, *90*, 5394 b) Marquis-Rigault, A., Dupont-Gervais, A., Baxter, P.N.W., Van Dosselaer, A. and Lehn, J.-M. *Inorg. Chem.* **1996**, *35*, 2307.
28. a) Van Stein, G.C., Van Koten, G., Passenire, H., Steinebach, O. and Vriete, K. *Inor. Chim. Acta* **1984**, *89*, 79 b) Van Stein, G.C., Van Koten, G., Vriete, K.Brevard, C. and Spek, A.L. *J. Am. Chem. Soc.* **1984**, *106*, 4486.
29. a) Hannon, M.J., Painting, C.L. and Alcock, N.W. *Chem. Commun*., **1999**, 2023 b) Hannon, M.J., Bunce, S., Clarke, A.J. and Alcock, N.W. *Angew. Chem. Int. Ed. Engl.* **1999**, *38*, 1277.
30. a) Yoshida, N., Ichikawa, K., Shiro, M. *J. Chem. Soc. Perkin Trans. 2* **2000**, *2*, 17 b) Yoshida, N., Oshio, H. and Ito, T. *J. Chem. Soc. Perkin Trans. 2* **1999**, 975 c) Yoshida, N., Oshio, H. and Ito, T. *Chem. Commun.* **1998**, 63.
31. Fleming, S., Mann, K.L.V., Couchman, S.M., Jeffery, J.C., McCleverty, A. and Ward, M.D. *J. Chem. Soc. Dalton Trans*, **1998**, 2047.

Triple helices

32. Harris, C.M. and Mc Kenzie, E.D. *J. Chem. Soc. (A)* **1969**, 746.
33. Potts, K.T., Horwitz, C.P., Fessak, A., Keshavarz-K, M., Nash, K.E. and Toscano, P.J. *J. Am. Chem. Soc.* **1993**, *115*, 10444.
34. Elliott, C.M., Derr, D.L., Ferrere, S., Newton, M.D. and Liu, Y.P. *J. Am. Chem. Soc.* **1996**, *118*, 5221.
35. Krämer, R., Lehn, J.-M., DeCIan, A. and Fisher, J. *Angew. Chem. Int. Ed. Engl.* **1993**, *32*, 704.
36. Zurita, D., Baret, P. and Pierre, J.-L., *New. J. Chem.* **1994**, *18*, 1143.
37. a) Charbonnière, L.J., Williams, A.F., Frey, U., Merbach, A.E., Kamalaprija, P. and Schaad, O. *J. Am. Chem. Soc.* **1997**, *119*, 2488 b) Piguet C., Bernardinelli G., Bocquet, B., Quattropani, A. and Williams, A.F. *J. Am. Chem. Soc.* **1992**, *114*, 7440 c) Piguet C., Bünzli, J.-C.G., Bernardinelli G., Hopfgartner G. and Williams, A.F. *J. Am. Chem. Soc.* **1993**, *115*, 8197 d) Elhabiri M., Scopelliti R., Bünzli J.-C.G. and Piguet C. *J. Am. Chem. Soc. 121*, **1999**, 10747 e) Rigault S., Piguet C., Bernardinelli G. and Hopfgartner G. *Angew. Chem. Int. Ed. Engl. 37*, 169 **1998** f) Edder, C., Piguet C., Bünzli, J.-C.G. and Hopfgartner G. *J. Chem. Soc., Dalton Trans.* **1997**, 4657 g) Renaud F., Piguet C., Bernardinelli G., Hopfgartner G. and Bünzli J.-C.G. *Chem. Commun.* **1999**, 457 h) Renaud F., Piguet C., Bernardinelli G., Hopfgartner G. and Bünzli J.-C.G. *J. Am. Chem. Soc.* **1999**, *121*, 9326.
38. Zelikovich, L., Libman, J., Schanzer, A., *Nature*, **1995**, *374*, 790.
39. Enemark, E.J., Stack, T.D. *P. Inorg. Chem.* **1996**, *35*, 2719.
40. Kersting, B., Telford, J.R., Meyer, M. and Raymond, K.N., *J. Am. Chem. Soc.* **1996**, *118*, 7221.
41. Albrecht, M.A. and Kotila, S. *Angew. Chem. Int. Ed. Engl.* **1996**, *35*, 1208.
42. Hogerheide, M.P., Jastrzebski, J.T.B., Boersma, J., Smeets, W.J.J., Spek, A.L. and Van Koten, G. *Inorg. Chem.* **1994**, *33*, 4431.
43. Grillo, V.A., Seddon, E.J., Grant, C.M., Aromí, G., Bollinger, J.C., Folting, K. and

Christou, G. *Chem. Commun.*, **1997**, 1561.
44. Scherer, M., Caulder, D.L, Darren W.J. and Raymond, K.N. *Angew. Chem. Int. Ed.* **1999**, *38*, 1588.
45. Rice, C.R., Wörl, S., Jeffery, J.C., Paul, R.L. and Ward, M.D. *Chem.Commun*, **2000**, 1529.
46. a) Tesouro Vallina, A. and Stoeckli-Evans, H. *Chimia* **1999**, *53*, 342 b) Cheng, H., Chun-ying, D. Chen-jie, F. and Qing-jin, M. *J. Chem. Soc., Dalton Trans.*, **2000**, 2419.
47. Yoshida, N. and Ichikawa, K. *Chem. Comm.*, **1997,** 1091.
48. Hannon, M.J., Painting, C.L., Jackson, A., Hamblin J. and Errington, W. *Chem. Comm.*, **1997,** 1807.
49. Yoshida, N., Ito, N. and Ichikawa, K. *J. Chem. Soc. Perkin Trans. 2*, **1997**, 2387.
50. Gampp, H., Maeder, M., Meyer, C.J. and Zuberbhehler, A.D. *Comments Inorg. Chem.* **1987**, *6*, 41.
51. Gulik-Krzywicki, T., Fouquey, C. and Lehn, J.-M. *Proc. Natl. Acad. Sci. U.S.A.* **1993**, *90*, 163.
52. Bilyk, A., Harding, M.M., Turner, P. and Hambley, T.W. *J. Chem. Soc. Dalton Trans.* **1995**, 2549.
53. Schoentjes, B. and Lehn, J.-M. *Helv. Chim. Acta* **1995**, *78*, 1.

Grids

54. Baxter, P.N.W., Lehn, J.-M., Fischer, J. and Youinou, M.-T. *Angew. Chem., Int. Ed. Engl.* **1994**, *33*, 2284.
55. Hanan, G.S., Volkmer, D., Schubert, U.S., Lehn, J.-M., Baum, G. and Fenske, D. *Angew. Chem., Int. Ed. Engl.* **1997**, *36*, 1842.
56. Waldmann, O., Hassmann, J., Müller, P., Hanan, G.S., Volkmer, D., Schubert, U.S. and Lehn, J.-M. *Phys. Rev. Lett*. **1997**, *79*, 3390.
57. Rojo, J., Lehn, J.-M., Baum, G., Fenske, D., Waldmann, O. and Müller, P. *Eur. J. Inorg. Chem.* **1999**, 517.
58. a) Baxter, P.N.W., Lehn, J.-M. and Rissanen, K. *Chem. Commun.* **1997**, 1323 b) Baxter, P.N.W., Lehn, J.-M., Kneisel, B.O. and Fenske, D. *Chem. Commun.* **1997**, 2231 c) Baxter, P.N.W., Lehn, J.-M., Kneisel, B.O. and Fenske, D. *Angew. Chem. Int. Ed. Engl.* **1997**, *36*, 1978.
59. a) Weissbuch, I., Baxter, P.N.W., Cohen, S., Cohen, H., Kjaer, K., Howes, P.B., Als-Nielsen, J., Hanan, G.S., Schubert, U.S., Lehn, J.-M., Leiserowitz, L. and Lahav, M. *J. Am. Chem. Soc.* **1998**, *120*, 4850 b) Weissbuch, I.; Baxter, P.N.W., Kuzmenko, I., Cohen, H., Cohen, S., Kjaer, K., Howes, P.B., Als-Nielsen, J., Lehn, J.-M., Leiserowitz, L. and Lahav, M. *Chem. Eur. J.* **2000**, *6*, 725.

Ladders and racks

60. Baxter, P.N.W., Hanan, G.S. and Lehn, J-M. *Chem. Commun.* **1996**, 2019.
61. a) Hanan, G.S., Arana, C. R., Lehn, J.-M., Fenske, D. *Angew. Chem. Int. Ed. Engl.* **1995**, *34*, 1122 b) Hanan, G.S., Arana, C.R., Lehn, J.-M., Baum, G. and Fenske, D. *Chem. Eur. J.* **1996**, *2*, 1292.
62. Drain, C.M., Nifiatis, F., Vasenko, A. and Batteas, J.D. *Angew. Chem. Int.Ed. Engl.* **1998**, *37*, 2344.

Cyclic motivs

63. Stang, P.J. and Olenyuk, B. *Acc. Chem. Res.* **1997**, *30*, 502.
64. Caulder, D.L., Raymond, K.N. *J. Chem. Soc., Dalton Trans.* **1999**, 1185.
65. a) Neels, A. and Stoeckli-Evans, H. *Inorg. Chem.* **1999**, *38*, 6164 b) Rüttimann, S., Bernardinelli, G. and Williams, A.F. *Angew. Chem. Int. Ed. Engl.* **1993**, *32*, 392 c) Carina,

R.F., Williams, A.F. and Bernardinelli, G. *J. Organomet. Chem.* **1997**, *548*, 45 d) Chi, X., Guerin, A.J., Haycock, R.A., Hunter, C.A. and Sarson, L.D., *J. Chem. Soc. Chem. Commun.* **1995**, 2567 e) Wojacczynski, J., Latos-Grazynski, L., Olmstead, M.M. and Balch, A.L. *Inorg. Chem.* **1997**, *36*, 4548 f) Yamarini, K., Fukuda, I., Kawamoto, K., Kushi, Y., Fikuhiro, A., Kubota, N., Fukuo, T. and Arakawa, R. *Inorg. Chem.* **1995**, *34*, 1054 g) Ma, G., Jung, Y.S., Chung, D.S. and Hong, J.-I. *Tetrahedron Lett.* **1999**, *40*, 531 h) Thompson, A., Rettig, S.J. and Dolphin, D. *Chem. Commun.* **1999**, 631 i) Schnebeck, R.-D., Randaccio, L., Zangrando, E. and Lippert, B., *Angew. Chem. Int. Ed. Engl.* **1998**, *37*, 119.

66. a) Bu, X.-H., Morishita, H., Tanaka, K., Biradha, K., Furusho, S. and Shionoya, M. *Chem. Commun.* **2000**, 971 b) Campos-Fernández, C.S., Clérac, R. and Dunbar, K.R. *Angew. Chem. Int. Ed.* **1999**, *38*, 3477 c) Gardner, M., Guerin, A.J., Hunter, C.A., Michelsen, U. and Rotger, C. *New. J. Chem.* **1999**, 309 d) Stang, P.J., Cao, D.H., Saito, S. and Arif, A.M. *J. Am. Chem. Soc.* **1995**, *117*, 6273 e) Whiteford, J.A., Lu, C.V. and Stang, P.J. *J. Am. Chem. Soc.* **1997**, *119*, 2524 f) Müller, C., Whiteford, J.A. and Stang, P.J. *J. Am. Chem. Soc.* **1998**, *120*, 9827 g) Habicher, T., Nierengarten, J.-F., Gramlich, V. and Diederich, F. *Angew. Chem. Int. Ed. Engl.* **1998**, *37*, 1916 h) Schmitz, M., Leininger, S., Fan, J., Arif, A.M. and Stang, P. J. *Organometallics*. **1999**, *18*, 4817 i) Cheng, H., Chun-ying, D., Chen-jie, F., Yong-jiang, L. and Qing-jin, M. *J. Chem. Soc. Dalton Trans.* **2000**, 1207 j) Duan, C.-Y., Liu, Z.-H., You, X.-Z., Xue, F. and Mak, T.C.W. *Chem. Commun.* **1997**, 381.

67. Woessner, S.M., Helms, J.B., Shen, Y. and Sullivan, B.P. *Inorg. Chem.* **1998**, *37*, 5406.

68. a) Kitagawa, S., Nozaka, Y. and Munakata, M. *J. Chem. Soc. Dalton Trans.* **1993**, 1399 b) López, C.A., Fackeler, J.P., Staples, R., Wang, S. and Winpenny, R.E.P. *Croat. Chem. Acta.* **1995**, *68*, 793 c) Constable, E.C., Elder, S.M., Palmer, C.A., Raithby, P.R. and Tocher, D.A. *Inorg. Chim. Acta* **1996**, *252*, 281.

69. a) Baxter, P., Lehn, J.-M., De Cian, A.and Fisher, J., *Angew. Chem. Int. Ed. Engl.* **1993**, *32*, 69 b) Baxter, P., Lehn, J.-M., Baum, G. and Fenske, D. *Chem Eur. J.* **1999**, *5*, 102 c) García, A.M., Bassani, D.M., Lehn, J.-M., Baum, G. and Fenske, D. *Chem. Eur. J.* **1999**, *5*, 1234.

70. a) Hannon, M.J., Painting, C.L. and Errington, W. *Chem. Commun.* **1997**, 307 b) Fujita, M., Nagao, S., Ogura, K. *J. Am. Chem. Soc.* **1995**, *117*, 1649 c) Chan, C.-K., Cheung, K.-K., Che, C.-M. *Chem. Commun.* **1996**, 227 d) Bark, T., Weyermüller, T., Heirtzler, F. *Chem. Commun.*, **1998**, 1475 e) O'Keefe, B.J., Steel, P.J. *Inorg. Chem. Commun.* **1998**, *1*, 147.

71. a) Stang, P.J., Olenyuk, B., Muddiman, D.C., Smith, R.D. *Organometallics*, **1997**, *16*, 3094 b) Fujita, M., Ogura, D., Miyazawa, M., Oka, H., Yamaguchi, K. and Okura, K. *Nature*, **1995**, *378*, 469 c) Kusukawa, T. and Fujita, M. *J. Am. Chem. Soc.* **1999**, *121*, 1397 d) Enemark, E.J. and Stack, T.D.P. *Angew. Chem. Int. Ed. Engl.* **1998**, *37*, 2082 e) Saalfrank, R.W., Burak, R., Reihs, S., Löw, N., Hample, F., Stachel, H.-D., Lentmaier, J., Peters, K., Peters, E.-M. and Von Schenering, H.G., *Angew. Chem. Int. Ed. Engl.* **1995**, *34*, 993 f) Parac, T.N., Caulder, D.L. and Raymond, K.N. *J. Am. Chem. Soc.* **1998**, *120*, 8003.

72. a) Hasenknopf, B., Lehn, J.-M., Boumediene, N., Dupont-Gervais, A., van Dorsselaer, A., Kneisel, B. and Fenske, D. *J. Am. Chem. Soc.* **1997**, *119*, 10956 b) Hasenknopf, B., Lehn, J.-M., Kneisel, B., Baum, G. and Fenske, D. *Angew. Chem. Int. Ed. Engl.* **1996**, *35*, 1838 c) Baum, G., Constable, E.C., Fenske, D., Housecroft, C.E. and Kulke, T. *Chem. Commun*, **1999**, 195 d) Mamula, O., Von Zelewsky, A. and Bernardinelli, G. *Angew. Chem. Int. Ed. Engl.* **1998**, *37*, 290.

Rods

73. a) Harriman, A. and Ziessel, R. *Chem Commun*, **1996**, 1707 b) Barigelletti, F., Flamigni, L., Balzani, V., Collin, J.-P., Sauvage, J.-P., Sour, A., Constable, E.C. and Cargill-Thompson, A.M. *J. Am. Chem. Soc.* **1994**, *116*, 7692 c) Constable, E.C. and Cargill-Thompson, A.M. *J.*

Chem. Soc. Dalton Trans. **1995**, 1615 d) Wärnmark, K., Baxter, P.N.W. and Lehn, J.-M., *Chem. Commun.*, **1998**, 993 e) Vögtle, F., Frank, M., Nieger, M., Belser, P., Von Zelewsky, A., Balzani, V., Barigelletti, F., De Cola, L. and Flamigni, L. *Angew. Chem. Int. Ed. Engl.* **1993**, *32*, 1643 f) Von Zelewsky, A. and Belser, P. *Chimia* **1998**, *52*, 620 g) Frank, M., Nieger, M., Vögtle, F., Belser, P., Von Zelewsky, A., De Cola, L., Balzani, V., Barigelletti, F. and Flamigni, L. *Inorg. Chim. Acta* **1996**, *242*, 281.

Dendrimers

74. Picture taken from the web page of the research group of Prof. A. Hirsch www.organik.uni-erlangen.de/hirsch/dend_chem.html.

75. a) Constable, E.C., Harverson, P., Ramsden, J.J. *Chem Commun.* **1997**, 1683 b) Hearshaw, M.A., Moss, J.R. *Chem. Commun.* **1999**, 1 c) Boulas, P.L., Gómez-Kaifer, M. and Echegoyen, L. *Angew. Chem. Int. Ed. Engl.* **1998**, *37*, 21 d) Constable, E.C., Housecroft, C.E. *Chimia* **1998**, *52*, 533.

Catenanes

76. a) Fujita, M. *Acc. Chem. Res.* **1999**, *32*, 53 b) Nierengarten, J.-F., Dietrich-Buchecker, C.O. and Sauvage, J.-P. *New J. Chem.* **1996**, *20*, 685 c) Fujita, M., Ibukuro, K., Seki, H., Kamo, O., Imanari, M. and Ogura, K. *J. Am. Chem. Soc.* **1996**, *118*, 899 d) Chambron, J.-C., Dietrich-Buchecker, C.O., Rapenne, G. and Sauvage, J.-P. *Chirality* **1998**, *10*, 125 e) Armaroli, N., Ceroni, P., Balzani, V., Kern, J.-M., Sauvage, J.-P. and Weidmann, J.L. *J. Chem. Soc. Faraday Trans.* **1997**, *93*, 4145 f) Sauvage, J.-P. *Acc. Chem. Res.* **1998**, *31*, 611.

Rotaxanes

77. a) Collin, J.-P., Gaviña, P. and Sauvage, J.-P. *Chem. Commun.* **1996**, 2005 b) Flamigni, L., Barigelletti, F., Armaroli, N., Collin, J.-P. and Sauvage, J.-P. *Chem. Eur. J.* **1998**, *4*, 1744 c) Armaroli, N., Dietrich, F., Dietrich-Buchecker, C.O., Flamigni, L., Marconi, G., Nierengarten, J.-F. and Sauvage, J.-P. *Chem. Eur. J.* **1998**, *4*, 406 d) Gaviña, P. and Sauvage, J.-P. *Tetrahedron Lett.* **1997**, 38, 3521 e) Ashton, P.R., Ballardini, R., Balzani, V., Constable, E.C., Credi, A., Kocian, O., Langford, S.J., Preece, J.A., Prodi, L., Schofield, E.R., Spencer, N., Stoddart, J.F. and Wenger, S. *Chem. Eur. J.* **1998**, *4*, 2413.

Knots and mixed motifs

78. a) Rapenne, G., Dietrich-Buchecker, C.O. and Sauvage, J.-P. *J. Am. Chem. Soc.* **1999**, *121*, 994 b) Meyer, M., Albrecht-Gary, A.M., Dietrich-Buchecker, C.O. and Sauvage, J.-P. *J. Am. Chem. Soc.* **1997**, *119*, 4599.

79. Baxter, P.N.W, Sleiman, H., Lehn, J.-M. and Rissanen, K. *Angew. Chem. Int. Ed. Engl.* **1997**, *36*, 1294.

80. Funerie, D.P., Lehn, J.-M., Baum, G. and Fenske, D *Chem. Eur. J.* **1997**, *3*, 681.

2. REFERENCES RESULTS

1. Gelling, O.J, van Bolhius, F. and Feringa, B.L. *J. Chem. Soc. Chem. Commun.* **1991**, 917.
2. Matsumoto, N., Nozaki, T., Ushio, H., Motoda, K., Ohba, M., Mago, G. and Okawa, H. *J. Chem. Soc. Dalton Trans.* **1993**, 2157.
3. Bowyer, P.K., Porter, K.A., Rae, A.D., Willis, C. and Wild, S.B. *Chem. Commun.*, **1998**, 1153.
4. Bermejo M.R., Fondo, M., González, A.M., Hoyos, O.L., Sousa, A., McAuliffe, C.A., Hussain, W., Pritchard, R. and Novotorsev, V.M., *J. Chem. Soc. Dalton Trans.*, **1999**, 2211.
5. a) Van Stein, G.C., Van Koten, G., Passenire, H., Steinebach, O. and Vriete, K. *Inor. Chim. Acta* **1984**, *89*, 79 b) Van Stein, G.C., Van Koten, G., Vriete, K.Brevard, C. and Spek, A.L. *J. Am. Chem. Soc.* **1984**, *106*, 4486.
6. a) Hannon, M.J., Painting, C.L. and Alcock, N.W. *Chem. Commun*., **1999**, 2023 b) Hannon, M.J., Bunce, S., Clarke, A.J. and Alcock, N.W. *Angew. Chem. Int. Ed. Engl.* **1999**, *38*, 1277 c) Hannon, M.J., Painting, C.L., Jackson, A., Hamblin J. and Errington, W. *Chem. Comm.*, **1997,** 1807.
7. a) Yoshida, N., Ichikawa, K., Shiro, M. *J. Chem. Soc. Perkin Trans. 2* **2000**, *2*, 17 b) Yoshida, N., Oshio, H. and Ito, T. *J. Chem. Soc. Perkin Trans. 2* **1999**, 975 c) Yoshida, N., Oshio, H. and Ito, T. *Chem. Commun.* **1998**, 63 c) Yoshida, N. and Ichikawa, K. *Chem. Comm.*, **1997,** 1091 d) Yoshida, N., Ito, N. and Ichikawa, K. *J. Chem. Soc. Perkin Trans. 2*, **1997**, 2387.
8. a) Tesouro Vallina, A. and Stoeckli-Evans, H. *Chimia* **1999**, *53*, 342 b) Cheng, H., Chun-ying, D. Chen-jie, F. and Qing-jin, M. *J. Chem. Soc., Dalton Trans.*, **2000**, 2419.
9. CSD, Cambridge Structural Database, Conquest Program, version 1.1, 2000 from the CCDC Cambridge Crystallographic Data Centre, 12 Union Road, Cambridge CB2 IEZ UK, www.ccdc.cam.ac.uk.
10. Abu-Surrah, A.S., Laine, T.V., Repo, T., Fawzi, R., Steimann, M. and Rieger, B. *Acta Cryst.* **1997**, *C53*, 1458.
11. Wright, M.E., Svejda, S.A. and Arif, A.M. *Inorg. Chim. Acta* **1990**, *175*, 13.
12. Krakowiak, K.E., Brandshaw, J.S., Tiang, W., Dalley, N.K., Wu, G. and Izatt, R.M. *J. Org. Chem.* **1991**, *56*, 2675.
13. McKee, V., Dorrity, M.R.J., Malone, J.F., Marrs, D. and Nelson, *J. Chem. Soc. Chem. Commun.* **1992**, 383.
14. Posel, M. Ph. D. Thesis, Université de Neuchâtel, **1998**.
15. Graf, M. Ph. D. Thesis, Université de Neuchâtel, **1995**.
16. a) Greaves, B. and Stoeckli-Evans, H. *Acta Cryst.* **1992**, *48*, 2269 b) Bock, H., Vaupel, C., Näther, C., Rupert, K. and Havlas, Z. *Angew. Chem. Int. Ed. Engl.* **1992**, *31*, 299.
17. Lewis, D.L. and Hodgson, D.J. *Inorg. Chem.* **1974**, *13*, 143.
18. O'Connor, C.J., Educk, E.E., Fronczek, F.R. and Kahn, O. *Inorg. Chim. Acta* **1985**, *105*, 107.
19. Moriuchi, T., Bandoh, S., Kamikawa, M. and Hirao, T. *Chem. Lett.* **2000**, 148.
20. Chakraborty, S., Munshi, P. and Lahiri, G.K. *Polyhedron*, **1999**, 18(10) 1437.
21. Haga, M. and Koizumi, K. *Inorg. Chim. Acta* **1985**, *104(1)*, 47.
22. Upadhyay, M.J., Bhattacharya, P.K., Ganeshpure, P.A. and Satish, S. *J. Mol.Catal.* **1992**, *73(3)* 277.
23. Mathew, J., Bhattacharya, P.K., Ganeshpure, P.A., Satish, S. and Sivaram, S. *J. Mol. Catal.* **1989**, *54(2)*, 131.
24. *International Tables for Crystallography C*, Kluwer Academic Publishers, Dordrecht, The Netherlands, **1995**.
25. Spek, A.L. *Acta Crystallogr.*, **1990**, *A46*, C34.

26. a) Ratilainen, J., Airola, K., Frohlich, R.and Nieger, M. *Polyhedron*, **1999**, *18*, 2265 b) Hueso Urena, F., Jimenez Pulido, S.B., Moreno Carretero, M.N., Quiros Olazabal, M. and Salas Peregrin, J.M. *Inorg. Chim. Acta.* **1998**, *277*, 103 c) Jantti, A., Wagner, M., Suontamo, R., Kolehmainen, E. and Rissanen, K. *Eur. J. Inorg. Chem.* **1998**, 1555 d) Neels, A. and Stoeckli-Evans, H. *Inorg. Chem.* **1999**, *38*, 6164.
27. a) Zacharias, P.S., Srinivas, B. and Aneetha, H. *Proc. Indian Acad. Sci., Chem. Sci.* **1995**, *107* (4), 297 b) Sureshan, C.A., Bhattacharya, P.K. *J. Mol. Catal. A: Chem.* **1998**, 130, 73.
28. Kato, T. and Kadowaki, K. *Japan. Chem. Express* **1988**, 3(11), 647.
29. a) Garg, R.K. and Sharma, L.M. *J. Indian Chem. Soc.* **1995**, 72(4), 231 b) Yoshida, N., Oshio, H. and Ito, T. *J. Chem. Soc. Perkin Trans. 2* **1999**, 975.
30. Hannon, M.J., Moreno, V., Prieto, M.J., Moldrheim, E., Sletten, E., Meistermann, I., Isaac, C.J., Sanders, K. and Rodger, A. *Angew. Chem. Int. Ed.* **2001**, *40*, 880.
31. a) Grillo, V.A., Seddon, E.J., Grant, C.M., Aromí, G., Bollinger, J.C., Folting, K. and Christou, G. *Chem. Commun.*, **1997**, 1561 b) Renaud F., Piguet C., Bernardinelli G., Hopfgartner G. and Bünzli J.-C.G. *J. Am. Chem. Soc.* **1999**, *121*, 9326.
32. Scherer, M., Caulder, D.L, Darren W.J. and Raymond, K.N. *Angew. Chem. Int. Ed.* **1999**, *38*, 1588.
33. Tesouro Vallina, A. and Stoeckli-Evans, H. *Acta Cryst.* **2001**, *C57*, 489.
34. Tesouro Vallina, A. and Stoeckli-Evans, H. *Acta Cryst.* **2001**, E57, m59.
35. Carlucci, L., Ciani, G., Proserpio, D.M. and Sironi, A. *Inorg. Chem. 37*, **1998**, 5941.
36. Suzuku, T., Kotsuki, H., Isobe, K., Moriya, N., Nakagawa, Y. and Ochi, M. *Inorg. Chem.*, **1995**, *35*, 530.
37. Withersby, M.A., Blake, A.J., Champeness, N.R., Hubberstey, P., Li, W.S. and Schröder, M. *Angew. Chem. Int. Ed. Engl.* **1997**, *36*, 2327.
38. a) Bailey, N.A., Barrass, A., Fenton, D.E., Leal Gonzalez, M.S., Moody, R. and Rodriguez de Barbarin, C.O. *J. Chem. Soc. Dalton Trans.* **1984**, 2741 b) Castro, J.A., Romero, J., García-Vazquez, J.A., Sousa, A. and Castañeiras, A. *Acta Cryst.* **1996**, *C52*, 2734 c) Castro, J.A., Castañeiras, A., Duran, M.L., García-Vazquez, J.A., Macias, A., Romero, J. and Sousa, A. *Z. Anorg. Allg. Chem.* **1990**, *586*, 203 d) Sakon, J., Reiter, A., Mertes, K.B. and Takusagawa, F. *Acta Cryst.* **1989**, *C45*, 1311 e) Muller-Westerhoff, U., Rheingold, A.L. and Allen, M.B. *Private Commun.* **1996** f) Parvez, M. and Birdsall, W.J. *Acta Cryst.* **1988**, *C44*, 1526 g) Borer, L.L. and Sin, E. *Inorg. Chim. Acta* **1988**, *142*, 197 h) Kanters, J.A., Spek, A.L., Postma, R., Van Stein, G.C. and Van Goten, G. *Acta Cryst.* **1983**, *C39*, 999 i) Franceschi, F., Guillemot, G., Solari, E., Floriani, C., Re, N., Birkedal, H. and Pattison, P. *Chem. Eur. J.* **2001**, *7*, 1468.
39. Cameron, A.F., Taylor, D.W. and Nuttall, R.H. *J. Chem. Soc. Dalton Trans.* **1973**, 2130.
40. a) Bermejo, E., Carballo, R., Castiñeiras, A., Dominguez, R., Liberta, A.E., Maichle-Moessner, C., Salberg, M.M. and Went, D.X. *Eur. J. Inor. Chem.* **1999**, 965 b) Pickardt, J. and Staub, B. *Z. Naturforsh. Teil B*, **1997**, *52*, 1456 c) Tian, Y.P., Yu, W.T., Jiang, M.H., Raj, S.S.S., Yang, P. and KunFun, H. *Acta Cryst.* C55, **1999**, 1639.
41. Amendola, V., Fabbrizzi, L., Mangano, C., Pallavicini, P., Perotti, A. and Taglietti, A. *J. Chem. Soc., Dalton Trans.*, **2000,** 185.
42. a) Asato, E., Furutachi, H., Kawahashi, T. and Mikuriya, M. *J. Chem. Soc., Dalton Trans.*, **1995,** 3897. b) Kahwa, I.A., Folkes, S., Williams, D.J., Ley, S.V., O'Mahoney and C.A., McPherson, G.L. *J. Chem. Soc. Chem. Comm.*, **1989**, 1531. c) Drew, M.G.B., McCann, M. and Nelson, S. M. *Inorg. Chim. Acta*, **1980**, *41*, 213.
43. Mikuriya, M., Hatano, Y. and Asato, E. *Bull. Chem. Soc. Jpn*, **1997**, *70*, 2495.
44. Hartman, J. R., Vachet, R.W., Callahan, J.H. *Inorg. Chim. Acta*, **2000**, *297*,79.
45. Lam, M.H.W., Lee, D.Y.K., Chiu, S.S.M., Man, K.W. and Wong, W.T. *Eur. J. Inorg. Chem*. **2000**,1483.

46. Beynek, N., McPartlin, M., Murphy, B.P. and Scowen, I. *Polyhedron*, **1998,** *17***,** 2137.
47. Hirayama, F., Zabel, V. and Saenger, W. *Acta Crystallogr*. **1985,** *C41*, 61.
48. Fu, Y.-J., Sun, W.-Y., Dai, W.-N., Shu, M.-H., Xue, F., Wang, D.-F., Mak, T.C.W., Tang, W.-X. and Hu, H.-W. *Inor. Chim. Acta*, **1999,** *290*, 127.
49. Fu, Y.-J., Yang, H., Wang, D.-F., Tang, W.-X., Wu, B.-M. and Mak, T.C.W. *Polyhedron*, **1997**, *16*, 1505.
50. Flack, H.D. *Acta Crystallogr*., **1983**, *A39*, 876.
51. Addison, A.W., Rao, T.N., Reedijk, J., van Rijn, J. and Verschor, G.C. *J. Chem. Soc., Dalton Trans.* **1984**, 1349.
52. a) Campos-Fernández, C.S., Clérac, R. and Dunbar, K.R. *Angew. Chem. Int. Ed.* **1999**, *38*, 3477 b) Bu, X.-H., Morishita, H., Tanaka, K., Biradha, K., Furusho, S. and Shionoya, M. *Chem. Commun.* **2000**, 971 c) Campos-Fernández, C.S., Clérac, R. Koomen, J.M., Rusell, D.H. and Dunbar, K.R. *J. Am. Chem. Soc.* **2001**, *123*, 773.
53. Roche, S., Yellowlees, L.J. and Thomas, J.A. *Chem. Commun.* **1998**, 1429.
54. a) Klein, A., Hasenzahl, S., Kaim, W. and Fiedler, J. *Organometallics*, **1998**, *17*, 3522. Barra, A.-L., Brunel, L.-C., Baumann, F., Schwach, M., Moscherosch, M. and Kaim, W. *J. Chem. Soc. Dalton Trans.* **1999**, *21*, 3855 b) Schwach, M., Hausen, H.-D. and Kaim, W. *Inorg. Chem.* **1999**, *38*, 2242 c) Kaim, W., Reinhardt, R. and Fiedler, J. *Angew. Chem. Int. Ed. Engl.* **1997**, *36*, 2493 d) Poppe, J., Kaim, W., Altabef, A. and Katz, N.E. *J. Chem. Soc. Perkin Trans. 2* **1993**, *11*, 2105.
55. Lagrenee, M., Sueur, S., Wignacourt, J.P., Mernari, B. and Boukhari, A. *J. Chim. Phys.-Chim. Biol.* **1991**, *88*, 2075.
56. a) Adams, H., Bailey, Carlisle, W.D., Fenton, D.E. and Rossi, G. *J. Chem. Soc. Dalton Trans.* **1990**, 1271 b) Adams, H., Bailey, N.A., Dwyer, M.J.S., Fenton, D.E., Hellier, P.C., Jempstead, P.D. and Latour, J.M. *J. Chem. Soc. Dalton Trans.* **1993**, 1207 c) Carlucci, L., Ciani, G., Proserpio, D.M. and Sironi, A. *Angew. Chem. Int. Ed. Engl.* **1995**, *34*, 1895 d) Constable, E.C., Khan, M.S., Liptrot, M.C., Lewis, J. and Raithby, P.R. *Inorg. Chim. Acta* **1991**, *179*, 239 e) Reger, D.L., Collins, J.E., Rheingold, A.L., Liable-Sands, L.M. and Yap, G.P.A. *Organometallics*, **1997**, *16*, 349 f) Abrahams, B.F., Jackson, P.A. and Rodson, R. *Angew. Chem. Int. Ed. Engl.* **1998**, *37*, 2656 g) Mendoza, J., Mesa, E., Rodriguez-Ubis, J.C., Vazquez, P., Vogtle, F., Windscheif, P.-M., Rissanen, K., Lehn, J.-M., Lilienbaum, D. and Ziessel, R. *Angew. Chem. Int. Ed. Engl.* **1991**, *30*, 1331.
57. a) Hunter, D. and Neilson, D. *J. Chem. Soc. Perkin Trans. 1* **1985**, 1081 b) Neilson, D.G., Mahmood, S. and Watson, K.M. *J. Chem. Soc. Perkin Trans. 1* **1973**, 335.

3. REFERENCES EXPERIMENTAL

1. Sheldrick, G.M. *SHELXS-97 Program for the Solution of Crystal Structures Acta Crystallogr*., **1990**, *A46*, 467.
2. Sheldrick, G.M. *SHELXL-97*, **1997**, *Program for the Refinement of Crystal Structures*, University of Göttingen, Germany.
3. Spek, A.L. *Acta Crystallogr.*, **1990**, *A46*, C34.
4. Keller, E. *Schakal 97*, **1997**, *A computer program for the graphic representation of molecular and crystallographic models*, University of Freiburg i. Br., Germany.
5. Visser, J. W. (1989). *J. Appl. Crystallogr*. 2, 89-95.
6. Altomare, A.; Burla, M. C.; Cascarano, G.; Giaccovazzo, C.; Guagliardi, A.; Moliterni, A.G.G.; Polidori, G. *EXPO, Program for Extracting Structure-Factor Amplitudes and Structure Solution from Powder Diffraction Data*, **1997**, Bari, Italy.
7. Larson, A.; Von Dreele, R.B. *GSAS*, *Generalized Structure Analysis System*, **1994**, Los Alamos National Laboratory, Los Alamos, NM.